

AD_____

AWARD NUMBER: DAMD17-02-1-0315

TITLE: Targeting Breast Cancer Vasculature

PRINCIPAL INVESTIGATOR: Erkki Ruoslahti, M.D., Ph.D.

CONTRACTING ORGANIZATION: The Burnham Institute
La Jolla, California 92037

REPORT DATE: March 2006

TYPE OF REPORT: Final

PREPARED FOR: U.S. Army Medical Research and Materiel Command
Fort Detrick, Maryland 21702-5012

DISTRIBUTION STATEMENT: Approved for Public Release;
Distribution Unlimited

The views, opinions and/or findings contained in this report are those of the author(s) and should not be construed as an official Department of the Army position, policy or decision unless so designated by other documentation.

REPORT DOCUMENTATION PAGE				Form Approved OMB No. 0704-0188	
<small>Public reporting burden for this collection of information is estimated to average 1 hour per response, including the time for reviewing instructions, searching existing data sources, gathering and maintaining the data needed, and completing and reviewing this collection of information. Send comments regarding this burden estimate or any other aspect of this collection of information, including suggestions for reducing this burden to Department of Defense, Washington Headquarters Services, Directorate for Information Operations and Reports (0704-0188), 1215 Jefferson Davis Highway, Suite 1204, Arlington, VA 22202-4302. Respondents should be aware that notwithstanding any other provision of law, no person shall be subject to any penalty for failing to comply with a collection of information if it does not display a currently valid OMB control number. PLEASE DO NOT RETURN YOUR FORM TO THE ABOVE ADDRESS.</small>					
1. REPORT DATE (DD-MM-YYYY) March 2006		2. REPORT TYPE Final		3. DATES COVERED (From - To) 1 Mar 02 – 28 Feb 06	
Targeting Breast Cancer Vasculature				5a. CONTRACT NUMBER	
				5b. GRANT NUMBER DAMD17-02-1-0315	
				5c. PROGRAM ELEMENT NUMBER	
6. AUTHOR(S) Erkki Ruoslahti, M.D., Ph.D. E-mail: ruoslahti@burnham.org				5d. PROJECT NUMBER	
				5e. TASK NUMBER	
				5f. WORK UNIT NUMBER	
7. PERFORMING ORGANIZATION NAME(S) AND ADDRESS(ES) The Burnham Institute La Jolla, California 92037				8. PERFORMING ORGANIZATION REPORT NUMBER	
9. SPONSORING / MONITORING AGENCY NAME(S) AND ADDRESS(ES) U.S. Army Medical Research and Materiel Command Fort Detrick, Maryland 21702-5012				10. SPONSOR/MONITOR'S ACRONYM(S)	
				11. SPONSOR/MONITOR'S REPORT NUMBER(S)	
12. DISTRIBUTION / AVAILABILITY STATEMENT Approved for Public Release; Distribution Unlimited					
13. SUPPLEMENTARY NOTES					
14. ABSTRACT The purpose of our project is to develop ways of reducing the toxic side effects thaty limit the usefulness of many of the existing anti-cancer drugs. The approach is to develop a strategy for physically concentrating therapeutic agents in tumor tissue. Our strategy makes use of unique features of tumor vasculature. We screen libraries of peptides displayed on phage <i>in vivo</i> to profile the specialization of breast cancer vasculature. We have isolated homing peptides that specifically recognize blood or lymphatic vessels in breast cancer and its metastases, and have even obtained peptides that specifically recognize the vessels in pre-malignant breast lesions. In addition, we have used methods based on phage library screening to discover a novel molecule that is involved in breast cancer metastasis The compounds developed in this work can be used to design new therapies that specifically target breast cancer. The vascular receptors for the homing peptides, some of which we have identified, represent novel "druggable" targets for the development of anti-cancer agents.					
15. Subject Terms (keywords previously assigned to proposal abstract or terms which apply to this award) Tumor vasculature, angiogenesis, lymphatic vessels, metastasis, drug delivery, peptides, phage display					
16. SECURITY CLASSIFICATION OF:			17. LIMITATION OF ABSTRACT	18. NUMBER OF PAGES	19a. NAME OF RESPONSIBLE PERSON
a. REPORT	b. ABSTRACT	c. THIS PAGE			USAMRMC
U	U	U	UU	143	19b. TELEPHONE NUMBER (include area code)

Targeting Breast Cancer Vasculature

Final Progress Report 03/01/02 - 2/28/06

Table of Contents

Cover	1
SF 298	2
Table of Contents	3
Introduction	4
Body.....	4
Key Research Accomplishments.....	15
Reportable Outcomes	15
Conclusions	17
References.....	18

Appendices

Bibliography

Personnel

- Akerman, M.E et al *Proc. Natl. Acad. Sci. USA*. 99:12617-12621 (2002)
Brown, D. and Ruoslahti, E. *Cancer Cell* 5: 365-374 (2004)
Brown, D.M., et al; *ChemBioChem*. 5: 871-875 (2004).
Christian, S., et al *J Cell Biol*. 163: 871-878 (2003).
Joyce, J.A., et al *Cancer Cell* 4:393-403 (2003).
Laakkonen, P., et al *Nature Med* 8: 743-751 (2002).
Laakkonen, P., et al *Proc. Natl. Acad. Sci. USA*. 101:9381-9386 (2004).
Pai, J-T. and Ruoslahti, E. *Gene*. 347: 21-33. (2005).
Pilch, J., et al *Proc. Natl. Acad. Sci. USA*. 103: 2800-2804 (2006)
Ruoslahti, E. *Drug Discovery Today*. 7:1138- 1143 (2002).
Ruoslahti, E. *The Biochemical Society Transactions* 32: 397-402 (2004).
Ruoslahti, E., et al *Current Pharmaceutical Design*. Special Issue, "Cell-penetrating Peptides, Mechanisms and Applications. 11: 3655-3660 (2005)
Zhang L., et al *Cancer Res.*, submitted.

INTRODUCTION

Toxic side effects limit the usefulness of many of the existing anti-cancer drugs. If it were possible to selectively target the drug into the tumor tissue, the efficacy of anti-tumor therapies could be enhanced while simultaneously decreasing the side effects. We are working on a targeting strategy that aims at physically concentrating therapeutic agents in tumor tissue by making use of the unique features of tumor vasculature.

Directing a therapy at the tumor vasculature has advantages: First, the vasculature is available for the therapeutic agent through the blood stream. In contrast, agents directed at the tumor cells often do not adequately penetrate into the tumor. Second, tumor cells depend on blood supply; an average of 100 tumor cells depends on one endothelial cell, making vascular therapy potentially highly effective. Finally, the vasculature is composed of normal cells, which, because they do not possess the genetic instability that is characteristic of tumor cells, are unlikely to develop resistance to treatments.

Tumor vasculature grows as the tumor grows, and this process – angiogenesis – makes tumor blood vessels distinct from normal resting blood vessels. Several anti-angiogenic therapies are in pre-clinical and clinical development. The approach we are working on, while it also targets the blood vessels, differs from these anti-angiogenic therapies in many important ways. The therapeutic agent is concentrated in tumor vessels, but it acts both on the endothelial cells and the tumor cells. Furthermore, the therapy can be directed specifically to breast cancer vasculature – both the blood vessels and the lymphatic vessels – eliminating potential side effects from targeting angiogenesis in tissue repair. Targeted destruction of tumor lymphatics eliminates a common route for metastasis. It is also possible to target pre-malignant lesions, or even normal breast tissue, for destruction, by using this approach.

In this project, we have used *in vivo* screening of libraries of peptides displayed on phage to profile the specialization of breast cancer vasculature. We have isolated homing peptides that specifically recognize blood or lymphatic vessels in breast cancer and its metastases, and even in pre-malignant breast lesions. In addition, we have developed new approaches to use phage library screening in discovering molecules involved in metastasis and have expanded the library screening from phage to chemical libraries. The compounds developed in this work can be used to design new therapies that specifically target breast cancer. The vascular receptors for the homing peptides, some of which we have identified, represent novel “druggable” targets for the development of anti-cancer agents.

BODY

The approved tasks for this project are:

Task 1: To identify peptides that specifically home to the blood and/or lymphatic vessels of MMTV-PyMT breast cancers.

Task 2: To validate the specific blood vessel and lymphatic vessel homing of the selected peptides.

Task 3: To identify and characterize receptors for the peptides that specifically home to the blood and/or lymphatic vessels of breast cancers.

Task 4: Study the specificity of vascular entry of tumor cells by using phage libraries.

Task 5: To study the use of homing peptides in breast cancer prevention and treatment in mouse models.

RESEARCH ACCOMPLISHED DURING THE GRANT PERIOD:

TASKS 1 AND 2: HOMING PEPTIDES

PEPTIDES THAT RECOGNIZE THE EXTRACELLULAR MATRIX IN BREAST CANCERS

In vivo homing peptide screening in the MMTV-PyMT breast cancer model yielded a pentapeptide with the sequence CREKA as the most promising tumor-homing peptide. The CREKA phage and fluorescein-labeled CREKA peptide home to the PyMT tumors as well as to MDA-MB-435 human breast cancer xenografts. The CREKA peptide binds to the tumor basement membrane material known as 'matrigel', and our results suggest that the binding epitope may be in altered type IV collagen (Task 3).

The superior tumor-homing properties of the CREKA peptide that emerged from our PyMT tumor screens, and that was described in the previous progress report, has been confirmed by two collaborators, AntiCancer Inc. and Dr. Gregory Lanza at the Washington University. Characterization of this peptide and other peptides that bind to breast cancer extracellular matrix is an ongoing project. In a separate project, we have shown that homing peptides can distinguish between the vasculature of premalignant lesions and fully developed tumors (Joyce et al., 2003).

Encouraged by this finding, we devised a screening protocol in which screening on tumor extracellular matrix *in vitro* was alternated with *in vivo* screening for tumor homing. To accomplish this, a CX7C phage library (C=cysteine; X=any amino acid) was screened *in vitro* on matrigel, a commercially available basement membrane material from the mouse EHS tumor, followed by *in vivo* screening for tumor homing to human breast cancer MDA-MB-435 xenografts. We also screened by reversing the order of the procedures (*in vivo* first). This novel combination screen yielded an interesting new peptide, which appeared in each of the two independent screens. This is a 9-amino acid cyclic peptide, which we refer to as CSG, based on its first 3 amino acids. Like CREKA, the CSG phage and peptide are highly efficient in tumor homing; fluorescein conjugated CSG gives strong tumor homing (Fig. 1) with a pattern compatible with matrix location *in vivo* (Fig. 2). Our current focus is to identify the receptors for these peptides (see below).

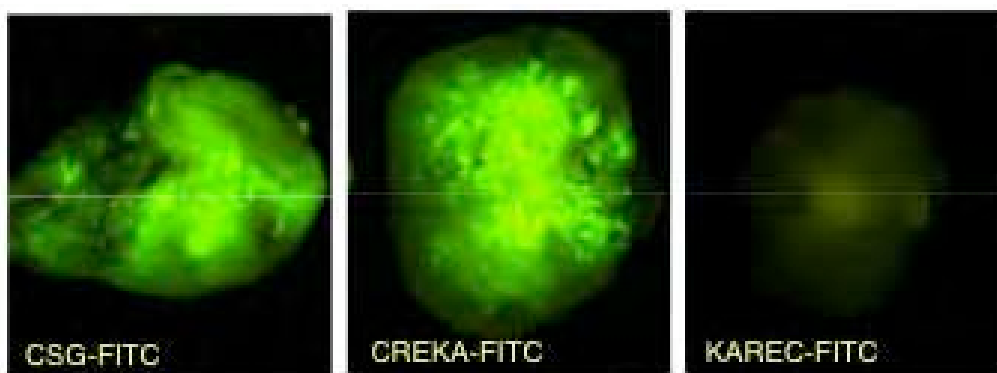


Fig. 1. The CREKA and CSG peptides home to breast cancer xenograft tumors. Tumor-bearing mice were intravenously injected with 500 μ g of fluorescein-labeled CREKA, CSG or control (KAREC) peptide. The mice were sacrificed 18 hours later, and the tumor and other tissues were removed and examined under blue light (Laakkonen et al., 2004). The tumors from the CREKA- and CSG-injected mice were strongly fluorescent.

KAREC, a scrambled variant of CREKA (negative control) produced no significant tumor fluorescence. A representative experiment out of 3 is shown.

LYMPHATIC HOMING PEPTIDES

We had previously shown that the lymphatic vessels in two breast cancer models carry a specific marker detectable with a peptide isolated from a phage library (Laakkonen et al., 2002). A nonapeptide (LyP-1) homes to lymphatic vessels in xenografted (MDA-MB-435) and in transgenic (PyMT) breast cancers. However, some tumors (particularly xenografts obtained with the human melanoma C8161 cells), even though they contained lymphatic vessels, were negative. We developed a new screening procedure based on the isolation of lymphatic endothelial cells (and phage bound to them) with anti-lymphatic endothelial antibodies. We then screened phage libraries for peptides that would bind to the lymphatics in the C8161 tumors or TRAMP transgenic prostate cancers. Through this procedure we have identified lymphatic homing peptides for each tumor. These peptides are tumor type-specific; they home poorly, or not at all, to other tumors, including the MDA-MB-435 tumors. Thus, a lymphatic vessel “zip code” system of the kind predicted in the original application is beginning to emerge. A surprising result was that a peptide (LyP-2) that we identified in a screen for homing peptides for skin cancer (Hoffman et al., 2003) and that differs little from LyP-1 (CGNKRTRGC for LyP-1 vs CNRRTKAGC for LyP-2) has a different specificity from LyP-1. Detailed comparison of the specificity of these two peptides, both of which recognize tumor lymphatics, showed a mutually exclusive range of tumor recognition (Fig. 3). A paper describing the new peptides and the unexpected specificity of the LyP family peptides is in revision for *Cancer Research* (Zhang et al., 2006).

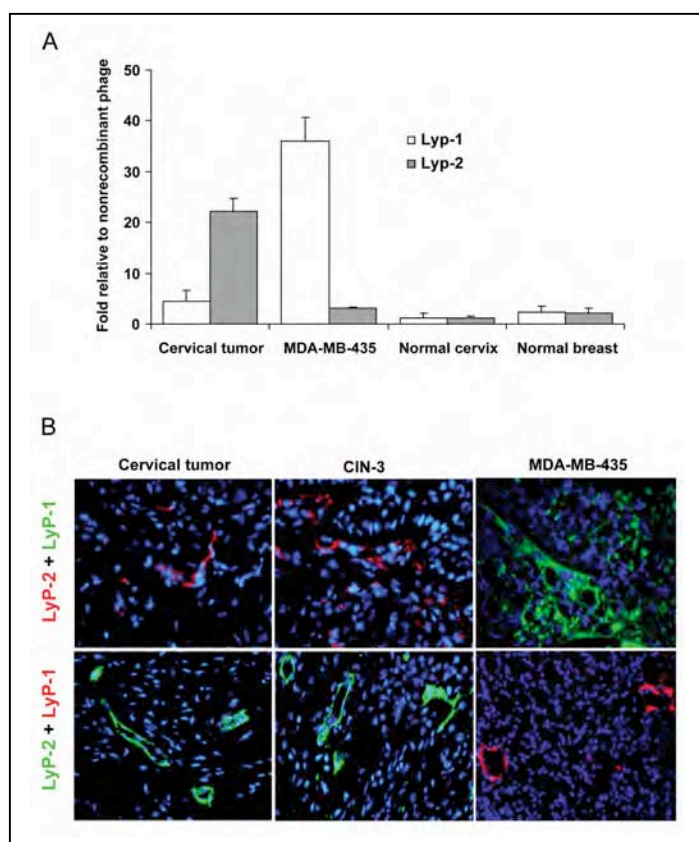


Fig. 2. Differential tumor-homing specificity of LyP-1 and LyP-2 peptides. A. LyP-1 and LyP-2 phage were intravenously injected into mice bearing MDA-MB-435 breast cancer xenografts or K14-HPV16/E₂ tumors (n=3). B. Fluorescein-labeled LyP-1 and rhodamine-labeled LyP-2 (upper row) were intravenously injected (100 µg of each peptide) into the mice bearing tumors or premalignant lesions. Alternatively, the injection consisted of rhodamine-labeled LyP-1 and fluorescein-labeled LyP-2 (lower row). Tissues were collected and processed for histological analysis 2 hrs later. LyP-1 homes to the MDA-MB-435 tumors, whereas LyP-2 homes to the cervical cancers and premalignant lesions. Phage homing to the premalignant lesions was significantly higher than to the corresponding tumors in both models (P<0.01). Original magnification: 400x. (From Zhang et al., *Cancer Res.*, submitted).

SPECIFIC BLOOD VESSEL MARKERS IN PREMALIGNANT LESIONS

There is abundant evidence that vasculature in malignant tumors is functionally and morphologically aberrant. We showed for the first time, using the *in vivo* phage display and a model of multistage tumorigenesis, that the angiogenic vasculature in premalignant lesions is distinguishable from normal as well as tumor vessels (Joyce et al., 2003). The tumor model was a transgenic pancreatic islet carcinoma and we also showed that both angiogenic progenitor and tumor vessels in the pancreas have molecular signatures distinct from tumors growing in or under the skin, even of the analogous cell type (and breast cancer xenografts). The stage and organ specificities of particular homing peptides may prove instructive about mechanisms regulating the neovasculature in different pathways of tumorigenesis, suggest means to detect and distinguish premalignant and malignant lesions noninvasively, and predict differential sensitivity to therapeutic agents targeting angiogenesis.

METADHERIN

We used *in vivo* screening of a cDNA library from a lung-metastasizing mouse 4T1 breast cancer cell to search for clones that would mediate binding of the phage to lung blood vessels. The rationale was that the procedure might reveal proteins that mediate the attachment of circulating 4T1 cells to lung vessels, thereby promoting the formation of lung metastases. The scheme worked and led to the identification of a novel protein we named metadherin. In a paper published in *Cancer Cell* we showed that metadherin mediates the binding and tissue-specific metastasis of experimental breast cancer to the lungs (Brown and Ruoslahti, 2004). Independent microarray analysis results from a large human breast cancer study show that elevated expression of an mRNA detected with an EST representing the metadherin mRNA is an excellent marker of aggressiveness in breast cancer (van't Veer et al., 2002). Our study, together with these microarray results, establishes metadherin as a novel metastasis-promoting protein that is likely to be clinically important. The studies in this grant period were to aim at identifying the protein to which metadherin binds in lung vasculature. Results described in the interim progress reports suggest that metadherin-mediated lung homing depends on a homotypic interaction between tumor cell metadherin and metadherin expressed on lung endothelial cells (but not in other endothelia). However, our recent results on possible involvement of metadherin in cell adhesion and migration, and by extension in tumor invasion, provided a compelling case for changing the focus of our metadherin work. The results are reported under Task 5. We also profiled the tissue-specific changes in lung endothelial cells by using microarrays (Pai and Ruoslahti, 2005).

CLOT-BINDING PEPTIDES

It was shown many years ago that tumors, but not normal tissues, contain fibrin. The reason is thought to be that the leakiness of tumor vessels allows plasma proteins to escape into tumor tissue, where clotting results in the conversion of fibrinogen into fibrin. We reasoned that peptides capable of binding to clotted plasma may specifically recognize tumors *in vivo*. We performed screening of a phage library for peptides that bind to clotted plasma in the presence of liquid plasma and obtained two cyclic decapeptides, CGLIIQKNEC (CLT1) and CNAGESSKNC (CLT2) (Pilch et al., 2006). When injected intravenously into mice bearing various types of tumors, fluorescein-conjugated CLT peptides accumulated in a fibrillar meshwork in the extracellular compartment of the tumors, but were not detectable in other tissues of the tumor-bearing mice. The tumor homing of both peptides was strongly reduced after coinjection with unlabeled CLT2, indicating that the two peptides recognize the same binding site. The CLT peptide fluorescence colocalized with staining for

fibrin(ogen) present in the extravascular compartment of tumors, but not in other tissues. The CLT peptides did not home to tumors grown in fibrinogen-null mice or in mice that lack plasma fibronectin. The CLT peptides also accumulated at the sites of injury in arteries, skeletal muscle, and skin. Our conclusion is that the CLT peptides recognize fibrin–fibronectin complexes formed by clotting of plasma proteins that have leaked into the extravascular space in tumors and other lesions. These peptides may be useful in targeting diagnostic and therapeutic materials into tumors and injured tissues.

***IN VIVO* SCREENING OF CHEMICAL LIBRARIES**

We have extended the *in vivo* tumor screening technology to include the screening of libraries of chemical compounds for accumulation in a specific tissue of live animals (Brown et al., 2004). We showed that it is possible to use *in vivo* screening to identify compounds that have specific affinities for individual normal tissues. One of the strongest indicators of the feasibility of such screening was that we correctly identified a benzodiazepine as a brain-homing compound from a small library. This work provides the first demonstration that it is possible to conduct large-scale screening of chemical libraries *in vivo*. The screening can identify targeted small molecules for use in a variety of applications and has some advantages over previous methods. *In vivo* phage screening primarily targets the vascular endothelium. Small molecular weight chemical compounds can target the vasculature, but are also likely to gain access to parenchymal cells in tissues. That parenchymal cells can be targets is suggested by the recovery of a benzodiazepine as a brain-homing molecule, as most receptors for these compounds are on the neurons. As an additional advantage, this screening approach does not require encoded or tagged library compounds. This is an improvement over other approaches that require separate chemistries for coupling different small molecules to synthetic or genetically engineered tags such as bacteriophage (Woiwode et al., 2003). In addition, the absence of compound tags eliminates the possibility of interference by the tag with the *in vivo* homing activity.

We next wanted to show proof of concept for a screen for compounds that accumulate in tumors. We tested an anti-tumor compound, the geldanamycin 17-AAG, which has been shown to specifically interact with a variant HSP-90 in tumors (Kamal et al., 2003). We found that intravenously injected 17-AAG could be detected in tumor tissue, but not in other tissues of the tumor mouse, with the exception of the kidneys (Fig 12; unpublished results). This result validates our approach to tumor targeting; the method can identify compounds that specifically bind to tumor tissue. These technical advances will allow screening of large numbers of compounds for tumor homing. We have initiated such screening and have so far screened about 2,000 compounds for homing to the mouse 4T1 breast cancer. No clear tumor homing compounds have been found so far. We have made arrangements to gain access to another 20,000 compounds for the screening (we need larger quantities of compounds at higher concentrations than are available in the libraries intended for the usual *in vitro* screening). We expect to find novel tumor-specific compounds, some of which may have anti-tumor activity, as we found to be the case with the LyP-1 peptide from an analogous phage library screen.

TASK 3: RECEPTORS FOR HOMING PEPTIDES

CREKA and CSG bind to matrigel

Fluorescein-labeled CREKA and CSG peptides, when injected intravenously into mice bearing MDA-MB-435 breast cancer xenografts, co-localize with the extracellular matrix of tumor vessels and stroma. As we had selected the CSG phage by alternating *in vitro* screening on matrigel (extracellular matrix from a tumor) and *in vivo* screening for tumor homing, we tested the CSG and CREKA phage for matrigel binding. As expected, the CSG phage binds to matrigel coated onto plastic. The binding is about 20 fold over the control phage in ELISA format assays. A surprising result was that the CREKA phage also binds to matrigel (Fig. 4). Moreover, inhibition assays with the cognate peptides show that the two peptides bind to different epitopes in matrigel. These findings will help in identifying the receptor for CREKA (which has proven elusive), and for the CSG peptide because matrigel can be used as the starting material for the isolation of the receptors.

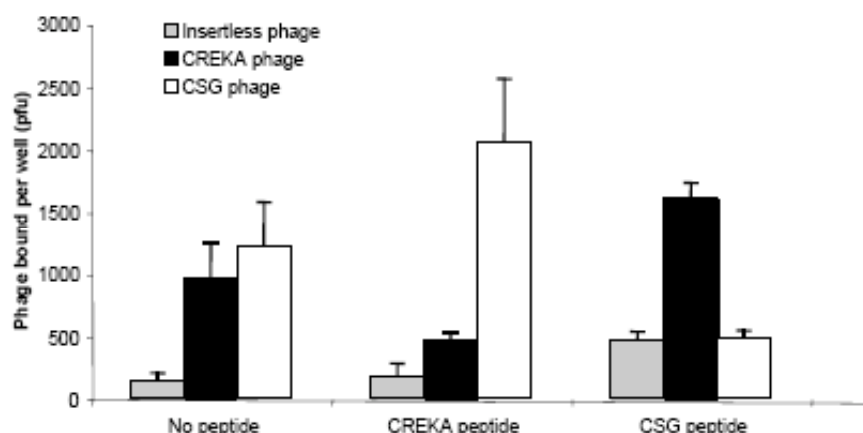


Fig. 3. Binding of CREKA phage and peptide to matrigel. The CREKA and CSG phage clones were incubated in microtiter wells coated with matrigel (coating concentration 3 ug/ml). The incubation was performed in the presence and absence of the cognate-free peptides (30 ug/well), the wells were washed, and the titers of bound phage were measured.

We will publish the CREKA/CSG results in two papers: one describing the peptides and their binding specificity still requires identification of the molecules in matrigel that the peptides recognize. Another paper where we have used CREKA to deliver iron oxide nanoparticles to tumor vasculature is being written.

F3

We have identified cell surface-expressed nucleolin as a receptor for a tumor-homing peptide on the MDA-MB-435 cells (Christian et al., 2003). The peptide, F3, is a fragment of the nuclear protein HMGN2. F3 binds to tumor blood vessel endothelial cells and tumor cells, and it also recognizes a small subpopulation of cells in the bone marrow that may represent endothelial precursor cells (Porkka et al., 2002). The identification of nucleolin as the F3 receptor identified cell surface nucleolin as a new angiogenesis marker in tumor vessels. This finding also made it possible for us to study the effect of anti-nucleolin on angiogenesis as described in the report on Task 5.

LyP-1

The main advance in the latest grant period has been the identification of the receptor for LyP-1, a peptide that specifically recognizes breast cancer lymphatics. We identified the receptor by performing affinity chromatography of MDA-MB-435 tumor extracts on insolubilized LyP-1 peptide. Mass spectrometry identified a specifically bound gel band as gC1q receptor. This protein is a little-studied complement receptor whose physiological role is unknown (Ghebrehiwet and Peerschke, 2004). We obtained a sample fusion protein from another group and showed that the LyP-1 phage specifically binds to gC1q and that a monoclonal anti-gC1qR antibody inhibits the binding (Fig. 4). We also used the antibodies to show that gC1q is greatly upregulated in the MDA-MB-435 tumors where the staining co-localizes both with lymphatic markers and with intravenously injected LyP-1 (Fig. 5). Moreover, treatment of the MDA-MB-435 cells with gC1q siRNA eliminated the binding of LyP-1 to the cells. Thus, multiple lines of evidence clearly identify gC1q as the receptor for LyP-1. While the over-expression of gC1q has been reported before, the association of this protein with lymphatic vessels and the possibility that it might be a suitable target for diagnostic probes and anti-cancer agents has not been noted before. In fact, we have reported (see Task 5) that the LyP-1 peptide has an inherent anti-tumor activity against MDA-MB-435 xenografts and that it also causes the destruction of the lymphatics in these tumors (Laakkonen et al., 2004). We are currently preparing a paper on the gC1qR results.

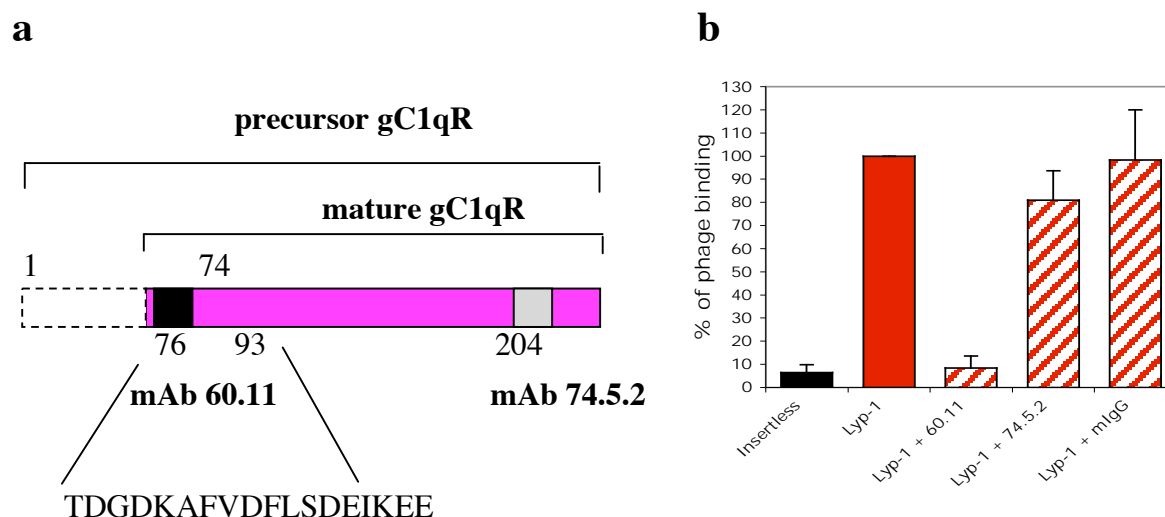


Fig. 4. Binding of LyP-1 phage to purified gC1qR. An antibody against the N-terminus of gC1qR inhibits LyP-1 phage binding to gC1qR. (a) Diagram of precursor (aa 1-282) and mature (aa 74-282) gC1qR protein. Boxes indicate the amino acid residues recognized by the monoclonal antibodies, mAb 60.11 and mAb 74.5.2, respectively at the N-terminus (aa 76-93) and C-terminus (aa 204-282) of the mature protein. The amino acid sequence recognized by mAb 60.11 is also indicated. (b) 1.5×10^7 pfu of insertless and LyP-1 phages were allowed to bind for 6h at 37°C to gC1qR protein coated onto microtiter plates in the presence or absence of 20µg/ml of either mAbs 60.11, 74.5.2 or purified mouse IgG1 (mlgG). The results are representative of three independent experiments and are expressed as percentage of phage binding, with LyP-1 phage binding alone as 100%.

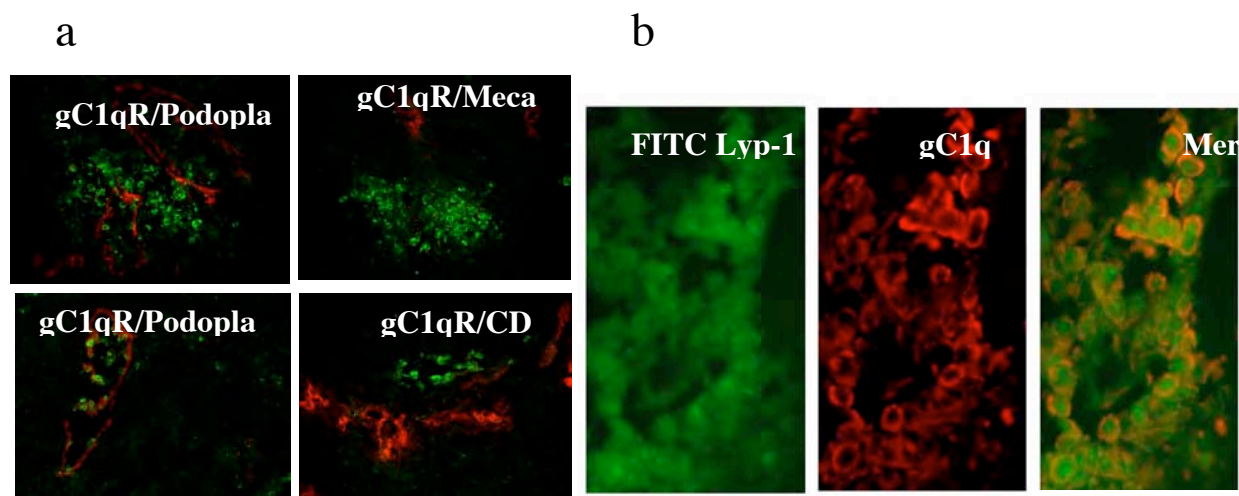


Fig. 5. Tumor localization of gC1qR and LyP-1 peptide. (a) Staining of gC1qR (green) and lymphatic (Podoplanin) or blood (Meca32/CD31) vessel endothelial markers (red) in MDA-MB-435 tumor xenografts. Polyclonal anti-gC1qR antibody recognizes cell clusters that lack blood vessels but contain lymphatics (upper panels), or cells lining vessel-like structures positive for Podoplanin but not CD31 or Meca32 (lower panels). (b) LyP-1 peptide localizes in gC1qR-positive patches within the tumor. Fluorescein-conjugated LyP-1 peptide was i.v. injected into mice bearing MDA-MB-435 tumors and allowed to circulate for 1h before removal of the tumor for gC1qR immunohistochemical analysis.

TASK 4

Our initial studies on the use of phage libraries to study tumor intravasation were hampered by varying uptake of the phage by the liver and spleen (presumably by the reticuloendothelial system). We were not able to reliably distinguish phage clones that were preferentially transported from tissue into the blood from phage that was not efficiently eliminated by the reticuloendothelial system. Thus, this project was assigned a secondary priority. We have recently selected phage that is not eliminated into the reticuloendothelial system, or does it slowly. We plan to use this phage to construct peptide libraries and will be using these libraries to screen for enhanced intravasation in future studies.

TASK 5**ANTI-NUCLEOLIN INHIBITS ANGIOGENESIS**

We reported last year that antibodies against the F3-binding domain of nucleolin inhibit angiogenesis in mice. Figure 6 illustrates the inhibition of endothelial cell tube formation and the reduction of blood vessels in a matrigel plug assay (Akerman et al., 2005) we have observed *in vitro* and *in vivo*. We have delayed publication of these results because the concept of “normalization” of tumor vasculature as a result of anti-angiogenic treatment has gained in prominence in the past year, and we want to see if the reduction in the density of tumor vessels we observe after anti-nucleolin treatment is associated with such normalization of the remaining vessels. If so, these remaining vessels will become a prime target for the screening of homing peptides that could be used to destroy these vessels. A DoD Idea grant for this project is about to be funded and will be used to continue the nucleolin project.

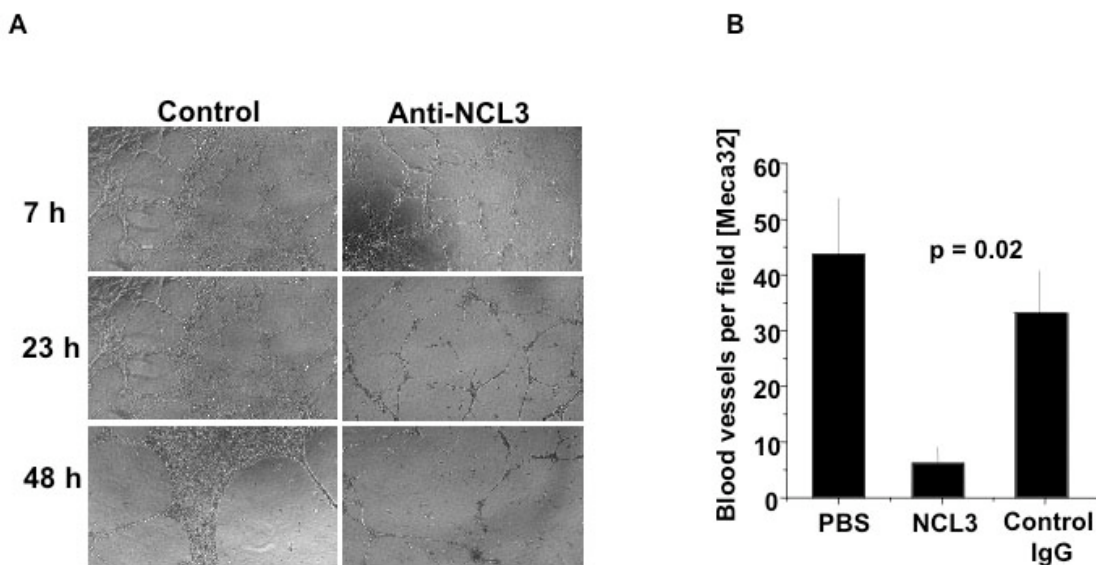


Fig. 6. Effect of anti-nucleolin antibodies on endothelial cell tube formation and on angiogenesis in subcutaneously implanted matrigel plugs. A. Endothelial tube formation assay. HUVECs were cultured under conditions (matrigel) that induce tube formation and the cultures were treated with either control IgG or anti-nucleolin IgG at 400µg/ml. The cultures with control IgG displayed robust tube formation within 24-48 hr (left panels), whereas the cells treated with anti-nucleolin initially (7 hr) developed tubes, but subsequently died of apoptosis (right panels). The pictures of tube forming cells were taken by bright field microscopy. **B.** Matrigel plug angiogenesis assay. Matrigel (0.1 ml) was supplemented with 100 ng of bFGF and

subcutaneously injected into mice. The mice were treated daily with intravenous injections of normal rabbit IgG (control) or anti-nucleolin IgG (NCL3; 0.2 mg of IgG). The plugs were removed on Day 7, sectioned, and blood vessels were visualized by staining with anti-CD31. There is a significant reduction in the number of blood vessels in the plugs from the anti-nucleolin-treated mice ($p < 0.02$). Representative experiments out of two or more are shown. (Christian et al., in preparation).

ANTI-TUMOR ACTIVITY OF LYP-1

We have shown that the LyP-1 peptide, which homes to tumor lymphatics, accumulates in MDA-MB-435 xenografts with an extraordinary efficiency and selectivity. In fact, we are able to detect the fluorescein-labeled LyP-1 in tumors of intact mice after an intravenous injection. We have now found that the LyP-1 peptide has an apoptotic effect on cells that bind this peptide, and that treatment of nude mice bearing MDA-MB-435 human breast cancer xenografts significantly suppresses tumor growth. Moreover, tumors from the mice treated with LyP-1 were almost completely devoid of lymphatic vessels. These results have now been published (Laakkonen et al., 2004). Thus, the LyP-1 receptor is not only a marker of tumor lymphatics, but is also important in tumorigenesis, and it may be possible to use this peptide or its mimics to reduce tumor mass (pro-apoptotic effect of tumor cells) and to reduce the number of lymphatics in and around the tumor (potentially preventing lymphatic metastasis). Now that we have identified the cell surface receptor for LyP-1 (Task 3), we are in a good position to elucidate the mechanism of action of this peptide and to develop antibodies and small molecule compounds that reproduce the anti-tumor activity of the peptide.

DRUG-HOMING PEPTIDE CONJUGATES

We recently received a proprietary doxorubicin compound from a Dutch biotech company that allows one to synthesize conjugates that release free doxorubicin intracellularly. We made conjugates with LyP-1 and an angiogenesis homing peptide similar to F3 and tested them with MDA-MB-435 xenografts. Unfortunately, these conjugates were not effective, possibly because the peptides take the conjugate to a cellular compartment in which the drug is not released.

POSSIBLE ROLE OF METADHERIN IN CELL ATTACHMENT, MIGRATION, AND INVASION

Metadherin expression in angiogenic vessels. To explore the role metadherin might play in biological functions other than metastasis, we tested for metadherin expression in angiogenesis. It has been reported that CEACAM-1 is required for VEGF-mediated responses in angiogenic vasculature (Ergün et al., 2000). Since we found that metadherin binds to CEACAM-1 in lung extracts, it seemed possible that metadherin might also play a role in angiogenesis. We detected metadherin expression in CD31+ and CD34+ cells within implanted matrigel plugs that were supplemented with bFGF, indicating that metadherin is expressed in angiogenic endothelial cells (Fig. 7). Metadherin was also detected in fibroblast-like cells throughout the matrigel plugs.

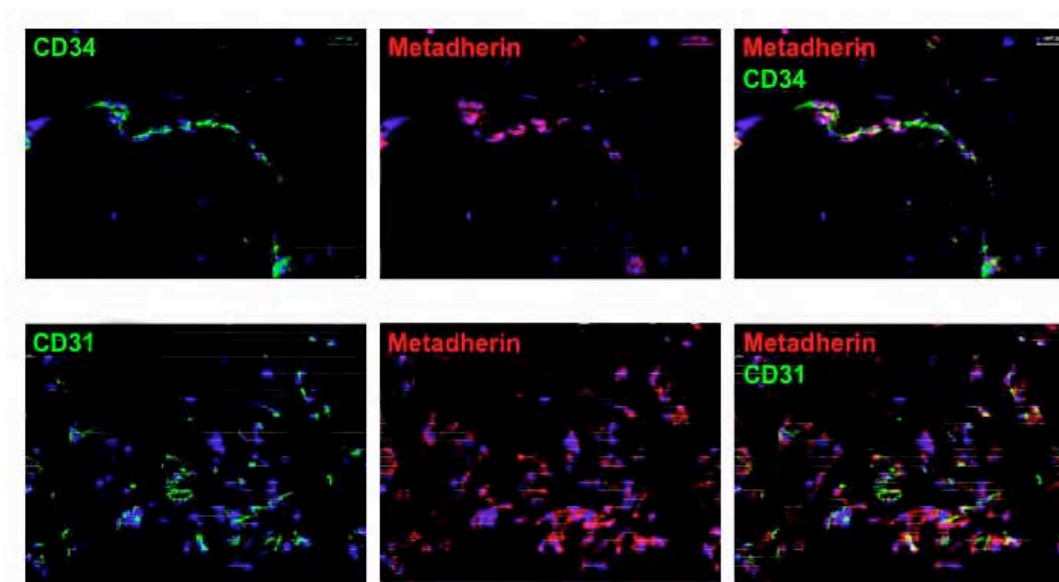


Fig. 7. Metadherin expression in matrigel plug angiogenesis. Matrigel supplemented with bFGF was implanted subcutaneously into BALB/c mice and incubated for nine days. Afterwards, the plugs were removed and frozen sections were prepared. The sections were fixed with acetone and then stained with rat anti-CD31 or anti-CD34 and rabbit anti- metadherin_{LHD} antibodies. Primary antibodies were detected with goat anti-rat IgG Alexa 488 (green) and goat anti-rabbit IgG Alexa 594 (red) and nuclei were stained with DAPI (blue).

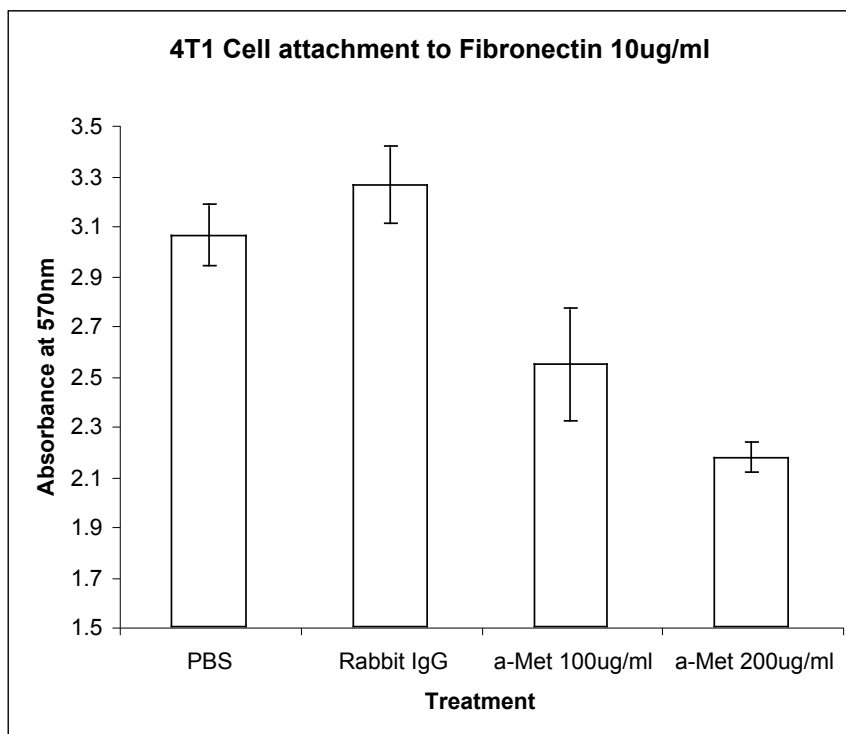
Effect of anti-metadherin on cell attachment and migration. Studying metadherin expression in cultured cells, we noted the preferential presence of metadherin at the leading edge of migrating KRIB cells. This observation, and the expression of metadherin in angiogenic endothelium, led us to examine the effect of blocking metadherin on cell adhesion and migration. We found that treatment of suspended 4T1 cells with the anti-metadherin_{LHD} antibody has a striking effect on the ability of the cells to attach upon plating onto culture plates. At antibody concentrations above 100 ug/ml, the treatment essentially abolished the subsequent attachment of cells. At the highest concentrations of the antibody, there were no attached cells at any time point. The final 72-hour time point is shown in Figure 8. Interestingly, the antibody had no effect on 4T1 cells that had already attached. This latter result also serves as a control regarding possible non-specific toxicity of the antibody preparation. TUNEL and propidium iodide staining suggested that the non-attached cells were dying by apoptosis (not shown).

Fig. 8. Anti-metadherin inhibits the attachment of tumor cells to culture dishes.

The 4T1 cells were suspended by treating attached cultures with 2mM EDTA in PBS. The cells were diluted to 1.5×10^6 cells/ml and mixed with antibody for 1 hr on ice. The suspension was then plated culture plates coated with fibronectin.

Three days later, the cells were examined to determine the effects of the metadherin antibody on cell attachment, spreading, and death. Smaller numbers of cells remained in the wells that received cells treated with anti-metadherin than in the controls. The reduction in cell number was dependent on the concentration of the antibody. Analysis of apoptosis markers revealed significantly more

apoptosis in the wells that received low concentrations of the antibody than in the control wells (not shown).



Cell migration was studied in an *in vitro* “wound” assay. The results show that the closure of the denuded areas is much slower (24h $p < 0.013$; 48h $p < 0.03$) in the cultures treated with the metadherin antibody (Fig 9). Similar results were obtained when metadherin expression was suppressed with siRNA.

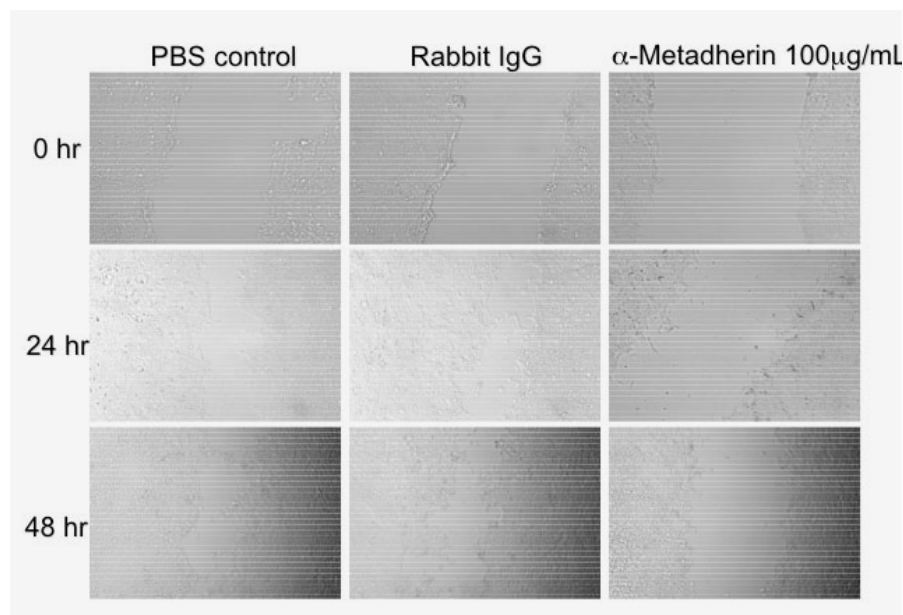


Fig. 9. Anti-metadherin inhibits wound closure *in vitro*. The 4T1 cells were grown in 6 well plates to confluency in IMEM/10%FBS. A streak was scraped in each well with a pipet tip and anti-metadherin antibodies at the indicated concentrations were added. PBS or rabbit IgG were used as control treatments. The cells treated with anti-metadherin antibody spread into the wounded region much less efficiently that the control cells. This same effect was seen 48 hr after treatment.

These results provide a strong indication that attachment to lung endothelium is not the only role of metadherin in tumor progression, but that metadherin is involved in tumor growth and invasion. This hypothesis will be tested in future work. Metadherin is a promising target for the development of anti-cancer agents, such as monoclonal antibodies that block its function.

KEY RESEARCH ACCOMPLISHMENTS

- Identified two peptides, CREKA and a nonapeptide designated as CSG, home to breast cancer blood vessels and extracellular matrix.
- Isolated peptides that home to lymphatic vessels in various tumors and shown that the lymphatics in different tumor types, including breast cancers, carry distinct, tumor type-specific markers.
- Shown that a lymphatic homing peptide (LyP-1) preferentially recognizes poorly vascularized areas in breast cancers and that it is extraordinarily effective in homing to MDA-MB-435 xenografts, suggesting applications in tumor imaging.
- Used the F3 and LyP-1 peptides to demonstrate that quantum dots (semiconductor material nanocrystals) coated with homing peptides specifically accumulate in breast cancer xenografts *in vivo*.
- Shown that homing peptides can distinguish the blood vessels of pre-malignant lesions from those of fully developed tumors (and from normal vessels).
- Discovered a breast cancer cell surface protein that binds tumor cells to lung endothelium promoting lung metastasis.
- Shown that peptides selected for binding to clotted plasma specifically home to breast cancers and other tumors.
- Provided proof-of-principle support for *in vivo* screening of small molecular weight chemical compounds for tumor-homing compounds by showing that a geldanamycin accumulates in breast cancer tissue and can be detected by mass spectrometry.
- Shown that the CREKA and CSG peptides both bind to matrigel *in vitro* and that the binding specificities of the two peptides are different.
- Identified a breast cancer cell receptor for a peptide that homes to tumor vasculature (F3) as cell surface-expressed nucleolin.
- Identified the breast cancer cell surface receptor for the LyP1 peptide as gC1q receptor.
- Shown that anti-nucleolin is anti-angiogenic and that systemically administered tumor lymphatic homing peptide has an anti-tumor effect.
- Shown that systemically administered LyP-1 peptide has inherent anti-lymphatics and anti-tumor effects.
- Discovered a homotypic metadherin interaction and provided evidence that this interaction is the basis of breast cancer cell binding to lung endothelium.
- Provided evidence that metadherin is involved in angiogenesis and in regulation of cell adhesion and migration, and by extension may be involved in tumor invasion.

REPORTABLE OUTCOMES**(1) Papers published, in press, and submitted:**

Akerman, M.E., Chan, W.C.W., Laakkonen, P., Bhatia, S.N., and Ruoslahti, E. Nanocrystal targeting *in vivo*. *Proc. Natl. Acad. Sci. USA*. 99:12617-12621 (2002).

Brown, D. and Ruoslahti, E. Metadherin, a novel cell-surface protein in breast tumors that mediates lung metastasis. *Cancer Cell* 5: 365-374 (2004)

Brown, D.M., Pelliccia, M., and Ruoslahti, E. Drug identification through *in vivo* screening of chemical libraries. *ChemBioChem*. **5**: 871-875 (2004).

Christian, S., Pilch, J., Porkka, K., Laakkonen, P., and Ruoslahti, E. Nucleolin expressed at the cell surface is a marker of endothelial cells in tumor blood vessels. *J Cell Biol.* **163**: 871-878 (2003).

Joyce, J.A., Laakkonen P., Bernasconi, M., Bergers, G., Ruoslahti, E., and Hanahan, D. Stage-specific vascular markers revealed by phage display in a mouse model of pancreatic islet tumorigenesis. *Cancer Cell* **4**:393-403 (2003).

Laakkonen, P., Porkka, K., Hoffman, J. A., and Ruoslahti, E. A tumor-homing peptide with a lymphatic vessel-related targeting specificity. *Nature Med* **8**: 743-751 (2002).

Laakkonen, P., Akerman, M.E., Biliran, H., Yang, M., Ferrer, F., Karpanen, T., Hoffman, R.M., and Ruoslahti, E. Antitumor activity of a homing peptide that targets tumor lymphatics and tumor cells. *Proc. Natl. Acad. Sci. USA*. **101**:9381-9386 (2004).

Pai, J-T. and Ruoslahti, E. Identification of genes up-regulated in endothelia. *Gene*. **347**: 21-33. (2005).

Pilch, J., Brown, D.M., Komatsu, M., Jarvinen, T., Yang, M., Pdeters, D., Hoffman, R.M., and Ruoslahti, E. Peptides selected for binding to clotted plasma accumulate in tumor stroma and wounds. *Proc. Natl. Acad. Sci. USA*. **103**: 2800-2804 (2006)

Ruoslahti, E. Drug targeting to specific vascular sites. *Drug Discovery Today*. **7**:1138- 1143 (2002).

Ruoslahti, E. Vascular Zipcodes in Angiogenesis and Metastasis. Jubilee Lecture published in *The Biochemical Society Transactions* **32**: 397-402 (2004).

Ruoslahti, E., Duza, T., and Zhang, L. Vascular Homing Peptides with Cell-penetrating Properties (2005). *Current Pharmaceutical Design*. Special Issue, "Cell-penetrating Peptides, Mechanisms and Applications. **11**: 3655-3660 (2005)

Zhang L., Giraudo, E., Hoffman, J.A., Hanahan, D. and Ruoslahti, E. Lymphatic Zip Codes in Premalignant Lesions and Tumors. *Cancer Res.*, submitted.

(2) Patent Applications

(2) Patent Applications

Metadherin polypeptides, encoding nucleic acids and methods of use; U.S. Application Serial No. 10/986,466; filed 11/10/04.

Metadherin polypeptides, encoding nucleic acids and methods of use; PCT Application No. PCT/US04/037471; filed 11/10/04.

Molecules that selectively home to vasculature of premalignant or malignant lesions of the pancreas and other organs; U.S. Application Serial No. 10/977,367; filed 10/29/04.

Molecules that selectively home to vasculature of premalignant or malignant lesions of the pancreas and other organs; PCT Application No. PCT/US04/36047; filed 10/29/04.

Peptides that home to tumor lymphatic vasculature and methods of using same; U.S. Application Serial No. 10/290,385; 2003-542899, originally filed 11/5/02.

Peptides that home to tumor lymphatic vasculature and methods of using same; PCT Application No. PCT/US02/035743; filed 11/5/02.

Peptides that home to tumor lymphatic vasculature and methods of using same; European Application No. 2795599.6; filed 11/5/02.

Peptides that home to tumor lymphatic vasculature and methods of using same; Japanese Application No. 2003-542899; filed 11/5/02.

Collagen-binding molecules that selectively home to tumor vasculature and methods of using same; U.S. Application Serial No. 10/648,813; filed 8/25/03.

Methods of modulating cell death based on the Bit1/AES regulatory pathway; U.S. Application Serial No. 10/655,755; filed 9/5/03.

Molecules that selectively home to vasculature of pre-malignant dysplastic lesions or malignancies; U.S. Application Serial No. 10/970,847; filed 10/20/04.

Molecules that selectively home to vasculature of pre-malignant dysplastic lesions or malignancies; PCT Application No. PCT/US04/034918; filed 10/21/04.

HMG2 peptides and related molecules that selectively home to tumor blood vessels and tumor cells; U.S. Application Serial No. 10/400,083; filed 3/20/03.

Methods and compositions for inhibiting tumor growth and angiogenesis; U.S. Application Serial No. 10/431,642; filed 5/5/03.

Lymphatic Zip Codes in Tumors and Pre-Malignant Lesions; U.S. Application Serial No. N/A; filed 2/1/06.

Methods and compositions related to targeting tumors, wounds and blood clots; U.S. Application Serial No. N/A; filed 2/6/06.

CONCLUSIONS

We have made significant progress toward completing each of the Tasks in the original application. A “zip code” system for lymphatic vessels in tumors is beginning to emerge. This heterogeneity of the lymphatics is similar to what we have established and continue to establish for tumor blood vessels. One of the lymphatic homing peptides and a new blood vessel homing peptide both show remarkably efficient and specific accumulation in breast cancer xenografts, boding well for future drug targeting experiments. We have added to the panel of blood vessel-targetors several promising new peptides, notably peptides that recognize the extracellular matrix of tumor vessels and tumor cells, and peptides that bind to plasma clots. We have also

shown that it is possible to distinguish the vasculature of premalignant lesions from both the vasculature of the corresponding normal tissue and fully developed tumors of the same tumor system.

The discovery of metadherin, a tumor cell surface protein involved in lung metastasis of breast cancer has opened up a new avenue of research on factors that affect tissue-specific cancer metastasis and determine the aggressiveness of individual cancers.

For the homing peptide technology to be maximally effective, it is important to identify the molecules the peptides recognize in tumor vessels. We successfully identified two such receptors. The angiogenesis-homing peptide F3 binds to nucleolin, which is aberrantly expressed at the surface of angiogenic endothelial cells and tumor cells. The latest, as yet unpublished results identify an obscure complement receptor as the receptor for the LyP-1 peptide. We have also have partial success with two peptides that recognize extracellular matrix in tumors; we have narrowed down the receptors to proteins present in the basement membrane material known as matrigel.

Antibodies against an appropriate domain of nucleolin have an anti-angiogenic/anti-tumor effect, and systemic administration of the LyP-1 peptide inhibits tumor growth and destroys tumor lymphatics in a breast cancer xenograft model. We have also found that metadherin regulates cell adhesion and migration and suspect that it may be important not only in lung metastasis, but as a factor that enhances tumor invasion. Next steps in this research will be directed at taking advantage of the diagnostic and therapeutic potential of the finding made under this grant. We want to preprepare human or humanized monoclonal antibodies against nucleolin, gC1qR and metadherin and test them for anti-tumor effects. We will also be searching for small molecular weight chemical compounds that would reproduce the anti-tumor effect of the LyP-1 peptides and would have better pharmacokinetic properties than the peptide. Our peptides are also actively tested as delivery vehicles for targeted drugs and gene therapies. In addition, my group are involved in nanoparticle targeting with the peptides. Thus, the technology we have developed under this grant is likely to result in novel diagnostic and therapeutic advances in the treatment of breast cancer.

REFERENCES

- Akerman, M.E., Pilch, P., Peters, D., and Ruoslahti, E. Anti-angiostatic peptides use plasma fibronectin to home to angiogenic vasculature. *Proc. Natl. Acad. Sci. USA*. **102**: 2040-2045 (2005).
- Brown, D. and Ruoslahti, E. Metadherin, a novel cell-surface protein in breast tumors that mediates lung metastasis. *Cancer Cell* **5**: 365-374 (2004)
- Brown, D.M., Pellecchia, M., and Ruoslahti, E. Drug identification through *in vivo* screening of chemical libraries. *ChemBioChem*. **5**: 871-875 (2004).
- Christian, S., Pilch, J., Porkka, K., Laakkonen, P., and Ruoslahti, E. Nucleolin expressed at the cell surface is a marker of endothelial cells in tumor blood vessels. *J Cell Biol*. **163**: 871-878 (2003).
- Ergün, S., Kilik, N., Ziegeler, G., Hansen, A., Nollau, P., Götze, J., Wurbach, J.H., Horst, A., Weil, J., Fernando, M., and Wagener, C. CEA-related cell adhesion molecule 1: a potent angiogenic factor and a major effector of vascular endothelial growth factor. *Mol Cell* **5**: 311-20. (2000).
- Hoffman, J.A., Giraudo E., Singh, M., Inoue, M., Porkka, K., Hanahan D., and Ruoslahti E. Progressive vascular changes in a transgenic mouse model of squamous cell carcinoma. *Cancer Cell* **4**:383-391 (2003).

- Ghebrehiwet, B. and Peerschke, EIB. CC1q-R (calreticulin) and gC1q-R/p33: ubiquitously expressed multi-ligand binding cellular proteins involved in inflammation and infection. *Mol. Immunol.* **41**, 173-183 (2004).
- Kamal, A., Thao, L., Sensintaffar, J., Zhang, L., Boehm, M.F. Fritz LC. Burrows FJ. A high-affinity conformation of Hsp90 confers tumour selectivity on Hsp90 inhibitors. *Nature* **425**: 407-10 (2003).
- Laakkonen, P., Porkka, K., Hoffman, J. A., and Ruoslahti, E. A tumor-homing peptide with a lymphatic vessel-related targeting specificity. *Nature Med* **8**: 743-751 (2002).
- Laakkonen, P., Akerman, M.E., Biliran, H., Yang, M., Ferrer, F., Karpanen, T., Hoffman, R.M., and Ruoslahti, E. Antitumor activity of a homing peptide that targets tumor lymphatics and tumor cells. *Proc. Natl. Acad. Sci. USA.* **101**: 9381-9386 (2004).
- Porkka, K., Laakkonen, P., Hoffman, J.A., Bernasconi, M., and Ruoslahti, E. Targeting of peptides to the nuclei of tumor cells and tumor endothelial cells in vivo. *Proc. Natl. Acad. Sci. USA.* **99**: 7444-7449. (2002).
- van 't Veer, L. J., Dai, H., van de Vijver, M. J., He, Y. D., Hart, A. A., Mao, M., Peterse, H. L., van der Kooy, K., Marton, M. J., Witteveen, A. T., *et al.* Gene expression profiling predicts clinical outcome of breast cancer. *Nature* **415**: 530-536 (2002).
- Woiwode, T.F., Haggerty, J.E., Katz, R., Gallop, M.A., Barrett, R.W., Dower, W.D., and Cwirla, S.E. Synthetic compound libraries displayed on the surface of encoded bacteriophage. *Chem. Biol.* **10**: 847-858 (2003).
- Zhang, L., Giraudo, E., Hoffman, J.A., Hanahan, D., and Ruoslahti, E. Lymphatic zip codes in tumors and premalignant lesions. *Cancer Cell.* Submitted.

BIBLIOGRAPHY

1. Akerman, M.E., Chan, W.C.W., Laakkonen, P., Bhatia, S.N., and Ruoslahti, E. Nanocrystal targeting *in vivo*. *Proc. Natl. Acad. Sci. USA*. 99:12617-12621 (2002).
2. Brown, D. and Ruoslahti, E. Metadherin, a novel cell-surface protein in breast tumors that mediates lung metastasis. *Cancer Cell* 5: 365-374 (2004)
3. Brown, D.M., Pellecchia, M., and Ruoslahti, E. Drug identification through *in vivo* screening of chemical libraries. *ChemBioChem*. 5: 871-875 (2004).
4. Christian, S., Pilch, J., Porkka, K., Laakkonen, P., and Ruoslahti, E. Nucleolin expressed at the cell surface is a marker of endothelial cells in tumor blood vessels. *J Cell Biol.* 163: 871-878 (2003).
5. Joyce, J.A., Laakkonen P., Bernasconi, M., Bergers, G., Ruoslahti, E., and Hanahan, D. Stage-specific vascular markers revealed by phage display in a mouse model of pancreatic islet tumorigenesis. *Cancer Cell* 4:393-403 (2003).
6. Laakkonen, P., Porkka, K., Hoffman, J. A., and Ruoslahti, E. A tumor-homing peptide with a lymphatic vessel-related targeting specificity. *Nature Med* 8: 743-751 (2002).
7. Laakkonen, P., Akerman, M.E., Biliran, H., Yang, M., Ferrer, F., Karpanen, T., Hoffman, R.M., and Ruoslahti, E. Antitumor activity of a homing peptide that targets tumor lymphatics and tumor cells. *Proc. Natl. Acad. Sci. USA*. 101:9381-9386 (2004).
8. Pai, J-T. and Ruoslahti, E. Identification of genes up-regulated in endothelia. *Gene*. 347: 21-33. (2005).
9. Pilch, J., Brown, D.M., Komatsu, M., Jarvinen, T., Yang, M., Pdeters, D., Hoffman, R.M., and Ruoslahti, E. Peptides selected for binding to clotted plasma accumulate in tumor stroma and wounds. *Proc. Natl. Acad. Sci. USA*. 103: 2800-2804 (2006)
10. Ruoslahti, E. Drug targeting to specific vascular sites. *Drug Discovery Today*. 7:1138- 1143 (2002).
11. Ruoslahti, E. Vascular Zipcodes in Angiogenesis and Metastasis. Jubilee Lecture published in *The Biochemical Society Transactions* 32: 397-402 (2004).
12. Ruoslahti, E., Duza, T., and Zhang, L. Vascular Homing Peptides with Cell-penetrating Properties (2005). *Current Pharmaceutical Design*. Special Issue, "Cell-penetrating Peptides, Mechanisms and Applications. 11: 3655-3660 (2005)
13. Zhang L., Giraudo, E., Hoffman, J.A., Hanahan, D. and Ruoslahti, E. Lymphatic Zip Codes in Premalignant Lesions and Tumors. *Cancer Res.*, submitted.

LIST OF PERSONNEL:

Ferrer, Fernando; Lu, Jerry; Nguyen Michael; Ponce, Elsa; Ruoslahti, Erkki; Simberg, Dmitri; Simon, Nicola; Wankell, Miriam; Zabetakis, Nicholas; Zhang, Lianglin;

Nanocrystal targeting *in vivo*

Maria E. Åkerman^{*†‡}, Warren C. W. Chan^{†‡}, Pirjo Laakkonen^{*}, Sangeeta N. Bhatia[†], and Erkki Ruoslahti^{*§}

^{*}Cancer Research Center, The Burnham Institute, 10901 North Torrey Pines Road, La Jolla, CA 92037; and [†]Department of Bioengineering, University of California at San Diego, 9500 Gilman Drive, La Jolla, CA 92093

Contributed by Erkki Ruoslahti, August 1, 2002

Inorganic nanostructures that interface with biological systems have recently attracted widespread interest in biology and medicine. Nanoparticles are thought to have potential as novel intravascular probes for both diagnostic (e.g., imaging) and therapeutic purposes (e.g., drug delivery). Critical issues for successful nanoparticle delivery include the ability to target specific tissues and cell types and escape from the biological particulate filter known as the reticuloendothelial system. We set out to explore the feasibility of *in vivo* targeting by using semiconductor quantum dots (qdots). Qdots are small (<10 nm) inorganic nanocrystals that possess unique luminescent properties; their fluorescence emission is stable and tuned by varying the particle size or composition. We show that ZnS-capped CdSe qdots coated with a lung-targeting peptide accumulate in the lungs of mice after i.v. injection, whereas two other peptides specifically direct qdots to blood vessels or lymphatic vessels in tumors. We also show that adding polyethylene glycol to the qdot coating prevents nonselective accumulation of qdots in reticuloendothelial tissues. These results encourage the construction of more complex nanostructures with capabilities such as disease sensing and drug delivery.

Hybrid organic/inorganic nanoparticles are thought to have potential as novel intravascular probes for diagnostics (e.g., imaging) and therapeutics (e.g., drug delivery) (1). For this potential to be realized, an ability to target the nanoparticles to specific tissues and cell types would be important. We used semiconductor quantum dots (qdots) coated with targeting peptides as prototypic nanostructures for intravascular delivery in live mice. Qdots are generally composed of atoms from groups II–VI or III–V of the periodic table and are defined as particles with physical dimensions smaller than the exciton Bohr radius (2). This size leads to a quantum confinement effect, which endows nanocrystals with unique optical and electronic properties. Qdots have size-tunable emission (from the UV to the IR), narrow spectral line widths, high luminescence, continuous absorption profiles, and stability against photobleaching (2–4). Furthermore, the large surface area-to-volume ratio of qdots makes them appealing for the design of more complex nanosystems.

Blood vessels express molecular markers that distinguish the vasculature of individual organs, tissues, and tumors. Peptides that recognize these vascular markers have been identified by screening phage libraries *in vivo*, a procedure in which peptides direct phage homing to individual sites (5). This approach has led to the identification of a unique set of homing peptides with high *in vivo* selectivity (6–9). We have used homing peptides to target i.v.-injected qdots to specific vascular sites in mice (Fig. 1). One of these peptides binds to membrane dipeptidase on the endothelial cells in lung blood vessels (9), and the other two preferentially bind to tumor blood vessels (10) or tumor lymphatic vessels (11) and the tumor cells. Each of the peptides directed the qdots to the appropriate site in the mice, showing that nanocrystals can be targeted *in vivo* with an exquisite specificity.

Materials and Methods

Preparation of Qdots and Peptide-Coated Qdots. Previously published procedures were used to synthesize tri-*n*-octylphosphine oxide-coated ZnS-capped CdSe qdots (12–15) and to modify their surface chemistry to render them water soluble (16, 17).

After this step, the surface of qdots was coated with mercaptoacetic acid.

Three peptides were used to coat qdots: CGFECVROCPCRC peptide (denoted as GFE) binds to membrane dipeptidase on the endothelial cells in lung blood vessels (9, 18), KDE-PQRRSARLSAKPAPPKPEPKPKKAPAKK (F3) preferentially binds to blood vessels and tumor cells in various tumors (10), and CGNKRTRGC (LyP-1) recognizes lymphatic vessels and tumor cells in certain tumors (11). The peptides were synthesized by *N*-(9-fluorenylmethoxycarbonyl)-L-amino acids chemistry with a solid-phase synthesizer and purified by HPLC. The composition of the peptides was confirmed by MS.

The peptides were thiolated by using 3-mercaptopropionimide hydrochloride (a.k.a. iminothiolane), an imidoester compound containing a sulfhydryl group. Peptides were incubated with iminothiolane for 1 h in 10 mM PBS, pH 7.4, at a 1:1 molar ratio. Afterward, mercaptoacetic acid-coated qdots were added to the solution to exchange some of the mercaptoacetic acid groups with the thiolated peptide incubated overnight at room temperature. For coadsorption of polyethylene glycol (PEG) and peptides, amine-terminated PEG (Shearwater Polymers, Huntsville, AL) was thiolated with iminothiolane. Thiolated PEG was directly added to a solution of mercaptoacetic acid-coated qdots in 10 mM PBS, pH 7.4, and allowed to incubate overnight at room temperature. Afterward, the thiolated peptide was added to the PEG/qdot solution and incubated overnight at room temperature. The coated qdots were purified with Microspin G-50 columns (Amersham Pharmacia) before assays or injection into a mouse. The coupling efficiency was determined by performing a Bradford assay (Bio-Rad) on the coated qdots.

Mice, Cell Lines, and Tumors. Lung endothelial (LE), brain endothelial, and human breast carcinoma MDA-MD-435 cells were maintained as described (7, 18). To establish tumor xenografts, 10⁶ exponentially growing MDA-MB-435 tumor cells were injected s.c. in the chest area of BALB/c *nu/nu* mice (Animal Technologies, Livermore, CA). The mice were used for *in vivo* targeting experiments 8–12 weeks after the tumor cell inoculation.

Qdot Injections and Histology. Peptide-coated qdots (100–200 μ g in 0.1–0.2 ml PBS) were injected into the tail vein of a mouse and allowed to circulate for 5 min (GFE qdots) or 20 min (F3 and LyP-1 qdots). Blood vessels were visualized by i.v. injecting tomato lectin conjugated with either fluorescein or biotin (Vector Laboratories), as reported (11). While still under anesthesia, the mouse was perfused with 4% paraformaldehyde through the heart. Tissues were frozen in Tissue Tek OCT embedding medium (Sakura Finetek, Torrance, CA) before sectioning. The sections were mounted with Vectashield mounting medium with or without 4',6-diamidino-2-phenylindole, dihydrochloride (Vector Laboratories) to visualize cell nuclei before examination under an inverted fluorescent microscope or a confocal microscope.

Abbreviations: qdot, quantum dot; PEG, polyethylene glycol; LE, lung endothelial.

^{*}M.E.Å. and W.C.W.C. contributed equally to this work.

[§]To whom correspondence should be addressed. E-mail: ruoslahti@burnham.org.

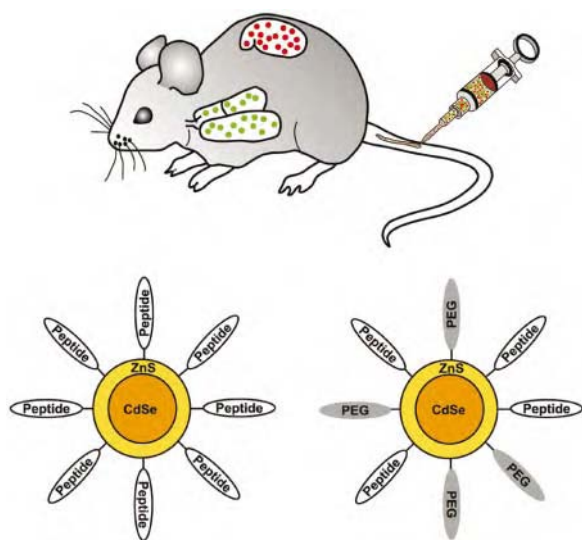


Fig. 1. Schematic representation of qdot targeting. Intravenous delivery of qdots into specific tissues of the mouse. (Upper) Design of peptide-coated qdots. (Lower) Qdots were coated with either peptides only or with peptides and PEG. PEG helps the qdots maintain solubility in aqueous solvents and minimize nonspecific binding.

Results

Peptide-Coated Qdots. We synthesized ZnS-capped CdSe qdots emitting in the green and the red (550 nm and 625 nm fluores-

cence maxima, respectively) and coated them with peptides by using a thiol-exchange reaction. The coupling of the GFE peptides yielded monodisperse qdots, whereas qdots coated with the F3 aggregated. The large number of positive residues in F3 may have caused colloidal aggregation by “bridging” negatively charged qdots. We overcame the aggregation problem by either decreasing the population of peptides on the qdot surface or by co-coupling peptides and PEG (molecular weight = 5,000 g/mol), a polymer known to minimize molecular interactions and improve colloidal solubilities (19) (Fig. 1). Protein assays revealed about 120 peptide molecules per qdot when peptide only was coupled. Co-coupling of PEG reduced this number to about 70.

Peptide Specificity *in Vitro*. To explore the binding activity and specificity of peptide-coated qdots, experiments were first conducted *in vitro*. LE and brain endothelial cells were grown in culture, and green-luminescent GFE-coated qdots were incubated with each cell type. The LE cells express membrane dipeptidase, the receptor for the GFE peptide, whereas the brain endothelial cells do not (9). On optical excitation, qdots coated with the lung-homing GFE peptide were observed decorating the surface of LE cells (Fig. 2*a*), whereas no visible signal was observed on the brain endothelial cells. Specificity of the GFE-qdot binding to LE cells was further demonstrated by inhibition of binding by both the addition of free GFE peptide or the organic molecule cilastatin, a known ligand and inhibitor of membrane dipeptidase (20) (Fig. 2*b* and *c*). This finding was quantified by using digital image analysis (Fig. 2*d*).

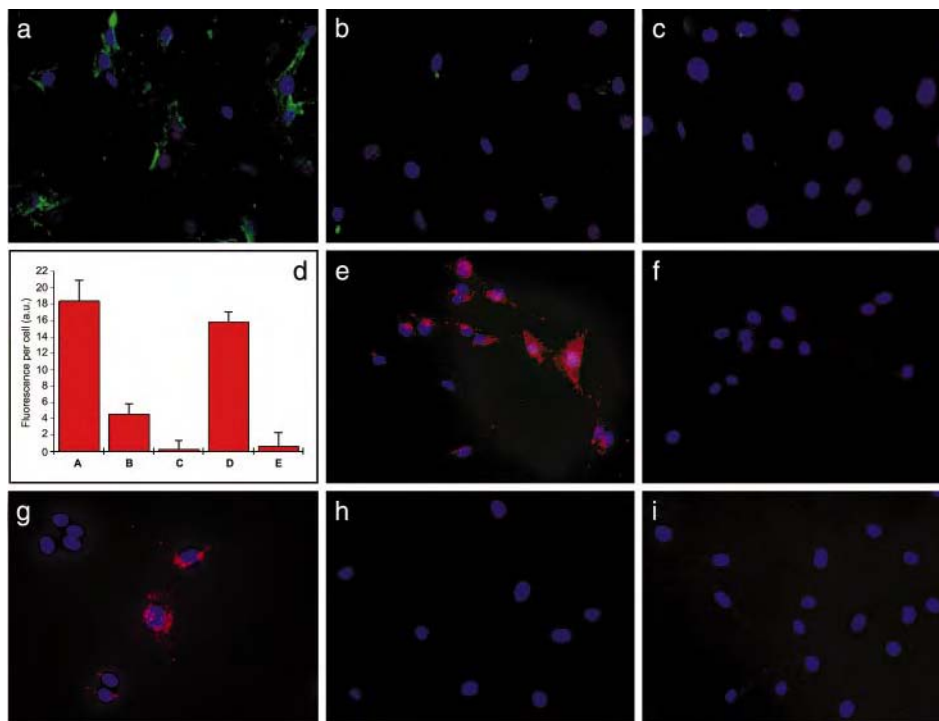


Fig. 2. Binding of peptide-conjugated qdots to endothelial cells and breast cancer cells *in vitro* is specific to peptide sequence. (a) Binding of green GFE-conjugated qdots to LE cells that express membrane dipeptidase. (b and c) Inhibition of GFE-qdot binding to LE cells by free GFE peptide (500 μM) (b) or with cilastatin, an inhibitor of the receptor, membrane dipeptidase (50 μM) (c). (d) Quantification of fluorescence intensity of an experiment similar to the one illustrated in a–c. (Columns A–C) GFE-qdot binding to LE cells; GFE concentration 250 μM; and cilastatin 50 μM. (Column D) The binding of GFE-qdots to the LE cells is not inhibited by a control peptide (LyP-1; 250 μM). (Column E) LyP-1-qdots do not bind to the LE cells. The fluorescence associated with 10 individual cells from each panel was measured by using digital image analysis. Background fluorescence from cells that received no qdots has been subtracted (2 a.u., arbitrary units). A representative experiment of five experiments was quantified. (e and f) F3 qdots bind to MDA-MB-435 breast carcinoma cells (e); free F3 peptide (500 μM) inhibits the binding (f). (g) Binding of LyP-1 qdots to MDA-MB-435 cells. (h and i) GFE qdots do not recognize the MDA-MB-435 cells (h) and LyP-1 qdots do not bind to the LE cells (i). Nuclei were visualized with 4',6-diamidino-2-phenylindole staining (blue). Cells were examined under an epifluorescence microscope with a 425/40-nm excitation and a 515-nm long-pass filter. (Original magnifications: a–c and i, ×200; and e–h, ×400.)

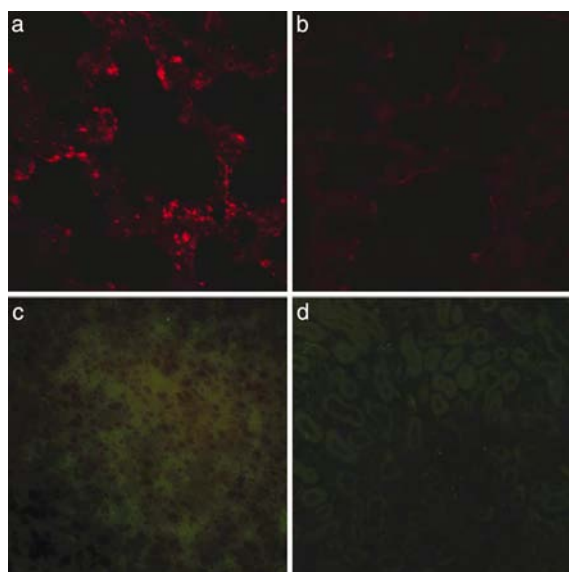


Fig. 3. *In vivo* targeting of qdots to normal lung vasculature is specific. Red GFE-conjugated qdots were injected into the tail vein of normal mice, and the presence of qdots in lung tissue was assessed by examining sections under a confocal microscope with UV excitation and a 585-nm long-pass filter (a and b) or an epifluorescent microscope as in Fig. 2 (c and d). (a) Red qdots localized in lung tissue. (b) Inhibition of qdot accumulation in the lungs by coinjected cilastatin. (c and d) Absence of GFE qdots in the brain (c) and kidney (d) demonstrates the specificity of binding. The results shown are representative of three experiments carried out with nine mice. (Original magnifications: a and b, $\times 600$; c and d, $\times 200$.)

Qdots coated with F3 or LyP-1 bound to the MDA-MB-435 human breast carcinoma cells (Fig. 2 e and g). As with GFE, specificity of F3- and LyP-1-coated qdots was demonstrated by

inhibition of binding by the appropriate cognate peptide (shown for the F3 qdots in Fig. 2f), and further confirmed by lack of inhibition by an unrelated (GFE) peptide or by cilastatin (not shown). The GFE-coated qdots did not bind to the MDA-MB-435 cells (Fig. 2h), and LyP-1-coated qdots did not bind to the endothelial cells (Fig. 2i). These experiments show that coating with GFE, F3, or LyP-1 peptides endows qdots with specific affinity to their corresponding cellular target *in vitro*.

Qdot Homing to Lung Endothelium *in Vivo*. Next, the ability of peptide-coated qdots to home to their targets *in vivo* was examined. Because red luminescent qdots were easier to distinguish from the autofluorescent tissue background than the green luminescent qdots, we i.v. injected red qdots coated with GFE into normal BALB/c mice and studied the tissue distribution of the injected qdots 5 min later. We detected bright GFE-qdot luminescence in the lungs (Fig. 3a), and its appearance was inhibited when the qdots were coinjected with cilastatin, similar to the *in vitro* studies (Fig. 3b). The GFE qdots were not found in various other organs (Fig. 3c, brain and Fig. 3d, kidney), except those with a prominent reticuloendothelial component (see below). Furthermore, we did not observe any acute toxicity, even after 24 h of circulation, caused by the i.v. administration of these nanoparticles (i.e., overt thrombosis or signs of complement activation).

Qdot Homing to Tumor Vasculature *in Vivo*. Qdots coated with peptides that home to tumor vasculature were examined in an MDA-MB-435 xenograft tumor system. Intravenously injected F3-coated and LyP-1-coated qdots accumulated in these tumors. As expected from their specificity for tumor blood vessels (10) and lymphatic vessels (11), the F3 and LyP-1 qdots targeted distinct structures within the tumors. The signal from F3-coated qdots colocalized with coinjected blood vessel marker lectin (Fig. 4a). The LyP-1-coated qdots did not

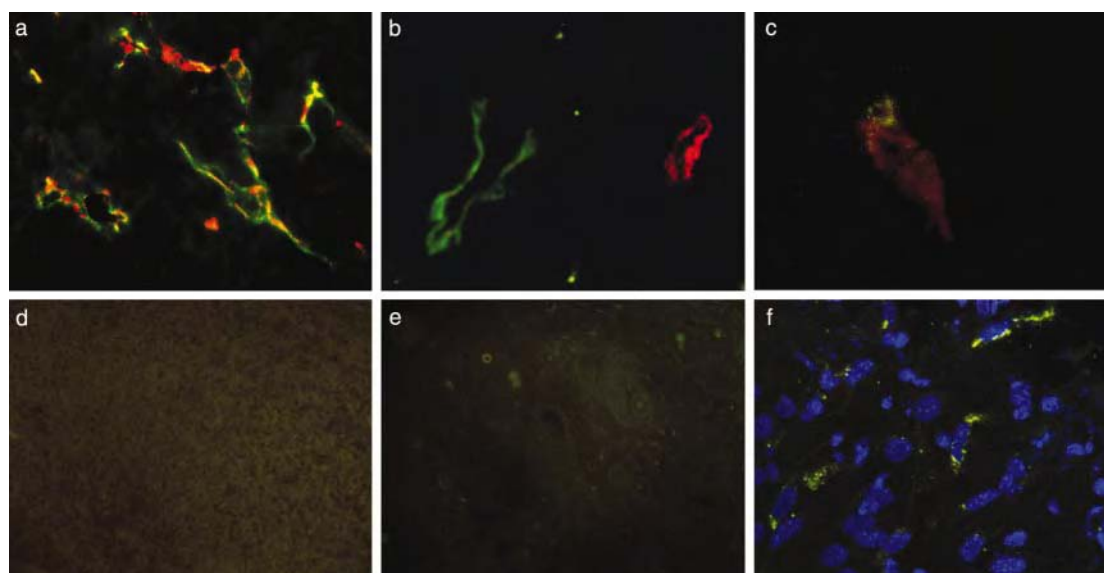


Fig. 4. *In vivo* targeting of qdots to tumor vasculature is specific. Red F3 or LyP-1 qdots, both PEG-coated, were injected into the tail vein of nude BALB/c mice bearing MDA-MB-435 breast carcinoma xenograft tumors. Blood vessels were visualized by coinjecting tomato lectin (green). (a) F3 qdots colocalize with blood vessels in tumor tissue. (b) LyP-1 qdots also accumulate in tumor tissue, but do not colocalize with the blood vessel marker. (c) Red F3 qdots and green LyP-1 qdots injected into the same tumor mouse target different structures in tumor tissue. (d) GFE qdots that bind to normal LE injected into tumor mice are not detected in tumor tissue. (e) F3 qdots injected into tumor mice do not appear in the skin taken from an area next to the tumor. A longer exposure was used in d and e to bring out the tissue background. (f) LyP-1 qdots are internalized by cells in tumor tissue. Images a, b, and f were obtained with a confocal microscope, and images c–e were obtained with an epifluorescent microscope as in Fig. 2. The results shown are representative of experiments carried out with six mice for the F3 qdots and 12 mice for the LyP-1 qdots. (Original magnifications: a and d, $\times 400$; b and c, $\times 600$; e, $\times 200$; and f, $\times 2,400$.)

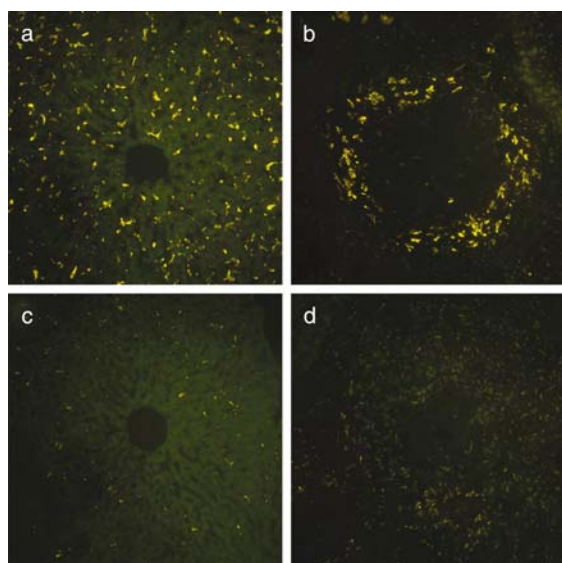


Fig. 5. Qdot uptake by the reticuloendothelial system is reduced by PEG coating. Green LyP-1 qdots with or without an added PEG coating were adjusted to an equal concentration by measuring absorbance at 540 nm and injected into the tail vein of mice bearing MDA-MB-435 tumors. Qdot localization in reticuloendothelial tissues was studied by epifluorescent microscopy of tissue sections as in Fig. 2. (a and b) LyP-1 qdots in the liver (a) and spleen (b). (c and d) LyP-1/PEG qdots in the liver (c) and spleen (d). These images are representative of three independent experiments. (Original magnifications: $\times 200$.)

colocalize with the lectin (Fig. 4b) or F3 qdots (Fig. 4c). They did colocalize with the lymphatic vessel marker, podoplanin (21) (not shown), as has been shown previously for fluorescein-labeled LyP-1 peptide (11). GFE-coated qdots injected as a control were not detected in the tumors (Fig. 4d). Brain, heart, kidney, or skin did not contain detectable qdots (Fig. 4e and data not shown), indicating specificity of the F3 and LyP-1 qdots for tumor components. The regional specificity of qdot delivery within a tumor demonstrates the feasibility of targeting functionally distinct components of a tumor (e.g., blood vessels vs. lymphatics, etc.). Furthermore, the subcellular pattern of qdot luminescence suggests that peptide-coated nanostructures are internalized after binding to the cell surface, which may have implications for drug delivery and other applications that require intracellular targeting (Fig. 4f).

Elimination of the Nonspecific Uptake by the Reticuloendothelial System. The *in vivo*-injected qdots, regardless of the peptide used for the coating, accumulated in both the liver and spleen, in addition to the targeted tissues. The mononuclear phagocytes of the reticuloendothelial system, characterized by their ability to mediate nonspecific uptake of circulating particulates, apparently participated in the clearance of a fraction of circulating qdots in our experimental system. Adsorption-resistant coatings such as PEG are often used to minimize recognition by the reticuloendothelial system, thereby increasing circulation half-life (22). We prepared LyP-1 qdots with and without PEG coating and found that PEG nearly eliminated the nonspecific

uptake into the liver and spleen (Fig. 5). Based on quantification of qdot fluorescence with digital image analysis, we estimate that coadsorption of PEG with peptide on the surface of qdots reduced the accumulation in the liver and spleen by about 95%. The PEG coating did not noticeably alter qdot accumulation in tumor tissue.

Discussion

In this article, we demonstrate the selective targeting of peptide-coated qdots to the vasculature of normal lungs and tumors, showing that it is possible to target hybrid organic/inorganic nanometer-sized colloidal material in a living mammal. In the future, the components and functions of a nanosystem will not be limited to peptide/semiconductor composites and luminescence.

Our peptide-coated qdots showed excellent homing specificity for the relevant vascular site, but we did not see accumulation of fluorescence within the targeted tissue. This finding is in contrast to what we have seen when the two tumor-homing peptides, F3 and LyP-1, were coupled to fluorescein. In that case, there was accumulation of fluorescence not only in the blood or lymphatic vessels, but also in the tumor cells. It is also possible that qdots did not penetrate into the tissue. The uncoated qdots have a diameter of 3.5 nm (green) or 5.5 nm (red) (14), which is equivalent to about 40 kDa, and the peptide coating adds another about 150 kDa. This may be a sufficiently large size to impede tissue penetration. However, F3 and LyP-1 qdots accumulated less well in cultured cells than the fluorescein-labeled peptide. It may be that the qdots were not sufficiently stable to remain luminescent in living cells and tissues. Alternatively, the fluorescence may be quenched by the qdots subjected to low pH in the microenvironment, by oxidation of the surface, or by factors adsorbed to the surface. For the delivery of nanocrystalline drugs, crystals that are unstable in tissue may offer an advantage, as the drug would dissolve at the target.

Our results suggest the potential selective targeting of other nanomaterials [e.g., optically active metallic colloids (23), near-IR emitting nanocrystals (24–26), and magnetic nanoparticles (27, 28)] as *in vivo* optical and magnetic probes for noninvasive imaging. The use of peptides to target drug-carrying nanostructures [such as those composed of fullerenes (29, 30) or dendrimers (31, 32), or stabilized drug nanocrystals] should also be possible. This targeting approach has been used recently to deliver nano-sized particles composed of lipids and DNA to tumor vasculature (33). Although the current nanosystems are rather simple, in the future we envision the fabrication of multifunctional nanosystems, known as nanomachines. Such devices may, as an example, sense the presence of disease, deliver a drug to the site of disease, and release the drug at that site.

We thank Drs. Darren Brown, Fernando Ferrer, Edward Monosov, Lea Rudee, and Michael Sailor for their help with this work. Oriaku A. Kas-Osoka assisted with qdot synthesis, and Robbin Newlin assisted with histology. This study was supported by grants from the National Cancer Institute (CA82713), the Department of Defense (DAMD 17-02-1-0315), and the Komen Foundation (99–3339) (to E.R.), and the David and Lucile Packard Foundation and the Defense Advanced Research Projects Agency (to S.N.B.). M.E.A. received support from the American-Scandinavian Foundation; W.C.W.C., received support from the National Institutes of Health; and P.L., received support from the Academy of Finland and the Finnish Cultural Foundation.

1. Niemeyer, C. M. (2001) *Angew. Chem.* **40**, 4128–4158.
2. Chan, W. C., Maxwell, D. J., Gao, X., Bailey, R. E., Han, M. & Nie, S. (2002) *Curr. Opin. Biotechnol.* **13**, 40–46.
3. Alivisatos, A. P. (1996) *Science* **271**, 933–937.
4. Han, M., Gao, X., Su, J. Z. & Nie, S. (2001) *Nat. Biotechnol.* **19**, 631–635.
5. Ruoslahti, E. (2000) *Semin. Cancer Biol.* **10**, 435–442.
6. Arap, W., Pasqualini, R. & Ruoslahti, E. (1998) *Science* **279**, 377–380.

7. Pasqualini, R., Koivunen, E. & Ruoslahti, E. (1997) *Nat. Biotechnol.* **15**, 542–546.
8. Pasqualini, R. & Ruoslahti, E. (1996) *Nature (London)* **380**, 364–366.
9. Rajotte, D. & Ruoslahti, E. (1999) *J. Biol. Chem.* **274**, 11593–11598.
10. Porkka, K., Laakkonen, P., Hoffman, J. A., Bernasconi, M. & Ruoslahti, E. (2002) *Proc. Natl. Acad. Sci. USA* **99**, 7444–7449.
11. Laakkonen, P., Porkka, K., Hoffman, J. A. & Ruoslahti, E. (2002) *Nat. Med.* **8**, 751–755.

12. Peng, X., Schlamp, M. C., Kadavanich, A. V. & Alivisatos, A. P. (1997) *J. Am. Chem. Soc.* **119**, 7019–7029.
13. Murray, C. B., Norris, D. J. & Bawendi, M. G. (1993) *J. Am. Chem. Soc.* **115**, 8706–8715.
14. Dabbousi, B. O., Rodriguez-Viejo, J., Mikulec, F. V., Heine, J. R., Mattoussi, H., Ober, R., Jensen, K. F. & Bawendi, M. G. (1997) *J. Phys. Chem. B* **101**, 9463–9475.
15. Hines, M. A. & Guyot-Sionnest, P. (1996) *J. Phys. Chem. B* **100**, 468–471.
16. Chan, W. C. & Nie, S. (1998) *Science* **281**, 2016–2018.
17. Mitchell, G. P., Mirkin, C. A. & Letsinger, R. L. (1999) *J. Am. Chem. Soc.* **121**, 8122–8123.
18. Rajotte, D., Arap, W., Hagedorn, M., Koivunen, E., Pasqualini, R. & Ruoslahti, E. (1998) *J. Clin. Invest.* **102**, 430–437.
19. Liu, V. A., Jastromb, W. E. & Bhatia, S. N. (2002) *J. Biomed. Mater. Res.* **60**, 126–134.
20. Kahan, F. M., Kropp, H., Sundelof, J. G. & Birnbaum, J. (1983) *J. Antimicrob. Chemother.* **12**, Suppl. D, 1–35.
21. Breiteneder-Geleff, S., Soleiman, A., Kowalski, H., Horvat, R., Amann, G., Kriehuber, E., Diem, K., Weninger, W., Tschachler, E., Alitalo, K., *et al.* (1999) *Am. J. Pathol.* **154**, 385–394.
22. Gref, R., Minamitake, Y., Peracchia, M. T., Trubetskoy, V., Torchilin, V. & Langer, R. (1994) *Science* **263**, 1600–1603.
23. Nie, S. & Emory, S. R. (1997) *Science* **275**, 1102–1106.
24. Bruchez, M., Jr., Moronne, M., Gin, P., Weiss, S. & Alivisatos, A. P. (1998) *Science* **281**, 2013–2016.
25. Schreder, B., Schmidt, T., Ptatschek, V., Winkler, U., Materny, A., Umbach, E., Lerch, M., Muller, G., Kiefer, W. & Spanhel, L. (2000) *J. Phys. Chem. B* **104**, 1677–1685.
26. Micic, O. I., Cheong, H. M., Fu, H., Zunger, A., Sprague, J. R., Mascarenhas, A. & Nozik, A. J. (1997) *J. Phys. Chem. B* **101**, 4904–4912.
27. Lewin, M., Carlesso, N., Tung, C., Tang, X., Cory, D., Scadden, D. T. & Weissleder, R. (2000) *Nat. Biotechnol.* **18**, 410–414.
28. Bulte, J. W. M., Douglas, T., Witwer, B., Zhang, S., Strable, E., Lewis, B. K., Zywicke, H., Miller, B., van Gelderen, P., Moskowitz, B. M., *et al.* (2001) *Nat. Biotechnol.* **19**, 1141–1147.
29. Kroto, H. W., Heath, J. R., O'Brien, S. C., Curl, R. F. & Smalley, R. E. (1985) *Nature (London)* **318**, 162–163.
30. Heath, J. R. (1998) *Nature (London)* **393**, 730–731.
31. Frechet, J. M. (1994) *Science* **263**, 1710–1715.
32. Grayson, S. M. (2001) *Chem. Rev.* **101**, 3819–3868.
33. Hood, J. D., Bednarski, M., Frausto, R., Guccione, S., Reisfeld, R. A., Xiang, R. & Cheresch, D. A. (2002) *Science* **296**, 2404–2407.

Metadherin, a cell surface protein in breast tumors that mediates lung metastasis

Darren M. Brown and Erkki Ruoslahti*

Cancer Research Center, The Burnham Institute, 10901 North Torrey Pines Road, La Jolla, California 92037

*Correspondence: ruoslahti@burnham.org

Summary

We used a phage expression library of cDNAs from metastatic breast carcinoma to identify protein domains that bind to the vasculature of the lung, a frequent site of breast cancer metastasis. We found that one protein domain selectively targeted phage as well as cells to the lung. This domain is part of the protein metadherin, shown by gene expression profiling to be overexpressed in metastatic breast cancer. Immunostaining revealed that metadherin is overexpressed in breast cancer tissue and breast tumor xenografts. Antibodies reactive to the lung-homing domain of metadherin and siRNA-mediated knockdown of metadherin expression in breast cancer cells inhibited experimental lung metastasis, indicating that tumor cell metadherin mediates localization at the metastatic site.

Introduction

Tumor metastasis is a complex, multistep process in which cancer cells detach from the original tumor mass and establish metastatic foci at organ-specific sites (Fidler, 2001). The location of the metastatic site depends on the particular type of cancer and stage of disease. For example, breast cancer spreads first to the lungs and liver (Kamby et al., 1987; Rutgers et al., 1989; Tomin and Donegan, 1987). Later in the disease, breast cancer spreads to the central nervous system and bone (Amer, 1982; Boogerd, 1996). The metastatic phase of the disease is devastating, given that conventional treatments are usually ineffective and patients typically survive only a few years after diagnosis (Harris et al., 1997).

Several factors affect the location and growth of metastases. Depending on the bloodflow pattern from the primary tumor, certain tumor cells are carried preferentially to particular organs (Weiss, 1992). While in circulation, some tumor cells selectively recognize particular endothelial cell surface molecules that mediate cell adhesion to specific organs (Abdel-Ghany et al., 2001; Cheng et al., 1998; Johnson et al., 1993). The arrest of tumor cells at the metastatic site, be it through mechanical trapping in small capillaries or through adhesive interactions with the endothelium, is a necessary step for tumors to establish at a secondary site (Chambers et al., 2002; Orr and Wang, 2001). Once the tumor cells have seeded the target organ, the local microenvironment influences whether or not a particular cancer cell will proliferate (Fidler, 2001; Radinsky, 1995). Unfortunately,

many of the factors that contribute to organ-specific metastasis have yet to be elucidated.

To identify tumor cell surface molecules that mediate breast cancer metastasis, we have used in vivo phage screening. This screening method has been used by our group to identify peptides and proteins that are capable of mediating selective in vivo localization of phage to individual organs as well as tumors and that reveal tissue-specific vascular differences (Arap et al., 1998, 2002; Laakkonen et al., 2002; Pasqualini and Ruoslahti, 1996; Porkka et al., 2002; Rajotte et al., 1998).

In this study, we isolated from phage expression libraries of breast carcinoma cDNAs a domain in a protein we call metadherin (for metastasis adhesion protein) that causes the phage to home specifically to lung microvasculature after intravenous injection. We show that the lung-homing domain of metadherin is extracellular. Antibodies to metadherin revealed high amounts of metadherin throughout human breast tumors and breast tumor xenografts while drastically lower levels of metadherin were present in normal breast tissue. We also show that antibodies reactive to the lung-homing domain of metadherin inhibited experimental breast cancer lung metastasis, as did siRNA-mediated knockdown of metadherin expression. These results suggest that metadherin plays an important role in breast cancer metastasis.

Results

Identification of cDNA clones by phage display

To identify candidate cell adhesion proteins that mediate breast cancer metastasis, we used an in vivo phage screening ap-

SIGNIFICANCE

Adhesive interactions with the endothelium have been shown to contribute to the localization and growth of tumors at particular secondary sites in experimental animals. In this report, we show that metadherin, a protein greatly overexpressed in breast cancers, mediates lung-specific dissemination of metastatic cells. Independent microarray data have identified high metadherin gene expression as a prognostic indicator of clinical metastasis in human breast cancer patients. Our results provide a possible mechanistic explanation for the clinical findings. Our demonstration that metastasis can be inhibited by blocking the lung-homing domain of metadherin with an antibody or by reducing metadherin expression identifies metadherin as a candidate target for therapeutic intervention in breast cancer and perhaps other cancers as well.

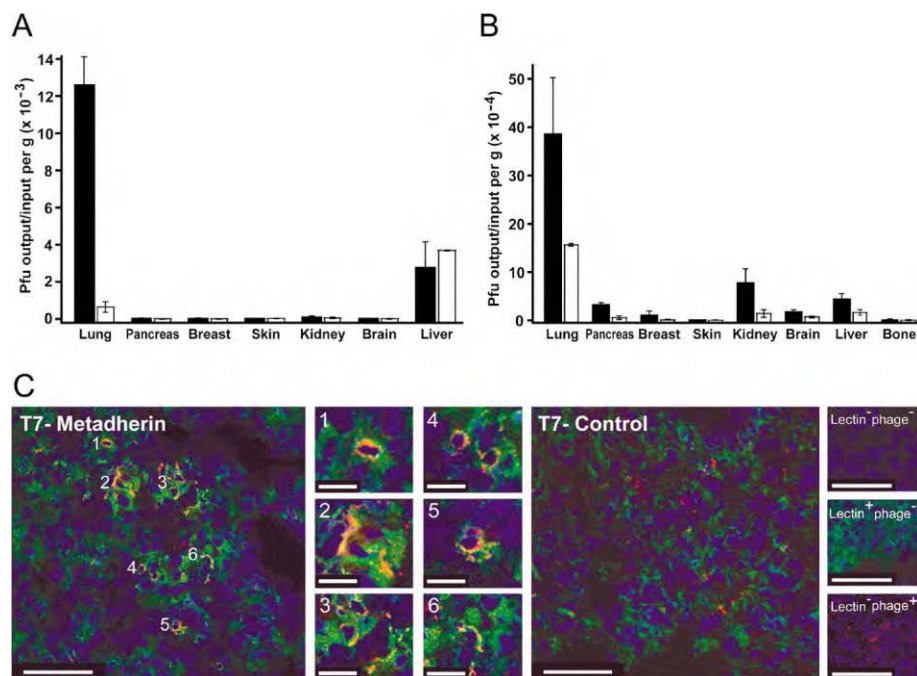


Figure 1. Homing specificity of metadherin phage

A: Metadherin (closed bars) and nonrecombinant (open bars) phage titers recovered from lung, pancreas, breast, skin, kidney, brain, and liver after injection into the tail vein of Balb/c mice and circulation for 5 min. Error bars represent mean \pm SD for 2–7 experiments per variable.

B: Metadherin (closed bars) and nonrecombinant (open bars) phage titers recovered from lung, pancreas, breast, skin, kidney, brain, liver, and bone (tibia) after injection into the left ventricle of the heart of Balb/c mice and circulation for 5 min. Error bars represent mean \pm SEM for 2–5 experiments per variable.

C: Confocal projections of anti-phage immunostained lungs from mice co-injected with fluorescein-labeled tomato lectin (green) and either metadherin phage (T7-metadherin) or T7-415 nonrecombinant phage (T7-Control). Control lungs were from noninjected mice (lectin⁻ phage⁻), mice injected with lectin alone (lectin⁺ phage⁻), or mice injected only with metadherin phage (lectin⁺ phage⁺). Anti-phage antibody was detected with Alexa 594 goat anti-rabbit IgG antibody (red). Nuclei were stained with DAPI (blue). The scale bars correspond to 50 μ m, except in panels 1–6, where the scale bars correspond to 10 μ m.

proach. We selected the highly metastatic, Balb/c-derived 4T1 mammary tumor cell line to study tumor metastasis because 4T1 cells and human mammary adenocarcinomas share similar sites of metastasis (Aslakson and Miller, 1992; Dexter et al., 1978; Miller et al., 1983). Human breast cancer spreads first to the lungs in 24%–77% of the cancers and to the liver in 22%–62% (Kamby et al., 1987; Rutgers et al., 1989; Tomin and Donegan, 1987). Similarly, 4T1 spreads in mice to the lungs and liver in >95% and >75% of the cancers, respectively (Pulaski and Ostrand-Rosenberg, 1998). We used the 4T1 cells to prepare a cDNA library enriched in transcripts that encode secreted and transmembrane proteins potentially involved in metastasis.

The 4T1 phage library was injected intravenously, and phage that localized to the lungs were isolated. After three rounds of selecting for lung-homing phage clones, 32 clones were initially isolated. We tested individual phage clones for their ability to specifically bind to lung vasculature. One of the five lung-specific clones we identified encoded a fragment of a protein recently deposited into GenBank (accession numbers AAL92861 and AAP30791).

The selected phage, when intravenously (i.v.) injected into mice and allowed to circulate for 5 min, bound to lungs almost 20-fold more than control phage (Figure 1A). In contrast, similar numbers of the selected phage and control phage accumulated in pancreas, breast, skin, kidney, brain, and liver. When injected into the left ventricle of the heart in mice, significantly more selected phage accumulated in the lungs, pancreas, kidney, brain, and liver than control phage (Figure 1B). Similar numbers of selected phage and control phage accumulated in breast, skin, and bone. The selected phage colocalized with blood vessels in the lungs (Figure 1C).

cDNA cloning and membrane topology of metadherin

The deduced amino acid sequence of the lung-homing domain of the lung-homing phage is shown in Figure 2A. Using BLAST

(Altschul et al., 1997), we found one cDNA clone (GenBank accession number AY082966) that encoded the putative full-length human protein corresponding to the phage clone. The GenBank entry refers to the protein as “LYRIC” and describes it as a putative CEACAM1-associated protein in colon carcinoma. These observations remain unpublished. Based on our results

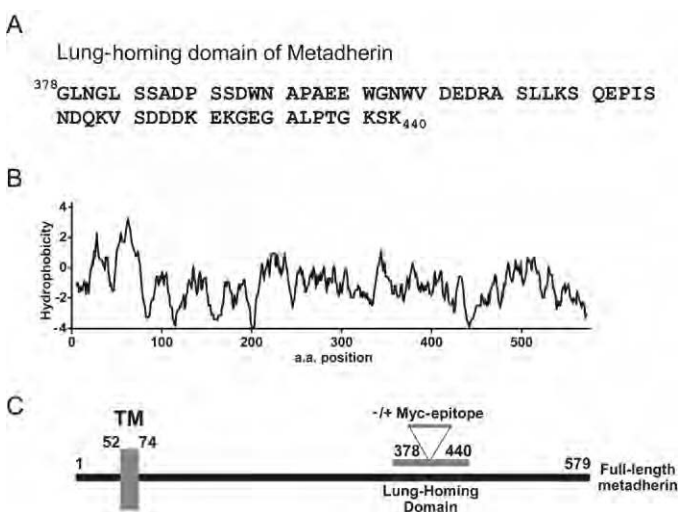


Figure 2. Sequence analysis of metadherin

A: Amino acid sequence of metadherin's lung-homing domain. This domain corresponds to residues 378–440 of the full-length mouse metadherin protein.

B: Hydrophobicity analysis of metadherin, using a window size of 9 amino acids.

C: Layout of the full-length metadherin protein. TM denotes the location of the putative transmembrane domain. The numbers denote the position of amino acids in the metadherin protein.

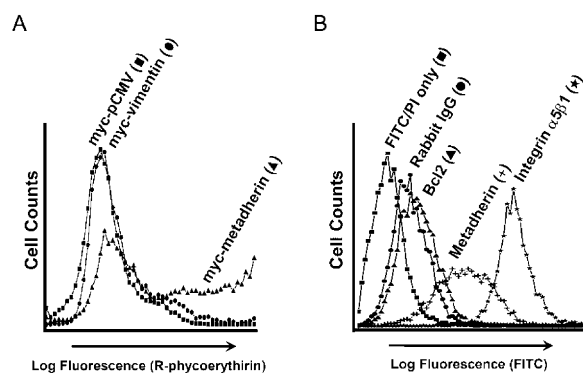


Figure 3. Lung-homing domain of metadherin is extracellular

A: HEK293T cells expressing full-length myc-tagged metadherin, myc-vimentin, or myc-pCMV were analyzed by flow cytometry. Anti-myc antibodies were applied to the cells and detected with a PE-labeled secondary Ab. **B:** Rabbit IgG, anti-Bcl2 polyclonal Ab (Bcl2), anti-integrin $\alpha 5 \beta 1$ polyclonal antibody (Integrin $\alpha 5 \beta 1$), or anti-metadherin₍₃₇₈₋₄₄₀₎ (metadherin) was applied to nonpermeabilized 4T1 tumor cells and detected with a FITC-labeled secondary Ab. Control cells were stained with FITC-labeled secondary Ab and propidium iodide alone (FITC/PI only).

that show the importance of this lung-homing protein in breast cancer metastasis, we have named this protein metadherin (metastasis adhesion protein). We used a reported mouse cDNA homolog of metadherin (GenBank accession number AK029915) to design oligonucleotides and amplified the full-length 1740 bp mouse metadherin cDNA by reverse transcription-polymerase chain reaction.

Analysis of the hydrophobic regions of metadherin (Kyte and Doolittle, 1982) revealed that amino acid residues 52–74 encode a putative transmembrane domain (Figure 2B). We did not find any domains in metadherin that were similar to other known proteins. Using a hidden Markov model to detect membrane helices and predict transmembrane topology in proteins (Glasgow, 1998; Krogh et al., 2001), we found that metadherin was predicted to be a type II transmembrane protein with an extracellular lung-homing domain. To confirm this prediction, we subcloned a c-myc epitope into the lung-homing domain of the metadherin cDNA, as shown in Figure 2C. This myc-tagged cDNA was expressed in HEK293T cells, and these cells were then stained with anti-myc antibodies. Using flow cytometry, we observed that intact myc metadherin-expressing cells were labeled with anti-myc antibodies (Figure 3A), indicating that the lung-homing domain of metadherin was extracellular. No cell surface labeling was detected in vector-transfected cells or nonpermeabilized cells expressing the intracellular protein myc-vimentin (Figure 3A). Anti-myc antibodies stained the myc vimentin-expressing cells when permeabilized, which confirms the expression of myc-vimentin, and permeabilized cells expressing vector alone were not stained with anti-myc antibodies (data not shown).

Metadherin expression in tumor cells and tumors

We also raised rabbit antibodies reactive to the lung-homing domain of metadherin to study endogenous metadherin in tumor cells and tumors. These antibodies bound to nonpermeabilized 4T1 cells in flow cytometry (Figure 3B). This result confirms the presence of the lung-homing domain of metadherin on tumor

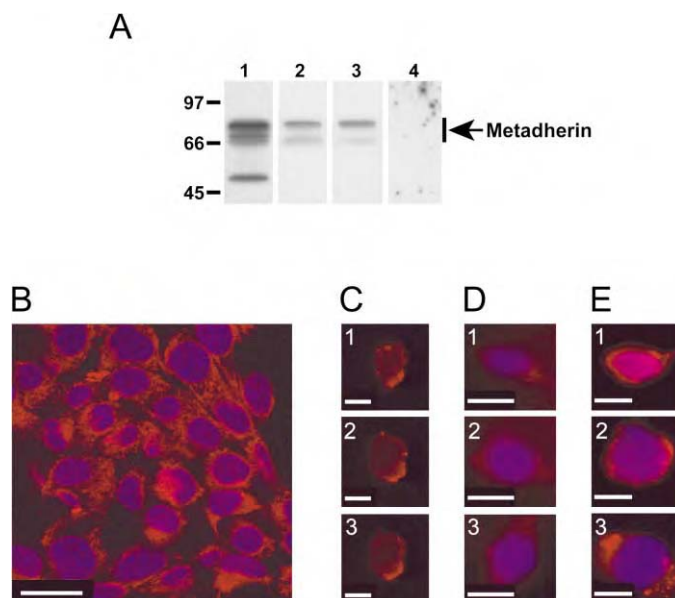


Figure 4. Metadherin expression in 4T1 tumor cells

A: Immunoblot of endogenous metadherin. Lanes 1 and 4, 4T1 cell extract; lane 2, KRIB cell extract; lane 3, MDA-MB-435 cell extract. Immunoblot detection of metadherin was performed with anti-metadherin₍₃₇₈₋₄₄₀₎ (lanes 1–3). Immunoblot detection of an unrelated protein, Clone D2, was performed with anti-Clone D2 polyclonal antibody (lane 4).

B: Confocal projection of permeabilized 4T1 cells stained with anti-metadherin₍₃₇₈₋₄₄₀₎. Scale bar corresponds to 50 μ m.

C: Confocal sections (0.15 μ m thick; panels 1–3) of nonpermeabilized 4T1 cells stained with anti-metadherin₍₃₇₈₋₄₄₀₎.

D and E: Nonpermeabilized 4T1 cells stained with anti-metadherin₍₃₇₈₋₄₄₀₎ that was pre-incubated with excess metadherin₍₃₇₈₋₄₄₀₎ peptide (**D**, panels 1–3) or excess control peptide (**E**, panels 1–3). In **B–E**, anti-metadherin₍₃₇₈₋₄₄₀₎ was detected with Alexa 594 goat anti-rabbit IgG antibody (red). Nuclei were stained with DAPI (blue). Images in **D** and **E** were captured using an inverted fluorescent microscope. The scale bars in **C–E** correspond to 5 μ m.

cells at the cell surface where it would be available to bind to vascular targets during metastasis. An antibody against a cytoplasmic protein (Bcl-2) and rabbit IgG did not bind to the surface of nonpermeabilized 4T1 cells, while the cells were strongly positive for integrin $\alpha 5 \beta 1$ (Figure 3B).

In 4T1 tumor cell extracts, anti-metadherin₍₃₇₈₋₄₄₀₎ detected proteins with apparent molecular weights of approximately 80 kDa, 75 kDa, and 55 kDa (Figure 4A, lane 1). KRIB and MDA-MB-435 cell extracts also contained the 80 kDa and 75 kDa proteins (Figure 4A, lanes 2 and 3, respectively). A control, affinity-purified polyclonal antibody reactive to a nonrelated protein (Clone D2) did not detect the anti-metadherin₍₃₇₈₋₄₄₀₎ immunoreactive bands (Figure 4A, lane 4). The 80 kDa and 55 kDa proteins detected by anti-metadherin₍₃₇₈₋₄₄₀₎ were also produced by an in vitro transcription and translation reaction using an epitope-tagged metadherin cDNA as template (data not shown); this suggests that the 55 kDa protein may be a degradation product of metadherin.

In fixed and permeabilized 4T1 cells, metadherin immunoreactivity localized throughout the cytoplasm (Figure 4B). In nonpermeabilized cells, the staining was concentrated at the edges of the cells (Figure 4C). Controls showed that pre-incubation of anti-metadherin₍₃₇₈₋₄₄₀₎ with the metadherin₍₃₇₈₋₄₄₀₎ lung-homing

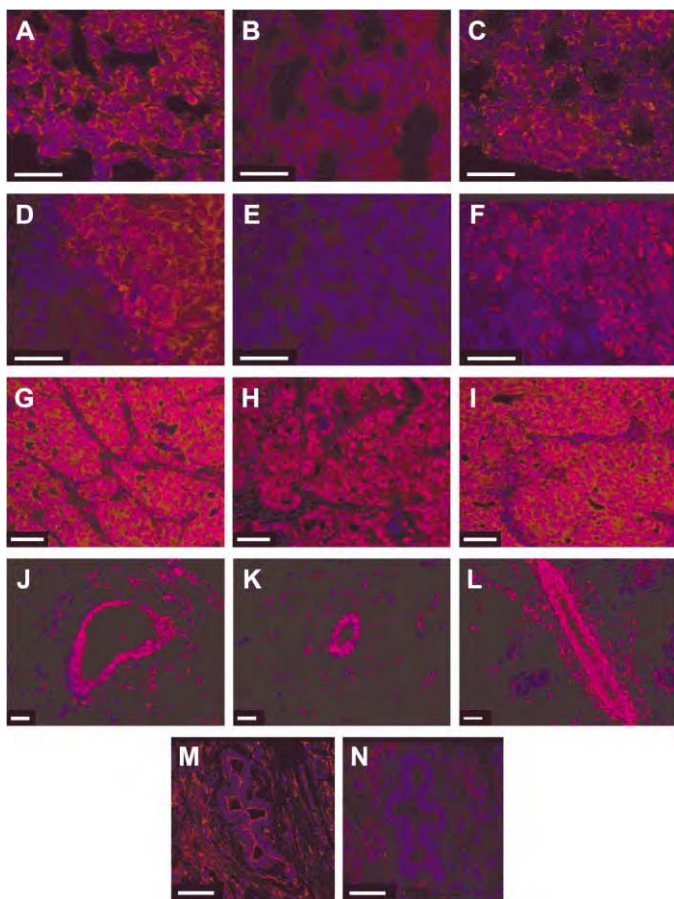


Figure 5. Metadherin expression in tumor xenografts and human breast cancer

MDA-MB-435 breast adenocarcinoma (A–C) or KRIB osteosarcoma (D–F) tumor xenografts grown in nude Balb/c mice were analyzed by immunostaining. Sections were stained with either anti-metadherin_(378–440) alone (A and D) or anti-metadherin_(378–440) pre-incubated with excess metadherin_(378–440) peptide (B and E) or excess control peptide (C and F). Sections of human breast tumor (G–I) or normal human breast tissue (J–L) were stained with either anti-metadherin_(378–440) alone (G and J) or anti-metadherin_(378–440) pre-incubated with excess metadherin_(378–440) peptide (H and K) or excess control peptide (I and L). Sections of mouse breast tissue were stained with either anti-metadherin_(378–440) alone (M) or anti-metadherin_(378–440) pre-incubated with excess metadherin_(378–440) peptide (N). In all panels, anti-metadherin_(378–440) was detected with Alexa 594 goat anti-rabbit IgG antibody (red) and nuclei were stained with DAPI (blue). The confocal projections in A–N were captured using a confocal microscope. The scale bars correspond to 50 μ m.

peptide inhibited the staining (Figure 4D), whereas a control peptide did not (Figure 4E).

We detected strong metadherin staining in sections of MDA-MB-435 and KRIB tumor xenografts (Figures 5A and 5D), which are two tumor models known to generate lung metastases (Berlin et al., 1993; Price et al., 1990). The anti-metadherin immunostaining was specific, since pre-incubation of antibody with the metadherin_(378–440) lung-homing peptide (Figures 5B and 5E) inhibited the staining and control peptide (Figures 5C and 5F) had no inhibitory effect. Subcutaneous tissue or skin adjacent to the tumors showed no anti-metadherin staining (e.g., Figure 5D, lower left corner).

Several human breast cancer sections stained with anti-

metadherin_(378–440) showed high amounts of metadherin throughout the tumor (Figure 5G). In contrast, we did not detect any cytoplasmic or cell surface-associated metadherin in normal human breast tissue, but nuclear staining was present (Figure 5J). The cell surface staining of breast cancer tissue could be inhibited with the metadherin_(378–440) peptide (Figure 5H), but not with control peptide (Figure 5I). Neither peptide inhibited nuclear staining (Figures 5H, 5I, 5K, and 5L). The human sections were paraffin embedded and processed with heat-induced target retrieval. Apparently, the antibody nonspecifically stains nuclei in such sections. In frozen tissue sections of normal mouse mammary tissue, we found specific metadherin staining at the apical surface of epithelial cells lining ducts of the mammary glands (Figures 5M and 5N), and a small amount of metadherin was dispersed through the mammary fat pad. We detected no metadherin in the spleen, kidney, lung, or skin, but minute amounts were seen in the liver. Purkinje neurons in the early postnatal and adult cerebellum were strongly positive for metadherin staining (data not shown). Tissue array slides of human breast tissue and breast adenocarcinomas were also stained with anti-metadherin_(378–440). We detected strong anti-metadherin_(378–440) staining throughout the tissue sections in 17 out of 31 breast adenocarcinomas, while metadherin was absent in 18 out of 20 samples of normal breast tissue. The other two normal breast tissue samples stained positive for metadherin at epithelial cells lining ducts of the mammary glands. These immunostaining results show that metadherin is selectively overexpressed in tumors.

Effect of metadherin expression on the localization of injected cells

To test the effect of metadherin on tissue distribution of i.v.-injected tumor cells, we studied HEK293T cells transiently transfected with metadherin. The cells were cotransfected with DsRed2 and metadherin, and DsRed2-positive cells were isolated using fluorescence-activated cell sorting (FACS). The cells were then i.v.-injected into mice. Fluorescent cells were detected in the blood vessels of lungs examined 2 hr after the injection; cell counting showed 22% more metadherin-transfected cells than that of vector-transfected cells (Figures 6A and 6B; Student's *t* test; $p < 0.001$). We did not see significant numbers of DsRed2 HEK293T cells in the brain, skin, liver, kidney, heart, spleen, or pancreas (Figure 6A). This result supports the phage homing data indicating that metadherin preferentially binds to lung vasculature. The relatively small incremental effect of metadherin overexpression on the lung localization of HEK293T cells is probably due to endogenous expression of metadherin by these cells, which immunoblotting showed to be about 45% of that in the 4T1 cells (data not shown).

Anti-metadherin and metadherin siRNA inhibit 4T1 lung metastasis

To gain information on the role of metadherin in metastasis, we decided to inhibit metadherin activity in the 4T1 cells with antibodies reactive to the lung-homing domain of metadherin. When co-injected with the 4T1 cells, anti-metadherin_(378–440) inhibited lung metastasis by about 40% (Figure 7, $p < 0.01$), compared to 4T1 cells treated with rabbit IgG. In a separate experiment, we did not observe any difference between the growth of mammary fat pad tumors formed from 4T1 cells pretreated with the anti-metadherin_(378–440) or rabbit IgG (data not shown).

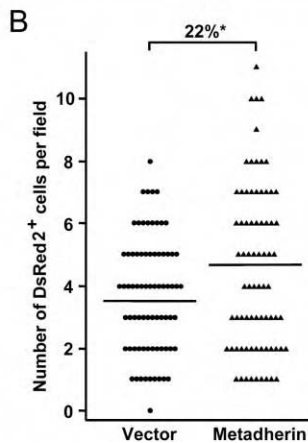
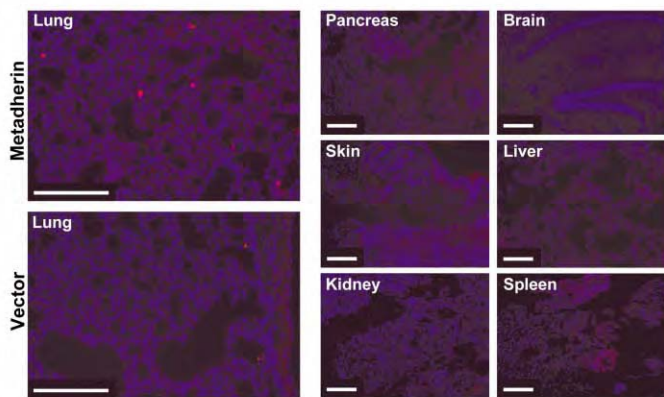


Figure 6. HEK293Ts overexpressing metadherin localize to lung

A: DAPI-stained (blue) lung sections from mice injected with HEK293T cells that were cotransfected with a DsRed2 expression vector (red) and either metadherin-pCMV or expression vector alone. Pancreas, skin, kidney, brain, liver, and spleen sections from mice injected with HEK293T cells that were transfected with a DsRed2 expression vector (red) and metadherin-pCMV. The scale bars correspond to 100 μm .

B: Number of DsRed2-positive cells per viewing field in the lung sections (n = 75; one-tailed Student's t test; *p < 0.001).

As a second approach, we measured the metastatic potential of breast cancer cells expressing reduced levels of metadherin. As shown in Figure 8A, siRNA reactive to metadherin, but not siRNA to GAPDH or scrambled-siRNA, was able to knock down expression of transfected myc-metadherin in HEK293T cells. We were unable to generate stable cell lines that expressed reduced levels of metadherin because metadherin expression levels returned to normal after 2 weeks. Instead, we coexpressed green fluorescent protein (EGFP) and the metadherin-reactive siRNA or scrambled-siRNA in 4T1 cells and selected for siRNA-transfected cells by FACS. The transfection with metadherin-siRNA did not affect the expression of β -actin or the type II transmembrane protein, transferrin receptor (Figure 8B). However, metadherin protein expression in metadherin-siRNA cells was reduced by about 40% relative to the scrambled-siRNA cells (Figure 8B). Measured by real-time PCR, metadherin-siRNA cells expressed about 40% less metadherin mRNA than the scrambled-siRNA cells, when metadherin mRNA levels were normalized to β -actin mRNA levels (Figure 8C).

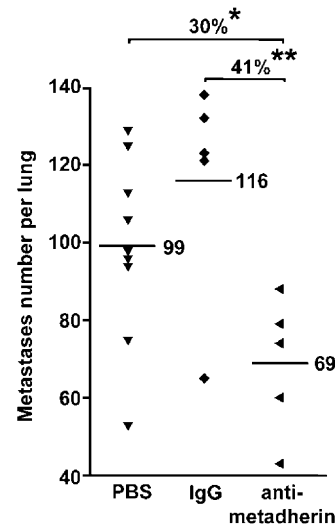


Figure 7. Anti-metadherin antibodies inhibit lung metastasis

Number of lung metastases from mice injected with 4T1 cells that were treated with anti-metadherin⁽³⁷⁸⁻⁴⁴⁰⁾, rabbit IgG, or PBS. Average number of metastases in each group is denoted with a horizontal line. The percent difference in average number of metastases between groups is denoted above the brackets, with significance measured using a one-tailed Student's t test (*p < 0.02, **p < 0.01).

Using flow cytometry, the effects of metadherin-reactive siRNA and scrambled-siRNA on cell growth and viability were assessed. In 4T1 cells cotransfected with EGFP and metadherin-reactive siRNA or scrambled-siRNA expression plasmids, we did not detect any significant difference in propidium iodide staining between the EGFP-positive populations from the metadherin-reactive siRNA or scrambled-siRNA cells (4.52% versus 5%, see Supplemental Figure S1 at <http://www.cancercell.org/cgi/content/full/5/4/365/DC1>). This suggested metadherin-reactive siRNA did not affect 4T1 cell viability under these conditions. In addition, the number of EGFP-positive cells in the metadherin-reactive siRNA and scrambled-siRNA transfected 4T1 cells was not significantly different, suggesting the metadherin-reactive siRNA plasmid did not inhibit cell growth during the 2 day transfection period (9.55% versus 9.95%, Supplemental Figure S1). Also, we counted the number of cells before and 2 days after transfecting the siRNA expression plasmids and did not see any significant effect of the metadherin-siRNA on the growth rate of the cells (data not shown).

Immunostaining confirmed that metadherin-siRNA cells expressed less metadherin (Figure 8D, 1 and 2) than scrambled-siRNA cells (Figure 8D, 3 and 4). Using FACS, we isolated EGFP-positive cells that excluded propidium iodide to select for viable siRNA-transfected cells (Figure 8D, 5–8). When injected into mice, the 4T1 cells expressing metadherin-reactive siRNA formed about 80% fewer experimental lung metastases than cells expressing scrambled-siRNA (Figure 8E, Student's t test, $p < 0.001$).

Discussion

We report here that a protein, metadherin, is overexpressed in breast tumors and binds to lung vasculature through a C-ter-

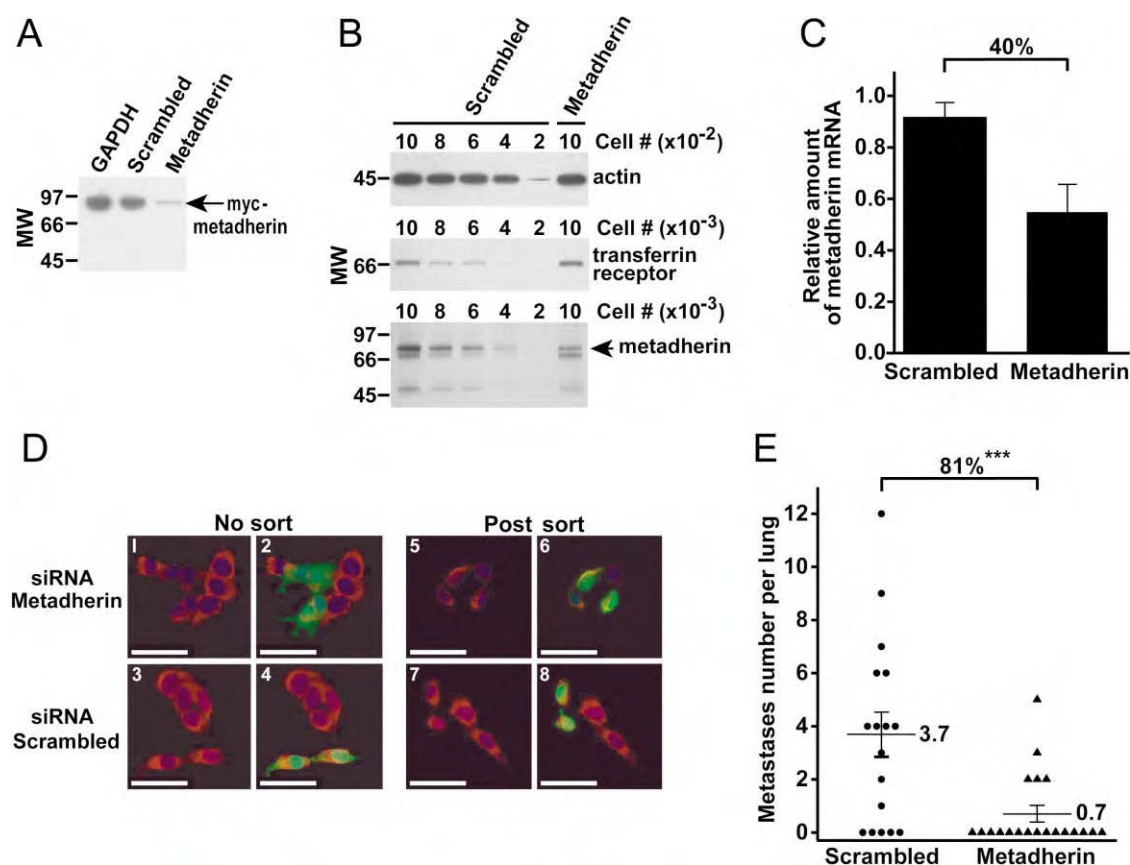


Figure 8. siRNA reactive to metadherin mRNA inhibits lung metastasis

A: Anti-myc immunoblot of HEK293T cell extracts expressing myc-tagged metadherin and siRNA reactive to GAPDH or metadherin, or scrambled-siRNA. **B:** Immunoblot quantitation of β -actin, transferrin receptor, or metadherin protein levels in 4T1 cells expressing siRNA reactive to metadherin or scrambled-siRNA. The arrow in **B** denotes the 80 kDa metadherin protein band quantified by densitometry.

C: Quantitation of metadherin mRNA in 4T1 cells expressing siRNA reactive to metadherin or scrambled-siRNA. The relative amount of metadherin mRNA was normalized to the abundance of β -actin mRNA, also detected by real-time PCR. Error bars represent mean \pm SD.

D: 4T1 cells were cotransfected with an EGFP expression vector and a vector expressing siRNA reactive to metadherin (panels 1, 2, 5, and 6) or scrambled-siRNA (panels 3, 4, 7, and 8). The cells were sorted by FACS to select for EGFP-expressing cells (Post sort). Nonsorted cells (No sort; panels 1–4) and postsorted cells (panels 5–8) were stained with anti-metadherin₍₃₇₈₋₄₄₀₎. Panels 2, 4, 6, and 8 show the EGFP-expressing cells (green) displayed in panels 1, 3, 5, and 7, respectively. In all panels, anti-metadherin₍₃₇₈₋₄₄₀₎ was detected with Alexa 594 goat anti-rabbit IgG antibody (red). Nuclei were stained with DAPI (blue). The scale bars correspond to 50 μ m.

E: siRNA reactive to metadherin transcripts inhibits 4T1 cell experimental lung metastasis. Values are expressed as the number of tumor foci per 10,000 cells injected. Bars represent mean \pm SEM (one-tailed Student's *t* test; ****p* < 0.001). In **C** and **E**, percentages indicate relative suppression compared to control group.

minimal segment in the extracellular domain. We also show that blocking the lung-homing domain with antibodies or inhibiting the expression of metadherin with siRNA can inhibit breast cancer metastasis. These results identify metadherin as a potential mediator of cancer metastasis.

Metadherin appears to detect a specific marker of lung vasculature. Metadherin phage accumulated in lung vasculature after either tail-vein or intracardiac injection, suggesting that among the various vascular beds, it primarily binds to lung endothelium. In this regard, metadherin is similar to lung-specific homing peptides isolated by *in vivo* phage display (Rajotte and Ruoslahti, 1999) and antibodies that specifically bind to lung vasculature (McIntosh et al., 2002). The ability of metadherin phage to specifically target lung vasculature suggests that among the various vascular beds, the molecule(s) metadherin binds ("metadherin receptor") is primarily expressed on lung endothelium. The identity of the receptor is currently unknown.

Tissue-specific expression of vascular markers is not limited to lung vasculature; recent data suggest that each tissue puts a specific signature on its vasculature (Ruoslahti, 2002). Thus, the binding of tumor cells to tissue-specific vascular markers may play a role in selective tumor metastasis to other tissues as well.

Metadherin appears to primarily mediate metastasis to one of the four sites commonly affected by human breast cancer: the lungs. The fact that metadherin phage primarily targeted the lungs after either intravenous or intracardiac injection and was not detected in substantial amounts in the liver, brain, or bone suggests that metadherin mediates specific adhesion to lung vasculature, even after passing through capillary networks of other organs. The ability of metadherin phage to accumulate in the lungs even after intracardiac injection suggests that metadherin also promotes selective binding of tumor cells to lung

vasculature, rather than helping them adhere to the first capillary bed the cells encounter.

Metadherin may be important to the pathogenesis of cancer. We found high expression of metadherin in cultured tumor cells, and its expression was higher in both experimental and clinical breast cancers than in normal breast tissue and in other normal tissues, as detected with specific metadherin antibodies. The only exception to the relatively low expression in the normal tissues we studied were the Purkinje cells in the cerebellum; metadherin may have a specific function in these cells.

A recent gene expression profiling study on breast cancer patients revealed that metadherin is overexpressed in many metastatic breast cancers. van 't Veer et al. (2002) found that metadherin mRNA expression levels (described as GenBank entry AK000745) in breast cancer patients were significantly correlated with a poor prognosis due to metastasis. Out of 25,000 genes analyzed, metadherin was ranked 25th when correlating gene expression levels with metastasis. Most of the patients who expressed high levels of these "poor prognosis" classified genes developed distant metastases within 5 years of observation. Thus, metadherin is overexpressed in breast cancer both at the protein and mRNA levels and is associated with increased malignancy of these cancers. Our results suggest that the association of metadherin overexpression with poor prognosis of breast cancer is due to an ability of metadherin to specifically promote tumor metastasis to the lungs.

There are other examples of adhesive interactions that are required in order for lung metastases to form. Dipeptidyl dipeptidase IV on lung endothelial cells was found to be an adhesion receptor for fibronectin on metastasizing breast and prostate carcinoma cells in a mouse model (Cheng et al., 1998; Johnson et al., 1993). In another mouse model, Ca²⁺-sensitive chloride channel, hCLCA2, expressed on lung endothelial cells was reported to be a ligand for β 4 integrins on metastasizing breast cancer cells (Abdel-Ghany et al., 2001; Elble et al., 1997). Most recently, the secreted chemokine, CXCL12, which is highly expressed in the lung, liver, and lymph nodes, was shown to bind to CXCR4 receptors on the surface of metastasizing breast cancer cells (Muller et al., 2001). Moreover, interfering with only one of these interactions was sufficient to inhibit metastasis (Abdel-Ghany et al., 2001; Cheng et al., 1998; Muller et al., 2001). Although there is no evidence available on the significance of these interactions in breast cancer, it seems that multiple interactions of cell adhesion molecules and growth factor receptors may be required for the attachment and growth of circulating tumor cells in the lung. Similar mechanisms based on unique vascular addresses may play a role in organ-specific metastasis to other organs.

The importance of metadherin in tumor cell metastasis might not only be limited to breast cancer. Using SAGEmap (Lal et al., 1999; Lash et al., 2000), a component of The Cancer Genome Anatomy Project at the National Center for Biotechnology Information, we found that metadherin is significantly overexpressed not only in breast cancers, but also in cancers of the brain and prostate ($p < 0.05$). This suggests that metadherin might also play a role in the metastasis of these cancers. Metadherin is conserved among mammals, and with the BLAST algorithm (Altschul et al., 1997), we found additional mouse and human metadherin-like molecules in the GenBank databases. It will be important to determine what role, if any, these related molecules might play in cancer.

Metadherin is a potential target for tumor diagnosis and preventative therapy. Given the cell surface localization of metadherin in tumor cells and the discrete overexpression of metadherin in primary tumors, therapeutics that target metadherin might prove to be selective for metastasis-prone tumors. Our results showing the antimetastatic activity of anti-metadherin antibodies and siRNA reactive to metadherin mRNA suggest that antibody or siRNA-based therapies that target metadherin might be effective in preventing certain tumors from metastasizing.

Experimental procedures

Cell lines, mice, and tumors

4T1, a cell line derived from a Balb/c breast adenocarcinoma, was obtained from ATCC and maintained as described by Pulaski and Ostrand-Rosenberg (1998). MDA-MB-435 and KRIB cell lines were maintained as described before (Laakkonen et al., 2002). Nude Balb/c mice were subcutaneously injected with 1×10^6 tumor cells and kept for 5 weeks (KRIB) or 10 weeks (MDA-MB-435). Tumors were then removed, frozen in OCT embedding medium (Tissue-Tek, Elkhardt, IN), and sectioned. The Burnham Institute Animal Research Committee approved the animal experimentation.

Phage library and screening

A cDNA library was prepared from membrane bound polyribosomal mRNA of 4T1 cells. Briefly, RNA from membrane bound polysomes of 3.2×10^8 4T1 cells was prepared using the methods described by Mechler (1987). Approximately 1 μ g of this RNA was used to generate 6 μ g of amplified antisense mRNA (aRNA), using the methods described by Luo et al. (1999). Using aRNA as template, mRNA was synthesized as described by Luo et al. (1999), except the primer, 5'-TTNNNNNN-3', was used instead of random hexamer primer, and methylated dNTPs were used instead of dNTPs. A cDNA library was prepared from the mRNA, as described in the manufacturer's protocol (OrientExpress Random Primer cDNA synthesis kit; Novagen, Madison, WI).

T7 phage vectors, designed to express cDNA library-encoded proteins fused at the N terminus to phage 10B coat protein and to a myc epitope at the C terminus, were then assembled. Oligonucleotides encoding myc epitopes in all three reading frames, internal *EcoRI* and *HindIII* restriction enzyme cleavage sites and flanking *EcoRI/HindIII* adapters, were synthesized. The oligonucleotides were then individually phosphorylated, annealed, and ligated to *EcoRI/HindIII*-digested T7Select 1-2a, 1-2b, or 1-2c vector arms (Novagen) to generate myc epitope phage vectors.

To prevent myc epitope expression in phage vectors that were unsuccessfully ligated to cDNA during library construction, a linker encoding stop codons in all three reading frames was inserted upstream of the myc epitope and downstream of the 10B coat protein in the phage vector. Oligonucleotides encoding stop codons in all three reading frames were synthesized, phosphorylated, annealed, and ligated to *EcoRI/HindIII*-digested myc epitope phage vectors to form myc-T7 vectors. A map of the myc epitope phage vector is shown in Supplemental Figure S2 at <http://www.cancer-cell.org/cgi/content/full/5/4/365/DC1>. The cDNA libraries were then ligated to *EcoRI/HindIII*-digested myc-T7 vector, phage were packaged, and libraries were amplified in *E. coli* BLT5615 cells (according to the manufacturer's protocol; Novagen). As measured by plaque assay, the library contained 4.7×10^6 primary recombinants.

Phage clones that expressed cDNA inserts with open reading frames were enriched by three rounds of selection with anti-myc mAb (3.1 μ g/ml MAB8864; Chemicon, Temecula, CA) bound to rat anti-mouse IgG1 magnetic beads (3.1 μ l per 1 ml of buffer; Miltenyi Biotec, Auburn, CA). Selections were performed with 10^{11} plaque forming units (pfu) of phage in 10 ml of Dulbecco's phosphate buffered saline containing 0.5% bovine serum albumin (PBSB). Phage were applied to a magnetized LS MACS column (Miltenyi Biotec), washed with buffer (50 mM Tris-HCl [pH 7.5], 150 mM NaCl, 1% NP-40, 0.5% sodium deoxycholate, 0.1% sodium dodecyl sulfate), eluted with PBSB after demagnetizing the column, and transferred to a second column for more washes. Phage were amplified in BLT5615 *E. coli* using the liquid lysate method after each anti-myc selection round and supernatants clarified by centrifugation were supplied with 1% vol/vol of *E. coli* protease

inhibitors cocktail (P-8465; Sigma-Aldrich, St. Louis, MO). After three rounds of myc antibody sorting, over 90% of the phage clones in the 4T1 library were found to contain open reading frame cDNA inserts. On average, the phage clones expressed protein fragments that were 75 amino acids long.

Ex vivo and in vivo screenings with the 4T1 phage library were performed as previously described (Hoffman et al., 2004). Briefly, cell suspensions were prepared from mouse lungs and incubated overnight at 4°C with 10^9 pfu of 4T1 phage library. The cells were washed to remove unbound phage, and the bound phage were rescued and amplified by adding BLT5615 *E. coli*. The amplified 4T1 phage library was applied to a lung cell suspension for a second ex vivo selection round, as before. The ex vivo preselected phage pool (200 μ l, or approximately 10^9 pfu) was injected intravenously into 2-month-old Balb/c mice through the tail vein, allowed to circulate for 5 min, and heart-perfused with PBS to remove unbound intravascular phage. Cell suspensions of tissue were prepared by mechanical disruption and washed to remove unbound phage, and the bound phage were rescued and amplified by adding BLT5615 *E. coli*. The phage pool was reinjected into Balb/c mice, and the cycle repeated twice. For each selection round, the number of phage recovered from the tissue was normalized to the number of injected phage and tissue mass. After three rounds of in vivo selections, cDNA inserts were sequenced from 32 phage clones as described before (Hoffman et al., 2004).

Cloning of full-length metadherin cDNA

The following primers were synthesized to amplify the full-length mouse metadherin cDNA: 5'-ACCATGGCTGCACGAAGCTGGCAGGACGAGCTG-3' and 5'-TCACGTTTCCCGTCTGGCCTTTTCTCTTTT-3'. RNA was isolated from 4T1 cells using a Total RNA Isolation Kit (Qiagen, Valencia, CA). The metadherin cDNA was amplified by RT-PCR using a Superscript One-Step RT-PCR Kit for Long Templates (according to manufacturer's protocol; Invitrogen, Carlsbad, CA) and subcloned into the TOPO-TA vector, pcDNA3.1-V5/His (according to the manufacturer's protocol; Invitrogen).

A myc epitope was added to metadherin protein by first inserting an *EcoRI* restriction enzyme site in the metadherin cDNA after nucleotide 1222 with a QuickChange site-directed mutagenesis kit (Stratagene, La Jolla, CA). Then, oligonucleotides encoding a myc epitope (EQKLISEEDL) and flanking *EcoRI* adapters were synthesized, phosphorylated, and ligated into the *EcoRI*-digested metadherin cDNA. The myc-metadherin cDNA was subcloned into the pCMV vector (Clontech, Palo Alto, CA). Human myc-vimentin cDNA was generated by reverse transcription-polymerase chain reaction, using vimentin-specific primers and human mRNA as template, and then subcloned into the pCMV-Myc vector (Clontech, Palo Alto, CA).

Antibodies, immunoblotting, and immunohistology

Anti-T7 phage affinity purified antibody was previously described (Laakkonen et al., 2002). A polyclonal antibody was generated in New Zealand White rabbits against the recombinant metadherin lung-homing domain that was fused to glutathione-S transferase. The initial immunization was done in complete Freund's adjuvant and boosters were with incomplete Freund's adjuvant. The antibody was affinity purified on recombinant hexahistidine-tagged metadherin₍₃₇₈₋₄₄₀₎ peptide coupled to SulfoLink Gel (Pierce, Rockford, IL) via a cysteine residue added to the amino terminus of the metadherin₍₃₇₈₋₄₄₀₎ peptide.

Blood vessel localization of metadherin phage was examined by i.v. injection of 2.5×10^{10} pfu metadherin phage (in 200 μ l M9LB) into the tail vein of a mouse. Blood vessels were visualized by co-injection of phage with 200 μ g of *Lycopersicon esculentum* (tomato) lectin conjugated to fluorescein. The injected materials were allowed to circulate for 10 min. Lungs were removed and frozen in OCT embedding medium (Tissue-Tek).

Tumor cell lysates were prepared in 2.5 \times Laemmli's sample buffer (Laemmli, 1970) at a ratio of 10^6 cells per 150 μ l and subjected to SDS-PAGE on 4%–20% acrylamide gradient gels. Proteins were transferred to PVDF membrane and immunoblots were performed with anti-metadherin₍₃₇₈₋₄₄₀₎ (0.1 μ g/ml) and goat anti-rabbit IgG-HRP (diluted 1:10,000; Bio-Rad, Hercules, CA) and developed using ECL+ plus chemiluminescence reagent (Amersham Biosciences, Piscataway, NJ), according to the manufacturer's instructions. The relative amount of metadherin detected by immunoblot was quantitated using an Alphamager (Alpha Innotech, San Leandro, CA). β -actin was detected with an anti-actin monoclonal antibody (10 μ g/ml, Chemicon). Transferrin receptor was detected with an anti-transferrin receptor polyclonal antibody (2 μ g/ml, Santa Cruz Biotech, Santa Cruz, CA). Affinity-purified

polyclonal antibody reactive to a 175 kDa protein, Clone D2, was prepared as described for anti-metadherin₍₃₇₈₋₄₄₀₎. Control immunoblots were performed with anti-Clone D2 (0.1 μ g/ml) and goat anti-rabbit IgG-HRP (described above).

For cell surface labeling, anti-metadherin₍₃₇₈₋₄₄₀₎, diluted to 20 μ g/ml in ice-cold IMEM (Invitrogen) with 10% fetal bovine serum (FBS), was added to cells cultured on chamber slides and incubated for 1 hr on ice. The cells were washed with IMEM and fixed with cold 4% paraformaldehyde in PBS for 15 min. Anti-metadherin antibodies were detected with Alexa 594 goat anti-rabbit IgG (diluted 1:500 in PBS with 1% FBS and 3% goat serum). Slides were mounted with Vectashield fluorescence mounting medium (Vector, Burlingame, CA). For permeabilized cell labeling, cells were first fixed with 4% paraformaldehyde (described above) and then treated with 0.1% Triton X-100 in PBSB for 15 min. The cells were washed with PBSB and incubated with anti-metadherin₍₃₇₈₋₄₄₀₎ (diluted to 20 μ g/ml in IMEM with 10% FBS) for 1 hr at room temperature. Anti-metadherin₍₃₇₈₋₄₄₀₎ was detected with Alexa 594 goat anti-rabbit IgG, as described above.

Paraffin-embedded human tissue sections (Spring Biosciences, Fremont, CA) and breast adenocarcinoma tissue array sections (InnoGenex, San Ramon, CA; NCI, Frederick, MD) were deparaffinized and then treated with Target Retrieval Solution (according to the manufacturer's instructions; DAKO, Carpinteria, CA). For immunofluorescence imaging, the sections were stained as described above, except PBSB was substituted for 0.5% Blocking Reagent (NEN Life Sciences, Boston, MA) in 0.1 M Tris/150 mM NaCl. The tissue array sections were stained as described above, except anti-metadherin₍₃₇₈₋₄₄₀₎ was detected with the EnVision + System (according to the manufacturer's instructions; DAKO) and cells were counterstained with hematoxylin (DAKO). To determine specificity, anti-metadherin₍₃₇₈₋₄₄₀₎ (20 μ g/ml) was pre-incubated overnight with 200 μ g/ml recombinant metadherin lung-homing protein or unrelated recombinant control protein (72 amino acid, lung-homing Clone D2) in blocking buffer before immunostaining the sections.

FACS analysis

Transiently transfected HEK293T cells expressing myc-vimentin, myc-metadherin, or myc-pCMV vector alone (Clontech) were detached from their culture dishes by gently washing with PBS containing 1% BSA (PBSB). The cells were then stained with anti-myc mAb (2 μ g/ml in PBSB; Chemicon) for 20 min at 4°C. The cells were washed with PBSB, stained with goat anti-mouse IgG PE-labeled antibody (4 μ g/ml in PBSB; Pharmingen, San Diego, CA), washed again with PBSB, fixed with 2% paraformaldehyde in PBS, resuspended in PBS, and analyzed using a FACScan flow cytometer (BD, San Jose, CA).

To analyze the 4T1 cells by FACS, the cells were detached from culture plates by incubating with PBS with 2 mM EDTA (PBSE) for 10 min. The cells were then washed with PBSB and incubated with 40 μ g/ml (in PBSB) of the following antibodies: anti-Bcl2 (SL-492, Santa Cruz Biotechnology, Santa Cruz, CA), normal rabbit IgG (Sigma, St. Louis, MO), anti-integrin $\alpha_5\beta_1$ (Protein G-purified from rabbit serum containing antibodies raised against human fibronectin receptor), and anti-metadherin₍₃₇₈₋₄₄₀₎. To detect bound antibodies, cells were incubated with goat anti-rabbit IgG-FITC (40 μ g/ml in PBSB; Molecular Probes, Eugene, OR). After the final wash, the cells were resuspended with PBS containing 2 μ g/ml of propidium iodide (PI) and analyzed by FACS.

HEK293T cell homing

HEK293T cells were cotransfected with DsRed2 (Clontech) and either metadherin-pCMV or empty myc-pCMV vector. 2 days posttransfection, the cells were detached with PBSE and filtered through a 40 μ m nylon filter. DsRed2-expressing cells were isolated using a FACS Vantage flow cytometer (BD Biosciences, San Jose, CA). 2.5×10^5 DsRed2-positive cells were injected into the tail vein of nude Balb/c mice. Five mice were injected with each cell type. After 2 hr, the mice were sacrificed, organs were removed and fixed with 4% paraformaldehyde in PBS, and 10 μ m thick frozen tissue sections were prepared. For each lung section, three different fields were counted. Clumps of DsRed2-positive cells with three or more cells were excluded from the count. Five sections per lung were counted.

Tumor metastasis studies

The 4T1 cells were detached from plates with PBSE, washed once with PBS, resuspended to 5×10^5 cells/ml in PBS, and placed on ice. Anti-

metadherin^[378-440] or rabbit IgG (200 µg) was added to 5×10^4 cells and the cells were then injected via the lateral tail vein into female Balb/c nu/nu mice. Animals were sacrificed 7 days after tumor cell injection. Lungs were recovered and fixed with Bouin's solution, and the tumor foci on the surface of the left lobe were counted under a dissecting microscope.

siRNA knockdown of metadherin expression

For the siRNA-mediated knockdown of metadherin expression, nucleotides 1597–1615 of the mouse metadherin cDNA (5'-GTGCCACCGATGTTAC AAG-3') were used as the target sequence. Oligonucleotides containing this target sequence were synthesized and subcloned into the pSilencer 3.0-H1 plasmid (Ambion, Austin, TX) according to the manufacturer's instructions. 4T1 cells were transfected with the metadherin or a negative control siRNA pSilencer vector together with an EGFP-expression vector (Clontech), using a 4:1 ratio of pSilencer to EGFP vectors. 2 days posttransfection, 4T1 cells that were labeled with EGFP and excluded propidium iodide were isolated by FACS. 10,000 or 50,000 of these selected 4T1 cells in 100 µl of PBS were injected into the tail vein of anesthetized nude Balb/c mice. The mouse lungs were harvested 22 days postinjection and fixed with Bouin's solution. The tumor foci on the lung surface were counted under a dissecting microscope. Data were recorded as the number of tumor foci formed per 10,000 cells injected. The levels of β-actin and metadherin mRNA in siRNA-transfected cells were determined using a one-step RT-PCR RNA Amplification Kit and LightCycler Instrument (according to manufacturer's protocol; Roche, Indianapolis, IN).

GenBank accession number

The nucleotide sequence of the mouse metadherin cDNA has been deposited in GenBank and received accession number AY553638.

Acknowledgments

We thank Drs. Kathryn Ely, Eva Engvall, and Yu Yamaguchi for comments on the manuscript. We also thank Yoav Altman for excellent technical assistance and Roslind Varghese for editing. This work was supported by grants PO1 CA 82713 and Cancer Center Support Grant CA 30199 from the NCI and DAMD17-02-1-0315 from the DOD. D.M.B. was supported by Postdoctoral training grant T32 CA 09579 from the NCI.

Received: September 5, 2003

Revised: February 13, 2004

Accepted: March 8, 2004

Published: April 19, 2004

References

- Abdel-Ghany, M., Cheng, H.C., Elble, R.C., and Pauli, B.U. (2001). The breast cancer beta 4 integrin and endothelial human CLCA2 mediate lung metastasis. *J. Biol. Chem.* 276, 25438–25446.
- Altschul, S.F., Madden, T.L., Schaffer, A.A., Zhang, J., Zhang, Z., Miller, W., and Lipman, D.J. (1997). Gapped BLAST and PSI-BLAST: a new generation of protein database search programs. *Nucleic Acids Res.* 25, 3389–3402.
- Amer, M.H. (1982). Chemotherapy and pattern of metastases in breast cancer patients. *J. Surg. Oncol.* 19, 101–105.
- Arap, W., Pasqualini, R., and Ruoslahti, E. (1998). Cancer treatment by targeted drug delivery to tumor vasculature in a mouse model. *Science* 279, 377–380.
- Arap, W., Haedicke, W., Bernasconi, M., Kain, R., Rajotte, D., Krajewski, S., Ellerby, H.M., Bredesen, D.E., Pasqualini, R., and Ruoslahti, E. (2002). Targeting the prostate for destruction through a vascular address. *Proc. Natl. Acad. Sci. USA* 99, 1527–1531.
- Aslakson, C.J., and Miller, F.R. (1992). Selective events in the metastatic process defined by analysis of the sequential dissemination of subpopulations of a mouse mammary tumor. *Cancer Res.* 52, 1399–1405.
- Berlin, O., Samid, D., Donthineni-Rao, R., Akesson, W., Amiel, D., and Woods, V.L., Jr. (1993). Development of a novel spontaneous metastasis model of human osteosarcoma transplanted orthotopically into bone of athymic mice. *Cancer Res.* 53, 4890–4895.
- Boogerd, W. (1996). Central nervous system metastasis in breast cancer. *Radiother. Oncol.* 40, 5–22.
- Chambers, A.F., Groom, A.C., and MacDonald, I.C. (2002). Dissemination and growth of cancer cells in metastatic sites. *Nat. Rev. Cancer* 2, 563–572.
- Cheng, H.C., Abdel-Ghany, M., Elble, R.C., and Pauli, B.U. (1998). Lung endothelial dipeptidyl peptidase IV promotes adhesion and metastasis of rat breast cancer cells via tumor cell surface-associated fibronectin. *J. Biol. Chem.* 273, 24207–24215.
- Dexter, D.L., Kowalski, H.M., Blazar, B.A., Fligiel, Z., Vogel, R., and Heppner, G.H. (1978). Heterogeneity of tumor cells from a single mouse mammary tumor. *Cancer Res.* 38, 3174–3181.
- Elble, R.C., Widom, J., Gruber, A.D., Abdel-Ghany, M., Levine, R., Goodwin, A., Cheng, H.C., and Pauli, B.U. (1997). Cloning and characterization of lung-endothelial cell adhesion molecule-1 suggest it is an endothelial chloride channel. *J. Biol. Chem.* 272, 27853–27861.
- Fidler, I.J. (2001). Seed and soil revisited: contribution of the organ microenvironment to cancer metastasis. *Surg. Oncol. Clin. N. Am.* 10, 257–269.
- Glasgow, J. (1998). Proceedings, Sixth International Conference on Intelligent Systems for Molecular Biology: June 28–July 1, 1998, Montreal, Quebec (Menlo Park, CA: AAAI Press).
- Harris, J., Morrow, M., and Norton, L. (1997). Malignant tumors of the breast. In *Cancer: Principles and Practice of Oncology* (Philadelphia: Lippincott-Raven), pp. 1557–1616.
- Hoffman, J.A., Laakkonen, P., Porkka, K., Bernasconi, M., and Ruoslahti, E. (2004). *In vivo* and *ex vivo* selections using phage-displayed libraries. In *Phage Display: A Practical Approach*, T. Clackson and H. Lowman, eds. (Oxford, UK: Oxford University Press).
- Johnson, R.C., Zhu, D., Augustin-Voss, H.G., and Pauli, B.U. (1993). Lung endothelial dipeptidyl peptidase IV is an adhesion molecule for lung-metastatic rat breast and prostate carcinoma cells. *J. Cell Biol.* 121, 1423–1432.
- Kamby, C., Dirksen, H., Vejborg, I., Daugaard, S., Guldhammer, B., Rossing, N., and Mouridsen, H.T. (1987). Incidence and methodologic aspects of the occurrence of liver metastases in recurrent breast cancer. *Cancer* 59, 1524–1529.
- Krogh, A., Larsson, B., von Heijne, G., and Sonnhammer, E.L. (2001). Predicting transmembrane protein topology with a hidden Markov model: application to complete genomes. *J. Mol. Biol.* 305, 567–580.
- Kyte, J., and Doolittle, R.F. (1982). A simple method for displaying the hydropathic character of a protein. *J. Mol. Biol.* 157, 105–132.
- Laakkonen, P., Porkka, K., Hoffman, J.A., and Ruoslahti, E. (2002). A tumor-homing peptide with a targeting specificity related to lymphatic vessels. *Nat. Med.* 8, 751–755.
- Laemmli, U.K. (1970). Cleavage of structural proteins during the assembly of the head of bacteriophage T4. *Nature* 227, 680–685.
- Lal, A., Lash, A.E., Altschul, S.F., Velculescu, V., Zhang, L., McLendon, R.E., Marra, M.A., Prange, C., Morin, P.J., Polyak, K., et al. (1999). A public database for gene expression in human cancers. *Cancer Res.* 59, 5403–5407.
- Lash, A.E., Tolstoshev, C.M., Wagner, L., Schuler, G.D., Strausberg, R.L., Riggins, G.J., and Altschul, S.F. (2000). SAGEmap: a public gene expression resource. *Genome Res.* 10, 1051–1060.
- Luo, L., Salunga, R.C., Guo, H., Bittner, A., Joy, K.C., Galindo, J.E., Xiao, H., Rogers, K.E., Wan, J.S., Jackson, M.R., and Erlander, M.G. (1999). Gene expression profiles of laser-captured adjacent neuronal subtypes. *Nat. Med.* 5, 117–122.
- McIntosh, D.P., Tan, X.Y., Oh, P., and Schnitzer, J.E. (2002). Targeting endothelium and its dynamic caveolae for tissue-specific transcytosis in vivo: a pathway to overcome cell barriers to drug and gene delivery. *Proc. Natl. Acad. Sci. USA* 99, 1996–2001.

- Mechler, B.M. (1987). Isolation of messenger RNA from membrane-bound polysomes. *Methods Enzymol.* 152, 241–248.
- Miller, F.R., Miller, B.E., and Heppner, G.H. (1983). Characterization of metastatic heterogeneity among subpopulations of a single mouse mammary tumor: heterogeneity in phenotypic stability. *Invasion Metastasis* 3, 22–31.
- Muller, A., Homey, B., Soto, H., Ge, N., Catron, D., Buchanan, M.E., McClanahan, T., Murphy, E., Yuan, W., Wagner, S.N., et al. (2001). Involvement of chemokine receptors in breast cancer metastasis. *Nature* 410, 50–56.
- Orr, F.W., and Wang, H.H. (2001). Tumor cell interactions with the microvasculature: a rate-limiting step in metastasis. *Surg. Oncol. Clin. N. Am.* 10, 357–381.
- Pasqualini, R., and Ruoslahti, E. (1996). Organ targeting in vivo using phage display peptide libraries. *Nature* 380, 364–366.
- Porkka, K., Laakkonen, P., Hoffman, J.A., Bernasconi, M., and Ruoslahti, E. (2002). A fragment of the HMGN2 protein homes to the nuclei of tumor cells and tumor endothelial cells in vivo. *Proc. Natl. Acad. Sci. USA* 99, 7444–7449.
- Price, J.E., Polyzos, A., Zhang, R.D., and Daniels, L.M. (1990). Tumorigenicity and metastasis of human breast carcinoma cell lines in nude mice. *Cancer Res.* 50, 717–721.
- Pulaski, B.A., and Ostrand-Rosenberg, S. (1998). Reduction of established spontaneous mammary carcinoma metastases following immunotherapy with major histocompatibility complex class II and B7.1 cell-based tumor vaccines. *Cancer Res.* 58, 1486–1493.
- Radinsky, R. (1995). Modulation of tumor cell gene expression and phenotype by the organ-specific metastatic environment. *Cancer Metastasis Rev.* 14, 323–338.
- Rajotte, D., and Ruoslahti, E. (1999). Membrane dipeptidase is the receptor for a lung-targeting peptide identified by in vivo phage display. *J. Biol. Chem.* 274, 11593–11598.
- Rajotte, D., Arap, W., Hagedorn, M., Koivunen, E., Pasqualini, R., and Ruoslahti, E. (1998). Molecular heterogeneity of the vascular endothelium revealed by in vivo phage display. *J. Clin. Invest.* 102, 430–437.
- Ruoslahti, E. (2002). Specialization of tumour vasculature. *Nat. Rev. Cancer* 2, 83–90.
- Rutgers, E.J., van Slooten, E.A., and Kluck, H.M. (1989). Follow-up after treatment of primary breast cancer. *Br. J. Surg.* 76, 187–190.
- Tomin, R., and Donegan, W.L. (1987). Screening for recurrent breast cancer—its effectiveness and prognostic value. *J. Clin. Oncol.* 5, 62–67.
- van 't Veer, L.J., Dai, H., van de Vijver, M.J., He, Y.D., Hart, A.A., Mao, M., Peterse, H.L., van der Kooy, K., Marton, M.J., Witteveen, A.T., et al. (2002). Gene expression profiling predicts clinical outcome of breast cancer. *Nature* 415, 530–536.
- Weiss, L. (1992). Comments on hematogenous metastatic patterns in humans as revealed by autopsy. *Clin. Exp. Metastasis* 10, 191–199.

Drug Identification through in vivo Screening of Chemical Libraries

Darren M. Brown, Maurizio Pellecchia, and
Erkki Ruoslahti*^[a]

Specific cell-surface molecules can direct leukocytes and certain tumor cells to particular organs.^[1–3] Recent work by our group has shown that peptides, selected by using the in vivo phage-screening approach, are also capable of mediating selective in vivo localization of phage to individual organs as well as tumors.^[4–6] To develop our targeting technology beyond peptide-based systems, we investigated the feasibility of screening a chemical library to identify small molecules other than peptides that possess a preferential affinity for particular organs or tissues. As a proof of principle, we screened

[a] Dr. D. M. Brown, Prof. M. Pellecchia, Prof. E. Ruoslahti
Cancer Research Center, The Burnham Institute
10901 North Torrey Pines Road, La Jolla, CA 92037 (USA)
Fax: (+1) 858-646-3198
E-mail: ruoslahti@burnham.org

two different chemical libraries *in vivo* and identified three compounds that preferentially accumulated in individual organs: a pharmacologically active benzodiazepine localized to the brain, another compound specifically homed in on the liver, and the third on the kidneys. These results show that it is possible to use *in vivo* chemical library screening to identify compounds that distribute themselves to specific sites in the body. Such knowledge can focus drug discovery on compounds with promising pharmacokinetic and tissue specificity profiles.

For *in vivo* screening of chemical libraries, we injected mixtures of small molecules into the circulation of mice, harvested selected organs in organic solvent to precipitate proteins, and detected the presence of compounds from the library in the soluble phase by mass spectrometry. We initially tested a library of ten compounds. Mass-spectrometric analysis of extracts from organs harvested 10 min after the intravenous injection of the library showed that one compound preferentially accumulated in the brain (Figure 1A). Breaking the code for the compounds revealed this 301 Da compound to be a benzodiazepine known as Oxazepam.^[7] A biologically inactive 265 Da benzodiazepine also present in the library was not detected in the brain (Figure 1A). Thus, it appeared possible to obtain organ-targeting small molecules by screening chemical libraries *in vivo*. We also learned from these early studies that it was easier to detect library compounds and differentiate them from endogenous tissue molecules in organic extracts analyzed by electrospray mass spectrometry when the library molecules had molar masses greater than 300 Da.

To test a larger library, we assembled a mixture of 75 compounds with molar masses between 300 and 600 Da and screened for compounds that home in on the brain, liver, lungs, or kidneys. Mass spectrometry performed on organ extracts from library-injected mice identified ten molecules as candidate organ-homing compounds. These ten compounds were tested individually for their ability to specifically target individual organs. Compounds 5862461 and 6074428 were found to accumulate in the kidneys (Figure 1B and C). The other tissues tested negative for these two compounds. Compound 5343617 was found primarily in the liver and, to a lesser extent, the lungs and kidneys (Figure 1D). The spectral patterns of compounds 5862461 and 5343617 were particularly distinct because these compounds contain bromine, which exists as two equally abundant natural isotopes,^[8] and causes a characteristic two-mass-unit split in the spectral peak (Figure 1B, inset). One compound accumulated in the lungs, kidneys, and liver, but not the brain; and another localized to the brain, kidneys, and liver, but not the lungs (data not shown). These compounds are likely to bind to receptors that are expressed in more than one tissue, but the varying tissue selectivity of these compounds clearly indicates tissue-specific homing. Extracts from the organs of control-injected mice confirmed that no molecules matched the spectral pattern of the homing compounds. Two other candidate organ-homing compounds localized to all

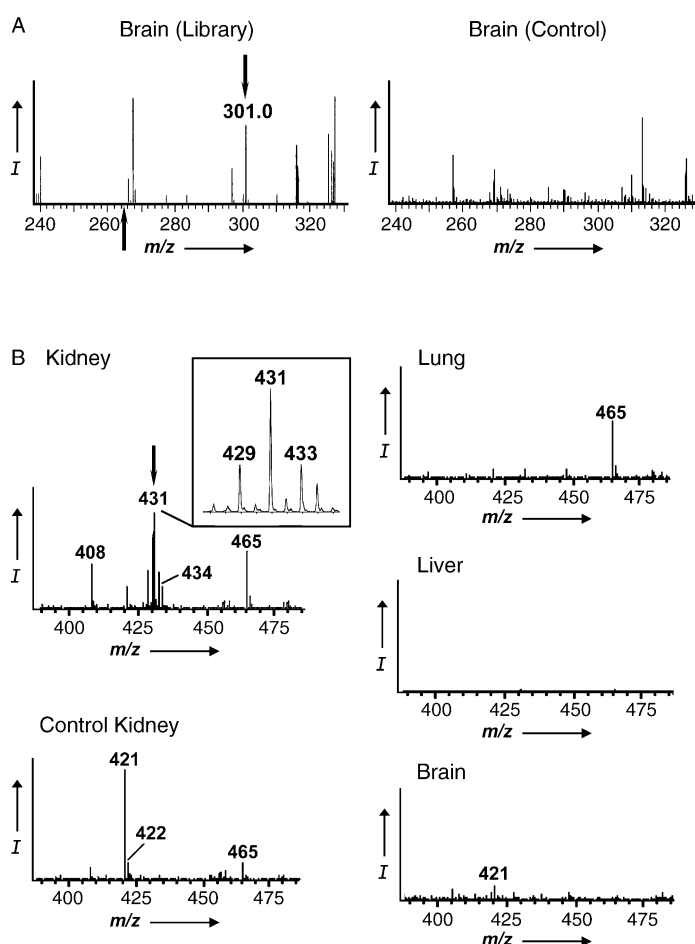


Figure 1. *In vivo* targeting of small molecules to particular organs. A) Detection of the benzodiazepine, Oxazepam, in the brain 10 min after intravenous injection with a ten-compound library. "Control" mice were injected with vehicle alone. The downward pointing arrow denotes the spectral peak for Oxazepam. The arrow below the axis denotes the m/z of the biologically inactive benzodiazepine in the library. No peak is seen at this position. B–D) Mice were intravenously injected with individual compounds from the 75-member library, and tissues were analyzed 10 min later by mass spectrometry. B) Detection of compound 5862461 in the kidneys after intravenous injection and circulation for 10 min. "Control" denotes mice injected just with DMSO. C) Compound 6074428 targets primarily the kidneys. D) Compound 5343617 targets the liver and lungs. Compound peak heights are shown as relative signal intensity (I). A "+" denotes compound-injected mice and "–" denotes DMSO-injected mice. The downward pointing arrows mark the spectral peaks for the organ-homing compounds.

four tested organs. These compounds might bind to molecules present in all tissues, but it is also possible that their concentration in blood remaining in tissues is high enough to allow detection. As these compounds did not show any tissue-specific homing, we did not study them further. For three compounds, the specific organ homing could not be confirmed in individual testing. The remaining 68 compounds were not detected in any tissue, apparently because they did not sufficiently accumulate in any of the test tissues to bring the concentration above the detection limit.

We next quantified the organ accumulation of the three compounds with the most promising organ-homing properties. We used the mass spectrometer to compare the relative

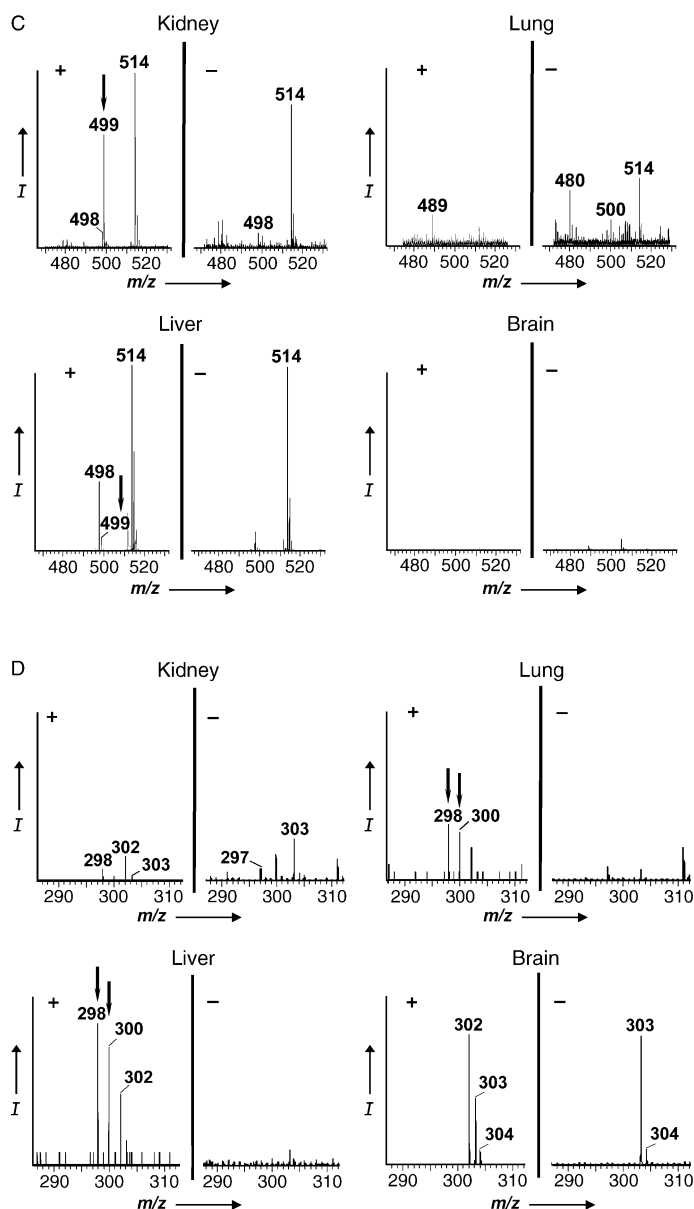
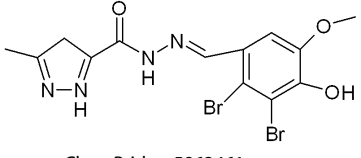
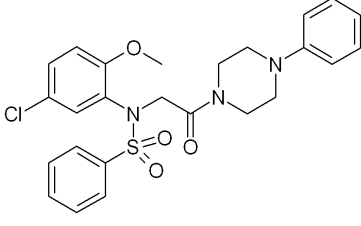
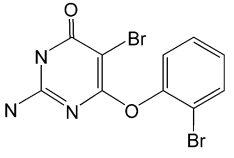


Figure 1. (Continued)

amounts of targeting compound in extracts of different organs. Compound 6074428 was at least 30-fold more concentrated in the kidneys than in the liver, lungs, and brain (Table 1). At least 2.4 times more compound 5862461 localized to the kidneys than to the liver, lungs, and brain. Compound 5343617 accumulated very strongly in the liver; about 55-fold higher levels were detected in the liver than in the kidneys, which contained a trace amount of the compound. This compound was also present at moderate levels in the lungs, but was not detectable in the brain. As each of these three compounds accumulated in different tissues, their organ-selective homing is clearly specific and not due to the presence of blood or nonspecific trapping in the target organs.

We then measured two parameters that influence the sensitivity of *in vivo* chemical library screening. First, we used the

Table 1. Homing specificity of compounds and their accumulation in target organs. The structure, target organ, and homing activity of the three organ-homing compounds are shown. The quantity of homing compound in the target organs 10 min after an intravenous injection of individual compounds was determined as described in the Experimental Section. The accumulation of targeting compound was expressed as normalized signal intensity level relative to the detection limit.

Organ-targeting compound	Target Organ(s)	Signal Intensity ^[a] (fold higher than detection limit)
 ChemBridge 5862461	kidney	2.4-fold (± 0.6)
 ChemBridge 6074428	kidney	32-fold (± 5.4)
 ChemBridge 5343617	liver lung kidney	67-fold (± 2.1) 8.2-fold (± 0.6) 1.2-fold (± 0.3)

[a] Accumulation data is represented as mean percentage (\pm standard deviation) for two experiments per variable.

mass spectrometer to analyze the spectral intensity of nine different compounds added to organ extracts, and found that the smallest amount of an individual compound that could be detected in a tissue extract was between 34 and 215 pmol. For the second parameter, we determined the smallest amount of homing compound that could be injected and still detected in our *in vivo* screening system. For this analysis, the signal intensity of compound 6074428 in kidney extracts from mice injected with various amounts (2 to 125 nmol) of the compound was determined by mass spectrometry. The spectral peak at *m/z* 499 from compound 6074428 was detectable in kidney extracts from mice injected with as little as 7.8 nmol of targeting compound (Figure 2). In the initial library screen with 75 compounds, about 33 nmol of each molecule was present in the injected library mix. Therefore, it is likely that 300 compounds could be tested in a single screening round for organ-targeting compounds. Given the ease and simplicity of this screening technique, a library of 10000 compounds could be screened *in vivo* in a few weeks with a relatively small-scale effort.

We encountered some limitations with *in vivo* chemical library screening that will be addressed in future studies. The volume of library injected into the mice (25 μ L) was limited by

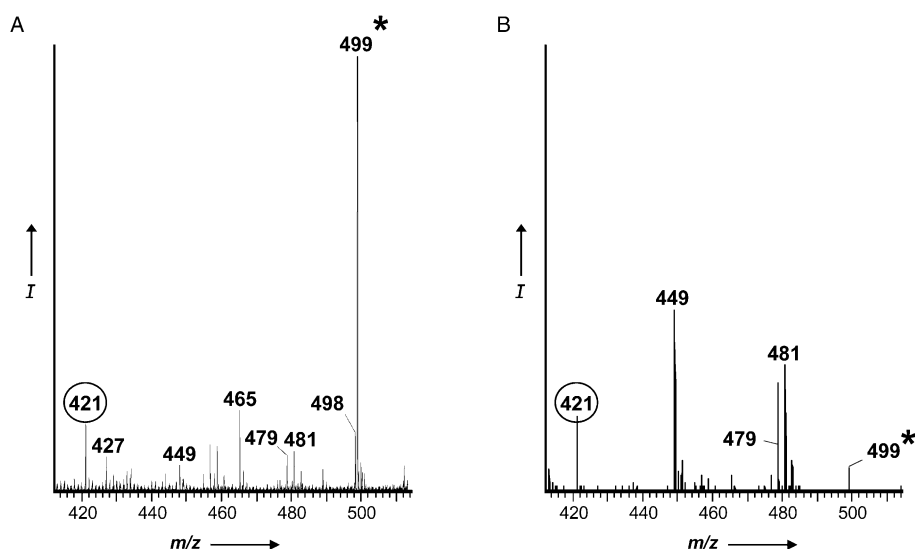


Figure 2. The lower detection limit of *in vivo* chemical library screening. Mass-spectrometric analysis of kidney extracts from mice injected with either A) 125 nmol or B) 7.8 nmol of compound 6074428. The peak intensities were normalized to the height of an endogenous tissue molecule at m/z 421 that was consistently detected in kidney extracts (circled). The asterisk denotes the spectral peak for the kidney-homing compound, 6074428. The spectral peak intensities of other endogenous tissue molecules (e.g. the molecules at m/z 449 and 481) varied between experiments; as a result, they were not used to normalize the spectral peak intensities of compound 6074428. Compound peak heights are shown as relative signal intensity (I).

the toxicity of the solvent, dimethyl sulfoxide (DMSO). With a less toxic solvent, it should be possible to inject up to 200 μ L of library and screen potentially as many as 3600 compounds in one round. Emulsifying agents like Cremophor® EL, Emulphor®, polysorbate 80, Solutol® HS15, or solvents containing *N*-methylpyrrolidone could be used as an alternative to DMSO when solubilizing the chemical library before *in vivo* screening. In addition, only 1% of the organ extract could be analyzed by mass spectrometry due to the presence of various endogenous tissue compounds in the acetone extracts. A more selective extraction and prepurification method could increase the sensitivity of the compound detection by mass spectrometry.

The biological basis for the targeting activity of some of the compounds identified in the screen has yet to be determined. However, it seems likely that binding to benzodiazepine receptors mediated the brain-homing activity of the pharmacologically active benzodiazepine, as the related inactive compound did not accumulate in the brain. The kidney-homing compound, 6074428, contains a benzenesulfonamide group that is known to have diuretic properties; perhaps this group mediates the kidney-homing activity of this compound.

This work provides the first demonstration that it is possible to conduct large-scale screening of chemical libraries *in vivo*. Such screening can identify targeted small molecules for use in a variety of applications and has some advantages over previous methods. *In vivo* phage screening primarily targets the vascular endothelium. Low-molecular-weight chemical compounds can target the vasculature, but are also likely to gain access to parenchymal cells in tissues. That parenchymal cells can be targets is suggested by our recovery of a benzodiazepine as a brain-homing molecule, as most receptors for these

compounds are on the neurons. As an additional advantage, this screening approach does not require encoded or tagged library compounds. This is an improvement over other approaches that require separate chemistries for coupling different small molecules to synthetic or genetically engineered tags such as bacteriophage.^[9] In addition, the absence of compound tags eliminates the possibility of interference by the tag with the *in vivo* homing activity.

The localization of selective molecules to specific “addresses” on the endothelium suggests that each tissue puts a specialized signature on its vasculature.^[10] Organ-specific vascular molecules are attractive targets for the delivery of therapeutics to particular sites. By conjugating targeting moieties to drugs, diseases such as

cancer can be treated with increased efficacy and fewer side effects;^[11,12] phage-derived homing peptides and peptidomimetics have been used in this manner to target malignant tumors.^[11–15] Organ-homing compounds isolated from chemical libraries are likely to be useful for similar purposes.

In vivo screening may also identify small molecules that have pharmacological effects at the target organ. The identification of a neuroactive compound and a potential diuretic as brain- and kidney-homing molecules, respectively, suggests that this may be possible. Thus, *in vivo* screening has the potential to advance drug discovery; it allows pharmacokinetics and specificity of action to be studied among large numbers of candidate compounds, or even from completely random libraries. Such approaches may accelerate the discovery and development of new drugs.

Experimental Section

A library of ten small molecules with molecular weights between 200 and 300 Da was prepared by a person not involved in the *in vivo* experimentation and was tested blindly. The ten-compound library was prepared in phosphate buffer (40 mM, pH 7.2) with each molecule at a final concentration of 1 mM. A larger library of small molecules was prepared from 75 organic molecules (purchased from ChemBridge, San Diego, CA) with molecular weights between 300 and 600 Da. The library compounds were randomly selected from a 420 000-member ChemBridge library, with each compound satisfying the following criteria: 1) the partition coefficient, expressed numerically as $\log P$, was less than 5 and 2) the molecular weights of the compounds differed from each other by at least 4 Da. There was high structural diversity in the library, given that the only limitation was the compounds selected from the 420 000-

member parent library needed to fit the parameters described above. The 75-compound library was resuspended in DMSO, with each molecule at a final concentration of 1.33 mM.

To identify molecules that localize to particular organs, two-month-old female Balb/c mice were anesthetized with avertin ($0.15 \mu\text{L g}^{-1}$) administered intraperitoneally. In experiments with the ten-compound library, 200 μL of library solution (200 nmol per compound) was intravenously injected into the tail vein. With the 75-compound library, 25 μL of library solution (33 nmol per compound) was intravenously injected into the tail-vein. After 10 min of circulation, the lungs, liver, kidneys, and brain were removed. We found 5–15 min to be optimal for the screening of intravenously injected phage for homing to individual tissues and tumors,^[16] and we wanted to keep the time short enough to prevent metabolism of the injected compounds, which would change their mass-spectrometric signature.

The organs were washed with PBS (5 mL) to remove excess blood and weighed. Each organ was mixed with acetone (5 mL) and then homogenized with a Handishear hand-held homogenizer (Virtis, Gardiner, NY). For certain organ homogenates, a control compound (ChemBridge 5116670, molar mass 340 Da, 0.25–2.5 nmol) was added as a reference to quantify the amount of homing compound in target organs. The organ/acetone homogenates were transferred to 15 mL centrifuge tubes and incubated at -80°C for 12 h to precipitate the proteins. Following centrifugation for 30 min at 3000g and 4°C , the supernatants were recovered and dried in a Speed Vac. A set of control organ extracts was also prepared from mice that were injected with pure DMSO (25 μL).

The dried organ extracts were resuspended in methanol (100 μL), spun in a vortex for about 10–20 min, and separated in a centrifuge to turn the debris into pellets. The supernatants were recovered, further diluted 1:20 in methanol, and the diluted sample (20 μL) was analyzed on a Waters Micromass[®] LCT mass spectrometer (Milford, MA) at The Scripps Research Institute (La Jolla, CA). Samples were injected into the electrospray by using a mobile solvent phase of methanol/water/acetonitrile (90:9:1). By comparing the masses of the individual compounds and the molecules in the organ extracts of mice injected with DMSO to the molecules in the organ extracts from the mice injected with the library, we were able to identify molecules in the library that localized to a particular organ.

The accumulation of compounds in organs was measured as follows:

We first measured the signal intensities of the targeting compounds using the mass spectrometer and compared them to the signal intensity of a standard compound that was added to the organ extracts; this enabled us to normalize the intensity value of compound peaks from experiments performed on different days. We then determined the smallest amount of an individual compound that could be detected in a tissue extract using mass spectrometry by measuring the spectral intensity of nine different compounds added in small amounts to organ extracts. The detection limit was defined as the spectral intensity level halfway between the background noise and the spectral intensity level generated from the smallest detectable amount of compound in organ extracts (averaged from nine different compounds whose spectra were analyzed and displayed with a scanning window of m/z 290–610). The normalized intensity values for homing compounds were compared to the detection limit to determine the degree of enrichment of compound in target organs relative to background levels. These enrichment values were not comparable from com-

pound to compound, since each compound has a different ionization efficiency and stability on the mass spectrometer.

The Burnham Institute Animal Research Committee approved the animal experimentation in compliance with the relevant US laws.

Acknowledgements

This work was supported by the U.S. National Cancer Institute (PO1 CA82713 and P30 CA30199) and the U.S. Department of Defense (DAMD17-02-1-0315). D.M.B. was supported by Post-doctoral training grant T32 CA09579 from the U.S. National Cancer Institute. We thank Drs. Eva Engvall and Douglas Hanahan for their valuable comments on the manuscript, and Roslind Varghese for editing.

Keywords: drug delivery • in vivo screening • mass spectrometry • tissue-specificity

- [1] I. J. Fidler, *Surg. Oncol. Clin. North Am.* **2001**, *10*, 257.
- [2] A. Müller, B. Homey, H. Soto, N. Ge, D. Catron, M. E. Buchanan, T. McClanahan, E. Murphy, W. Yuan, S. N. Wagner, J. L. Barrera, A. Mohar, E. Verastegui, A. Zlotnik, *Nature* **2001**, *410*, 50.
- [3] E. J. Kunkel, E. C. Butcher, *Immunity* **2002**, *16*, 1.
- [4] R. Pasqualini, E. Ruoslahti, *Nature* **1996**, *380*, 364.
- [5] D. Rajotte, W. Arap, M. Hagedorn, E. Koivunen, R. Pasqualini, E. Ruoslahti, *J. Clin. Invest.* **1998**, *102*, 430.
- [6] P. Laakkonen, K. Porkka, J. A. Hoffman, E. Ruoslahti, *Nat. Med. (N.Y. U.S.)* **2002**, *8*, 751.
- [7] *Clinical Handbook of Psychotropic Drugs*, 11th rev. ed. (Eds.: K. Z. Bezchlibnyk-Butler, J. J. Jeffries), Huber, Seattle, **2001**, p. 273.
- [8] *CRC Handbook of Chemistry and Physics*, 84 ed. (Ed.: D. R. Lide), CRC Press, Boca Raton, **2003**, p. 11.
- [9] T. F. Woiwode, J. E. Haggerty, R. Katz, M. A. Gallop, R. W. Barrett, W. J. Dower, S. E. Cwirla, *Chem. Biol.* **2003**, *10*, 847.
- [10] E. Ruoslahti, *Nat. Rev. Cancer* **2002**, *2*, 83.
- [11] W. Arap, W. Haedicke, M. Bernasconi, R. Kain, D. Rajotte, S. Krajewski, H. M. Ellerby, D. E. Bredesen, R. Pasqualini, E. Ruoslahti, *Proc. Natl. Acad. Sci. USA* **2002**, *99*, 1527.
- [12] F. Curnis, A. Sacchi, L. Borgna, F. Magni, A. Gasparri, A. Corti, *Nat. Biotechnol.* **2000**, *18*, 1185.
- [13] J. D. Hood, M. Bednarski, R. Frausto, S. Guccione, R. A. Reisfeld, R. Xiang, D. A. Cheres, *Science* **2002**, *296*, 2404.
- [14] D. Hallahan, L. Geng, S. Qu, C. Scarfone, T. Giorgio, E. Donnelly, X. Gao, J. Clanton, *Cancer Cell* **2003**, *3*, 63.
- [15] W. Arap, R. Pasqualini, E. Ruoslahti, *Science* **1998**, *279*, 377.
- [16] J. A. Hoffman, P. Laakkonen, K. Porkka, M. Bernasconi, E. Ruoslahti in *Phage Display: A Practical Approach* (Eds.: T. Clackson, H. Lowman), Oxford University Press, Oxford, **2004**.

Received: November 19, 2003

Nucleolin expressed at the cell surface is a marker of endothelial cells in angiogenic blood vessels

Sven Christian,¹ Jan Pilch,¹ Maria E. Akerman,^{1,2} Kimmo Porkka,^{1,3} Pirjo Laakkonen,¹ and Erkki Ruoslahti¹

¹Cancer Research Center, The Burnham Institute, La Jolla, CA 92037

²Department of Bioengineering, University of California, San Diego, La Jolla, CA 92093

³Department of Medicine, Division of Hematology, Stem Cell and Basic Science Laboratory, Helsinki University Central Hospital, FIN-00029 HUS, Helsinki, Finland

A tumor-homing peptide, F3, selectively binds to endothelial cells in tumor blood vessels and to tumor cells. Here, we show that the cell surface molecule recognized by F3 is nucleolin. Nucleolin specifically bound to an F3 peptide affinity matrix from extracts of cultured breast carcinoma cells. Antibodies and cell surface biotin labeling revealed nucleolin at the surface of actively growing cells, and these cells bound and internalized fluorescein-conjugated F3 peptide, transporting it into the nucleus. In contrast, nucleolin was exclusively nuclear

in serum-starved cells, and F3 did not bind to these cells. The binding and subsequent internalization of F3 were blocked by an antinucleolin antibody. Like the F3 peptide, intravenously injected antinucleolin antibodies selectively accumulated in tumor vessels and in angiogenic vessels of implanted "matrigel" plugs. These results show that cell surface nucleolin is a specific marker of angiogenic endothelial cells within the vasculature. It may be a useful target molecule for diagnostic tests and drug delivery applications.

Introduction

Tumor growth is critically dependent on angiogenesis, which is the sprouting of new blood vessels from existing ones (Hanahan and Folkman, 1996). Angiogenic vessels differ from normal vessels in their morphological and molecular characteristics. The molecular markers of angiogenic vessels include endothelial growth factor receptors, integrins, proteolytic enzymes, and extracellular matrix components (Ruoslahti, 2002), as well as membrane proteins of unknown function (St Croix et al., 2000; Christian et al., 2001a). A specific marker for tumor lymphatics has also been described previously (Laakkonen et al., 2002).

The molecular markers that distinguish tumor vasculature from that of normal tissues are important in a number of ways. Many of the molecules that are selectively expressed in tumor blood vessels play a functional role in development and maintenance of new blood vessels. Examples include endothelial cell growth factor receptors and integrins (Eliceiri

and Cheresh, 1999; Ferrara and Alitalo, 1999; Hynes, 2002), matrix metalloproteases (Brooks et al., 1998; Bergers et al., 2000), and aminopeptidase N (Pasqualini et al., 2000). Blocking the function of these proteins inhibits angiogenesis. Furthermore, these and other molecules selectively expressed in tumor vasculature can be made use of in targeting diagnostic and therapeutic agents in tumors (Arap et al., 1998; Nilsson et al., 2001; El-Sheikh et al., 2002; Hood et al., 2002).

The identification of additional tumor blood vessel markers helps in the understanding of angiogenesis and could be useful for tumor targeting. We set out to identify the molecule, "receptor," that is recognized by a tumor-homing peptide recently identified by our laboratory. This peptide, F3, was discovered in a screening procedure that used a phage-displayed cDNA library and combined ex vivo screening on cell suspensions prepared from mouse bone marrow and in vivo screening for tumor homing. F3 is a 34-amino acid fragment of a high mobility group protein, HMG2N (Porkka et al., 2002). F3 homes to the vasculature of various types of tumors by binding to the endothelial cells. F3 also binds to a subpopulation of bone marrow cells that may be precursors for endothelial cells. In some tumors, the F3

Address correspondence to Erkki Ruoslahti, The Burnham Institute, 10901 North Torrey Pines Rd., La Jolla, CA 92037. Tel.: (858) 646-3125. Fax: (858) 646-3198. email: ruoslahti@burnham.org

Pirjo Laakkonen's present address is Molecular/Cancer Biology Laboratory, Biomedicum Helsinki, University of Helsinki, P.O. Box 63, Haartmaninkatu 8, FIN-00014 Helsinki, Finland.

Key words: angiogenesis; bone marrow; cell-penetrating peptides; nuclear proteins

Abbreviation used in this paper: HUVEC, human umbilical vein endothelial cell.

peptide also recognizes the tumor cells. A striking property of the F3 peptide is that it is internalized by its specific target cells and transported to the nucleus.

We have now identified cell surface-expressed nucleolin as the receptor for F3 on tumor cells and angiogenic endothelial cells. Cell surface nucleolin expression is a novel angiogenesis marker. It provides a tool for studying tumor angiogenesis, including the contribution of precursor cells to this process, and for targeting drugs into tumors.

Results

Nucleolin binds to F3 in affinity chromatography

The F3 peptide binds to and accumulates within both tumor endothelial cells and tumor cells *in vivo* (Porkka et al., 2002). Because F3 also binds to cultured tumor cells such as the human breast carcinoma cell line MDA-MB-435, we decided to use this cell line to identify a receptor for F3. Affinity chromatography of MDA-MB-435 cell extracts on an F3 peptide affinity matrix revealed a major F3-binding band at a molecular mass of 110 kD and several bands in the 20-kD range that did not bind to a control peptide matrix (Fig. 1 A). Mass spectrometry analysis indicated that the 110-kD band is nucleolin. Although the calculated mass of nucleolin is 76 kD, it migrates at 110 kD in SDS-PAGE, most likely because of posttranslational modifications and high content of negatively charged amino acids in the NH₂-terminal region of the protein (Harms et al., 2001). The 20-kD range bands were identified as various histones.

The identification of the 110-kD protein as nucleolin was confirmed by immunoblotting. A monoclonal antinucleolin antibody, MS-3, revealed a major 110-kD band and faint lower molecular mass bands in the F3-bound material (Fig. 1 B, a). These bands were not present in eluates from the control peptide matrix. The faint bands are probably fragments of nucleolin, as they aligned with some of the several lower molecular mass bands detected by the antibody in a whole cell extract. These results show that the F3 peptide can specifically interact with nucleolin, suggesting nucleolin as a candidate receptor for F3.

We prepared antisera against nucleolin by immunizing rabbits with two different synthetic peptides from the human nucleolin sequence. Affinity-purified antibodies recognized a band that aligned with the 110-kD nucleolin band defined by the MS-3 antibody (Fig. 1 B, b). Like MS-3, the rabbit antibodies also detected smaller molecular mass bands that presumably represent nucleolin fragments. As expected, based on the fact that the immunizing peptides came from different regions of the nucleolin molecule, the sets of minor bands detected by each antibody did not overlap. Immunoblotting showed that the NCL3 antibody also recognizes a 110-kD protein in extracts of mouse cells. (Fig. 1 B, c).

Nucleolin is expressed at the cell surface

To serve as an F3 receptor, nucleolin would have to be present at the cell surface. Nucleolin is primarily known as a nuclear and cytoplasmic protein, but recent studies have shown that a cell surface form of nucleolin also exists (Said et al., 2002; Sinclair and O'Brien, 2002). To determine if F3-binding nucleolin in the MDA-MB-435 cells is ex-

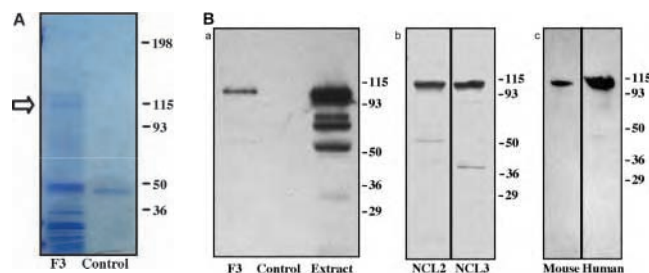


Figure 1. Nucleolin binds to immobilized F3 peptide. (A) SDS gel electrophoresis of Coomassie blue-stained proteins isolated from MDA-MB-435 cell extracts on F3 affinity matrix (F3) or control peptide matrix (Control). The arrow indicates a specific 110-kD band, which was identified as nucleolin by mass spectrometry. (B) Immunoblotting of eluates from F3 and control affinity matrices with a monoclonal mouse antinucleolin antibody (a); immunoblotting of MDA-MB-435 cell extracts with polyclonal rabbit antinucleolin antibodies NCL2 and NCL3 (b); immunoblotting of extracts generated from the human cell line C8161 and the mouse cell line 4T1 with NCL3 (c). The F3 bound material (a, F3) contains full-length nucleolin and a faintly staining 75-kD band. In the original cell extract (a, Extract), the antibody recognizes full-length nucleolin at 110 kD, along with several faster migrating bands (presumably nucleolin fragments), including one at 75 kD. No antinucleolin reactive bands are detected in eluates from the control matrix (a, Control). Affinity-purified polyclonal antibodies NCL2 and NCL3 recognize a band that aligns with the 110-kD nucleolin band in human extracts, and NCL3 crossreacts with mouse nucleolin (c, Mouse). Both antibodies also detect smaller bands that presumably represent nucleolin fragments.

pressed at the cell surface, exponentially growing cells were biotinylated with a cell-impermeable biotin reagent, and cell extracts were subjected to affinity chromatography on immobilized F3. Two biotinylated bands at 110 and 75 kD specifically bound to F3 (Fig. 2 A, a). The surface biotinylated 75-kD band was stronger than the 110-kD band, whereas the opposite was true in the affinity chromatography, possibly because the cell surface expression or accessibility to biotinylation may be different for the two forms. Notably, the histones that bound to the F3 matrix from the cell extract did not become biotin-labeled in intact cells, but were the most prominent F3-binding bands from cell surface-biotinylated serum-starved cultures, which contain many dead cells (Fig. 2 A, b). No nucleolin band was detectable in the serum-starved cells, suggesting a lack of cell surface nucleolin expression.

Nucleolin was also detected at the cell surface of growing MDA-MB-435 in FACS[®] analysis using antibodies. Both the polyclonal NCL3 and monoclonal MS-3 antibodies bound to MDA-MB-435 cells, producing a distinct shift of the fluorescence peak relative to control IgG and nonsurface reactive antibody, respectively. That result was consistent in repeated experiments (Fig. 2 B, a and b). Gating for cells that were negative for propidium iodide uptake showed that the antinucleolin-positive cells were alive and their cell membranes were intact. We used the polyclonal antibody, which gave a stronger signal with the MDA-MB-435 cells than the monoclonal, to test cultured human umbilical vein endothelial cells (HUVECs) for cell surface nucleolin. A small shift in the fluorescence peak was observed (Fig. 2 B, c). These results show that nucleolin is expressed on the surface of the MDA-MB-435

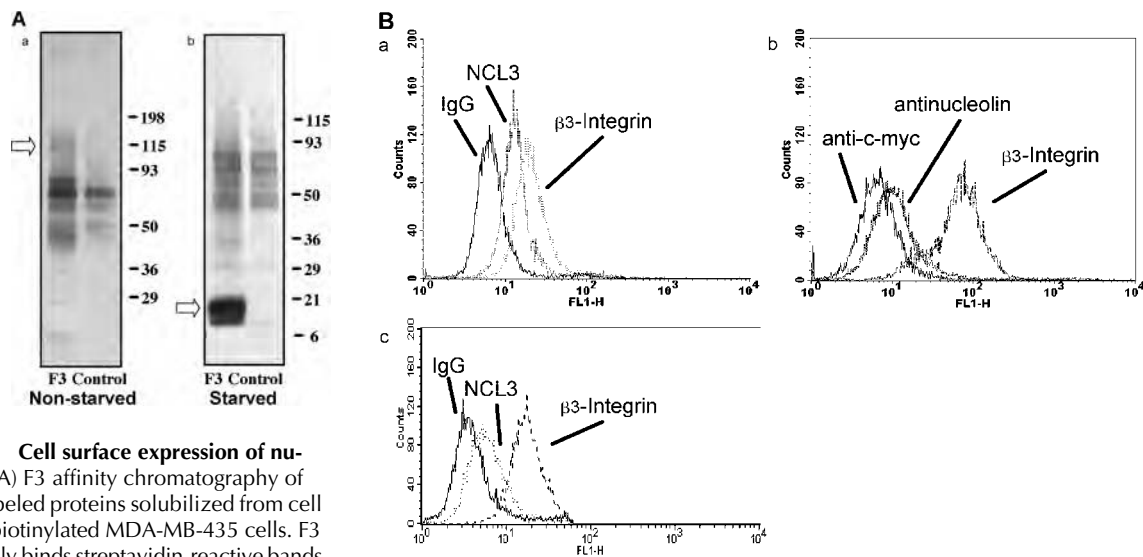


Figure 2. Cell surface expression of nucleolin. (A) F3 affinity chromatography of biotin-labeled proteins solubilized from cell surface-biotinylated MDA-MB-435 cells. F3 specifically binds streptavidin-reactive bands at 110 (arrow) and 75 kD in nonstarved cells (a). These bands are not detectable in serum-starved cells, but a set of low molecular mass bands is prominent (b, arrow).

(B) FACS[®] analysis of antibody binding to MDA-MB-435 cells (a and b) and HUVECs (c). Propidium iodide-negative (living) cells were gated for the analysis. Polyclonal antinucleolin NCL3 (a and c) and monoclonal antinucleolin antibody MS-3 (b) cause a shift of the FACS[®] peak compared with controls (rabbit IgG and an isotype-matched monoclonal antibody with an unrelated specificity, respectively), indicating cell surface expression of nucleolin on the MDA-MB-435 and HUVECs. A positive control, an anti- β 3 integrin, gives a strong shift, reflecting a high cell surface expression of this integrin subunit in both types of cells.

cells and that HUVECs may also express some cell surface nucleolin. Because the presence of many dead cells prevented a FACS[®] analysis on serum-starved MDA-MB-435 cells, we used immunostaining to study their subcellular nucleolin distribution. The NCL3 antibody stained the surface of MDA-MB-435 cells when the cells were actively growing, but there was no surface staining of these cells after they were rendered stationary by serum withdrawal (Fig. 3). Nuclear nucleolin was detected in permeabilized cells under both conditions. These results agree with the cell surface biotinylation data shown in Fig. 2 and suggest that cell surface expression of nucleolin is a characteristic of actively growing cells.

Antinucleolin antibodies inhibit internalization of F3 by cells

Nucleolin has been reported to shuttle between the cytoplasm and the nucleus (Shibata et al., 2002) and between the cell surface and the nucleus (Said et al., 2002). We used antibodies to study whether nucleolin is involved in the internalization and nuclear transport of F3. As shown previously (Porkka et al., 2002), fluorescein-labeled F3 was taken up by the MDA-MB-435 cells and localized in the cytoplasm and nucleus of 100% of the cells (Fig. 4, a–c). Coincubation of the cells with the NCL3 antibody inhibited the appearance of F3 in the cytoplasm and nucleus of the cells (Fig. 4, e–g). Instead, the antibody was internalized into the MDA-MB-435 cells and transported into the nucleus. NCL2, although it bound to the MDA-MB-435 cells, was not internalized and did not inhibit the cytoplasmic and nuclear localization of F3 (Fig. 4, i–k). Neither antibody affected the internalization of the cell-penetrating peptide from the Tat protein (Fig. 4, d, h, and l). These results indicate that F3 binds to cells and is internalized by them in a nucleolin-dependent manner that involves the NH₂-terminal acidic domain of nucleolin.

Internalization of the F3 peptide into cultured cells is independent of heparan sulfates

Next, we determined whether glycosaminoglycans play a role in the internalization of F3 into cells. The F3 peptide is a highly basic peptide and, as such, has an affinity for negatively charged glycosaminoglycans. Previous studies have shown that binding to heparan sulfates can be sufficient for the internalization of a heparan sulfate-binding protein (Roghani and Mos-

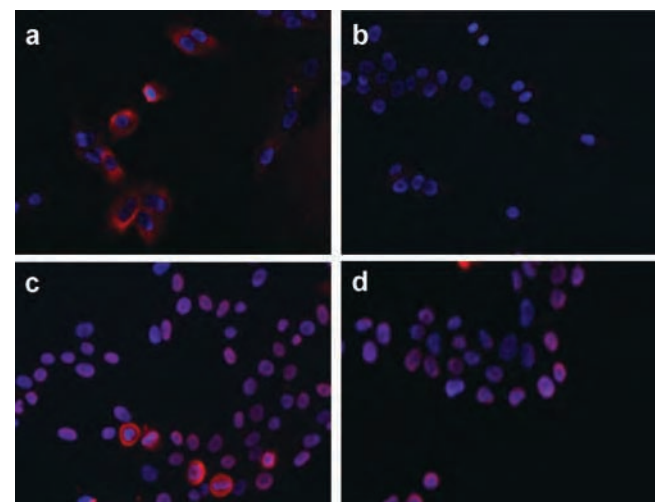
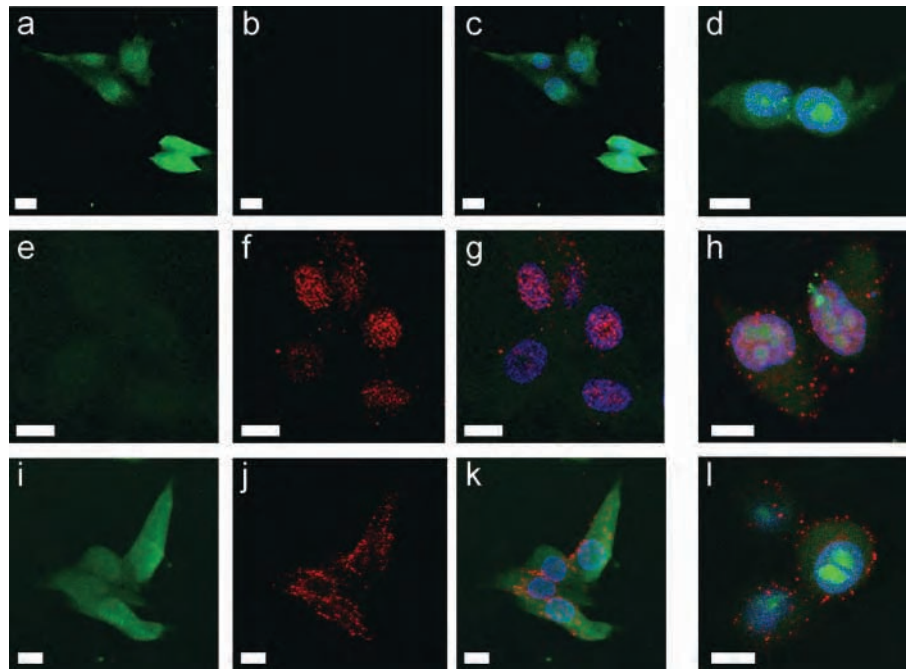


Figure 3. Subcellular distribution of nucleolin in dividing and stationary cells. MDA-MB-435 cells were cultured in standard culture media (a and c) or in media lacking serum (b and d). Nucleolin was detected using polyclonal NCL3 antibody in fixed cells without permeabilizing the cells (a and b) or after permeabilization with Triton X-100 (c and d). Nucleolin appears both on the surface and in the nuclei of the actively growing cells cultured in the standard media, but is exclusively nuclear in serum-starved cells.

Figure 4. Antinucleolin antibodies inhibit F3 internalization by cells.

Exponentially growing MDA-MB-435 cells were incubated with 1 μ M FITC-F3 or FITC-Tat peptide for 2 h at 37°C. FITC-F3 is internalized and transported into the nucleus (a, FITC-F3, green; b, red channel; c, merge). Coincubation with antinucleolin antibody NCL3 inhibits the cellular uptake and subsequent nuclear transport of the peptide (e, F3-FITC, green; f, NCL3, red; g, merge). NCL2 has no influence on uptake of F3 (i, F3-FITC, green; j, NCL2, red; k, merge). Internalization of FITC-Tat peptide (d) is not affected by NCL3 (h) or NCL2 (l). The antibodies were detected with Alexa-594 anti-rabbit IgG (red). Nuclei were stained with DAPI (blue). The images were obtained by confocal microscopy. Bars, 10 μ m.



catelli, 1992). CHO cells that produce no glycosaminoglycans because of a mutated xylosyl transferase gene (pgsA-745 cells; Esko et al., 1985) internalized fluorescein-conjugated F3 and transported it into the nucleus as efficiently as the wild-type cells (Fig. 5). Neither cell type internalized a fluorescein-conjugated control peptide. Thus, glycosaminoglycans do not seem to be involved in the uptake of the F3 peptide into cells.

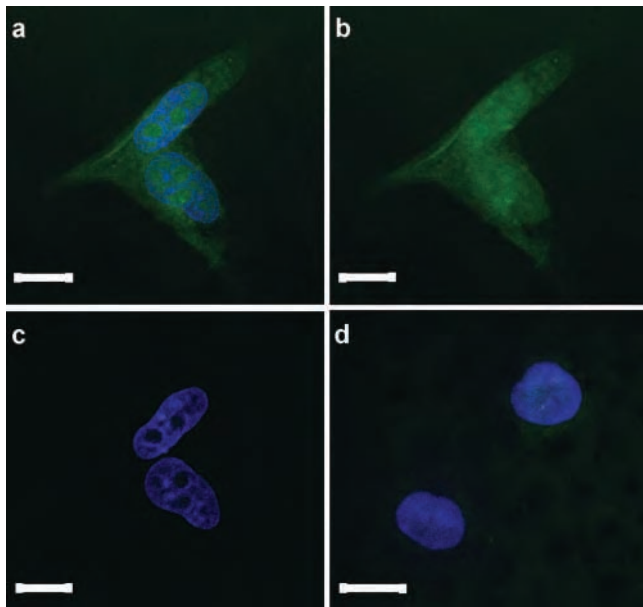


Figure 5. Glycosaminoglycan-deficient cells bind and internalize F3. FITC-F3 is internalized by the glycosaminoglycan-deficient pgsA-745 cells and transported into the nucleus. (a) pgsA-745 cells incubated with FITC-F3 and stained with DAPI to visualize the nuclei. (b and c) The same field as in panel a viewed separately for the F3 fluorescence (b) or the nuclear DAPI staining (c). (d) A FITC-labeled control peptide is not internalized by the pgsA-745 cells. The images were obtained by confocal microscopy. Bars, 10 μ m.

Circulating antinucleolin antibodies selectively localize in angiogenic blood vessels

The F3 peptide, when expressed on the surface of phage, or labeled with fluorescein or quantum dots, selectively homes to tumor blood vessels and vessels in a matrigel angiogenesis

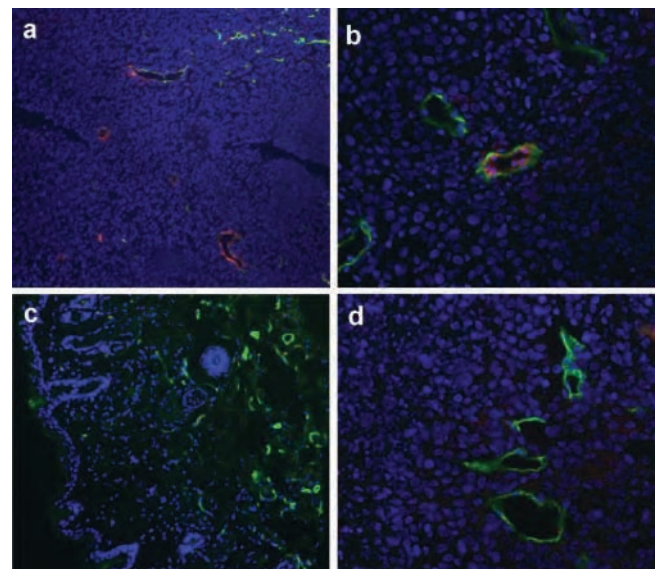


Figure 6. Intravenously injected antinucleolin antibody accumulates in tumor blood vessels. An affinity-purified rabbit antinucleolin antibody (NCL3) was injected into the tail vein of mice bearing MDA-MB-435 xenograft tumors. The tumor and various organs were removed 1 h after the injection, sectioned, and examined for the presence of rabbit IgG using Alexa-594 anti-rabbit IgG (red). Blood vessels were stained with anti-CD31 antibody (green), and nuclei were counterstained with DAPI (blue). The antinucleolin antibody has bound to tumor blood vessels (a and b), but is not seen in the skin (c). Rabbit IgG injected similarly as a control does not bind to tumor blood vessels (d).

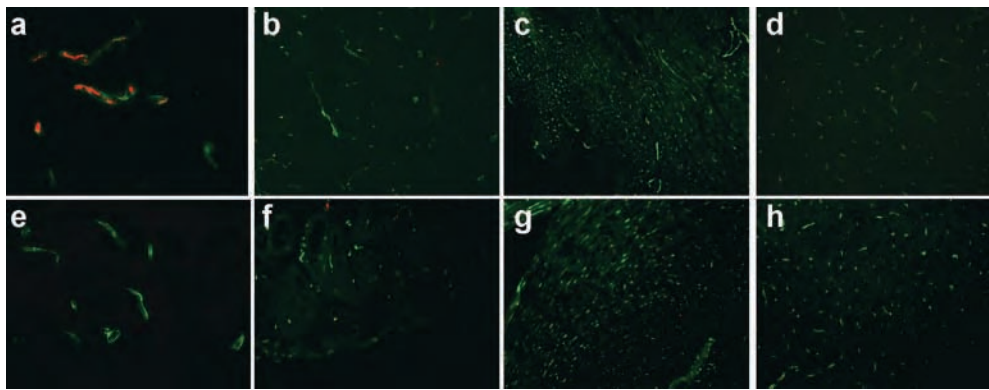


Figure 7. **Cell surface nucleolin is expressed in angiogenic blood vessels.** Balb/c *nu/nu* mice were subcutaneously injected with matrigel supplemented with bFGF. 8 d later, an antinucleolin antibody (NCL3) or control IgG was injected into the tail vein of the mice. The matrigel plugs were removed 1 h after the injection, sectioned, and examined for the presence of rabbit IgG using Alexa-594 anti-rabbit IgG (red). Blood vessels were stained with anti-CD31 antibody (green), and nuclei were counterstained with DAPI (blue). The injected NCL3 colocalizes the blood vessel staining in the matrigel plugs (a), but no injected rabbit IgG is detected in the plugs (e). No specific NCL3 accumulation over the IgG control is seen in any of the tissues examined: b and f, skin; c and g, heart; or d and h, brain. b–d, NCL3; f–h, IgG.

model but not to normal blood vessels. (Akerman et al., 2002; Porkka et al., 2002; Joyce et al., 2003).

To determine whether antinucleolin would similarly accumulate in tumor vessels and/or tumor cells, we intravenously injected the NCL3 antibody into mice bearing MDA-MB-435 tumors. Tissues collected 60 min after injection showed selective accumulation of the antibody in tumor blood vessels (Fig. 6, a and b). No antibody was detected in association with the tumor cells. About 70% of the tumor vessels were positive for the antibody, whereas no positive vessels were seen in the blood vessels of the normal tissues tested (skin and lung; shown for skin subcutaneous tissue in Fig. 6, c). Purified rabbit IgG, injected as a control, was not detected in tumor blood vessels (Fig. 6, d).

Next, we examined the binding of antinucleolin antibodies to angiogenic blood vessels in a nonmalignant tissue (matrigel plugs impregnated with basic FGF as an angiogenesis inducer). Intravenously injected NCL3 antibodies selectively accumulated in 70% of the blood vessels of subcutaneously implanted matrigel plugs (Fig. 7, a). Control IgG was not detectable in the matrigel plug vessels (Fig. 7, e), and NCL3 was not detectable in the blood vessels of various control organs (Fig. 7, b–d). Thus, nucleolin appears to be selectively expressed on the cell surface of angiogenic blood vessels but not on blood vessels of other tissues in vivo.

Discussion

Here, we show that the tumor-homing F3 peptide, which binds to and is internalized by endothelial and tumor cells (Porkka et al., 2002), interacts with nucleolin. We also show that antinucleolin antibodies detect nucleolin at the surface of cultured tumor cells and endothelial cells of angiogenic vessels in vivo. These results support the previously proposed role for nucleolin as a shuttle molecule between the nucleus and the cell surface, and they define cell surface nucleolin as a novel vascular marker for angiogenic endothelium.

Several approaches were used to identify the binding molecule for the F3 peptide as nucleolin. First, nucleolin and histones were identified as the main cellular proteins that

specifically bound to immobilized F3 peptide. Cell surface labeling indicated that the bound nucleolin was derived from the surface of intact cells, whereas the histones were not labeled and, therefore, likely originated from dead cells. Second, inhibition of F3 uptake into cultured cells by an antinucleolin antibody that is internalized into the nucleus provides additional evidence for the specificity of the F3–nucleolin interaction and its occurrence in intact cells. Third, the specific binding of injected antinucleolin antibodies to tumor blood vessels extends the association of F3 binding and cell surface nucleolin expression to an in vivo animal model.

The nucleolin polypeptide consists of a negatively charged NH₂-terminal domain, an RNA-binding domain, and a COOH-terminal domain rich in RGG motifs. The main functions of nucleolin relate to rRNA maturation and ribosome assembly (Ginisty et al., 1999; Srivastava and Pollard, 1999). Although nucleolin was originally described as a nuclear and cytoplasmic protein, a number of studies show that it can also be expressed at the cell surface (Deng et al., 1996; Larrucea et al., 1998; Said et al., 2002; Sinclair and O'Brien, 2002). Recent results also ascribe additional functions to nucleolin as a shuttle protein between the cytoplasm and the nucleus (Borer et al., 1989; Yu et al., 1998), and between the cell surface and the nucleus (Schmidt-Zachmann and Nigg, 1993; Said et al., 2002; Shibata et al., 2002). The localization of nucleolin within the cell may be regulated by phosphorylation of its NH₂ terminus (Schwab and Dreyer, 1997). Our results provide additional evidence for the cell surface localization and shuttle function of nucleolin.

The expression of nucleolin at the cell surface seems to correlate with growth and metabolic activity of cells. Both the uptake of the F3 peptide and the staining of intact cells with antinucleolin antibodies were suppressed in serum-starved cells. This may be a proliferation-related effect. An association of cell surface nucleolin expression with cell proliferation in vitro has been described previously (Hovanessian et al., 2000). Other factors besides proliferation may contribute to the regulation of cell surface nucleolin expression. We found only modest levels of cell surface nucleolin on actively prolifer-

erating endothelial cells *in vitro*, whereas antinucleolin binding to angiogenic endothelium was readily detectable *in vivo*. The differentiation state of the cells may be a factor contributing to nucleolin regulation, as cultured human leukemia-60 cells induced to differentiate into nonproliferating macrophages lose their ability to bind F3 (unpublished data). The restricted expression of cell surface nucleolin and the cell-type specificity of the expression may explain why some investigators have not been able to document the presence of nucleolin at the cell surface (Yu et al., 1998). A similar explanation may apply to the heterogeneity of the cell surface nucleolin expression in the vasculature of tumors and matrigel plugs; local variation in endothelial cell proliferation is likely to occur in angiogenic lesions *in vivo*.

F3-displaying phage selectively homes to tumor vasculature *in vivo*, and fluorescein-tagged F3 also binds to and is taken up by endothelial cells in tumor vasculature. However, the peptide also spreads to tumor cells, and it appears in a few individual nonvascular cells in the skin and the gut (Porkka et al., 2002). Intravenously injected antinucleolin antibody was only detected in angiogenic vessels of tumors as well as of matrigel plugs. The restricted distribution of the antibody resembles that of the phage, probably because the size of phage and antibody limit their access to tissues, whereas the relatively small molecular mass of the peptide conjugate (~5 kD) may permit wider distribution. Nonetheless, each of these reagents demonstrates the specificity of cell surface nucleolin for angiogenic vessels within the vasculature.

F3 is rich in basic amino acids and binds to cell surface heparan sulfate. However, our demonstration that CHO cells lacking heparan sulfate (and other glycosaminoglycans) internalize F3 excludes a direct role of heparan sulfate as the internalizing molecule. Indeed, binding and antibody inhibition studies show that F3 internalization is mediated by cell surface nucleolin. El-Sheikh et al. (2002) have described a peptide from the heparin-binding domain of vascular endothelial growth factor that selectively homes to tumor vasculature. The authors attributed the tumor homing to affinity of the peptide for heparan sulfate. It will be interesting to see whether this peptide might also bind to nucleolin.

The internalization of the F3 peptide and NCL3 antibody may reflect a physiological function of cell surface nucleolin. Midkine is a 13-kD cytokine that, like F3, contains a high proportion of basic amino acids (Said et al., 2002). It plays a role in neurite outgrowth and neuronal differentiation, and its mRNA is up-regulated in several human carcinomas (Tsutsui et al., 1993). The internalization of midkine by cells has been reported to be nucleolin dependent (Said et al., 2002), although lipoprotein receptor-related protein can also serve as the internalizing receptor for midkine (Shibata et al., 2002). The binding site for midkine in nucleolin has been localized to the RGG domain of nucleolin (Said et al., 2002), whereas our antibody inhibition results implicate the domain rich in acidic amino acids as the binding site for F3. Cell surface nucleolin may also be involved in the activities of basic FGF, which has been shown to bind to nucleolin in nuclear extracts (Bonnet et al., 1996). Thus, F3, midkine, and possibly basic FGF, might be internalized by a nucleolin-dependent mechanism, but distinct binding sites on nucleolin may exist to mediate the uptake.

A highly basic peptide derived from the HIV Tat protein also binds to cells and is internalized by them. The Tat peptide allows internalization of conjugated proteins and is commonly used as a cell-penetrating agent (Fawell et al., 1994; Langel, 2002). It is unlikely that the Tat peptide would use nucleolin for its internalization and nuclear transport. First, the internalization of Tat is independent of the cell type, even *in vivo*, whereas our results show that cell surface nucleolin is limited, it is expressed in angiogenic endothelium but not in the blood vessels in normal tissues. Second, treatment of cells with heparinase to remove heparan sulfates inhibits internalization of the Tat peptide (Suzuki et al., 2002), whereas we found that lack of heparan sulfates did not affect F3 uptake. Third, Tat internalization is independent of temperature and does not require energy, and several other cell-penetrating peptides are similar to Tat in this regard (Langel, 2002). In contrast, F3 uptake is blocked at 4°C (Porkka et al., 2002). Finally, our antibody inhibition data also suggest that Tat peptide internalization is independent of nucleolin because an antinucleolin antibody inhibited the uptake of F3 but not of the Tat peptide.

Our laboratory has recently described yet another type of a cell-penetrating peptide, LyP-1, which is also rich in basic amino acids (Laakkonen et al., 2002). This peptide specifically homes to the endothelium of tumor lymphatics and the tumor cells in certain, but not all, tumors. The internalization of this peptide is not affected by antinucleolin antibodies (unpublished data). Thus, several different internalization mechanisms for basic peptides appear to exist, both universal and cell-type specific.

Cell-penetrating peptides rich in basic amino acids are transported into the nucleus after internalization (Langel, 2002). This is also the case with F3 and LyP-1 (Laakkonen et al., 2002; Porkka et al., 2002). Nucleolin is thought to be responsible for the nuclear transport of midkine (Shibata et al., 2002), and the same may be the case with F3. It is also possible that the multiple basic amino acids in F3 form one or more independent nuclear localization signals.

The selective *in vivo* homing of the two nucleolin-binding reagents, the F3 peptide and the NCL3 antibody, to angiogenic blood vessels establishes cell surface nucleolin as a new angiogenesis marker. Tumor blood vessels undergo angiogenesis (Hanahan and Folkman, 1996) and have specific markers in common with other angiogenic vessels (Ruolahti, 2002). Future studies will determine whether cell surface nucleolin might play a role in angiogenesis, possibly by binding and internalizing growth factors such as midkine and bFGF. The restricted expression of cell surface nucleolin in angiogenic vessels and in tumor cells *in vivo*, and its ability to internalize molecules bound to it, make nucleolin an attractive potential target for the development of agents for vascular therapy of tumors.

Materials and methods

Cells and antibodies

MDA-MB-435 cells were grown in RPMI 1640 medium with 10% FCS and 1% Glutamine Pen-Strep (Irvine Scientific). CHO-K1 and pgsA-745 cells were grown in α MEM Earle's salt with 10% FCS and 1% Glutamine Pen-Strep. The antibodies used were mouse monoclonal antinucleolin (IgG₁; MS-3; Santa Cruz Biotechnology, Inc.) and rabbit polyclonal antibodies

raised against peptides synthesized according to the nucleolin sequence. NCL2 and NCL3 were raised against amino acids 43–51 and 221–232 of human nucleolin, respectively. The peptides were coupled to keyhole limpet hemocyanin and used to immunize rabbits according to the manufacturer's instructions. Antibodies were affinity purified from the sera on the appropriate synthetic peptide immobilized on a SulfoLink Column (Pierce Chemical Co.; 2 mg of peptide covalently coupled/column). Bound antibodies were eluted with a glycine-hydrochloride buffer, pH 2.5, and neutralized with 1 M Tris-HCl, pH 8. Each antibody immunoblotted the same 110-kD nucleolin band in cell extracts as the monoclonal antinucleolin.

F3 affinity chromatography and mass spectroscopy

Affinity purification of nucleolin from MDA-MB-435 detergent extracts was performed as described previously (Christian et al., 2001b). In brief, 6×10^8 cells were pelleted and lysed in 60 ml of RIPA buffer (1% Triton X-100, 0.5% deoxycholic acid, 0.1% SDS, 10 mM Tris-HCl, pH 7.6, 150 mM NaCl, and 1% protease inhibitor cocktail for mammalian cells; Sigma-Aldrich). The lysate was incubated with 20 μ l F3 (AKVKDEPQRSSARLSAKPAPPKPEPKPKKAPAKK) affinity matrix (2 mg of peptide covalently coupled to 1 ml of affigel 10). Control fractionation was performed on a 34-amino acid peptide that represents a scrambled version of F3. The matrix beads were washed three times with 0.025% Triton X-100, 50 mM Tris-HCl, pH 8.4, 150 mM NaCl, 1 mM CaCl_2 , and 0.02% azide; washed twice with 25 mM Tris-HCl, pH 8.4, and 250 mM NaCl; and the bound proteins were eluted with 30 μ l SDS gel sample buffer. The affinity-purified proteins were reduced with 50 mM DTT and separated on an 8–20% polyacrylamide gel and visualized by colloidal blue staining (Invitrogen). The molecular masses of the gel bands were determined by comparing to the standards in an Alphamanager instrument (Alpha Innotech Corp.). Bands that appeared in the F3 eluate, but not in the control, were cut out, digested with trypsin, and analyzed by mass spectroscopy using a matrix-assisted laser desorption ionization, time of flight instrument (model Voyager DE-PRO; Applied Biosystems) using an α -cyano-4-hydroxycinnamic acid/nitrocellulose matrix.

Immunoblot analysis

Cell extracts or affinity-purified samples were separated on an SDS-PAGE and transferred onto nitrocellulose membranes for 1 h at 100 V. The membranes were blocked overnight at 4°C with 5% milk powder in TBS-T (140 mM NaCl, 10 mM Tris-HCl, pH 7.4, and 0.05% Tween) and incubated with mouse monoclonal or rabbit polyclonal antinucleolin antibody (10 μ g/ml in TBS-T) for 1 h at RT. After extensive washing, the membranes were incubated with peroxidase-coupled rabbit anti-mouse or goat anti-rabbit antibody, and bound antibody was detected with ECL (Amersham Biosciences) and exposure to Biomax MR (Kodak).

Cell surface biotinylation

For cell surface expression analysis, MDA-MB-435 cells (5×10^6 cells) were washed three times with cold PBS on a cell culture plate and incubated with biotinylation buffer (20 mM HEPES, pH 7.45, 5 mM KCl, 130 mM NaCl, 0.8 mM MgCl_2 , 1 mM CaCl_2 , and 0.5 mg/ml EZ link Sulfo-NHS-Biotin; Pierce Chemical Co.) for 1 h at 4°C. After the removal of the reagent, the cells were washed three times with wash buffer (50 mM Tris, pH 7.5, 150 mM NaCl, 1 mM MgCl_2 , and 1 mM CaCl_2) and lysed in 1% Triton X-100 lysis buffer for 1 h. The lysates were centrifuged for 15 min at 15,000 g. F3 binding proteins were isolated by affinity chromatography as described above, separated on SDS-PAGE, and transferred to nitrocellulose. The nitrocellulose membranes were incubated after blocking with ExtrAvidin-peroxidase conjugates diluted at 1:5,000 (Sigma-Aldrich) for 1 h at RT. Bands were detected after incubation with ECL reagent and exposure to Biomax MR.

FACS analysis of cell surface nucleolin

For FACS[®] analysis, MDA-MB-435 or HUVEC were detached with EDTA and 10^6 cells/sample were incubated with either polyclonal rabbit antinucleolin antibody NCL3 (10 μ g/ml) or monoclonal antinucleolin antibody MS-3 (Santa Cruz Biotechnology, Inc.; 10 μ g/ml) for 45 min on ice. Cells were washed with ice-cold PBS and incubated with Alexa-488 (Molecular Probes) secondary antibody (1:50 in PBS). As a negative control, the cells were incubated with 10 μ g/ml of rabbit IgG or with 10 μ g/ml monoclonal anti-c-myc antibody (Santa Cruz Biotechnology, Inc.), followed by the secondary antibody. As a positive control, the cells were incubated with 10 μ g/ml of mouse monoclonal anti- β_3 -integrin (CBL 479; Cymbus Biotechnology Ltd.). The antibody-treated cells were washed and resuspended in 50 μ l PBS containing 2 μ g/ml propidium iodide to distinguish between live and dead cells, and 10,000 cells per sample were analyzed using a FACSCalibur flow cytometer.

Detection of peptides and antibodies in cells and tissues

For internalization experiments, cells were incubated with 1 μ M of fluorescein-conjugated peptide for 2 h at 37°C. The cells were washed with PBS, fixed with 4% PFA in PBS, and analyzed by confocal microscopy. The cell-penetrating basic peptide from the human immunodeficiency virus Tat protein (GRKKRRQRRR; Fawell et al., 1994) was used as a positive control in the internalization experiments. To detect nucleolin, cells were fixed with 4% PFA in PBS and stained with 10 μ g/ml antinucleolin antibodies either directly or after permeabilization with Triton X-100. Bound antibodies were detected with Alexa-594-labeled anti-rabbit antibody (Molecular Probes) and visualized by fluorescence microscopy.

In vivo distribution of circulation-accessible cell surface nucleolin was examined in mice bearing xenograft tumors or basement membrane (matrigel) plugs. Xenograft tumors were generated by subcutaneously injecting exponentially growing MDA-MB-435 human breast cancer cells (10^6 cells in 200 μ l of culture media) into the mammary fat pad area of 2-mo-old Balb/c *nu/nu* mice (Animal Technologies). The animals were used for experiments 8 wk after injection. Nontumor angiogenesis was studied in matrigel plugs (Fulgham et al., 1999; Ngo et al., 2000). 2-mo-old Balb/c *nu/nu* mice were subcutaneously injected with 100 μ l of Matrigel (Becton Dickinson) at two or three locations in the abdominal area. Each 100- μ l plug contained 100 ng of recombinant human bFGF as an angiogenesis stimulant (R&D Systems). The animals were used for antibody injection experiments 8 d after the implantation.

In vivo distribution of antibodies was studied by intravenously injecting mice with 200 μ g of polyclonal rabbit antinucleolin antibody or rabbit IgG. 1 h after the injection, the mice were anesthetized, perfused through the heart with 10 ml PBS, and killed by infusing 10 ml of 4% PFA in PBS. Tumors or matrigel plugs, along with various control tissues were removed, fixed in 4% PFA, and frozen in OCT embedding medium (Tissue-Tek). All procedures were performed under anesthesia induced by intraperitoneal injection of 2,2,2-tribromoethanol (Avertin) at a dosage of 0.4–0.75 mg/gram of body weight (500–700 μ l/mouse). All animal experiments were approved by the Animal Review Committee of the Burnham Institute.

For histological analyses, 5- μ m sections were cut. The injected rabbit antinucleolin antibody and anti-CD31 antibody (10 μ g/ml; BD Biosciences) applied on the tissue sections were detected with Alexa-594- and Alexa-488-conjugated secondary antibodies, respectively. The sections were examined under an inverted fluorescent microscope (Nikon) or a confocal microscope (Bio-Rad Laboratories). Nuclei were counterstained using DAPI (Vector Laboratories).

We thank Dr. Ed Monosov, Jennifer Freund, and Jeff Nickel for their help with microscopy; Dr. Fernando Ferrer for peptide synthesis; and Tristan Williams for mass spectroscopy.

This work was supported by grants from the National Cancer Institute (CA82713), the Department of Defense (DAMD 17-02-1-0315; given to E. Ruoslahti), and the Cancer Center (CA30199). S. Christian is supported by a fellowship from the Deutsche Forschungsgemeinschaft.

Submitted: 24 April 2003

Accepted: 7 October 2003

References

- Akerman, M.E., W.C. Chan, P. Laakkonen, S.N. Bhatia, and E. Ruoslahti. 2002. Nanocrystal targeting in vivo. *Proc. Natl. Acad. Sci. USA*. 99:12617–12621.
- Arap, W., R. Pasqualini, and E. Ruoslahti. 1998. Cancer treatment by targeted drug delivery to tumor vasculature in a mouse model. *Science*. 279:377–380.
- Bergers, G., R. Brekken, G. McMahon, T.H. Vu, T. Itoh, K. Tamaki, K. Tanzawa, P. Thorpe, S. Itohara, Z. Werb, and D. Hanahan. 2000. Matrix metalloproteinase-9 triggers the angiogenic switch during carcinogenesis. *Nat. Cell Biol.* 2:737–744.
- Bonnet, H., O. Filhol, I. Truchet, P. Brethenou, C. Cochet, F. Amalric, and G. Bouche. 1996. Fibroblast growth factor-2 binds to the regulatory beta subunit of CK2 and directly stimulates CK2 activity toward nucleolin. *J. Biol. Chem.* 271:24781–24787.
- Borer, R.A., C.F. Lehner, H.M. Eppenberger, and E.A. Nigg. 1989. Major nuclear proteins shuttle between nucleus and cytoplasm. *Cell*. 56:379–390.
- Brooks, P.C., S. Silletti, T.L. von Schalscha, M. Friedlander, and D.A. Cheresh. 1998. Disruption of angiogenesis by PEX, a noncatalytic metalloproteinase fragment with integrin binding activity. *Cell*. 92:391–400.
- Christian, S., H. Ahorn, A. Koehler, F. Eisenhaber, H.P. Rodi, P. Garin-Chesa, J.E. Park, W.J. Rettig, and M.C. Lenter. 2001a. Molecular cloning and

- characterization of endosialin, a C-type lectin-like cell surface receptor of tumor endothelium. *J. Biol. Chem.* 276:7408–7414.
- Christian, S., H. Ahorn, M. Novatchkova, P. Garin-Chesa, J.E. Park, G. Weber, F. Eisenhaber, W.J. Rettig, and M.C. Lenter. 2001b. Molecular cloning and characterization of EndoGlyx-1, an EMILIN-like multisubunit glycoprotein of vascular endothelium. *J. Biol. Chem.* 276:48588–48595.
- Deng, J.S., B. Ballou, and J.K. Hofmeister. 1996. Internalization of anti-nucleolin antibody into viable HEP-2 cells. *Mol. Biol. Rep.* 23:191–195.
- El-Sheikh, A., C. Liu, H. Huang, and T.S. Edgington. 2002. A novel vascular endothelial growth factor heparin-binding domain substructure binds to glycosaminoglycans in vivo and localizes to tumor microvascular endothelium. *Cancer Res.* 62:7118–7123.
- Eliceiri, B.P., and D.A. Cheresh. 1999. The role of alphav integrins during angiogenesis: insights into potential mechanisms of action and clinical development. *J. Clin. Invest.* 103:1227–1230.
- Esko, J.D., T.E. Stewart, and W.H. Taylor. 1985. Animal cell mutants defective in glycosaminoglycan biosynthesis. *Proc. Natl. Acad. Sci. USA.* 82:3197–3201.
- Fawell, S., J. Seery, Y. Daikh, C. Moore, L.L. Chen, B. Pepinsky, and J. Barsoum. 1994. Tat-mediated delivery of heterologous proteins into cells. *Proc. Natl. Acad. Sci. USA.* 91:664–668.
- Ferrara, N., and K. Alitalo. 1999. Clinical applications of angiogenic growth factors and their inhibitors. *Nat. Med.* 5:1359–1364.
- Fulgham, D.L., S.R. Widhalm, S. Martin, and J.D. Coffin. 1999. FGF-2 dependent angiogenesis is a latent phenotype in basic fibroblast growth factor transgenic mice. *Endothelium.* 6:185–195.
- Ginisty, H., H. Sicard, B. Roger, and P. Bouvet. 1999. Structure and functions of nucleolin. *J. Cell Sci.* 112:761–772.
- Hanahan, D., and J. Folkman. 1996. Patterns and emerging mechanisms of the angiogenic switch during tumorigenesis. *Cell.* 86:353–364.
- Harms, G., R. Kraft, G. Grelle, B. Volz, J. Dernedde, and R. Tauber. 2001. Identification of nucleolin as a new L-selectin ligand. *Biochem. J.* 360:531–538.
- Hood, J.D., M. Bednarski, R. Frausto, S. Guccione, R.A. Reisfeld, R. Xiang, and D.A. Cheresh. 2002. Tumor regression by targeted gene delivery to the neovasculature. *Science.* 296:2404–2407.
- Hovanessian, A.G., F. Puvion-Dutilleul, S. Nisole, J. Svab, E. Perret, J.S. Deng, and B. Krust. 2000. The cell-surface-expressed nucleolin is associated with the actin cytoskeleton. *Exp. Cell Res.* 261:312–328.
- Hynes, R.O. 2002. A reevaluation of integrins as regulators of angiogenesis. *Nat. Med.* 8:918–921.
- Joyce, J.A., P. Laakkonen, M. Bernasconi, G. Bergers, E. Ruoslahti, and D. Hanahan. 2003. Stage-specific vascular markers revealed by phage display in a mouse model of pancreatic islet tumorigenesis. *Cancer Cell.* In press.
- Laakkonen, P., K. Porkka, J.A. Hoffman, and E. Ruoslahti. 2002. A tumor-homing peptide with a targeting specificity related to lymphatic vessels. *Nat. Med.* 8:751–755.
- Langel, Ü. 2002. Cell-Penetrating Peptides: Processes and Applications. CRC Press, Boca Raton, FL. 406 pp.
- Larrucea, S., C. Gonzalez-Rubio, R. Cambronero, B. Ballou, P. Bonay, E. Lopez-Granados, P. Bouvet, G. Fontan, M. Fresno, and M. Lopez-Trascasa. 1998. Cellular adhesion mediated by factor J, a complement inhibitor. Evidence for nucleolin involvement. *J. Biol. Chem.* 273:31718–31725.
- Ngo, C.V., M. Gee, N. Akhtar, D. Yu, O. Volpert, R. Auerbach, and A. Thomas-Tikhonenko. 2000. An in vivo function for the transforming Myc protein: elicitation of the angiogenic phenotype. *Cell Growth Differ.* 11:201–210.
- Nilsson, F., H. Kosmehl, L. Zardi, and D. Neri. 2001. Targeted delivery of tissue factor to the ED-B domain of fibronectin, a marker of angiogenesis, mediates the infarction of solid tumors in mice. *Cancer Res.* 61:711–716.
- Pasqualini, R., E. Koivunen, R. Kain, J. Lahdenranta, M. Sakamoto, A. Stryhn, R.A. Ashmun, L.H. Shapiro, W. Arap, and E. Ruoslahti. 2000. Aminopeptidase N is a receptor for tumor-homing peptides and a target for inhibiting angiogenesis. *Cancer Res.* 60:722–727.
- Porkka, K., P. Laakkonen, J.A. Hoffman, M. Bernasconi, and E. Ruoslahti. 2002. A fragment of the HMGN2 protein homes to the nuclei of tumor cells and tumor endothelial cells in vivo. *Proc. Natl. Acad. Sci. USA.* 99:7444–7449.
- Roghani, M., and D. Moscatelli. 1992. Basic fibroblast growth factor is internalized through both receptor-mediated and heparan sulfate-mediated mechanisms. *J. Biol. Chem.* 267:22156–22162.
- Ruoslahti, E. 2002. Specialization of tumour vasculature. *Nat. Rev. Cancer.* 2:83–90.
- Said, E.A., B. Krust, S. Nisole, J. Svab, J.P. Briand, and A.G. Hovanessian. 2002. The anti-HIV cytokine midkine binds the cell surface-expressed nucleolin as a low affinity receptor. *J. Biol. Chem.* 277:37492–37502.
- Schmidt-Zachmann, M.S., and E.A. Nigg. 1993. Protein localization to the nucleolus: a search for targeting domains in nucleolin. *J. Cell Sci.* 105:799–806.
- Schwab, M.S., and C. Dreyer. 1997. Protein phosphorylation sites regulate the function of the bipartite NLS of nucleolin. *Eur. J. Cell Biol.* 73:287–297.
- Shibata, Y., T. Muramatsu, M. Hirai, T. Inui, T. Kimura, H. Saito, L.M. McCormick, G. Bu, and K. Kadomatsu. 2002. Nuclear targeting by the growth factor midkine. *Mol. Cell. Biol.* 22:6788–6796.
- Sinclair, J.F., and A.D. O'Brien. 2002. Cell surface-localized nucleolin is a eukaryotic receptor for the adhesin intimin-gamma of enterohemorrhagic *Escherichia coli* O157:H7. *J. Biol. Chem.* 277:2876–2885.
- Srivastava, M., and H.B. Pollard. 1999. Molecular dissection of nucleolin's role in growth and cell proliferation: new insights. *FASEB J.* 13:1911–1922.
- St Croix, B., C. Rago, V. Velculescu, G. Traverso, K.E. Romans, E. Montgomery, A. Lal, G.J. Riggins, C. Lengauer, B. Vogelstein, and K.W. Kinzler. 2000. Genes expressed in human tumor endothelium. *Science.* 289:1197–1202.
- Suzuki, T., S. Futaki, M. Niwa, S. Tanaka, K. Ueda, and Y. Sugiura. 2002. Possible existence of common internalization mechanisms among arginine-rich peptides. *J. Biol. Chem.* 277:2437–2443.
- Tsutsui, J., K. Kadomatsu, S. Matsubara, A. Nakagawara, M. Hamanoue, S. Takao, H. Shimazu, Y. Ohi, and T. Muramatsu. 1993. A new family of heparin-binding growth/differentiation factors: increased midkine expression in Wilms' tumor and other human carcinomas. *Cancer Res.* 53:1281–1285.
- Yu, D., M.Z. Schwartz, and R. Petryshyn. 1998. Effect of laminin on the nuclear localization of nucleolin in rat intestinal epithelial IEC-6 cells. *Biochem. Biophys. Res. Commun.* 247:186–192.

Stage-specific vascular markers revealed by phage display in a mouse model of pancreatic islet tumorigenesis

Johanna A. Joyce,^{1,3} Pirjo Laakkonen,^{2,3,4} Michele Bernasconi,^{2,5} Gabriele Bergers,^{1,6} Erkki Ruoslahti,^{2,*} and Douglas Hanahan^{1,*}

¹Department of Biochemistry and Biophysics, Diabetes and Comprehensive Cancer Centers, University of California, San Francisco, 513 Parnassus Avenue, San Francisco, California 94143

²Cancer Research Center, The Burnham Institute, 10901 North Torrey Pines Road, La Jolla, California 92037

³These authors contributed equally to this work.

⁴Present address: Molecular/Cancer Biology Laboratory, Biomedicum Helsinki, University of Helsinki, P.O.B. 63 (Haartmaninkatu 8), FIN-00014 Helsinki, Finland.

⁵Present address: Functional Genomics Unit, Divisions of Infectious Diseases and Oncology, The University Children's Hospital of Zürich, August-Forel Strasse 1 CH-8008 Zürich, Switzerland.

⁶Present address: Department of Neurological Surgery, University of California, San Francisco, 513 Parnassus Avenue, San Francisco, California 94143.

*Correspondence: dh@biochem.ucsf.edu (D.H.); ruoslahti@burnham.org (E.R.)

Summary

The vasculature in the angiogenic stages of a mouse model of pancreatic islet carcinogenesis was profiled in vivo with phage libraries that display short peptides. We characterized seven peptides distinguished by their differential homing to angiogenic progenitors, solid tumors, or both. None homed appreciably to normal pancreatic islets or other organs. Five peptides selectively homed to neoplastic lesions in the pancreas and not to islet β cell tumors growing subcutaneously, xenotransplant tumors from a human cancer cell line, or an endogenously arising squamous cell tumor of the skin. Three peptides with distinctive homing to angiogenic islets, tumors, or both colocalized with markers that identify endothelial cells or pericytes. One peptide is homologous with pro-PDGF-B, which is expressed in endothelial cells, while its receptor is expressed in pericytes.

Introduction

Angiogenesis, the formation of new blood vessels, is essential for tumor growth. The transition from normal to neoplastic vasculature during tumorigenesis has been termed the "angiogenic switch," and both positive and negative regulators of the switch have been identified (Hanahan and Folkman, 1996). The vascular anatomy of tumors is typically distinct from that of normal tissues (Carmeliet and Jain, 2000). In contrast to their normal counterparts, tumor vessels are tortuous and dilated and show reduced vessel integrity. Tumor vessels often have numerous fenestrae or discontinuities, loose interendothelial junctions, and a discontinuous or absent basement membrane, collectively resulting in vessel leakiness (Carmeliet and Jain, 2000; Hashizume et al., 2000).

We are only beginning to understand the molecular events underlying the pronounced abnormalities evident in the angiogenic vasculature of tumors and progenitor lesions. Previous

studies have shown that a number of genes are upregulated during the transition from normal to tumor blood vessels, including the integrins $\alpha v\beta 3$, $\alpha v\beta 5$, and $\alpha 5\beta 1$; several matrix metalloproteinases; and various endothelial growth factor receptors (Hanahan and Folkman, 1996; Ruoslahti, 2002). Recently, St. Croix et al. further showed, using a comparative RNA expression profiling technology (SAGE), that a number of genes or EST's were selectively expressed or upregulated in the tumor endothelium of human colorectal cancer, relative to the corresponding normal colonic vasculature (St. Croix et al., 2000). This approach relied on substantive differences in gene expression to identify tumor-specific endothelial markers, which will likely only reveal a subset of alterations that distinguish normal and tumor blood vessels. Specific binding of phage from libraries that can display more than a billion random peptide sequences offers a complementary approach for comparative screening. In vivo phage display screening has proven to be a powerful method for un-

SIGNIFICANCE

While there is abundant evidence that tumor vasculature is functionally and morphologically aberrant, we show herein using a peptide epitope profiling technology that the angiogenic vasculature in premalignant lesions is distinguishable from normal as well as tumor vessels in a model of multistage tumorigenesis. Moreover, both angiogenic progenitor and tumor vessels in the pancreas have molecular signatures distinct from tumors growing in or under the skin, even of the analogous cell type. The stage and organ specificities of particular homing peptides may prove instructive about mechanisms regulating the neovasculature in different pathways of tumorigenesis, suggest means to detect and distinguish premalignant and malignant lesions noninvasively, and predict differential sensitivity to therapeutic agents targeting angiogenesis.

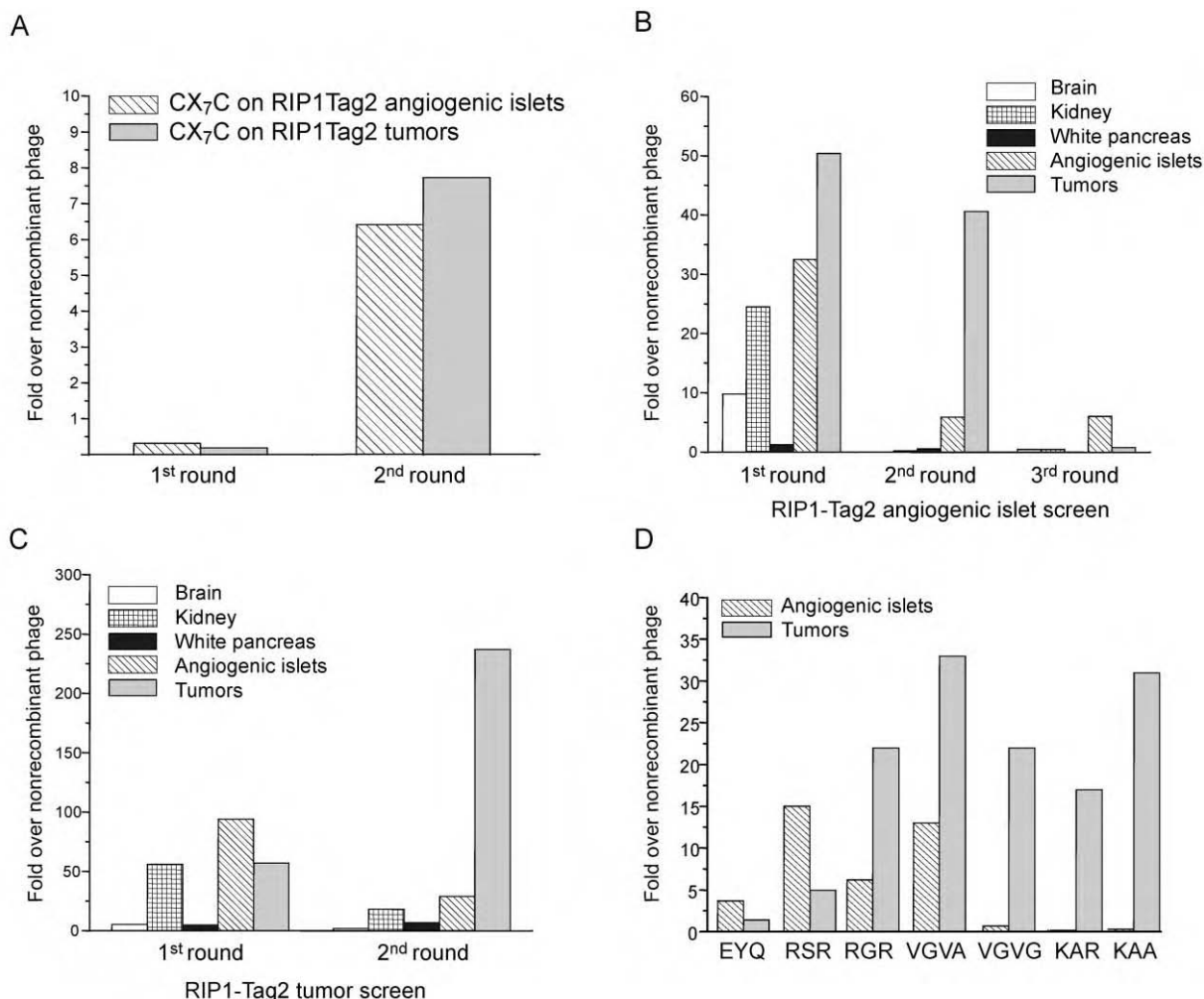


Figure 1. Isolation of stage-specific phage using ex vivo and in vivo phage display

A: Ex vivo screening on cells derived from RIP1-Tag2 angiogenic islets or tumors using the CX₇C peptide library displayed on T7 phage. The enriched phage pools were used for subsequent in vivo homing to RIP1-Tag2 angiogenic islets (three rounds of selection) (**B**) and tumors (two rounds of selection) (**C**). **D:** In vivo homing of individual phage to RIP1-Tag2 angiogenic islets and tumors.

covering differences among individual vascular beds in normal organs (Pasqualini and Ruoslahti, 1996; Rajotte et al., 1998) and has also yielded peptides that specifically home to blood vessels or lymphatics in tumors (Arap et al., 1998; Laakkonen et al., 2002; Porkka et al., 2002). The targets for these peptides in blood vessels include the $\alpha v\beta 3$ and $\alpha v\beta 5$ integrins (Arap et al., 1998) and aminopeptidase N (Pasqualini et al., 2000).

In this and a companion study (Hoffman et al., 2003 [this issue of *Cancer Cell*]), we set out to use phage-display profiling to ask whether additional levels of neoplastic vascular specialization might exist in tumor development. We sought to distinguish the vessels of premalignant angiogenic lesions from those of angiogenic solid tumors and to examine whether differences exist between angiogenic vessels of tumors developing in different organs. Previous studies have profiled differences between normal blood vessels and the vasculature of transplanted tumors in immunodeficient mice. Unlike these transplanted tumors, transgenic tumor models provide an opportunity to examine pre-neoplastic changes unfolding in different organs in a more physiologically relevant microenvironment.

We used a prototypical mouse model of multistage tumorigenesis, the RIP1-Tag2 transgenic model of islet cell carcinoma (Hanahan, 1985), to address our hypothesis that the vasculature of pre-neoplastic lesions differs from that of established tumors. RIP1-Tag2 transgenic mice express the SV40 T antigens (Tag) under the control of the insulin gene promoter, which elicits the sequential development of tumors in the islets of Langerhans over a period of 12–14 weeks. Hyperplastic islets begin to appear at around 4 weeks of age, and angiogenesis is activated a few weeks later in a subset of the hyperplastic islets, producing angiogenic (dysplastic) islets (Bergers et al., 1998; Folkman et al., 1989). Solid tumors form beginning at 9 to 10 weeks, initially presenting as small nodules that grow and progress to large islet tumors with well-defined margins, as well as two classes of invasive carcinoma (Lopez and Hanahan, 2002). We set out to identify stage-specific molecular markers accessible via the circulation, either on the surface of endothelial cells, their periendothelial support cells (pericytes and smooth muscle cells), or even tumor cells themselves (as a result of the hemorrhagic,

leaky angiogenic vasculature). We successfully selected phage pools that homed preferentially to different stages during RIP1-Tag2 tumorigenesis. In addition to “pan-angiogenic” markers shared by many types of tumors, we identified vascular target molecules that are characteristic of this tumor’s tissue of origin and are not expressed in the vessels of several tumor types growing in or under the skin. We have begun to investigate the binding partners for these peptides and present evidence linking one peptide to a vascular signaling circuit involving PDGF ligands expressed in endothelial cells and their receptor PDGFR β , expressed in pericytes of the angiogenic vasculature.

Results

Isolation of stage-specific phage from RIP1-Tag2 mice

RIP1-Tag2 mice develop multifocal angiogenic islet progenitors and then solid tumors in a stepwise manner, such that at 12 weeks of age, each mouse will typically have approximately 50 angiogenic islets and 2–6 small tumors. This circumstance allowed us to use 12-week-old mice to select for phage binding to angiogenic islet progenitors and/or tumors in the same mouse. In order to enrich for phage that bind to RIP1-Tag2 target cells (endothelial, perivascular, and tumor), we included a pre-selection step (Laakkonen et al., 2002; Porkka et al., 2002) on cell suspensions prepared from pancreatic lesions. Two rounds of *ex vivo* selection from a CX₇C peptide library on cell suspensions from angiogenic islets or solid tumors yielded phage pools that bound 7- to 8-fold over a control, nonrecombinant phage to their respective target cells (Figure 1A). These enriched phage pools were used in subsequent *in vivo* rounds to select for phage that would home specifically to either angiogenic islets or tumors in RIP1-Tag2 mice.

Three rounds of *in vivo* selection on angiogenic islets resulted in a phage pool that selectively homed to angiogenic islets. The homing to the islets was 7-fold higher than to tumors in the same mouse (Figure 1B). There was no homing to control organs. The tumor selection yielded a pool that showed an 8-fold preference for tumors versus angiogenic islets in the same mouse following two rounds of *in vivo* selection (Figure 1C).

Sequencing of phage from the selected pools identified a number of peptide sequences that were represented more than once, and these were tested for their ability to bind cell suspensions prepared from angiogenic islets and tumors. Six of the phage selected for further analysis were from the tumor screen (referred to as KAA, RGR, RSR, VGVA, VGVG, and KAR), and one (EYQ) was picked from the angiogenic screen. Peptide sequences corresponding to each of these peptide motifs are shown in Table 1. All of these peptides are linear, although the phage library used here (CX₇C) was designed to express peptides cyclized by a covalent bond between two cysteine residues. However, a library of this design does contain a minority of linear peptides. A stop codon occurring within the random insert will cause truncation of the peptide, and a frameshift mutation frequently changes the second cysteine into valine. It may be that the target molecules in the RIP1-Tag2 tumors selected for linear peptides. In the companion study (Hoffman et al., 2003), the same library yielded cyclic homing peptides. The RIP1-Tag2 homing phage fall into three classes based on their homing either to angiogenic islets or to tumors *in vivo* (Figure 1D) and their *ex vivo* binding patterns: tumor-selective phage

(KAA, KAR, and VGVG), angiogenic islet-selective phage (RSR and EYQ), and phage that home to both types of angiogenic lesions (VGVA and RGR). Some of the selected peptides that share similar peptide motifs also display similar homing patterns. For example, KAA and KAR (CKAAKNK and CKGAKAR = XBXXBXXB, where B represents basic residues and X denotes uncharged residues) both preferentially home to tumors over angiogenic islets. However, other related peptides such as RGR and RSR (CRGRRST and CRSRKG = XBXXBXX) have quite different homing capabilities. Interestingly, all of these peptides are distinct from those found previously in phage display screens of transplant tumors (Arap et al., 1998; Laakkonen et al., 2002; Porkka et al., 2002).

Stage-specific homing of fluorescein-conjugated peptides

To confirm that the selective phage homing was due to the displayed peptide sequences, we studied the localization of fluorescein-conjugated peptides after intravenous injection; one peptide from each homing class was selected for detailed analysis. We used 8-week-old RIP1-Tag2 mice to examine peptide localization during the angiogenic switch and 12-week-old RIP1-Tag2 mice to visualize both angiogenic islets and tumors.

The observed peptide localization profiles in each case closely mimicked that of the cognate phage, as shown in Figure 1D, with each peptide falling into the same of the three homing classes. Figure 2 illustrates the peptide localization for these three representative fluorescein-conjugated peptides: RSR (angiogenic-selective), KAA (tumor-selective), and RGR (angiogenic- and tumor-homing). RSR shows abundant accumulation in RIP1-Tag2 angiogenic islets (Figure 2B) but little or no localization in tumors (Figure 2C) or normal islets (Figure 2A). KAA shows abundant localization in RIP1-Tag2 tumors (Figure 2F) but little or no localization in angiogenic islets (Figure 2E) or normal islets (Figure 2D). Finally, RGR localizes in both RIP1-Tag2 angiogenic islets (Figure 2H) and tumors (Figure 2I) but there is little or no peptide in normal islets (Figure 2G). It was somewhat unexpected that RSR, which was selected from the tumor phage screening, preferentially bound to angiogenic islets. It seems that the epitope this peptide binds to is present both in tumors and angiogenic islets, but is more abundant in angiogenic islets. This result could also be indicative of the heterogeneity of the pools of angiogenic islets or tumors isolated by gross examination, in which there are multiple lesions of differing grades within each group. Hence, a gross selection of the tumor pool may in fact include some large, advanced angiogenic islets that can only be definitively distinguished by histological grading, which was performed in conjunction with the peptide homing to the different lesions.

Homing of the peptides to the pancreatic islet lesions was specific: little or no homing was detected in normal islets, brain, liver, lung, and spleen (Figures 2K and 2L and data not shown). Fluorescence was detected in kidney, presumably as a result of uptake from glomerular filtrate (Figure 2J). Representative figures of control tissues from a RIP1-Tag2 mouse injected with fluorescein-conjugated RGR peptide are shown in Figures 2J–2L. A similar absence of fluorescence in control tissues was observed for all other injected peptides (data not shown). In addition, control peptides did not show specific homing to any of the RIP1-Tag2 lesional stages or to a number of normal tissues.

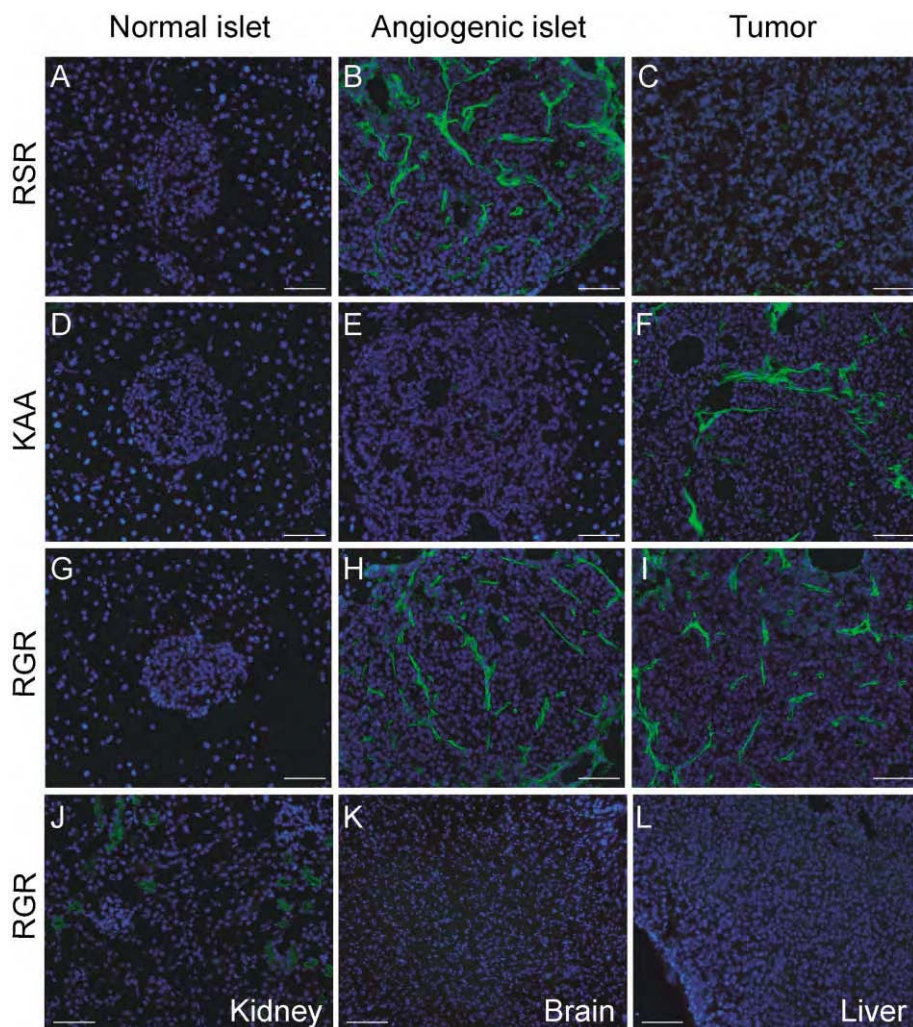


Figure 2. Stage-specific homing of fluorescein-conjugated peptides in RIP1-Tag2 model

Visualization of an angiogenic islet-selective peptide (RSR) homing is shown in normal islet (A), angiogenic islet (B), and tumor (C). Homing profiles are also shown for a tumor-selective peptide (KAA) to normal islet (D), angiogenic islet (E), and tumor (F), as well as of a peptide (RGR) that homes to both angiogenic islets and tumors (G, normal islet; H, angiogenic islet; and I, tumor). Control tissues (J, kidney; K, brain; and L, liver) from a RIP1-Tag2 mouse injected with fluorescein-conjugated RGR peptide are also presented. Similar absence of fluorescence in control tissues was observed for all other injected peptides, indicative of a lack of specific homing. The scale bar corresponds to 50 μ M.

Fluorescein-conjugated peptides colocalize with vascular markers

We reasoned that intravenous administration of the phage libraries would select for phage carrying peptides that bind to endothelial molecules specific for the target vasculature. The expectation of endothelial selectivity is based upon the preferential exposure of phage to luminal cells of the vasculature, as well as the appreciable size of the phage and the short time the phage are allowed to circulate (Pasqualini and Ruoslahti, 1996). In order to test this expectation, tissues were collected following i.v. infusion with the various fluorescein-conjugated peptides, sectioned, and evaluated with endothelial cell markers. The primary analysis involved immunostaining with a mouse pan-endothelial cell antigen (MECA32) antibody that recognizes a dimer of 50–55 kDa protein subunits present on all endothelial cells (Hallman et al., 1995; Leppink et al., 1989) (Figures 3B, 3C, 3H, 3I, 3N, and 3O). Additional analyses (not shown) involved immunostaining to reveal CD31/PECAM or systemic infusion of a fluorescent-labeled lectin that binds to the endothelial lumen. In addition, tissue sections from peptide-infused mice were stained with an antibody recognizing NG2, a marker of the neovascular pericytes (Schlingemann et al., 1990, 1991) (Figures 3E, 3F, 3K, 3L, 3Q, and 3R). Remarkably, all three peptides (RSR, KAA, and RGR) show some colocalization both with endo-

thelial cell and pericyte markers, indicating that each homes to and binds moieties associated with both cell types (Figure 3 and data not shown). Again, there was no colocalization of these peptides with those same markers in the adjacent exocrine pancreas or in normal pancreatic islets; tissue sections stained with MECA32 and NG2 showed some colocalization, consistent with the proximity of endothelial cells and pericytes (Figures 3S–3U).

The apparent homing of peptides representing all three classes of stage specificity to both pericytes and endothelial cells was unexpected. It may be pertinent that the RIP1-Tag2 tumor vasculature is known to be leaky, as evidenced by extensive microhemorrhaging (Parangi et al., 1995) and morphometric analysis (Hashizume et al., 2000; Morikawa et al., 2002; Thurston et al., 1998), such that the circulating phage pool likely had access to the extraluminal vascular microenvironment, where receptors on pericytes and in the extracellular matrix could be accessible. It is known that the vasculature of both angiogenic islets and tumors is leaky (Morikawa et al., 2002). However, reciprocal homing of the peptides that recognize the angiogenic islet but not tumor vessels, and vice versa, excludes the possibility that the recognition of angiogenic islet versus tumor vessels would simply be caused by differences in the leakiness of the

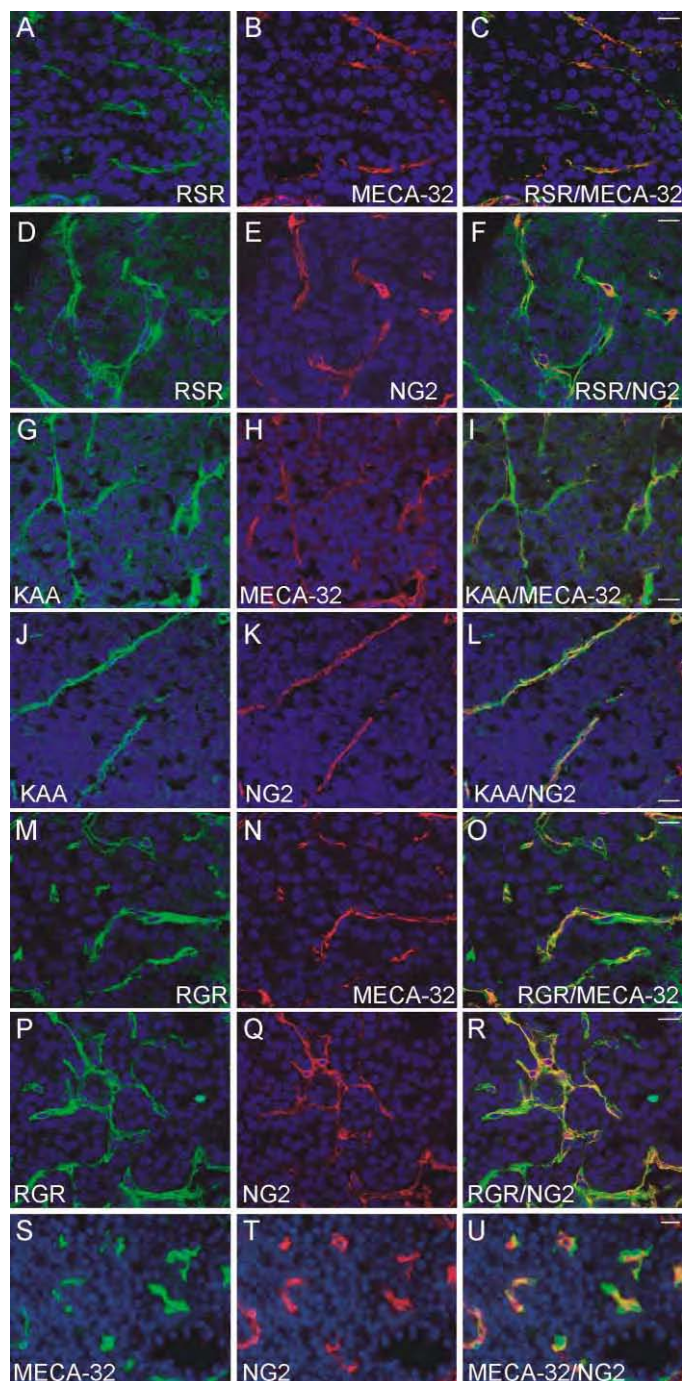


Figure 3. Colocalization of fluorescein-conjugated peptides with vascular markers in RIP1-Tag2 islet lesions

RSR peptide localization in an angiogenic islet is shown in (A) and (D) (green), while co-staining for MECA32 (red) and the merge are shown in (B) and (C). Co-staining for NG2 (red) is shown in (E), with the merge in (F). KAA peptide localization in a tumor is shown in (G) and (J) (green), while co-staining for MECA32 (red) and the merge are shown in (H) and (I). Co-staining for NG2 (red) is shown in (K), with the merge in (L). RGR peptide localization in an angiogenic islet is shown in (M) and (P) (green), while co-staining for MECA32 (red) and the merge are shown in (N) and (O). Co-staining for NG2 (red) is shown in (Q), with the merge in (R). Staining for endothelial cells (MECA32) (S) and pericytes (NG2) (T) in tumor sections demonstrated their close association (U). Scale bar: 10 μ m.

vessels. The ex vivo pre-selection step we used to enrich for RIP1-Tag2-specific targets may have similarly selected for non-luminal endothelial binding partners, but it should be emphasized that any peptide selected ex vivo must also have been accessible via the circulation during the in vivo selections. Consistent with this logic, phage-displaying peptides that bind to the pericyte marker, NG2, have previously been shown to home to a transplant tumor in vivo (Burg et al., 1999).

Specificity of in vivo homing to islet tumors in the pancreas

Selection of phage that home to the vasculature of neoplastic lesions in RIP1-Tag2 mice can be envisioned to identify two classes of peptides: those whose cognate receptors are specific to angiogenic islets and/or tumors in the pancreas and those that also home to the angiogenic vasculature in other tumor types. Therefore, we asked whether phage and peptides selected in pancreatic neoplasias would home to two different transplant tumors growing subcutaneously or to de novo skin tumors induced in another transgenic mouse model.

β TC3 transplant tumors arise following subcutaneous inoculation of nude mice with cultured islet tumor-derived (β TC3) cells (Efrat et al., 1988), allowing the study of islet tumors and their vasculature outside of their natural environment in the pancreas. Because the vasculature of a subcutaneously grown β TC3 tumor derives from skin, we also tested another subcutaneous transplant tumor, arising from inoculation of the MDA-MB-435 human breast carcinoma cell line. Finally, K14-HPV16 mice, another well-studied transgenic mouse model of cancer that develop tumors of the squamous epithelial cells of the skin (Arbeit et al., 1994; Coussens et al., 1996), allowed us to compare RIP1-Tag2 islet tumors to a tumor with similar multistage pathogenesis arising in a different tissue. The relative homing efficiencies in the various tumor models of the phage from the RIP1-Tag2 tumor screen fall broadly into two categories: those that selectively home to RIP1-Tag2 tumors (KAA, RGR, VGVA) and those that show a more general homing to other tumors in addition to RIP1-Tag2 (VGVG, KAR) (Figure 4A). The phage homing data were supported by i.v. injection of fluorescein-conjugated peptides corresponding to the phage. Results for the three representative peptides are summarized in Figure 4B, and an example of the tissue fluorescence produced following injection of the KAR peptide in different tumors is shown in Figures 4C–4E.

Homing during non-tumor angiogenesis was examined using angiogenesis in subcutaneously implanted matrigel plugs. All peptides except one showed no homing to the matrigel plugs. The RGR peptide appeared in a punctate manner in some blood vessels. However, the intensity was much lower and the pattern quite different than in RIP1-Tag lesions (data not shown). This indicates that this set of peptides are selective for neovascularization during tumorigenesis and are not general markers of neovessel formation.

Identification of candidate vascular receptors

The set of peptides homing to angiogenic neoplasias in the pancreas were applied to database searches, seeking to identify mouse proteins with sequences homologous to the peptides. Table 1 lists candidate proteins with such homologies that were deemed to be of interest. In theory, these proteins could correspond to putative ligands mimicked by the phage-displayed

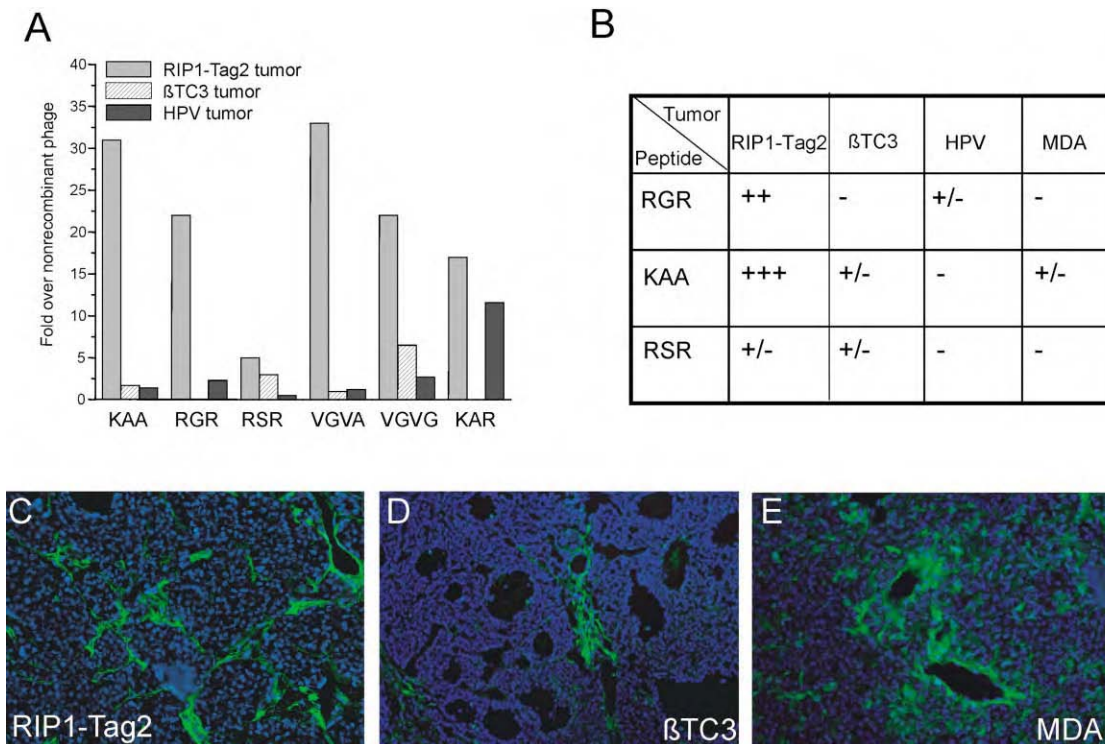


Figure 4. Evaluation of the neoplastic specificity of selected homing phage and peptides

A: Bar graph showing homing efficiency of individual phage to a pancreatic islet tumor in a RIP1-Tag2 mouse, a βTC3-derived subcutaneous transplant tumor in a nude mouse, and a squamous cell carcinoma in a K14-HPV16 mouse.

B: Table summarizing the relative homing of fluorescein-conjugated peptides to different tumor models. +++ indicates strong homing, as revealed by the fluorescent intensity of i.v. injected peptide, ++ indicates moderate homing, + indicates weak homing, - indicates absence of homing. Representative images of fluorescein-conjugated KAR peptide homing to a RIP1-Tag2 pancreatic islet tumor (C), a βTC3 subcutaneous tumor (D), and an MDA subcutaneous tumor (E) are also shown. Magnification 200×.

peptides. Many of the candidate proteins have been previously associated with the vasculature. One protein, collagen XII, was found to share homology with two peptides: KAR (CKGAKAR) and VGVA (FRVGADV), though in different structural domains. It is interesting to note that collagen XII was also identified by gene expression profiling as a gene that is overexpressed in tumor endothelial cells (St. Croix et al., 2000; and <http://mendel.imp.univie.ac.at/SEQUENCES/TEMS/mainpgs/temtable.html>).

It was somewhat surprising that homologies to peptide se-

quences in two cell surface receptors, fibroblast growth factor receptor 1 (FGFR1) and Tie-1, were revealed by homology searching, as phage-displayed peptides have traditionally been thought to mimic ligands not receptors. However, in the case of FGFR1, the particular peptide sequence (YQLDV) has been reported to be in the ligand binding domain D2 (Plotnikov et al., 1999), suggesting the possibility that the phage displaying this peptide may in fact be binding to FGFR1 ligands, i.e., the fibroblast growth factors (FGFs). It is well known that many of the

Table 1. Candidate mouse proteins sharing motifs with homing peptides

Peptide	Peptide sequence	Extended motif	Mouse protein with the motif	Accession number
RGR	CRGRRST	RGRRS RGRR	PDGF-B Stromal interaction molecule 2	P31240 Q9P246
RSR	CRSRKG	CRSR-G	Cadherin EGF LAG receptor 1	O35161
KAA	CKAAKNK	CKA-K	WNT-2	NPO76142
KAR	CKGAKAR	CKGAKA AKAR GAKAR	Collagen XII Collagen XII Claudin 9	Q60847 Q60847 Q9ZOS7
VGVA	FRVGADV	F-VGVADV RVGV	Collagen XII Collagen XII	Q60847 Q60847
EYQ	CEYQLDVE	CEYQL YQLDV YQLDV	Semaphorin 4C FGFR1 Tie-1	Q64151 P16092 Q06806

Peptides were analyzed using a BLAST (NCBI) search against the SWISSPROT database, using the option for short nearly exact matches, to identify mouse proteins with homologous sequences.

heparin binding FGFs are sequestered in the extracellular matrix and basement membrane by binding to heparan sulfate proteoglycans (Ornitz and Itoh, 2001), which is consistent with phage homing to these FGF depots in vivo. As the Tie-1 receptor is an orphan receptor tyrosine kinase, ligand binding information is not currently available; however, the peptide sequence homology is in the extracellular domain (Sato et al., 1993).

Another provocative homology was seen for the RGR peptide (CRGRRST), which is contained within the B chain of the pro-form of platelet-derived growth factor (PDGF-B), a known ligand for the transmembrane receptor tyrosine kinase PDGFR β . The RGR sequence homology (RGRRS) spans the pro-peptide cleavage site of pro-PDGF-B (Johnsson et al., 1984). To investigate the hypothesis that the RGR peptide was homing to PDGFR β by virtue of this homology, we transfected 293T cells with a fusion gene designed to overexpress PDGFR β . The binding of RGR phage was 20-fold more efficient to PDGFR β -transfected cells than nontransfected cells. In contrast, no binding above the background was detected toward cells transfected with vascular endothelial growth factor receptor 2 (VEGFR2) (Figure 5A). Moreover, when we tested the RSR phage, which has a peptide sequence similar to RGR, no specific binding was observed either to PDGFR β - or VEGFR2-transfected cells (Figure 5A). The association of RGR with PDGFR β was further substantiated when intravenously injected fluorescein-conjugated RGR peptide was shown to colocalize with PDGFR β , visualized by subsequent immunostaining of tissue sections from RIP1-Tag2 tumors. Merging of the RGR-FITC image (Figure 5B, panel a) with the antibody staining for PDGFR β (Figure 5B, panel b) revealed almost complete colocalization (Figure 5B, panels c and d).

Discussion

We set out in this and the companion study (Hoffman et al., 2003) to characterize the vasculature during the discrete stages of organ-specific carcinogenesis, using a profiling technology based on peptide libraries displayed on the surface of bacteriophage. Phage that display a peptide with an appropriate binding specificity home via the circulation to the site of binding affinity. As such, phage profiling can reveal differences in the composition and properties of the vasculature of different organs and pathological lesions. Using as a target the RIP1-Tag2 mouse model of multistage tumorigenesis involving the pancreatic islets of Langerhans, we have identified peptides that discriminate between the vasculature of the premalignant angiogenic islets and the fully developed tumors. Most of the identified homing peptides appear to selectively detect vascular changes induced during tumorigenesis in the endocrine pancreas, but not in other tumors growing in or under the skin. Remarkably, three peptides representing one of the distinctive homing classes (to angiogenic progenitors, to tumors, or to both) each colocalized with markers separately identifying endothelial cells and pericytes in the angiogenic lesions. The sequences of the homing peptides suggest candidate proteins containing homologous sequences that are mimicked by peptide binding to the angiogenic vasculature.

Insights into organ-specific differences in neoplastic vasculature

The influence of tissue microenvironment in tumor development is increasingly appreciated (Coussens and Werb, 2002; Liotta

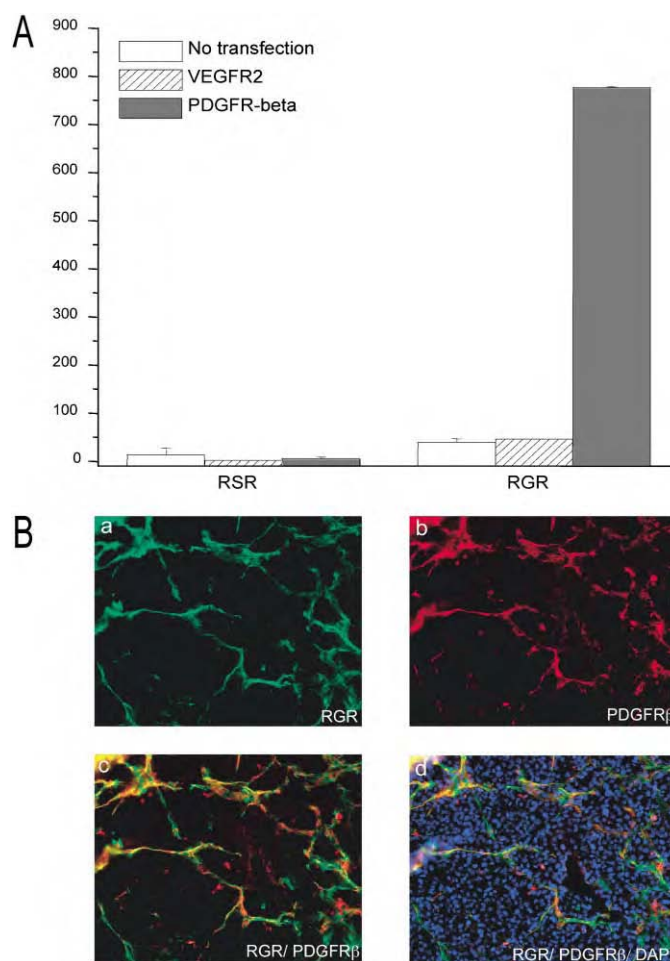


Figure 5. PDGFR β is a candidate receptor for RGR peptide

A: Bar graph showing binding of RGR or RSR phage to 293T cells transfected with either the PDGFR β , the related VEGFR2, or nontransfected cells. Y axis = fold over nonrecombinant phage.

B: Colocalization of fluorescein-conjugated RGR peptide (a, green) with the PDGFR β antibody (b, red) and merged images (c and d) in RIP1-Tag2. Magnification 400 \times .

and Kohn, 2001). As developing neoplasias activate angiogenesis and recruit a neovasculature from the surrounding tissue microvascular bed, the organ microenvironment may influence the morphology and physiology of the tumor neovasculature. Evidence in support of organ-specific differences has come, for example, by comparing permeability in the vessels of transplant tumors as a function both of tumor type and the host tissue site (Hobbs et al., 1998; Roberts et al., 1998).

We asked whether tumors arising in their natural microenvironment are different from those developing in another "foreign" location by comparing endogenously arising RIP1-Tag2 tumors in the pancreas with β TC3 cell-derived tumors grown subcutaneously (the β TC3 cell line was established from a RIP1-Tag2 pancreatic islet tumor; Efrat et al., 1988). The results from both phage and peptide binding (Figure 4 and data not shown) indicate that some phage/peptides home to β TC3 subcutaneous tumors in addition to RIP1-Tag2 endogenous tumors, albeit less efficiently (e.g., VGVG). However, most of the other phage/

peptides do not show any appreciable homing to β TC3 tumors by comparison to RIP1-Tag2 tumors (e.g., KAA and VGVA), supporting the predominant role of the tissue microenvironment in influencing some of the receptors that are displayed on the cell surface.

Similar results were found for the two other tumor types we studied: squamous cell carcinomas of the epidermis arising in K14-HPV16 transgenic mice and subcutaneous xenograft tumors of the human MDA-MB-435 breast cancer cell line. KAR and VGVG were the only phage/peptides that homed appreciably to these models, whereas the other peptides showed a similar lack of homing, as for β TC3 tumors. Thus, the majority of phage-displayed and soluble peptides homed selectively to the tumor vasculature of RIP1-Tag2 tumors arising in their natural environment in the endocrine pancreas, showing little affinity for tumors growing subcutaneously or in the skin itself. By contrast, in the aforementioned study of tumor endothelial genes revealed by expression profiling (St. Croix et al., 2000), a number of the tumor-specific endothelial genes identified as upregulated in a colorectal cancer screen were also found in the tumor endothelium of other cancers (lung, brain, pancreas, and breast primary tumors; and a colorectal metastasis to the liver). Our method has clearly revealed a partially overlapping but distinctive set of markers. These results support the existence of both tumor-specific and tumor-generic vascular markers and may have implications for interpretation of data forthcoming from xenograft tumor models. If vascular markers are not recapitulated in transplant models representing a particular organ-specific cancer, then aspects of its phenotypic behavior and response to therapy (particularly targeted antiangiogenic and antivascular agents) may differ as well. Similar results have been seen in the companion study (Hoffman et al., 2003) comparing *de novo* epidermal squamous cell carcinomas in the K14-HPV16 mice with transplant tumors in the adjacent subcutaneous microenvironment.

Homing peptides revealing molecular anatomy of tumor vasculature

We have begun to investigate candidate binding moieties ("receptors") for the RIP1-Tag2 homing peptides, initially by searching protein databases for proteins that contain the homing peptide sequences and thus might represent the endogenous protein mimicked by the peptide. It is striking that a number of the candidate proteins revealed by the search have been implicated in some aspect of angiogenesis (PDGFs, WNTs, claudins, collagen XII, FGFR1, Tie-1). We chose to evaluate the PDGF-B homology in light of recent evidence implicating PDGF signaling in the angiogenic phenotype in the RIP-Tag2 model: three PDGF ligand genes are expressed in the tumor endothelial cells, while PDGF receptor β is expressed in tumor pericytes (Bergers et al., 2003). Pharmacological inhibition of PDGFR signaling in RIP1-Tag2 mice disrupted pericyte association with the tumor endothelium, inhibited angiogenesis, and reduced the vascularity of the islet tumors (Bergers et al., 2003). The results add to a knowledge base implicating PDGF signaling in pericyte-endothelial cell homeostasis, both in developing vessels (Betsholtz et al., 2001; Leveen et al., 1994; Lindahl et al., 1997; Soriano, 1994) and in tumors (Heldin and Westermark, 1999; Ostman and Heldin, 2001).

The evaluation of RGR in light of its homology to PDGF-B clearly suggests its homing is associated with PDGFR expres-

sion and/or signaling. The most compelling evidence comes from overexpressing PDGFR β in cultured cells. There was a striking increase in the binding of the RGR phage to cells transfected with PDGFR β , whereas transfection with a structurally related receptor tyrosine kinase, VEGFR2, had no effect on the binding. Moreover, systemically infused RGR colocalizes with virtually all of the PDGFR β detected by immunostaining in angiogenic islets and tumors. Both lines of evidence support the model that RGR binds to PDGFR β . There are, however, other data that complicate this simple conclusion. First, RGR colocalizes not only with a pericyte marker, NG2, consistent with PDGFR β expression in pericytes, but also with an endothelial cell marker, MECA32, indicative of homing to endothelial cells (which do not typically express PDGFR β —see Bergers et al., 2003). Second, the RGR peptide sequence overlaps the pro-peptide processing site and is thus only partially represented in mature PDGF-B ligand; moreover, the sequences for PDGF homo- and heterodimerization and for receptor binding are not at the N terminus of the mature ligand (Clements et al., 1991; Heldin and Westermark, 1999; Ostman et al., 1991). Thus it is not clear how RGR might bind either to PDGF ligands or receptors. These data lead us to suggest that RGR mimics a protein-protein interaction site in pro-PDGF-B that mediates its specific homing and mimics bona fide associations of pro-PDGF-B. One possible association for RGR is either with PDGFR β itself or with a protein induced by its expression, given the enhanced binding seen in the transfected cells overexpressing PDGFR β as well as the observed colocalization of RGR with PDGFR β in angiogenic islets and tumors. It is interesting to note that a similar sequence is found in PDGF-D, a related PDGF ligand that also signals through PDGFR β . The sequence RGRS is located in the secreted PDGF-D at the site of processing from the inactive to active form of PDGF-D (Bergsten et al., 2001; LaRoche et al., 2001).

The additional colocalization of RGR with the endothelial cell marker MECA32 suggests that an RGR binding moiety is also expressed by endothelial cells or shared between pericytes and endothelial cells. While there is no obvious coimmunostaining of either endothelial cell marker (CD31, MECA32) with any of several pericyte markers (desmin, SMA, NG2) in the angiogenic islets or tumors (J.J. and G.B., unpublished observations), a small subset of FAC-sorted cells within RIP1-Tag2 tumors are positive for both CD31 and NG2 (G.B., unpublished observations). In addition, both cell types contribute to the vascular basement membrane and the extracellular matrix that separates and envelops them, and these structures could contain RGR binding motifs produced by one or both cell type and localized amongst them. Indeed, purified PDGF-B has been shown to bind various ECM and BM proteins, including collagens I-IV (Somasundaram and Schuppan, 1996), laminin-1, nidogen, and perlecan (Gohring et al., 1998). Another attractive candidate for RGR binding is the predicted prohormone processing enzyme that binds and cleaves pro-PDGF-B within the RGR homology. Interestingly, while the RGR phage and peptide homed effectively to angiogenic progenitor islets and solid tumors in RIP1-Tag2 mice, neither homed to angiogenic dysplasias or tumors in the HPV16 transgenic mice nor to the MDA-MB-435 subcutaneous tumors. These results suggest that PDGF signaling and the resultant vessel stabilization by pericytes may differ among tumors or that there are differences in pericyte activation and/or maturation (Morikawa et al., 2002). Alternatively, the blood

vessels in the squamous cell carcinomas, being less hemorrhagic, may limit the accessibility of the blood-borne phage and labeled peptides to the perivascular cells (see below).

Other homologies between homing peptides and endogenous proteins listed in Table 1 may also be significant. The fact that many of these proteins have been implicated in angiogenesis, or related biological processes, supports this prediction. For example, two of the peptides, KAR and VGVA, show homology to collagen XII, which is associated with blood vessels in the developing embryo (Bohme et al., 1995; Oh et al., 1993). Colocalization of both peptides with vascular markers (data not shown) is consistent with the predicted localization of collagen XII.

Lessons from profiling different tumor types

It is of interest to compare and contrast the results reported here to that of the companion study (Hoffman et al., 2003), which similarly used phage display libraries to profile the angiogenic dysplasias and squamous cell carcinomas that arise in the skin of K14-HPV16 transgenic mice. That study produced a series of homing peptides that were selective for angiogenic progenitors or solid tumors. And again, both tumor type-selective and tumor-generic phage were identified; their analysis focused on skin tumor-specific phage that did not home to the angiogenic vasculature in the stages of pancreatic islet carcinogenesis in RIP1-Tag2 mice. The skin-tumor homing peptides had different sequences from those identified herein, and their candidate cellular homologs (and prospective binding moieties) were distinctive. In sum, each study identified both tumor type-specific and stage-specific vascular homing peptides, further supporting the proposition that organ microenvironment imparts distinctive constraints on neoplastic development that affects the characteristics of the neovasculature induced to sustain tumor development and progression.

It is intriguing that the two organ sites of neoplastic development (skin and pancreas) preferentially selected phage with different cellular specificity. The HPV phage all homed exclusively to endothelial cells, whereas each of the RIP1-Tag2 phage representing the three homing classes (angiogenic progenitor, tumor, or both) chosen for analysis homed both to pericytes and to endothelial cells. This suggests significant differences in the vascular morphology and/or functionality in the skin and pancreas. One difference may be in vascular permeability. The islet tumors are blood red from hemorrhaging and the angiogenic vasculature is permeable to a variety of macromolecules (Hashizume et al., 2000; Thurston et al., 1998). By contrast, the skin tumors are white, indicative of less hemorrhagic vessels or higher interstitial pressure. Thus the phage population circulating through the vascular system in RIP1-Tag2 mice may have had ready access to the perivascular microenvironment, whereas the "tighter" vessels in the skin lesions may limit such accessibility. Future studies on the expression of the "receptors" identified by these distinctive classes of homing peptides should clarify whether their binding moieties are differentially expressed and/or differentially accessible via the vasculature in these distinctive tumor types and their angiogenic progenitor lesions, providing further insight into the dynamics and tissue-specific qualities of the angiogenic phenotype.

The selective accumulation of fluorescein-conjugated peptides in the RIP-Tag lesions indicates that a monovalent peptide-receptor interaction is robust enough to carry a payload to the

target. As such, these peptides could be used as biomarkers or for imaging, particularly of pre-neoplastic lesions, which are notoriously difficult to detect. The peptides homing to angiogenic islets, for example, could be used both as markers of the angiogenic switch and to monitor therapeutic response to antiangiogenic agents, in much the same way as parameters such as microvessel density are currently employed. Future experiments will test the efficacy of targeting of imaging agents and active drugs to multiple stages of tumorigenesis.

In conclusion, we have used phage display to profile the vasculature during the distinctive stages of multistep tumorigenesis in a prototypical mouse model of cancer. We have identified three different classes of stage-specific peptides suggestive of distinctive characteristics of the neovasculature in premalignant and malignant lesions. We expect that the selectivity in peptide homing will help us understand the stage-specific differences in efficacy observed for angiogenesis inhibitor therapy in the RIP1-Tag2 model (Bergers et al., 1999). In addition, it may be possible to selectively target antitumor therapies to individual or multiple cell types during RIP-Tag tumorigenesis using these homing peptides conjugated to, for example, proapoptotic sequences, as previously reported (Ellerby et al., 1999). It will be of further interest to ask whether these homing peptides can similarly characterize the neovasculature of stages in human pancreatic islet carcinogenesis, as well as in other organ-specific cancers in mouse models and humans.

Experimental procedures

Generation of mice and tissue isolation

The generation of RIP1-Tag2 mice (Hanahan, 1985) and K14-HPV16 mice (Arbeit et al., 1994; Coussens et al., 1996) has been reported. Angiogenic islets were isolated from 8- and 12-week-old RIP1-Tag2 mice by collagenase digestion of the excised pancreas and selected based on their red, hemorrhagic appearance (Parangi et al., 1995). Tumors were microdissected from the excised pancreas of 12-week-old RIP1-Tag2 mice and the surrounding exocrine tissue was carefully removed. The synchronicity of tumorigenesis in the RIP1-Tag2 model allowed us to simultaneously isolate pools of angiogenic islets and tumors from the same mouse at 12 weeks of age, thus affording us the opportunity to directly compare homing of individual phage to different stages in an individual mouse/pancreas. Tumors were dissected from the ear or chest of K14-HPV16 mice. For the β TC3 allograft models, 10^6 β TC3 tumor cells (Efrat et al., 1988) were inoculated under the skin of the rear flank of *nu/nu* mice in a BALB/c background and allowed to grow until approximately 5 mm in size, and then used for experimental analysis. MDA-MB-435 xenograft models were generated by inoculating 10^6 tumor cells subcutaneously in the chest of *nu/nu* BALB/c mice. Tumors were used for the homing/binding experiments at 8–12 weeks after injection of the tumor cells. Matrigel plug angiogenesis was induced as previously described (Fulgham et al., 1999; Ngo et al., 2000; Yi et al., 2003). Briefly, 100 μ l of Matrigel containing 80 ng/ml bFGF was injected subcutaneously in the abdominal area of BALB/c/*nu/nu* mice, and at day 8, the mice were injected with fluorescein-conjugated peptides as detailed below.

Phage libraries and library screening

The screening process involved two *ex vivo* selection rounds followed by 2–3 *in vivo* selection rounds. For the *ex vivo* selections, cell suspensions were prepared from the different RIP1-Tag2 lesions in 12-week-old RIP1-Tag2 mice and incubated overnight at 4°C with 10^9 plaque forming units (p.f.u.) of a T7 phage (Novagen) displayed CX₂C peptide library. The cells were washed to remove unbound phage and the bound phage rescued and amplified in *E. coli*. This procedure enriches for phage that bind to tumor, endothelial, and other stromal cells present in the suspension. The *ex vivo* pre-selected phage pool was injected intravenously into 12-week-old RIP1-Tag2 mice through the tail vein, allowed to circulate for 7 min, and heart-perfused with PBS to remove unbound intravascular phage. As the vascula-

ture is preferentially available for the phage to bind in this selection, there is an enrichment of phage that bind to the endothelium of the target tissue. The RIP1-Tag2 lesions and control tissues (brain, kidney, spleen, lung, "white" pancreas [i.e., not containing any hemorrhagic lesions], and liver) were excised to allow for comparison of homing efficiencies. Cell suspensions were prepared by mechanical disruption of the tissues, washed to remove unbound phage, and the bound phage rescued and amplified by adding *E. coli*. The phage pool was reinjected into mice at a similar disease stage, and the cycle repeated. In each experiment, nonrecombinant control phage was used as a control for relative selectivity. Sets of 96 phage clones were randomly collected from each homing phage population. The peptide-encoding DNA inserts were amplified by PCR, and the PCR products sequenced. Phage representing the most frequently appearing peptide motifs were individually tested for their ability to selectively home to the lesions on which they were selected, relative to other stages in the tumorigenesis pathway and to control organs. Fluorescein-conjugated peptides corresponding to these phage insert sequences were synthesized using an automated peptide synthesizer with standard solid-phase fluorenylmethoxycarbonyl (Fmoc) chemistry. One hundred micrograms of each individual fluorescein-conjugated peptide was injected intravenously into the tail vein of RIP1-Tag2 mice at 8 or 12 weeks of age and into normal BL/6 mice. The peptide was allowed to circulate for 7 min, followed by heart perfusion first with PBS and then with Zn-buffered formalin. The RIP1-Tag2 pancreas and control organs (brain, kidney, liver, lung, and spleen) were removed, fixed for 1 hr in formalin, washed with $1 \times$ PBS, placed in 30% sucrose for several hours, washed with $1 \times$ PBS, and embedded in OCT (Tissue-Tek). Each peptide was injected into at least three individual RIP1-Tag2 or normal mice at each of the different stages.

Histology and immunohistochemistry

To examine the localization of injected fluorescein-conjugated peptides, frozen sections ($10 \mu\text{m}$ thick) were cut on a cryostat, mounted in Vectashield Mounting Medium with DAPI (Vector Laboratories), and visualized under an inverted fluorescent microscope or a confocal microscope (Zeiss LSM 510 META). For immunohistochemistry, frozen slides were preincubated with blocking buffer ($1 \times$ PNB from NEN Biosciences) for 1 hr, washed several times in $1 \times$ PBS, and incubated with the primary antibody of interest overnight at 4°C . The cell-specific antibodies used were rat monoclonal anti-mouse CD31 (1:200; BD Pharmingen), rat monoclonal anti-mouse MECA32 (1:200; BD Pharmingen), rabbit polyclonal anti-mouse NG2 (1:200; Chemicon), and rat monoclonal anti-mouse PDGFR β (CD140b) (1:200; eBioscience). The corresponding secondary antibodies; Cy-3 donkey anti-rabbit IgG and Rhodamine Red donkey anti-rat IgG (Jackson ImmunoResearch), were used at a 1:200 dilution and incubated for 1 hr at room temperature. The following species-matched immunoglobulins were used as negative controls: rabbit IgG (Vector Laboratories) and rat IgG (Jackson ImmunoResearch) at a 1:200 dilution. The slides were washed several times in $1 \times$ PBS and mounted in Vectashield Mounting Medium with DAPI (Vector Laboratories). Hematoxylin and eosin (H&E) staining was performed for histological grading of adjacent sections by standard methods, and lesions were graded as previously described (Lopez and Hanahan, 2002).

Transfection and phage binding assay

293T cells were transfected with plasmids encoding PDGFR β or VEGFR2 (Borges et al., 2000) using Fugene transfection reagent (Roche Diagnostics). Briefly, $10 \mu\text{g}$ of plasmid was mixed with $700 \mu\text{l}$ of DMEM without serum and $30 \mu\text{l}$ of Fugene and incubated for 15 min at room temperature before adding the mixture to the cells. Forty-eight hours posttransfection, the cells were detached from the culture plates using EDTA and washed $1 \times$ with PBS. RSR, RGR, and the control nonrecombinant phage (about 1×10^9 pfu) were incubated with the transfected cells for 2 hr at 4°C , followed by five washes with 1% BSA in PBS to remove the unbound phage. The bound phage were rescued by adding bacteria, and the binding efficiencies were determined by plaque assay.

Acknowledgments

We thank Cherry Concengco for excellent technical assistance and Fernando Ferrer for peptide synthesis. We thank Dr. Kristian Pietras for reading the manuscript and for helpful suggestions. This study was supported by a grant

from the National Cancer Institute CA82713 (to E.R. and D.H.) and by grants from the Department of Defense DAMD 17-02-1-0315 (E.R.) and the N.C.I. (D.H.). J.A.J. received support from the Leukemia and Lymphoma Society. P.L. received support from the Academy of Finland and the Finnish Cultural Foundation.

Received: June 5, 2003

Revised: September 10, 2003

Published: November 24, 2003

References

- Arap, W., Pasqualini, R., and Ruoslahti, E. (1998). Cancer treatment by targeted drug delivery to tumor vasculature in a mouse model. *Science* 279, 377–380.
- Arbeit, J., Munger, K., Howley, P.M., and Hanahan, D. (1994). Progressive squamous epithelial neoplasia in K14-human papillomavirus type 16 transgenic mice. *J. Virol.* 68, 4358–4368.
- Bergers, G., Hanahan, D., and Coussens, L.M. (1998). Angiogenesis and apoptosis are cellular parameters of neoplastic progression in transgenic mouse models of tumorigenesis. *Int. J. Dev. Biol.* 42, 995–1002.
- Bergers, G., Javaherian, K., Lo, K.M., Folkman, J., and Hanahan, D. (1999). Effects of angiogenesis inhibitors on multistage carcinogenesis in mice. *Science* 284, 808–812.
- Bergers, G., Song, S., Meyer-Morse, N., Bergsland, E., and Hanahan, D. (2003). Benefits of targeting both pericytes and endothelial cells in the tumor vasculature with kinase inhibitors. *J. Clin. Invest.* 111, 1287–1295.
- Bergsten, E., Uutela, M., Li, X., Pietras, K., Ostman, A., Heldin, C.-H., Alitalo, K., and Eriksson, U. (2001). PDGF-D is a specific protease-activated ligand for the PDGF β -receptor. *Nat. Cell Biol.* 3, 512–516.
- Betsholtz, C., Karlsson, L., and Lindahl, P. (2001). Developmental roles of platelet-derived growth factors. *Bioessays* 23, 494–507.
- Bohme, K., Li, Y., Oh, P.S., and Olsen, B.R. (1995). Primary structure of the long and short splice variants of mouse collagen XII and their tissue-specific expression during embryonic development. *Dev. Dyn.* 204, 432–445.
- Borges, E., Jan, Y., and Ruoslahti, E. (2000). Platelet-derived growth factor receptor beta and vascular endothelial growth factor receptor 2 bind to the beta 3 integrin through its extracellular domain. *J. Biol. Chem.* 275, 39867–39873.
- Burg, M.A., Pasqualini, R., Arap, W., Ruoslahti, E., and Stallcup, W.B. (1999). NG2 proteoglycan-binding peptides target tumor neovasculature. *Cancer Res.* 59, 2869–2874.
- Carmeliet, P., and Jain, R. (2000). Angiogenesis in cancer and other diseases. *Nature* 407, 249–257.
- Clements, J.M., Bawden, L.J., Bloxidge, R.E., Catlin, G., Cook, A.L., Craig, S., Drummond, A.H., Edwards, R.M., Fallon, A., Green, D.R., et al. (1991). Two PDGF-B chain residues, arginine 27 and isoleucine 30, mediate receptor binding and activation. *EMBO J.* 10, 4113–4120.
- Coussens, L.M., and Werb, Z. (2002). Inflammation and cancer. *Nature* 420, 860–867.
- Coussens, L.M., Hanahan, D., and Arbeit, J.M. (1996). Genetic predisposition and parameters of malignant progression in K14-HPV16 transgenic mice. *Am. J. Pathol.* 149, 1899–1917.
- Efrat, S., Linde, S., Kofod, H., Spector, D., Delannoy, M., Grant, S., Hanahan, D., and Baekkeskov, S. (1988). Beta-cell lines derived from transgenic mice expressing a hybrid insulin gene-oncogene. *Proc. Natl. Acad. Sci. USA* 85, 9037–9041.
- Ellerby, H.M., Arap, W., Ellerby, L.M., Kain, R., Andrusiak, R., Rio, G.D., Krajewski, S., Lombardo, C.R., Rao, R., Ruoslahti, E., et al. (1999). Anti-cancer activity of targeted pro-apoptotic peptides. *Nat. Med.* 5, 1032–1038.
- Folkman, J., Watson, K., Ingber, D., and Hanahan, D. (1989). Induction of

- angiogenesis during the transition from hyperplasia to neoplasia. *Nature* 339, 58–61.
- Fulgham, D.L., Widhalm, S.R., Martin, S., and Coffin, J.D. (1999). FGF-2 dependent angiogenesis is a latent phenotype in basic fibroblast growth factor transgenic mice. *Endothelium* 6, 185–195.
- Gohring, W., Sasaki, T., Heldin, C.H., and Timpl, R. (1998). Mapping of the binding of platelet-derived growth factor to distinct domains of the basement membrane proteins BM-40 and perlecan and distinction from the BM-40 collagen-binding epitope. *Eur. J. Biochem.* 255, 60–66.
- Hallman, R.D., Mayer, D.N., Berg, E.L., Broermann, R., and Butcher, E.C. (1995). Novel mouse endothelial cell surface marker is suppressed during differentiation of the blood brain barrier. *Dev. Dyn.* 202, 325–332.
- Hanahan, D. (1985). Heritable information of pancreatic beta-cell tumors in transgenic mice expressing recombinant insulin/simian virus 40 oncogenes. *Nature* 315, 115–122.
- Hanahan, D., and Folkman, J. (1996). Patterns and emerging mechanisms of the angiogenic switch during tumorigenesis. *Cell* 86, 353–364.
- Hashizume, H., Baluk, P., Morikawa, S., McLean, J.W., Thurston, G., Roberge, S., Jain, R.K., and McDonald, D.M. (2000). Openings between defective endothelial cells explain tumor vessel leakiness. *Am. J. Pathol.* 156, 1363–1380.
- Heldin, C.H., and Westermark, B. (1999). Mechanism of action and in vivo role of platelet-derived growth factor. *Physiol. Rev.* 79, 1283–1316.
- Hobbs, S.K., Monsky, W.L., Yuan, F., Roberts, W.G., Griffith, L., Torchilin, V.P., and Jain, R.K. (1998). Regulation of transport pathways in tumor vessels: Role of tumor type and microenvironment. *Proc. Natl. Acad. Sci. USA* 95, 4607–4612.
- Hoffman, J.A., Giraudo, E., Singh, M., Zhang, L., Inoue, M., Porkka, K., Hanahan, D., and Ruoslahti, E. (2003). *Cancer Cell* 4, this issue, 383–391.
- Johnsson, A., Heldin, C.H., Wasteson, A., Westermark, B., Deuel, T.F., Huang, J.S., Seeburg, P.H., Gray, A., Ullrich, A., Scrace, G., et al. (1984). The c-sis gene encodes a precursor of the B chain of platelet-derived growth factor. *EMBO J.* 3, 921–928.
- Laakkonen, P., Porkka, K., Hoffman, J.A., and Ruoslahti, E. (2002). A tumor-homing peptide with a targeting specificity related to lymphatic vessels. *Nat. Med.* 8, 751–755.
- LaRochelle, W.J., Jeffers, M., McDonald, W.F., Chillakuru, R.A., Giese, N.A., Lokker, N.A., Sullivan, C., Boldog, F.L., Yang, M., Vernet, C., et al. (2001). PDGF-D, a new protease-activated growth factor. *Nat. Cell Biol.* 3, 517–521.
- Leppink, D.M., Bishop, D.K., Sedmak, D.D., Henry, M.L., Ferguson, R.M., Streeter, P.R., Butcher, E.C., and Orosz, C.G. (1989). Inducible expression of an endothelial cell antigen on murine myocardial vasculature in association with interstitial cellular infiltration. *Transplantation* 48, 874–877.
- Leveen, P., Pekny, M., Gebre-Medhin, S., Swolin, B., Larsson, E., and Betsholtz, C. (1994). Mice deficient for PDGF-B show renal, cardiovascular and hematological abnormalities. *Genes Dev.* 8, 1875–1887.
- Lindahl, P., Johansson, B.R., Leveen, P., and Betsholtz, C. (1997). Pericyte loss and microaneurysm formation in PDGF-B deficient mice. *Science* 277, 242–245.
- Liotta, L.A., and Kohn, E.C. (2001). The microenvironment of the tumour-host interface. *Nature* 411, 375–379.
- Lopez, T., and Hanahan, D. (2002). Elevated levels of IGF-1 receptor convey invasive and metastatic capability in a mouse model of pancreatic islet tumorigenesis. *Cancer Cell* 1, 339–353.
- Morikawa, S., Baluk, P., Kaidoh, T., Haskell, A., Jain, R.K., and McDonald, D.M. (2002). Abnormalities in pericytes on blood vessels and endothelial sprouts in tumors. *Am. J. Pathol.* 160, 985–1000.
- Ngo, C.V., Gee, M., Akhtar, N., Yu, D., Volpert, O., Auerbach, R., and Thomas-Tikhonenko, A. (2000). An in vivo function for the transforming Myc protein: elicitation of the angiogenic phenotype. *Cell Growth Differ.* 11, 201–210.
- Oh, S.P., Griffith, C.M., Hay, E.D., and Olsen, B.R. (1993). Tissue-specific expression of type XII collagen during mouse embryonic development. *Dev. Dyn.* 196, 37–46.
- Ornitz, D.M., and Itoh, N. (2001). Fibroblast growth factors. *Genome Biol.* 2, 3005.1–3005.12.
- Ostman, A., and Heldin, C.H. (2001). Involvement of platelet-derived growth factor in disease: development of specific antagonists. *Adv. Cancer Res.* 80, 1–38.
- Ostman, A., Andersson, M., Hellman, U., and Heldin, C.H. (1991). Identification of three amino acids in the platelet-derived growth factor (PDGF) B-chain that are important for binding to the PDGF- β receptor. *J. Biol. Chem.* 266, 10073–10077.
- Parangi, S., Dietrich, W., Christofori, G., Lander, E.S., and Hanahan, D. (1995). Tumor suppressor loci on mouse chromosomes 9 and 16 are lost at distinct stages of tumorigenesis in a transgenic model of islet cell carcinoma. *Cancer Res.* 55, 6071–6076.
- Pasqualini, R., and Ruoslahti, E. (1996). Organ targeting *in vivo* using phage display peptide libraries. *Nature* 380, 364–366.
- Pasqualini, R., Koivunen, E., Kain, R., Lahdenranta, J., Sakamoto, M., Stryhn, A., Ashmun, R.A., Shapiro, L.H., Arap, W., and Ruoslahti, E. (2000). Aminopeptidase N is a receptor for tumor-homing peptides and a target for inhibiting angiogenesis. *Cancer Res.* 60, 722–727.
- Plotnikov, A.N., Schlessinger, J., Hubbard, S.R., and Mohammadi, M. (1999). Structural basis for FGF receptor dimerization and activation. *Cell* 98, 641–650.
- Porkka, K., Laakkonen, P., Hoffman, J.A., Bernasconi, M., and Ruoslahti, E. (2002). A fragment of the HMGN2 protein homes to the nuclei of tumor cells and tumor endothelial cells *in vivo*. *Proc. Natl. Acad. Sci. USA* 99, 7444–7449.
- Rajotte, D., Arap, W., Hagedorn, M., Koivunen, E., Pasqualini, R., and Ruoslahti, E. (1998). Molecular heterogeneity of the vascular endothelium revealed by *in vivo* phage display. *J. Clin. Invest.* 102, 430–437.
- Roberts, W.G., Delaat, J., Nagane, M., Huang, S., Cavenee, W.K., and Palade, G.E. (1998). Host microvasculature influence on tumor vascular morphology and endothelial gene expression. *Am. J. Pathol.* 153, 1239–1248.
- Ruoslahti, E. (2002). Specialization of tumour vasculature. *Nat. Rev. Cancer* 2, 83–90.
- Sato, T.N., Qin, Y., Kozak, C.A., and Audus, K.L. (1993). Tie-1 and Tie-2 define another class of putative receptor tyrosine kinase genes expressed in early embryonic vascular system. *Proc. Natl. Acad. Sci. USA* 90, 9355–9358.
- Schlingemann, R.O., Rietveld, F.J., de Waal, R.M., Ferrone, S., and Ruiter, D.J. (1990). Expression of the high molecular weight melanoma-associated antigen by pericytes during angiogenesis in tumors and in healing wounds. *Am. J. Pathol.* 136, 1393–1405.
- Schlingemann, R.O., Rietveld, F.J., Kwaspen, F., van de Kerkhof, P.C., de Waal, R.M., and Ruiter, D.J. (1991). Differential expression of markers for endothelial cells, pericytes, and basal lamina in the microvasculature of tumors and granulation tissues. *Am. J. Pathol.* 138, 1335–1347.
- Somasundaram, R., and Schuppan, D. (1996). Type I, II, III, IV, V, and VI collagens serve as extracellular ligands for the isoforms of platelet-derived growth factor (AA, BB, and AB). *J. Biol. Chem.* 271, 26884–26891.
- Soriano, P. (1994). Abnormal kidney development and hematological disorders in PDGF β -receptor mutant mice. *Genes Dev.* 8, 1888–1896.
- St. Croix, B., Rago, C., Velculescu, V., Traverso, G., Romans, K.E., Montgomery, E., Lal, A., Riggins, G.J., Lengauer, C., Vogelstein, B., and Kinzler, K.W. (2000). Genes expressed in human tumor endothelium. *Science* 289, 1197–1202.
- Thurston, G., McLean, J.W., Rizen, M., Baluk, P., Haskell, A., Murphy, T.J., Hanahan, D., and McDonald, D.M. (1998). Cationic liposomes target angiogenic endothelial cells in tumors and chronic inflammation in mice. *J. Clin. Invest.* 101, 1401–1413.
- Yi, M., Sakai, T., Fassler, R., and Ruoslahti, E. (2003). Antiangiogenic proteins require plasma fibronectin or vitronectin for in vivo activity. *Proc. Natl. Acad. Sci. USA*, in press.

A tumor-homing peptide with a targeting specificity related to lymphatic vessels

PIRJO LAAKKONEN¹, KIMMO PORKKA¹, JASON A. HOFFMAN² & ERKKI RUOSLAHTI¹

¹Cancer Research Center, The Burnham Institute, La Jolla, California, USA

²Program in Molecular Pathology, The Burnham Institute and Department of Pathology, University of California San Diego School of Medicine, La Jolla, California, USA

Correspondence should be addressed to E.R.; email: ruoslahti@burnham.org

Published online: 10 June 2002, doi:10.1038/nm720

Blood vessels of tumors carry specific markers that are usually angiogenesis-related^{1,2}. We previously used phage-displayed peptide libraries *in vivo* to identify peptides that home to tumors through the circulation and that specifically bind to the endothelia of tumor blood vessels^{3,4}. Here we devised a phage screening procedure that would favor tumor-homing to targets that are accessible to circulating phage, but are not blood vessels. Screening on MDA-MB-435 breast carcinoma xenografts yielded multiple copies of a phage that displays a cyclic 9-amino-acid peptide, LyP-1. Homing and binding to tumor-derived cell suspensions indicated that LyP-1 also recognizes an osteosarcoma xenograft, and spontaneous prostate and breast cancers in transgenic mice, but not two other tumor xenografts. Fluorescein-labeled LyP-1 peptide was detected in tumor structures that were positive for three lymphatic endothelial markers and negative for three blood vessel markers. LyP-1 accumulated in the nuclei of the putative lymphatic cells, and in the nuclei of tumor cells. These results suggest that tumor lymphatics carry specific markers and that it may be possible to specifically target therapies into tumor lymphatics.

We combined *ex vivo* and *in vivo* phage selections⁵ to search for peptides that recognize tumor-specific vessels other than blood vessels. We selected phage from a cyclic peptide library for binding to cell suspensions prepared from MDA-MB-435 breast cancer xenografts. To increase the likelihood of obtaining new kinds of homing peptides, we reduced the number of blood vessel endothelial cells by treating the cell suspension with anti-CD31 magnetic beads before recovering and amplifying bound phage. Blood-vessel endothelial cells express high levels of CD31, whereas lower levels are expressed by lymphatic endothelial cells^{6,7} (and this study). Three rounds of *ex vivo* selection yielded a phage pool that bound to the primary tumor-derived cells approximately 350-fold over control, non-recombinant phage. Subsequent *in vivo* selections of this pool in a nude mouse bearing an MDA-MB-435 tumor resulted in 30-fold enrichment in the tumor relative to non-recombinant phage.

One of the peptide sequences enriched in the selected phage pool was CGNKRTRGC. The phage displaying this peptide bound to primary MDA-MB-435 tumor-derived cell suspensions about 7,000 times more than non-recombinant phage (Fig. 1a). The synthetic CGNKRTRGC peptide (LyP-1) inhibited the binding of the phage (data not shown). The LyP-1 phage bound cultured MDA-MB-435 cells on average about 100-fold over

non-recombinant phage. The LyP-1-displaying phage also bound to cell suspensions prepared from KRIB osteosarcoma xenografts, and from transgenic mouse mammary carcinomas (Fig. 1a). This phage did not bind to cell suspensions from HL-60 leukemia or C8161 melanoma xenografts (Fig. 1a). Two permutations (CGEKRTRGC and CGNKRTRGV) arose spontaneously during the phage amplification and were recognized because of an altered plaque size. They did not significantly bind to MDA-MB-435 tumor-derived cell suspensions.

The LyP-1-displaying phage homed to the MDA-MB-435 and KRIB tumors *in vivo*. On the average, the mean phage titer in tumor tissue was 60-fold greater than non-recombinant phage in MDA-MB-435 tumors and 15-fold in KRIB tumors (Fig. 1b). In agreement with the cell-binding data, the phage did not home *in vivo* to HL-60 or C8161 xenografts (Fig. 1b), nor to brain, spleen, skin, kidneys and lungs; there may have been some homing to normal breast tissue (Fig. 1c). The MDA-MB-435 homing of the variant CGEKRTRGC-displaying phage was only 10% of the homing of the LyP-1.

When we treated MDA-MB-435 tumor-derived cells with 0.5% NP-40 before recovering homed phage, we found 10–20 times more LyP-1 phage than without the detergent, suggesting that the phage was internalized by cells. *In vitro* experiments showed that cultured MDA-MB-435 cells internalized fluorescein-conjugated LyP-1 peptide. The labeled peptide initially appeared in the cytoplasm and, with time, increasingly in the nucleus (Fig. 1d). There was no detectable cellular uptake of a fluorescein-labeled control peptide (ARALPSQSR), which like CGNKRTRGC has three basic residues (data not shown).

Intravenously (i.v.) injected LyP-1 phage localized to vessel-like structures and to some single cells within the MDA-MB-435 tumors. The vessels containing the phage were negative for CD31 (Fig. 2a). Fluorescein-conjugated synthetic LyP-1 peptide, when injected into the tail vein of MDA-MB-435 tumor-bearing mice, also localized to vessel-like structures and to individual cells within the tumor mass. The peptide-stained vessels did not appear to be blood vessels, because they were negative for MECA-32 staining (Fig. 2b). In addition, there was a lack of colocalization with blood vessels labeled by i.v.-injected tomato lectin⁸. When the peptide and lectin fluorescence were captured in the same microscopic field, they were separate (Fig. 2c), and many fields contained only peptide fluorescence (Fig. 2d) or only lectin fluorescence (Fig. 2e). Fluorescein-conjugated LyP-1 localized to MDA-MB-435 tumors regardless of whether the tumors were grown subcutaneously or in the mammary fat pad,



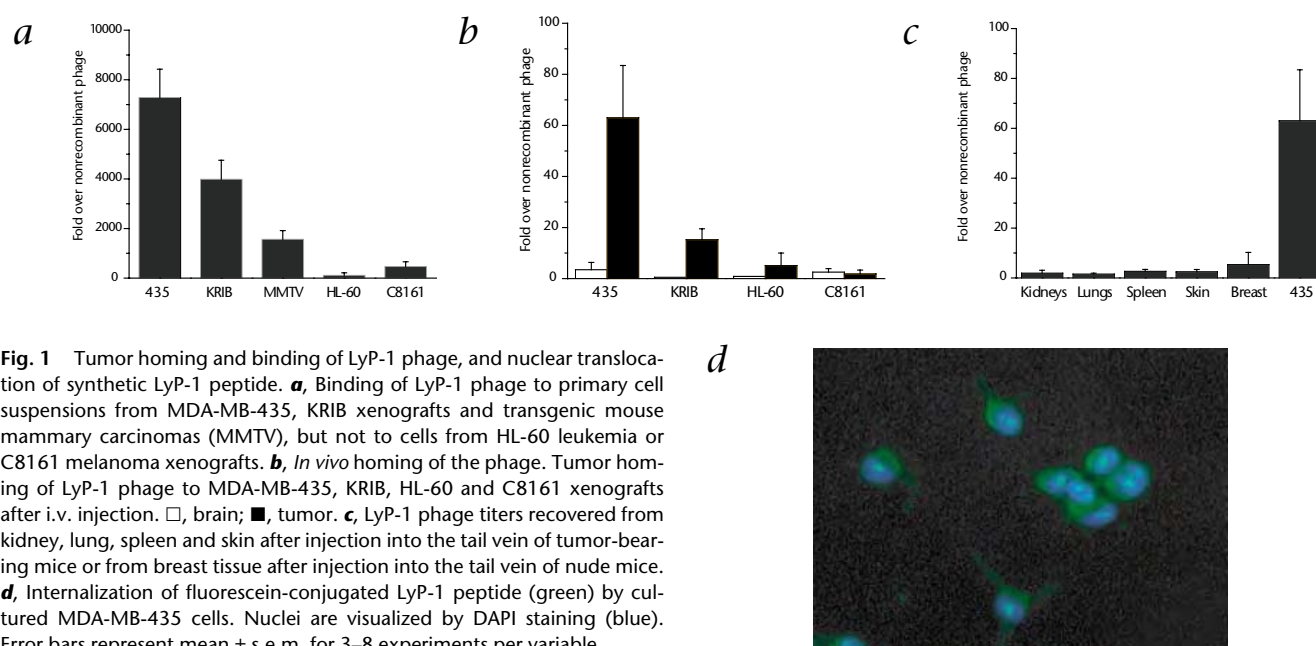


Fig. 1 Tumor homing and binding of LyP-1 phage, and nuclear translocation of synthetic LyP-1 peptide. **a**, Binding of LyP-1 phage to primary cell suspensions from MDA-MB-435, KRIB xenografts and transgenic mouse mammary carcinomas (MMTV), but not to cells from HL-60 leukemia or C8161 melanoma xenografts. **b**, *In vivo* homing of the phage. Tumor homing of LyP-1 phage to MDA-MB-435, KRIB, HL-60 and C8161 xenografts after i.v. injection. □, brain; ■, tumor. **c**, LyP-1 phage titers recovered from kidney, lung, spleen and skin after injection into the tail vein of tumor-bearing mice or from breast tissue after injection into the tail vein of nude mice. **d**, Internalization of fluorescein-conjugated LyP-1 peptide (green) by cultured MDA-MB-435 cells. Nuclei are visualized by DAPI staining (blue). Error bars represent mean \pm s.e.m. for 3–8 experiments per variable.

but more fluorescence accumulated in the subcutaneous tumors (data not shown). The fluorescein-conjugated peptide also homed to transgenic prostate carcinomas (TRAMP), again failing to colocalize with tomato lectin (Fig. 2f). Among several normal tissues studied, fluorescence was only seen in kidney tubuli, presumably as a result of uptake of free fluorescein-conjugated LyP-1 from the glomerular filtrate. Fluorescence from the labeled control peptide also localized in kidney tubuli (data not shown).

Our data suggested that the vessel-like structures targeted by LyP-1 were not blood vessels, so we hypothesized that they might be lymphatic vessels. To investigate whether LyP-1 homed to tumor lymphatics, we stained MDA-MB-435 tumor sections with lymphatic markers: lymphatic vessel endothelial hyaluronin acid receptor-1 (LYVE-1), a transmembrane hyaluronin acid receptor^{9,10}; podoplanin, a glomerular podocyte membrane protein¹¹; and vascular endothelial growth factor receptor-3 (VEGFR-3)^{12–14}. In accordance with earlier results^{13–15}, antibodies against each of these markers stained vessel-like structures in the MDA-MB-435 tumors. These structures frequently lacked a detectable lumen. The staining rarely overlapped with lectin staining, indicating that few, if any, of these vessels were blood vessels.

Fluorescein-conjugated LyP-1 injected into the tail vein of tumor-bearing mice colocalized with LYVE-1 (Fig. 3a), podoplanin (Fig. 3b and c) and VEGFR-3 (Fig. 3d and e) in vessel-like structures within MDA-MB-435 tumor tissue. Some of these structures appeared to be vessels filled with tumor cells (Fig. 3f). LyP-1 also accumulated outside the structures positive for the lymphatic markers, including the tumor cells, individual VEGFR3-positive cells and what appeared to be connective tissue between tumor cells. However, LyP-1 fluorescence typically centered around the structures detected with the lymphatic marker antibodies, implicating the lymphatic structures as the likely primary site of LyP-1 recognition. High-magnification images (Fig. 3c and g) show that fluorescein-conjugated LyP-1 accumulated in the nuclei of cells lining vessel-like structures, while the lymphatic marker antibodies (anti-podoplanin in Fig. 3c) stained the plasma membranes of the same cells. We also injected i.v. mice

with monoclonal antibody to podoplanin, and could detect the antibody in tissues. The injected antibody colocalized with LYVE-1 (Supplementary Fig. A online), and LyP-1 (Fig. 3h), but not with MECA-32 (data not shown).

The LyP-1 phage did not recognize C8161 xenografts in homing or cell-binding assays, but these tumors did contain vessel-like structures that stained positive for both LYVE-1 and podoplanin, but not for the tomato lectin (Supplementary Fig. B online). These results indicate that LyP-1 recognizes lymphatic vessel-associated structures in some tumors but not in others.

Previous *in vivo* phage-screening experiments have yielded peptides that recognize markers that are selectively expressed in tumor vasculature^{3,4}. The structures recognized by LyP-1 in the target tumors seem to be related to lymphatic vessels, rather than blood vessels, as shown by colocalization of LyP-1 with three lymphatic markers and lack of colocalization with three blood-vessel markers. Probes for lymphatic vessels that require transport of the probe through the lymphatic vessels have generally revealed such vessels around, but not within tumors^{16–18}. However, the use of molecular markers for lymphatic endothelial cells has revealed lymphatic structures inside many tumors^{9,13–15}.

Each of the lymphatic markers that we used colocalized with LyP-1 in the MDA-MB-435 tumors. None of these markers are completely specific for lymphatic endothelial cells^{19,20}, but the presence of all three markers in the LyP-1-positive structures strongly suggests that these structures are lymphatic vessels. These LyP-1-binding cells are not tumor cells, because they stained with antibody against mouse VEGFR-3 and with antibodies against mouse major histocompatibility complex (MHC) antigen H-2K^d (data not shown). The VEGFR-3 antibody is known not to recognize human VEGFR-3 (K. Alitalo and H. Kubo, pers. comm.).

LyP-1 often colocalized with lymphatic markers in structures that appeared in tissue sections as thin strands that form loops. These structures may be collapsed lymphatic vessels. Moreover, the reticular architecture with numerous ill-defined lumina described for tumor lymphatics in the recent study of human head and neck cancers is similar to ours¹⁵. Alternatively, these struc-

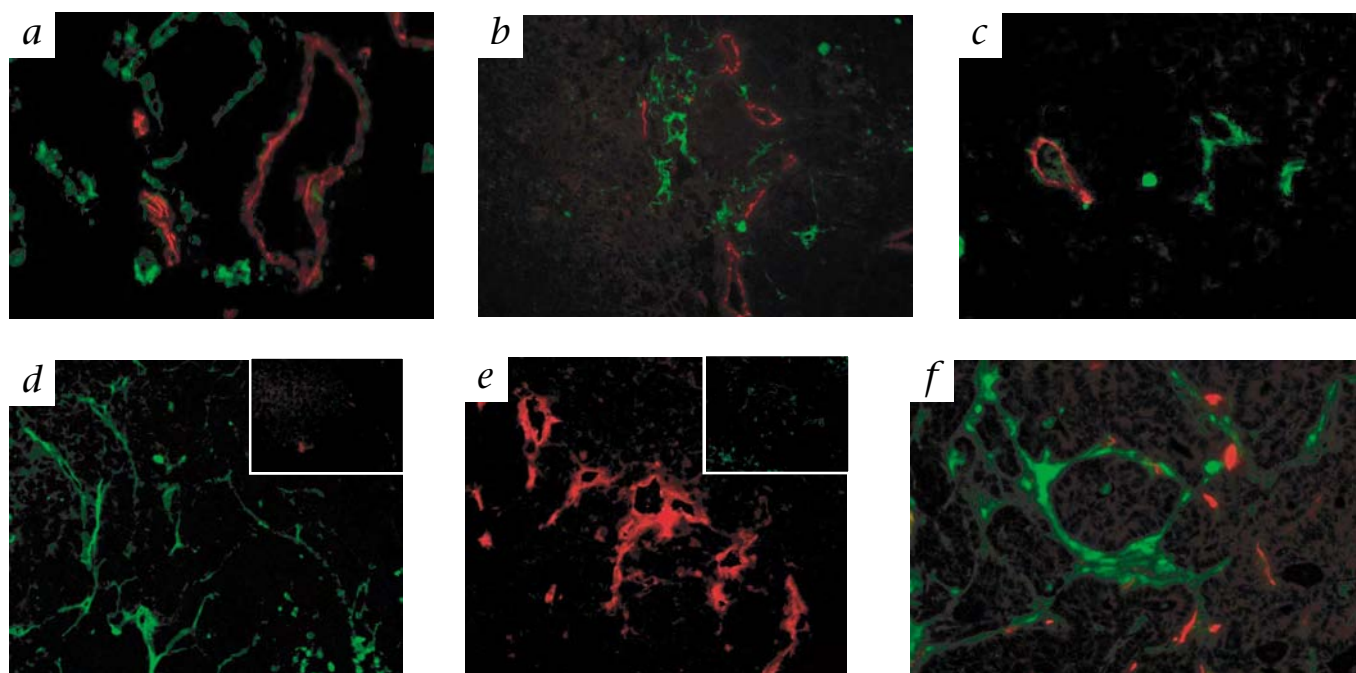


Fig. 2 LyP-1 phage and LyP-1 peptide do not colocalize with blood vessel markers. **a–e**, LyP-1 phage (**a**) or fluorescein-conjugated LyP-1 peptide (**b–e**) injected into the tail vein of a mouse bearing an MDA-MB-435 tumor. **a**, Tumor blood vessels were stained with anti-CD31 antibody (red) and phage was visualized using anti-T7 antibody followed by fluorescein-conjugated anti-rabbit IgG (green). **b–e**, Tumor blood vessels (red) were detected with MECA-32 (**b**) or i.v. injected, biotinylated tomato lectin (**c–e**). The green color shows the localization of LyP-1 peptide. **c**, A microscopic field contain-

ing both LyP-1 peptide and lectin fluorescence. **d**, Areas where peptide staining was abundant were often devoid of blood vessels. (the *inset*, blood vessel staining in the same microscopic field) **e**, Other areas of the tumor contained numerous blood vessels, but no peptide (*inset*, peptide staining in the same microscopic field). **f**, LyP-1 peptide (green) homed also to the transgenic mouse prostate tumor (TRAMP). Blood vessels (red) were detected with i.v. injected biotinylated tomato lectin. **d**, **e** and the insets in **d** and **e** are single color images. Magnification, $\times 400$ in **a**, **c**, and **e**; $\times 200$ in **b**, **d** and **f**.

tures could be dilated lymphatic vessels filled with tumor. It may be that most intra-tumor lymphatics are not patent vessels functional in transporting lymph. Because we access the tumor lymphatics through blood circulation, the accumulation of our

phage and peptide in these structures may not be dependent on functionality of the targeted lymphatics.

Although these results strongly suggest that LyP-1 binds to tumor lymphatics, we cannot exclude the possibility that the

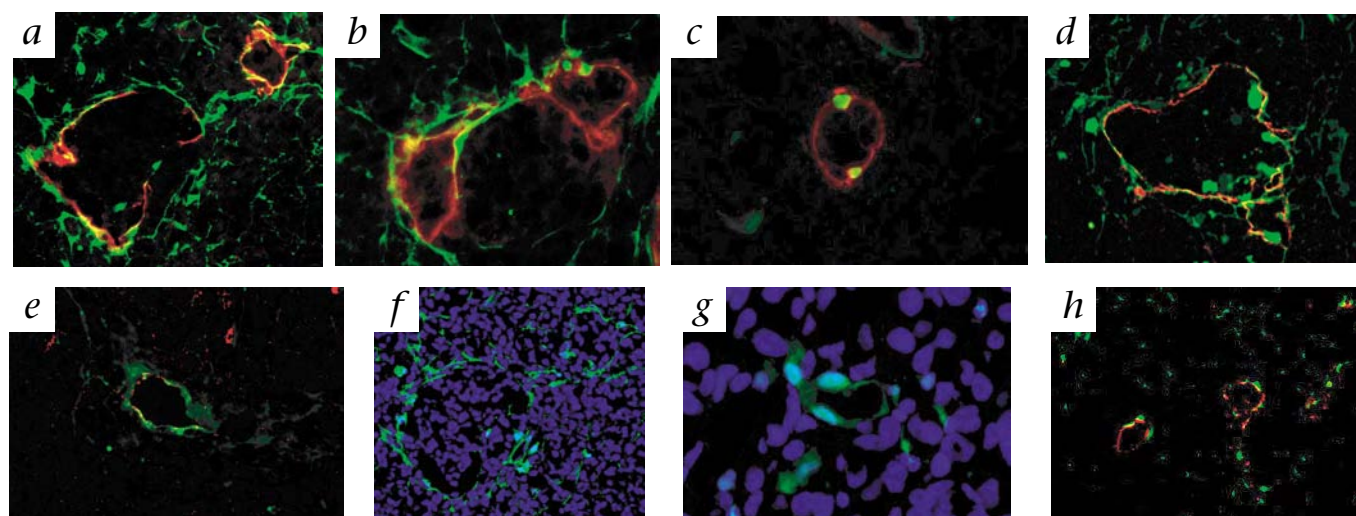


Fig. 3 Colocalization of LyP-1 with lymphatic markers. Fluorescein-conjugated LyP-1 peptide was injected into the tail vein of mice bearing MDA-MB-435 xenografts. **a–e**, LyP-1 (green) colocalizes with red staining for the lymphatic vessel markers LYVE-1 (**a**), podoplanin (**b** and **c**) and VEGFR-3 (**d** and **e**) in reticular and vessel-like structures within the tumor tissue. Some of the peptide fluorescence accumulates in the nu-

clei of the cells lining the vessels positive for the lymphatic markers and LyP-1, as shown by examination at a higher magnification (podoplanin costaining; **c**) and by using blue counter staining of nuclei with DAPI (**f** and **g**). **h**, LyP-1 fluorescence also partially colocalized with i.v. injected anti-podoplanin antibody in tumor tissue. Magnification, $\times 200$ in **a–d** and **h**; $\times 400$ in **g** and **f**.



target cell would be a transitional cell in between the lymphatic and blood vessel endothelial lineages⁶. There are also some similarities in the distribution of LyP-1 and periodic acid Schiff (PAS)-positive structures in melanomas, which may represent alternate vascular channels²¹.

The binding of LyP-1 to putative tumor lymphatics and tumor cells is not universal for all tumors. Although we found LyP-1 to recognize two xenograft tumors and three transgenic mouse tumors, a leukemia (HL-60) and a melanoma (C8161) xenograft were negative. This was the case despite the fact that the C8161 tumors contained lymphatics as identified by positive staining for LYVE-1 and podoplanin and the lack of staining for a blood vessel marker. As the binding of LyP-1 to the cultured tumor cells correlated with its ability to recognize the putative tumor lymphatics in the xenografts, it may be that the tumor cells induce the expression of the LyP-1 binding molecule in the intratumoral lymphatic cells.

Our results suggest that tumor lymphatics may be specialized in a way similar to what has been shown for tumor blood vessels^{3,4,22,23}. Moreover, the LyP-1 peptide may make it possible to specifically target tumor lymphatics and their adjacent tumor tissues for destruction. The nuclear localization of fluorescein coupled to LyP-1 suggests that LyP-1 could be a particularly effective carrier of drugs that act inside the nucleus. Given the importance of the lymphatic route in metastasis, such a treatment may destroy the most deadly parts of tumors.

Methods

Mice, cell lines and tumors. MDA-MB-435, KRIB and C8161 cell lines were maintained in DMEM supplemented with 10% FBS. Nude BALB/c mice were subcutaneously injected with 1×10^6 tumor cells, and tumor-bearing mice were used to prepare cell suspensions and for homing experiments at 3–6 weeks (KRIB or C8161) or 9–12 weeks (MDA-MB-435) post-injection. The animal experimentation was approved by the Burnham Institute Animal Research Committee.

Phage libraries and screening. The libraries were prepared as described⁵. NNK-oligonucleotides encoding a random library of cyclic peptides of the general structure CX₂C (ref. 24) were cloned into the T7Select 415-1 vector according to the manufacturer's instructions (Novagen, Madison, Wisconsin). This vector displays peptides in all 415 copies of the phage capsid protein as a C-terminal fusion.

Tumor-homing phage were isolated from the phage library by combining *ex vivo* and *in vivo* screening. For the *ex vivo* screening, tumor-cell suspensions were prepared from human MDA-MB-435 breast carcinoma xenograft tumors using collagenase (0.5 mg/ml, Sigma) to disperse the tissue. A cell suspension was incubated with the phage library (3.7×10^{10} plaque-forming units (p.f.u.)) overnight at 4 °C and unbound phage were removed by serially washing with 1% BSA in DMEM. Magnetic beads (Dyna, Oslo, Norway) coated with anti-mouse CD31 (MEC 13.3; Pharmingen, San Diego, California) were used to preferentially deplete the tumor-derived cell suspension of blood vessel endothelial cells. Phage bound to the CD31-deficient cell population were rescued and amplified. The phage selection process was repeated 3 times. The *ex vivo* pre-selected phage pool was then subjected to an *in vivo* selection round by injecting it (1.7×10^9 p.f.u.) into the tail vein of a nude mouse bearing an MDA-MB-435 tumor. 48 individual clones were then picked from this *in vivo*-selected, tumor-homing pool and their peptide-encoding inserts were sequenced. Nine peptides appearing more than once were amplified and their ability to bind to cultured cells and tumor-derived cell suspensions was tested⁵. The 5 individual phage that bound better to cell suspensions from MDA-MB-435 tumors than to cultured MDA-MB-435 cells were tested for their ability to home to tumors *in vivo*. In some experiments, the phage were rescued from tissues by treating the tissue with 0.5% NP-40 in PBS.

Peptide synthesis. Peptides were synthesized in our peptide synthesis facility using Fmoc chemistry in a solid-phase synthesizer. The peptides were purified by HPLC, and their sequence and structure was confirmed by mass

spectrometry. Fluorescein-conjugated peptides were synthesized as described²⁵.

Antibodies and immunohistology. To produce antibodies to T7, New Zealand White rabbits were immunized with 10^{10} p.f.u. of T7 nonrecombinant phage (Novagen). The initial immunization was done in complete Freund's adjuvant and boosters were with incomplete Freund's adjuvant. The antibody titer was estimated by using ELISA, and the antiserum was absorbed against BLT5615 bacterial and mouse liver lysates. The LYVE-1 antibody was produced by immunizing New Zealand White rabbits with a peptide encoding the 19 C-terminal residues of mouse LYVE-1 (ref. 10) conjugated to keyhole limpet hemocyanin (KLH; Pierce, Rockford, Illinois). The initial immunization was done in complete Freund's adjuvant and boosters were with incomplete Freund's adjuvant. The antibodies were affinity purified with the peptide coupled to Sulfolink Gel (Pierce) and tested for tissue reactivity by immunofluorescence, where they gave a characteristic lymphatic staining pattern. The specificity of this antibody and that of an antibody against the ectodomain of LYVE-1 (ref. 10) have been reported to be similar⁷. Other primary antibodies used in immunohistochemistry were rat anti-mouse VEGFR-3 (ref. 12) (provided by K. Alitalo and H. Kubo), rat anti-mouse podoplanin¹¹ (provided by T. Petrova), rat anti-mouse MECA-32 (Pharmingen), rat anti-mouse CD31 (Pharmingen), and biotin anti-mouse H-2Kd, clone SF1-1.1 (Pharmingen).

Tissue distribution of fluorescein-labeled peptides was examined by i.v. injection of the peptide (100 µg in 200 µl PBS) into the tail vein of a mouse. Blood vessels were visualized by i.v. injection of *Lycopersicon esculentum* (tomato) lectin conjugated either to fluorescein or biotin (100 µg in 200 µl of PBS; Vector, Burlingame, California). The biotinylated lectin was detected with streptavidin-conjugated Alexa-594 (red). In some experiments, the anti-podoplanin antibody was similarly injected. The injected materials were allowed to circulate for 5–15 min and the mouse was perfused with 4% paraformaldehyde through the heart. Tissues were removed and frozen in OCT embedding medium (Tissue-Tek, Elkhart, Indiana). The biotin-conjugated lectin was detected with streptavidin-conjugated Alexa-594 (Molecular Probes, Eugene, Oregon) and the anti-podoplanin antibody with goat anti-rat Alexa-488 or Alexa-594 (Molecular Probes).

Note: Supplementary information is available on the Nature Medicine website.

Acknowledgments

We thank E. Engvall and E. Pasquale for comments on the manuscript; K. Alitalo, H. Kubo, T. Petrova and M. Quintanilla for antibodies; M. Bernasconi and A. Man for tumor materials; F. Ferrer for peptide synthesis; and R. Newlin for assistance with histology. This study was supported by grants CA74238, CA82715, the Cancer Center Support Grant CA 30199 from the NCI, and grant 99-3339 from the Komen Foundation. P.L. is supported by fellowship 69768 from the Academy of Finland and a fellowship from the Finnish Cultural Foundation. J.A.H. is a recipient of a National Cancer Institute Training Grant fellowship in the Molecular Pathology of Cancer.

Competing interests statement

The authors declare that they have no competing financial interests.

RECEIVED 28 FEBRUARY; ACCEPTED 13 MAY 2002

1. Hanahan, D. & Folkman, J. Patterns and emerging mechanisms of the angiogenic switch during tumorigenesis. *Cell* **86**, 353–364 (1996).
2. Ruoslahti, E. Specialization of tumour vasculature. *Nature Rev. Cancer* **2**, 83–90 (2002).
3. Arap, W., Pasqualini, R. & Ruoslahti, E. Cancer treatment by targeted drug delivery to tumor vasculature in a mouse model. *Science* **279**, 377–380 (1998).
4. Porkka, K., Laakkonen, P., Hoffman, J.A., Bernasconi, M. & Ruoslahti, E. A fragment of the HMGN2 protein homes to the nuclei of tumor cells and tumor endothelial cells *in vivo*. *Proc. Natl. Acad. Sci. USA* (in the press).
5. Hoffman, J.A., Laakkonen, P., Porkka, K., Bernasconi, M. & Ruoslahti, E. *In vivo* and *ex vivo* selections using phage-displayed libraries. in *Phage Display: A Practical Approach* (eds. Clackson, T. & Lowman, H.) (Oxford University Press, Oxford, UK, in the press).

6. Oliver, G. & Detmar, M. The rediscovery of the lymphatic system: old and new insights into the development and biological function of the lymphatic vasculature. *Genes Dev.* **16**, 773–783 (2002).
7. Makinen, T. *et al.* Isolated lymphatic endothelial cells transduce growth, survival and migratory signals via the VEGF-C/D receptor VEGFR-3. *EMBO J.* **20**, 4762–4773 (2001).
8. Chang, Y.S. *et al.* Mosaic blood vessels in tumors: frequency of cancer cells in contact with flowing blood. *Proc. Natl. Acad. Sci. USA* **97**, 14608–14613 (2000).
9. Jackson, D.G., Prevo, R., Clasper, S. & Banerji, S. LYVE-1, the lymphatic system and tumor lymphangiogenesis. *Trends Immunol.* **22**, 317–321 (2001).
10. Prevo, R., Banerji, S., Ferguson, D.J., Clasper, S. & Jackson, D.G. Mouse LYVE-1 is an endocytic receptor for hyaluronan in lymphatic endothelium. *J. Biol. Chem.* **276**, 19420–19430 (2001).
11. Breiteneder-Geleff, S. *et al.* Angiosarcomas express mixed endothelial phenotypes of blood and lymphatic capillaries: Podooplanin as a specific marker for lymphatic endothelium. *Am. J. Pathol.* **154**, 385–394 (1999).
12. Kubo, H. *et al.* Involvement of vascular endothelial growth factor receptor-3 in maintenance of integrity of endothelial cell lining during tumor angiogenesis. *Blood* **96**, 546–553 (2000).
13. Stacker, S.A. *et al.* VEGF-D promotes the metastatic spread of tumor cells via the lymphatics. *Nature Med.* **7**, 186–191 (2001).
14. Skobe, M. *et al.* Induction of tumor lymphangiogenesis by VEGF-C promotes breast cancer metastasis. *Nature Med.* **7**, 192–198 (2001).
15. Beasley, N.J.P. *et al.* Intratumoral lymphangiogenesis and lymph node metastasis in head and neck cancer. *Cancer Res.* **62**, 1315–1320 (2002).
16. Mandriota, S.J. *et al.* Vascular endothelial growth factor-C-mediated lymphangiogenesis promotes tumour metastasis. *EMBO J.* **20**, 672–682 (2001).
17. Leu, A.J., Berk, D.A., Lymboussaki, A., Alitalo, K. & Jain, R.K. Absence of functional lymphatics within a murine sarcoma: a molecular and functional evaluation. *Cancer Res.* **60**, 4324–4327 (2000).
18. Karpanen, T. *et al.* Vascular endothelial growth factor C promotes tumor lymphangiogenesis and intralymphatic tumor growth. *Cancer Res.* **61**, 1786–1790 (2001).
19. Carreira, C.M. *et al.* LYVE-1 is not restricted to the lymph vessels: Expression in normal liver blood sinusoids and down-regulation in human liver cancer and cirrhosis. *Cancer Res.* **61**, 8079–8084 (2001).
20. Valtola, R. *et al.* VEGFR-3 and its ligand VEGF-C are associated with angiogenesis in breast cancer. *Am. J. Pathol.* **154**, 1381–1390 (1999).
21. Maniotis, A.J. *et al.* Vascular channel formation by human melanoma cells *in vivo* and *in vitro*: Vasculogenic mimicry. *Am. J. Pathol.* **155**, 739–752 (1999).
22. Brooks, P.C. *et al.* Integrin $\alpha v \beta 3$ antagonists promote tumor regression by inducing apoptosis of angiogenic blood vessels. *Cell* **79**, 1157–1164 (1994).
23. St Croix, B. *et al.* Genes expressed in human tumor endothelium. *Science* **289**, 1197–1202 (2000).
24. Smith, G.P. & Scott, J.K. Libraries of peptides and proteins displayed on filamentous phage. *Methods Enzymol.* **217**, 228–257 (1993).
25. Wender, P.A. *et al.* The design, synthesis, and evaluation of molecules that enable or enhance cellular uptake: peptoid molecular transporters. *Proc. Natl. Acad. Sci. USA* **97**, 13003–13008 (2000).

Antitumor activity of a homing peptide that targets tumor lymphatics and tumor cells

Pirjo Laakkonen^{*†}, Maria E. Åkerman^{*‡}, Hector Biliran^{*§}, Meng Yang[¶], Fernando Ferrer^{*}, Terhi Karpanen[†], Robert M. Hoffman[¶], and Erkki Ruoslahti^{*||}

^{*}The Burnham Institute, La Jolla, CA 92037; [†]Molecular/Cancer Biology Laboratory, Biomedicum Helsinki, University of Helsinki, P.O.B. 63 (Haartmaninkatu 8), FIN-00014 Helsinki, Finland; [‡]Department of Bioengineering, University of California at San Diego, La Jolla, CA 92093; and [§]AntiCancer, Inc., San Diego, CA 92111

Contributed by Erkki Ruoslahti, May 10, 2004

LyP-1 is a peptide selected from a phage-displayed peptide library that specifically binds to tumor and endothelial cells of tumor lymphatics in certain tumors. Fluorescein-conjugated LyP-1 and a related peptide, LyP-1b, strongly accumulated in primary MDA-MB-435 breast cancer xenografts and their metastases from i.v. peptide injections, allowing visualization of orthotopic tumors in intact mice. The LyP peptide accumulation coincided with hypoxic areas in tumors. LyP-1 induced cell death in cultured human breast carcinoma cells that bind and internalize the peptide. Melanoma cells that do not bind LyP-1 were unaffected. Systemic LyP-1 peptide treatment of mice with xenografted tumors induced with the breast cancer cells inhibited tumor growth. The treated tumors contained foci of apoptotic cells and were essentially devoid of lymphatics. These results reveal an unexpected antitumor effect by the LyP-1 peptide that seems to be dependent on a proapoptotic/cytotoxic activity of the peptide. As LyP-1 affects the poorly vascularized tumor compartment, it may complement treatments directed at tumor blood vessels.

phage display | tumor targeting | live imaging | therapy

Tumor blood vessels express molecular markers that distinguish them from normal blood vessels. Many of these tumor vessel markers are related to angiogenesis, but some are selective for certain tumors (1). Markers that distinguish the vasculature of tumors at the premalignant stage from the vasculature of fully malignant tumors in the same tumor system have also been described (2, 3). Recent data from our laboratory indicate that lymphatic vessels in tumors are also specialized, because a cyclic 9-amino acid peptide, LyP-1, binds to the lymphatic vessels in certain tumors, but not to the lymphatics of normal tissues (4).

The lymphatic system is an important route of tumor metastasis. Many cancers preferentially spread through the lymphatics. Recent discoveries of growth factors and molecular markers for lymphatic endothelial cells have made possible detailed studies of the relationship of tumor cells and the lymphatic vasculature of tumors (5–9). The use of marker proteins such as LYVE-1 (6), podoplanin (5), and Prox-1 (10) has shown that lymphatic vessels are abundant in the periphery of tumors and that many tumors also contain lymphatics within the tumor mass (4, 11). However, the intratumoral lymphatic vessels are generally not functional in transporting tissue fluid (12) and are often filled with tumor cells (4, 13). Recent experimental and clinical data strongly suggest that the number of lymphatics in a tumor, perhaps their size as well, and the expression of lymphangiogenic growth factors are important determinants in the ability of a tumor to metastasize (14–18).

Thus, it may become possible to reduce metastasis by specifically targeting tumor lymphatics (and the tumor tissue adjacent to these vessels) for destruction. The LyP-1 peptide, which specifically binds to tumor lymphatics (4), provides one potential avenue for developing reagents that can specifically destroy tumor lymphatics. This peptide also binds to the tumor cells in

tumors that contain LyP-1-positive lymphatics, further expanding the potential of this peptide.

We show here that i.v. injected LyP-1 strongly and specifically accumulates in breast cancer xenografts over time, localizing preferentially in hypoxic areas. We also report that LyP-1 has a proapoptotic/cytotoxic effect on tumor cells and that systemic administration of the LyP-1 peptide inhibits breast cancer xenograft growth in mice. The treated tumors contain foci of apoptotic cells and reduced numbers of lymphatic vessels. These findings suggest that LyP-1 may provide a starting point for the development of new antitumor agents.

Materials and Methods

Cell Lines and Tumors. MDA-MB-435 human breast carcinoma cells and C8161 human melanoma cells were maintained in DMEM supplemented with 10% FCS. Nude BALB/c *nu/nu* mice were injected s.c. or into the mammary fat pad with 1×10^6 tumor cells to induce tumors. A vascular endothelial growth factor (VEGF)-C-transfected MDA-MB-435 cell line was prepared as previously reported for MCF7 cells (13).

Antibodies and Immunohistology. Blood vessels were visualized by staining tissue sections with monoclonal antibodies against CD-31, CD-34, or MECA-32 (all rat anti-mouse antibodies from Pharmingen). A polyclonal rabbit anti-mouse LYVE-1 antibody (4) and a rat monoclonal anti-mouse podoplanin antibody (provided by Kari Alitalo, University of Helsinki) were used to visualize lymphatic vessels. The primary antibodies were detected with goat anti-rabbit or anti-rat Alexa 594 (Molecular Probes).

Biodistribution of fluorescein-conjugated peptides was examined after i.v. injection (100 μ l of 1 mM peptide solution in 200 μ l of PBS) into the tail vein of a mouse. The peptide was allowed to circulate for various periods of time, and the mouse was perfused through the heart with 4% paraformaldehyde. Tissues were removed, soaked in 30% sucrose in PBS overnight, and frozen in OCT embedding medium (Tissue-Tek). Alternatively, tumor-bearing mice were i.v. injected with 500 μ l of 1 mM fluorescein-conjugated peptide in PBS, and the peptide was allowed to circulate for 16–20 h.

The whole-body imaging was done under a blue light, by using the imaging system of a fluorescence stereo microscope (model LZ12; Leica, Deerfield, IL) equipped with a mercury 50-W lamp (19).

Determination of Vessel Density in Tissues. Frozen tumor sections were stained with antibodies against CD-34 and podoplanin (5) to visualize the tumor-associated blood and lymphatic vessels. Using $\times 200$ magnification, each microscopic field in the hori-

Abbreviation: VEGF, vascular endothelial growth factor.

[§]Present address: Department of Pathology, School of Medicine, Wayne State University, 540 East Canfield Road, Detroit, MI 48201.

^{||}To whom correspondence should be addressed. E-mail: ruoslahti@burnham.org.

© 2004 by The National Academy of Sciences of the USA

zontal and the vertical directions was counted for the presence of the two types of vessels.

Hypoxia. Hypoxic areas in the tumor were visualized by i.v. injection of a hypoxia marker 2-nitroimidazole (EF5) (20) into tumor-bearing mice (10 μ l of 10 mM EF5 per g), followed by Cy3-conjugated mouse anti-EF5 (provided by Randall S. Johnson, University of California at San Diego). Cultured MDA-MB-435 cells were grown on coverslips and incubated overnight at 37°C to allow for attachment and spreading of the cells. Half of the cells were transferred to a hypoxia chamber (0.1% oxygen/5% CO₂) and incubated overnight under hypoxic conditions. Fluorescein-conjugated peptides (10 μ M) were added to the cells in 1% BSA in DMEM and incubated for 3 h, followed by fixation with 4% paraformaldehyde in PBS. The coverslips were mounted on glass slides by using Vecta-Shield mounting media with 4',6-diamidino-2-phenylindole (Vector Laboratories).

Cytotoxicity Assay. Cytotoxic efficacy of the different peptides was judged by measuring the release of a cytoplasmic enzyme, lactate dehydrogenase, from damaged cells into the supernatant by using a colorimetric assay Cytotoxicity Detection Kit (LDH assay; Roche Diagnostics). MDA-MB-435 cells were plated on 96-well plates (6,000 cells per well) and incubated overnight at 37°C to allow for attachment and spreading of the cells. Cells were washed once with PBS, and 50 μ l of 2% BSA in DMEM was added to the cells. Peptides were added in 50 μ l of H₂O and incubated for 24–72 h at 37°C. After the incubation, the cells were spun down (1,000 rpm, 10 min), and the supernatant was transferred to a new plate. The color reaction was added to the cells and incubated for 25 min before the absorbance was read at 492 nm. Cells incubated with 50 μ l of H₂O and 50 μ l of 2% BSA in DMEM served as a background control, and cells incubated with 1% Nonidet P-40 showed the maximal cytotoxic value. The cytotoxicity was determined as a percentage of the maximal value after the subtraction of the background.

Tumor Treatment Studies. Tumor-bearing mice were treated with i.v. injections of peptides beginning 4 weeks after tumor cell inoculation. The injections were administered twice a week for 4–5 weeks. Tumor volumes were measured once a week and were calculated according to the formula $V = \text{width} \times \text{height} \times \text{depth}/2$, derived from the formula for the volume of an ellipsoid (21). Student's *t* test was used for statistical analysis of the results. The animal experiments reported here were approved by The Burnham Institute Animal Research Committee.

Synthesis of Fluorescein-Conjugated Peptides. Peptides were synthesized by using Fmoc-protected amino acids (Nova Biochem) and HATU (PE Biosystems, Foster City, CA) as a coupling reagent in dimethylformamide activated with diisopropylethylamine. All peptides were amide-capped at the C terminus by the use of Fmoc-PAL-PEG-PS resin (PE Biosystems). The peptides were conjugated with fluorescein at the N terminus by reacting with fluorescein isothiocyanate isomer (FITC, Aldrich) in dimethylformamide for 20 h in the presence of diisopropylethylamine.

Results

Fluorescein-Conjugated Homing Peptides Accumulate in Tumor Tissue. Intravenously injected LyP-1 peptide was observed to home to tumor-associated lymphatic vessels and tumor cells in MDA-MB-435 xenografts and some other tumors (4). In this earlier work, the peptide was allowed to circulate for <20 min. To optimize the accumulation of LyP-1 in these tumors, we

studied the distribution of the peptide for longer periods of time. We found striking accumulation of fluorescein-conjugated LyP-1 in tumors several hours after the injection. At 16–20 h, the tumors of the LyP-1-injected mice were brightly fluorescent in whole-body fluorescent imaging (19) of intact mice (Fig. 1A). Tumors from the mice injected with a control peptide showed no fluorescence (Fig. 1B). Imaging of dissected tumors and organs from the same animals revealed strong fluorescence in tumors from mice injected with LyP-1, whereas no fluorescence was detectable in the tumors from the control peptide-injected mice. Other tissues showed no specific fluorescence with either peptide (Fig. 1C and D).

We then confirmed the tumor-specificity of LyP-1 by quantifying the fluorescence in the dissected tissues. Tumor fluorescence from the control peptide injection was too low to be accurately distinguished from the background, but LyP-1 concentration was at least 15- to 40-fold higher in the tumors than that of the control peptide, whereas fluorescence in other tissues was not significantly different from the background (Fig. 1E). A peptide closely related to LyP-1 (CNKRTRGGC; H.B., J. A. Hoffman, P.L., and E.R., unpublished data) also strongly accumulated in the tumors (LyP-1b in Fig. 1E). These results show that the LyP-1 peptides accumulate in the MDA-MB-435 tumors with extraordinary efficiency and that the accumulation is specific. The LyP-1 fluorescence was mainly present in tumor cell nuclei (Fig. 1F), whereas the control peptide was essentially negative in tumor tissue (Fig. 1G). No fluorescence was detected in other tissues with any of the peptides (shown for LyP-1 in brain tissue in Fig. 1H).

LyP-1 Recognizes Metastatic Lesions. MDA-MB-435 tumor cells transfected with the lymphangiogenic growth factor VEGF-C produce tumors with increased number of lymphatic vessels and enhanced propensity to metastasize into regional lymph nodes and the lungs (13, 16, 22). In agreement with the ability of LyP-1 to recognize tumor lymphatics, LyP-1 accumulation in the VEGF-C-expressing tumors seemed to be stronger than in the parental-line tumors (data not shown). LyP-1 peptide also homed to the metastatic lymph nodes of the MDA-MB-435/VEGF-C tumor mice (Fig. 2A–E), colocalizing with lymphatic endothelial markers (arrows in Fig. 2C) and tumor cells (Fig. 2E) within the lymph nodes. No LyP-1 fluorescence was detected in the vessels of normal lymph nodes; the nuclei of a few isolated cells that appeared to be leukocytes were positive (Fig. 2B *Inset*). Metastatic foci in lungs were also positive for LyP-1 (Fig. 2F). These results show that metastases can retain the LyP-1 binding of the primary tumor and that the same tumor can induce the LyP-1-binding epitope in the lymphatic vessels of more than one tissue.

LyP-1 Peptide Recognizes Hypoxic Areas in Tumors. The tumor cells that accumulated LyP-1 formed clusters within the tumors, and these clusters contained few blood vessels (Fig. 3A) but were positive for lymphatic endothelial markers (Fig. 3B). The LyP-1-positive tumor cell clusters were strikingly similar to clusters of tumor cells revealed by uptake of hypoxia markers (23). This similarity, and the lack of blood vessels, led us to examine a possible connection between LyP-1 binding and hypoxia. Intravenously injected hypoxia reagent EF5 and fluorescein-labeled LyP-1 accumulated in the same areas in the tumors, but the staining for the two markers seemed to be mutually exclusive at the level of individual cells (Fig. 3C and D). If EF5 was injected first, the homing of LyP-1 was reduced (Fig. 3C) and vice versa (Fig. 3D). Moreover, injecting LyP-1 or EF5 alone gave a stronger tumor signal for both compounds than the coinjections. In contrast, the accumulation of EF5 in C8161 melanoma xenografts, which are not recognized by LyP-1 (4), was unaffected by coinjecting LyP-1 (data not shown). These results

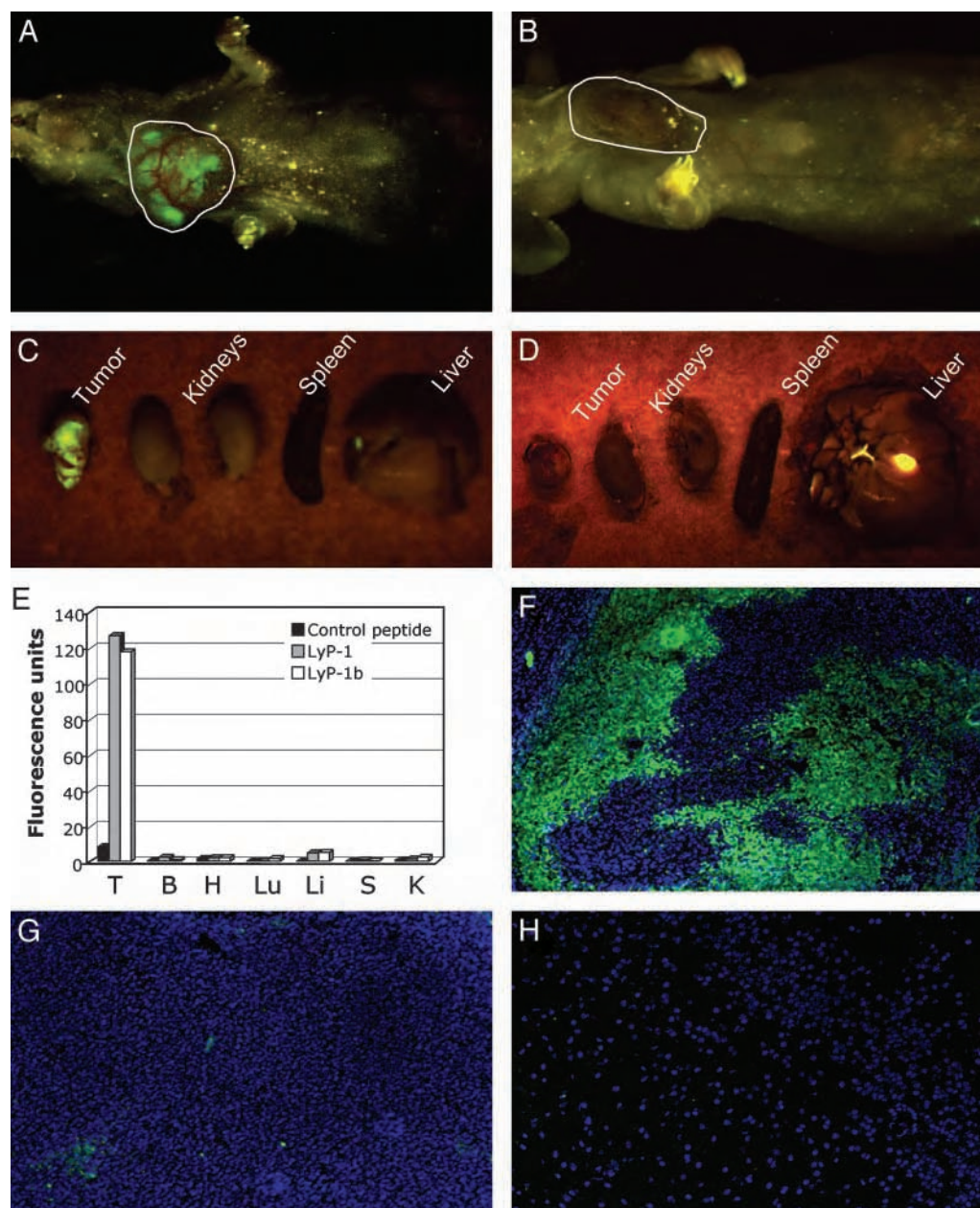


Fig. 1. Specific accumulation of lymphatic homing peptides in tumors. Mice bearing orthotopic MDA-MB-435 xenograft tumors were i.v. injected with fluorescein-conjugated LyP-1 (A) or a fluorescein-conjugated control peptide (ARALPSQRSR) (B). The mice were anesthetized 16–20 h later and examined for fluorescence under blue light. Tumor fluorescence of a LyP-1-injected tumor mouse is shown in A. No fluorescence was detected in tumors of mice injected with the control peptide (B). After the external examination, the mice were killed, and tumor, kidneys, spleen, and liver were excised and examined for fluorescence. LyP-1 produced intense fluorescence in the tumor, whereas no fluorescence was detectable in other organs (C). Even when imaged directly, no fluorescence was observed in the control peptide-injected tumor (D). The gallbladder is autofluorescent and appears as a green spot in C and D. E shows quantification of the imaging results for LyP-1 and for LyP-1b, which was analyzed in similar experiments. Mice that did not receive any fluorescent compound were used to determine the level of autofluorescence in tissues, and this background was subtracted from the experimental values. The graph shows a representative experiment of three. (F–H) Mice injected with peptides as in A and B were perfused through the heart, and their tumors were examined microscopically. Strong LyP-1 fluorescence is seen in the nuclei (visualized by 4',6-diamidino-2-phenylindole staining) of tumor cells (F). No appreciable fluorescence from the control peptide is seen in tumor tissue (G), and all normal tissues tested were negative for all peptides (the result for LyP-1 in the brain is shown in H). T, tumor; B, brain; H, heart; Lu, lungs; Li, liver; S, spleen; K, kidneys. Magnification: F and G, $\times 100$; H, $\times 200$.

indicate that LyP-1 preferentially localizes in hypoxic parts of tumors and that LyP-1 and EF5 specifically affect one another's recognition of hypoxic tumor cells.

Serum Starvation Increases Binding of Fluorescein-Conjugated LyP-1 to Cultured MDA-MB-435 Cells. We next sought to reproduce the effect of hypoxia on tumor cell recognition *in vitro*. We cultured

MDA-MB-435 cells under hypoxic conditions but detected no increase in the number of cells that were positive for fluorescein-conjugated LyP-1 (data not shown). However, we did see an increase in the number of cells that had taken up LyP-1 when we maintained the cells in low serum (compare Fig. 3 E and F). Counting of LyP-1-positive cells showed that the difference was 2.5-fold. These results suggest that LyP-1 homing to tumors may

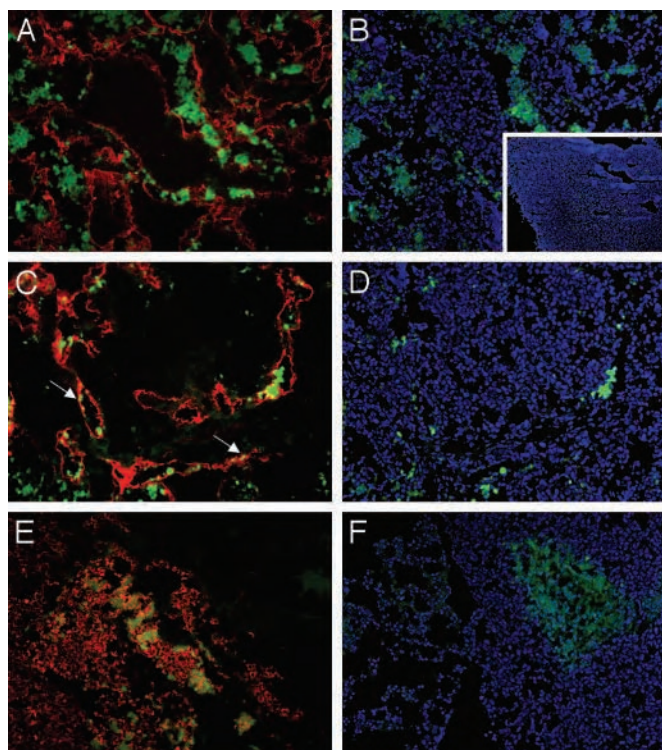


Fig. 2. Lymphatic homing peptide recognizes metastases of VEGF-C-expressing tumors. Fluorescein-conjugated LyP-1 peptide was i.v. injected into mice bearing orthotopic VEGF-C-expressing MDA-MB-435 tumors and allowed to circulate for 15 min. The tumor, lymph nodes, lungs, kidneys, and liver were removed and prepared for immunohistology. Lymphatic vessels in lymph node metastases (A–D) were visualized by staining with anti-LYVE-1 antibodies followed by goat anti-rabbit Alexa 594 (red, A and C). Nuclei were visualized by 4',6-diamidino-2-phenylindole staining (blue, B and D). A and B and C and D show the same microscopic fields with different staining. LyP-1 peptide (green) is present in the nuclei of cells in and around enlarged lymphatic vessels in lymph node metastases. These cells are tumor cells as judged by their intense staining with anti-VEGF-C antibody (red, E). The peptide is also seen in the nuclei of lymphatic endothelial cells (arrows in C). No LyP-1 accumulated in a tumor-free lymph node (B Inset). A metastatic lung tumor also accumulates LyP-1 (F; LyP-1, green; nuclei, blue). Magnification, $\times 200$; Inset, $\times 50$.

not be directly related to hypoxia but may result from the attendant nutrient starvation.

LyP-1 Binding and Internalization Induce Cell Death. Studying the internalization of the fluorescein-conjugated LyP-1 peptide in cultured cells, we noticed that the LyP-1 positive cells tended to round up, and the morphology of their nuclei frequently suggested apoptosis. To investigate whether LyP-1 caused cell death, we incubated MDA-MB-435 cells with unlabeled LyP-1 and monitored cell lysis. Incubation with LyP-1 resulted in a concentration-dependent increase in cell lysis with an IC_{50} of $\approx 66 \mu M$ (Fig. 4A). C8161 human melanoma cells, which do not bind LyP-1 (4), were not affected by the peptide. Control peptides that resemble LyP-1 in their amino acid composition and/or cyclic structure (CRVTRSGC, Fig. 4A) and two other peptides [CGEKTRTGC, a variant of LyP-1, which has no cell-binding activity (4); and KECQSRLSCP, (data not shown)] had no effect on the viability of either cell line. Thus, LyP-1 specifically kills cells that bind this peptide.

Systemic Treatment with LyP-1 Inhibits Tumor Growth and Reduces the Number of Tumor Lymphatics. Given that LyP-1 had an *in vitro* cytotoxic effect on the MDA-MB-435 tumor cells, we examined

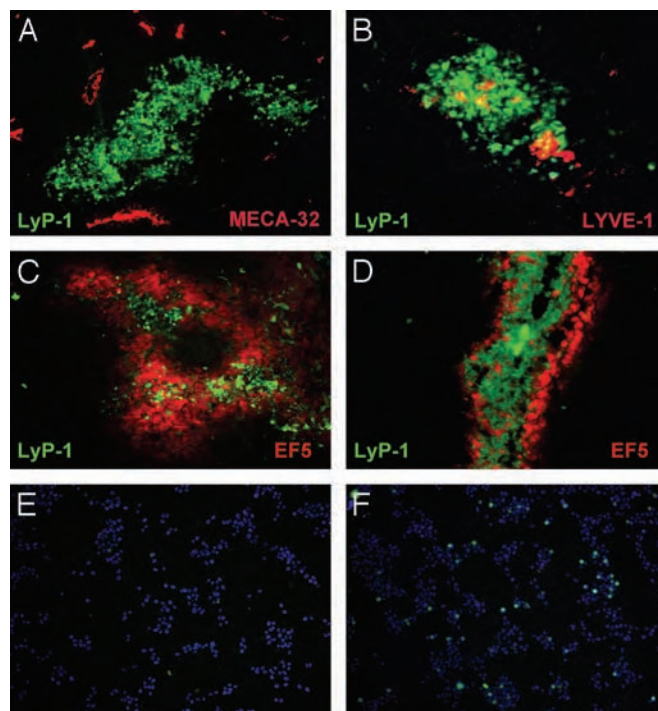


Fig. 3. LyP-1 peptide recognizes cell clusters that lack blood vessels but contain lymphatics. Fluorescein-conjugated LyP-1 peptide was i.v. injected into MDA-MB-435 tumor-bearing mice and allowed to circulate for 15 min. LyP-1 peptide was seen in cell clusters throughout the tumor (green, A and B). These areas did not contain blood vessels, as judged by staining with the blood vessel endothelial marker, MECA-32 (red, A) but were often positive for the lymphatic endothelial markers, LYVE-1 (red, B) and podoplanin (not shown). The hypoxia marker EF5 (red), injected 8 h before LyP-1 (green), localized in the LyP-1-positive patches within the tumors (C). Reversing the order of the injections reduced the amount of EF5 in the LyP-1-positive patches (D). The presence of the two compounds at the cellular level seemed to be mutually exclusive. (E and F) LyP-1 binding to cultured cells is increased by serum starvation. Fluorescein-conjugated LyP-1 peptide was added to MDA-MB-435 cells cultured either in 10% (E) or 0.1% (F) serum, and the binding and uptake of the peptide by the cells was determined 3 h later. Serum starvation increased the number of LyP-1-positive cells (LyP-1, green; nuclei, blue). Magnification: A–D, $\times 200$; E and F, $\times 100$.

the effect of LyP-1 on tumor growth *in vivo*. We gave MDA-MB-435 or MDA-MB-435/VEGF-C tumor mice biweekly i.v. injections of the LyP-1 peptide, starting after the mice had established palpable tumors. Fig. 4B shows one of three similar treatment experiments. The LyP-1 peptide inhibited tumor growth formed by both cell lines. The average reduction of tumor volume relative to the control-treated mice was $\approx 50\%$ and highly significant ($P < 0.005$). Increasing the dose of the LyP-1 peptide did not improve the efficacy of the compound (data not shown). The tumors of the LyP-1-treated animals contained numerous TUNEL-positive cells, indicating apoptosis, whereas little apoptosis was detected in the tumors of the control-treated mice (Fig. 4C and D). The increased apoptosis in the LyP-1 group was specific for the tumor tissue; other tissues did not contain significant numbers of TUNEL-positive cells (data not shown).

LyP-1-treatment selectively reduced the number of lymphatic vessels in the tumors, while having a less prominent effect on the blood vessel density in the same tumors (Fig. 5). These results are in agreement with the *in vivo* homing pattern of the fluorescein-conjugated LyP-1 peptide to the lymphatics in MDA-MB-435 tumor-bearing mice (4). It seems that the lymphatic endothelial cells in the tumor are also susceptible to LyP-1.

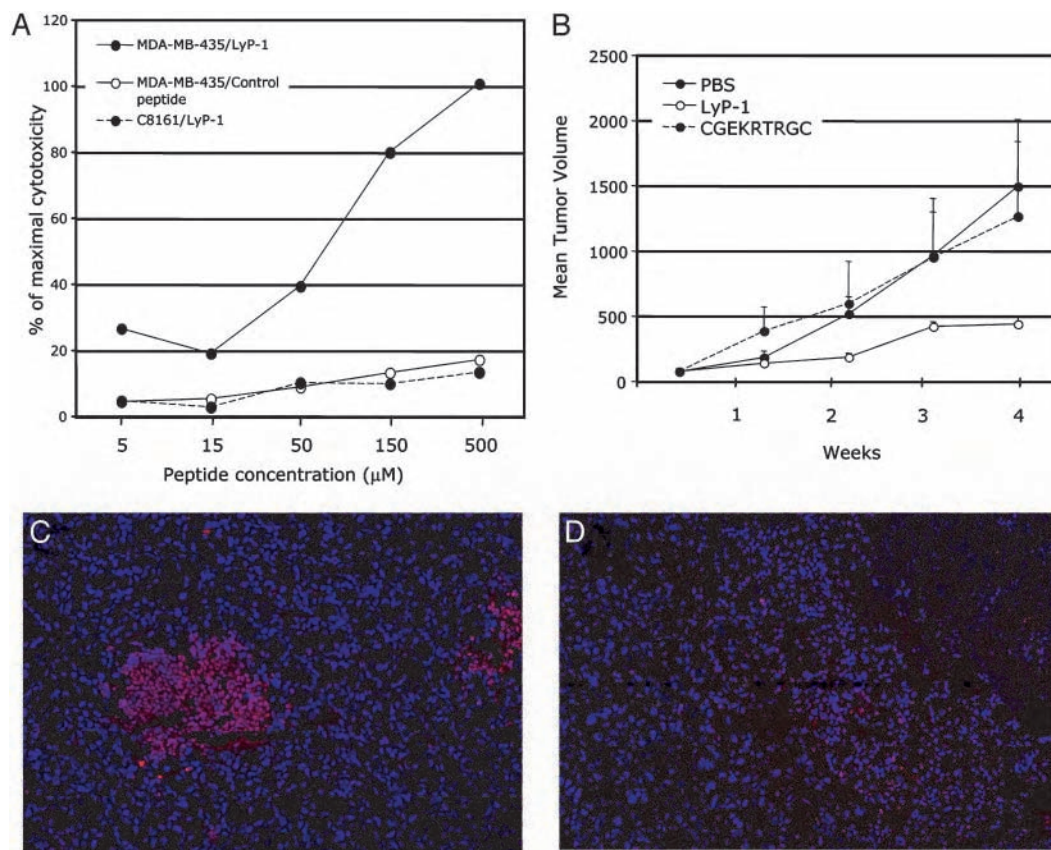


Fig. 4. LyP-1 peptide causes cell death *in vitro* and inhibits tumor growth *in vivo*. (A) LyP-1 (●, solid line) causes a dose-dependent release of lactate dehydrogenase from the cultured MDA-MB-435 cells, whereas a control peptide (CRVTRTSGC, ○) has no effect. LyP-1 does not release lactate dehydrogenase from human C8161 melanoma cells (●, dotted line). (B) Mice bearing MDA-MB-435 tumors were injected twice a week with 60 μg of LyP-1 or its inactive variant (CGEKRTGRC), or with PBS. There were five mice/group; the treatment was started 4 weeks after the inoculation of the tumor cells (1–2 weeks after the tumors became palpable) and lasted 4 weeks. One experiment of three is shown. LyP-1 reduced the mean tumor volume by an average of 50% ($P < 0.05$). (C and D) TUNEL staining (red) reveals clusters of apoptotic cells in the LyP-1-treated (C), but not control-treated (D), tumors. Blue, 4',6-diamidino-2-phenylindole staining of nuclei. Magnification, $\times 200$. The error bars in B show SEM.

Discussion

We report here that LyP-1, a peptide that specifically binds to tumor lymphatics and tumor cells, strongly accumulates in breast

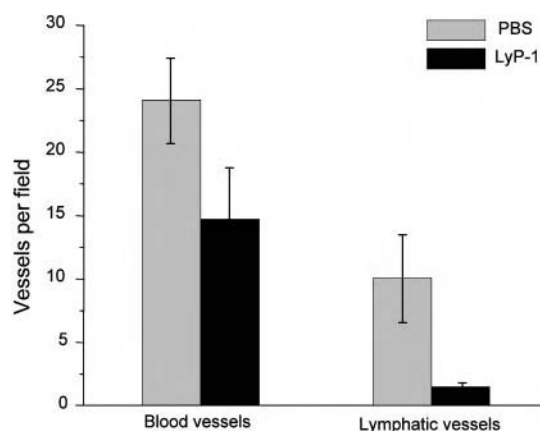


Fig. 5. LyP-1 peptide reduces the number of tumor lymphatics. Tumor sections were stained with antibodies against CD-34 and podoplanin to visualize and count tumor-associated blood vessels and lymphatics. LyP-1 reduced the number of lymphatic vessels by an average of 85% (three experiments). Blood vessel density in the same tumors was affected less (average reduction, 39%). The error bars show SD.

cancer xenografts after an i.v. injection. The peptide and a closely related variant of it preferentially localize in hypoxic areas within the tumors. We also show that systemically administered LyP-1 causes tumor cell apoptosis, reduces the number of tumor lymphatics, and inhibits tumor growth in mice bearing breast cancer xenografts. These results suggest that it may be possible to develop LyP-1-based cancer therapies.

The LyP-1 peptide shows strong accumulation in the MDA-MB-435 tumors, including metastases from these tumors. The efficacy and specificity of this peptide was sufficient to allow us to visualize orthotopic tumors in intact mice based on fluorescence. Although fluorescence-based imaging of tumors formed by GFP-producing cells in intact animals is possible (19), achieving it with an i.v. injected material may be unique. The remarkable tumor-homing efficiency of the LyP-1 peptide may be because of the propensity of this peptide to become internalized by cells. Cells that bind the LyP-1 peptide transport it across the cell membrane, into the cytoplasm and the nucleus. In this regard, LyP-1 is similar to the Tat peptide and other cell-penetrating peptides, which are also taken up by cells (24). An important difference is that our LyP-1 peptides are cell type-specific and deliver a payload to specific target cells: the lymphatic endothelial and tumor cells in tumors that display the "receptor" for these peptides. The internalization is likely to contribute to the effectiveness of these peptides in becoming concentrated in the targeted tumors. If this efficacy can be reproduced in clinical settings, LyP-1-directed targeting of contrast agents may become useful in tumor detection.

Our results show that treatment of tumor cells with the LyP-1 peptide causes cell death. This effect is specific because cells that do not bind LyP-1 were not affected. The tumor cell apoptosis we observed *in vivo* indicates that the LyP-1-binding cells die by apoptosis.

Whereas the mechanism whereby LyP-1 kills cells remains to be elucidated, the proapoptotic effect seems to be directed against tumor cells that are under stress, as LyP-1 colocalized with a tissue hypoxia marker *in vivo*, and serum starvation enhanced LyP-1 binding and internalization by cultured tumor cells *in vitro*. It will be important to identify the molecule (receptor) to which LyP-1 binds at the cell surface (and that may mediate the proapoptotic effect of LyP-1). Our efforts to isolate a LyP-1 receptor by affinity chromatography and various cloning methods have not yet been successful.

Treatment of tumor-bearing mice with the LyP-1 peptide suppressed tumor growth. It also drastically reduced the expression of lymphatic endothelial markers in the treated tumors. This latter result suggests that LyP-1 is also cytotoxic/proapoptotic for lymphatic endothelial cells in tumors. As tumor lymphatics have not been shown to be important for tumor growth (25), it is likely that the antitumor activity of LyP-1 is related to its effect on tumor cells rather than tumor lymphatics. However, given the demonstrated role of tumor lymphatics in metastasis (15, 16, 22), destroying tumor lymphatics with LyP-1 may be particularly

effective in curtailing lymphatic spread of tumors. As lymphatics appear to be the first target of LyP-1 in tumors (4), the antitumor effect of LyP-1 may be particularly pronounced on tumor cells within and close to the lymphatics, which are likely to be the cells most probable to spread through the lymphatic system.

Hypoxia enhances metastasis (23, 26), and LyP-1 selectively targets tumor cells in the hypoxic areas of tumors. This may be another pathway through which LyP-1 could suppress metastasis. MDA-MB-435 tumors are highly metastatic, and the VEGF-C-expressing cells are even more aggressive in that regard. In this study, we evaluated the effects of LyP-1 on established primary tumors. As metastasis had already occurred at the time the treatment began, we could not evaluate the effect of LyP-1 on the metastatic spread. Studies to determine the effects of LyP-1 on metastasis are underway. Nonetheless, the data already at hand define this peptide as a potentially unique tool for tumor diagnosis and treatment.

We thank Dr. Randall Johnson for reagents, Drs. Kari Alitalo and Eva Engvall for comments on the manuscript, and Roslind Varghese for editing. This work was supported by National Cancer Institute Grant CA82713, Department of Defense Grant DAMD 17-02-1-0315 (to E.R.), Cancer Center Support Grant CA30199, and National Cancer Institute Grant CA099258-01 (to AntiCancer, Inc.). P.L. received support from the Academy of Finland and Biocentrum Helsinki. M.E.A. was supported by Department of Defense Fellowship DAMD17-02-1-0308.

1. Ruoslahti, E. (2002) *Nat. Rev. Cancer* **2**, 83–90.
2. Hoffman, J. A., Giraudo, E., Singh, M., Zhang, L., Inoue, M., Porkka, K., Hanahan, D. & Ruoslahti, E. (2003) *Cancer Cell* **4**, 383–391.
3. Joyce, J. A., Laakkonen, P., Bernasconi, M., Bergers, G., Ruoslahti, E. & Hanahan, D. (2003) *Cancer Cell* **4**, 393–403.
4. Laakkonen, P., Porkka, K., Hoffman, J. A. & Ruoslahti, E. (2002) *Nat. Med.* **8**, 751–755.
5. Breiteneder-Geleff, S., Soleiman, A., Kowalski, H., Horvat, R., Amann, G., Kriehuber, E., Diem, K., Weninger, W., Tschachler, E., Alitalo, K. & Kerjaschki, D. (1999) *Am. J. Pathol.* **154**, 385–394.
6. Banerji, S., Ni, J., Wang, S. X., Clasper, S., Su, J., Tammi, R., Jones, M. & Jackson, D. G. (1999) *J. Cell Biol.* **144**, 789–801.
7. Wigle, J. T. & Oliver, G. (1999) *Cell* **98**, 769–778.
8. Achen, M. G., Jeltsch, M., Kuk, E., Makinen, T., Vitali, A., Wilks, A. F., Alitalo, K. & Stacker, S. A. (1998) *Proc. Natl. Acad. Sci. USA* **95**, 548–553.
9. Jeltsch, M., Kaipainen, A., Joukov, V., Meng, X., Lakso, M., Rauvala, H., Swartz, M., Fukumura, D., Jain, R. K. & Alitalo, K. (1997) *Science* **276**, 1423–1425.
10. Wigle, J. T., Harvey, N., Detmar, M., Lagutina, I., Grosveld, G., Gunn, M. D., Jackson, D. G. & Oliver, G. (2002) *EMBO J.* **21**, 1505–1513.
11. Jackson, D. G., Prevo, R., Clasper, S. & Banerji, S. (2001) *Trends Immunol.* **22**, 317–321.
12. Leu, A. J., Berk, D. A., Lymboussaki, A., Alitalo, K. & Jain, R. K. (2000) *Cancer Res.* **60**, 4324–4327.
13. Karpanen, T., Egeblad, M., Karkkainen, M. J., Kubo, H., Yla-Herttuala, S., Jaattela, M. & Alitalo, K. (2001) *Cancer Res.* **61**, 1786–1790.
14. Pepper, M. S. (2001) *Clin. Cancer Res.* **7**, 462–468.
15. Stacker, S. A., Caesar, C., Baldwin, M. E., Thornton, G. E., Williams, R. A., Prevo, R., Jackson, D. G., Nishikawa, S., Kubo, H. & Achen, M. G. (2001) *Nat. Med.* **7**, 186–191.
16. Mandriota, S. J., Jussila, L., Jeltsch, M., Compagni, A., Baetens, D., Prevo, R., Banerji, S., Huarte, J., Montesano, R., Jackson, D. G., *et al.* (2001) *EMBO J.* **20**, 672–682.
17. Valtola, R., Salven, P., Heikkilä, P., Taipale, J., Joensuu, H., Rehn, M., Pihlajaniemi, T., Weich, H., de Waal, R. & Alitalo, K. (1999) *Am. J. Pathol.* **154**, 1381–1390.
18. Saharinen, P., Tammela, T., Karkkainen, M. J. & Alitalo, K. (2004) *Trends Immunol.*, in press.
19. Yang, M., Baranov, E., Jiang, P., Sun, F. X., Li, X. M., Li, L., Hasegawa, S., Bouvet, M., Al-Tuwaijri, M., Chishima, T., *et al.* (2000) *Proc. Natl. Acad. Sci. USA* **97**, 1206–1211.
20. Lord, E. M., Harwell, L. & Koch, C. J. (1993) *Cancer Res.* **53**, 5721–5726.
21. Schueneman, A. J., Himmelfarb, E., Geng, L., Tan, J., Donnelly, E., Mendel, D., McMahon, G. & Hallahan, D. E. (2003) *Cancer Res.* **63**, 4009–4016.
22. Skobe, M., Hawighorst, T., Jackson, D. G., Prevo, R., Janes, L., Velasco, P., Riccardi, L., Alitalo, K., Claffey, K. & Detmar, M. (2001) *Nat. Med.* **7**, 192–198.
23. Rofstad, E. K., Rasmussen, H., Galappathi, K., Mathiesen, B., Nilsen, K. & Graff, B. A. (2002) *Cancer Res.* **62**, 1847–1853.
24. Lundberg, P. & Langel, U. (2003) *J. Mol. Recognit.* **16**, 227–233.
25. He, Y., Kozaki, K., Karpanen, T., Koshikawa, K., Yla-Herttuala, S., Takahashi, T. & Alitalo, K. (2002) *J. Natl. Cancer Inst.* **94**, 819–825.
26. Zhong, H., De Marzo, A. M., Laughner, E., Lim, M., Hilton, D. A., Zagzag, D., Buechler, P., Isaacs, W. B., Semenza, G. L. & Simons, J. W. (1999) *Cancer Res.* **59**, 5830–5835.

Identification of endothelial genes up-regulated in vivo

Jih-tung Pai, Erkki Ruoslahti*

Cancer Research Center, The Burnham Institute, 10901 North Torrey Pines Road, La Jolla, CA 92037, USA

Received 1 June 2004; received in revised form 25 November 2004; accepted 15 December 2004

Received by R. Di Lauro

Abstract

We have used microarrays to identify genes that are selectively expressed in endothelial cells in vivo. Analysis of freshly isolated endothelial cells from the lungs and kidneys reveals that 350 out of the 10,000 genes represented on the microarrays were expressed at higher levels than by the corresponding parenchymal cells. Thirteen of these genes were identified both in the lung and kidney screens from a subset of about 5000 genes. Many of these genes are known to be specifically expressed in endothelial cells, but about 200 genes were potentially novel endothelial genes. The preferential endothelial expression of a selected group of these genes was confirmed by quantitative polymerase chain reaction or in situ mRNA hybridization. Comparison of the genes expressed in lung and kidney endothelia revealed numerous differences. Notably, genes encoding components of an ephrin signaling pathway were highly expressed in lung endothelial cells. In summary, the genes we have identified represent potentially new pan-endothelial and tissue-specific endothelial markers.

© 2004 Elsevier B.V. All rights reserved.

Keywords: Microarray; Gene expression; Organ specificity; Ephrins

1. Introduction

The endothelial cells (EC) lining the vascular lumen are a highly specialized cell type. The gene expression pattern of EC includes many proteins that are specific for EC (Peale and Gerritsen, 2001). In addition, actively proliferating EC express their own set of markers that are not present at significant levels in resting cells, and EC from one tissue differ from those in another (Ruoslahti, 2002). An under-

standing of the role of EC in normal physiology and in various pathologies requires identifying and characterizing the genes that are expressed by various types of EC.

A global analysis of gene expression patterns makes it possible to simultaneously identify and classify large numbers of expressed genes. The methods previously used to study EC gene expression include proteomic approaches, differential hybridization, subtraction hybridization, differential display, Serial Analysis of Gene Expression, and microarrays (St Croix et al., 2000; Ho et al., 2003). The majority of these studies used cultured EC, leaving open the possibility that changes may have occurred during cell culture. For example, in vitro proliferation induces an angiogenic phenotype in EC, which may be quite different from the phenotype of the non-proliferating cells in vivo. During the past few years, microarray analyses have emerged as a useful technology in delineating expression patterns. Microarrays have been used to study EC biology under different conditions: human umbilical vein EC under shear stress and various EC lines under various growth stimuli (Dekker et al., 2002; Zhao et al., 2003). These studies have provided insights into EC biology and

Abbreviations: EC, endothelial cells; PE, R-Phycoerythrin; DEPC, diethyl pyrocarbonate; aRNA, antisense RNA; HRP, horseradish peroxidase; DAB, diaminobenzidine; PECAM, platelet-endothelial cell adhesion molecule; Icam2, intercellular adhesion molecule 2; Esam, endothelial cell-selective adhesion molecule; Gata2, GATA binding protein 2; Ets2, v-ets avian erythroblastosis virus E26 oncogene homolog 2; EST, expression sequence tag; PEM, pan endothelial marker; LEM, lung endothelial marker; KEM, kidney endothelial marker; Sdf1, stromal cell-derived factor 1; Arap3, ARP-GAP, RHO-GAP, ankyrin repeat and plekstrin homology domains-containing protein 3; PI3K, phosphatidylinositol 3-kinase; RGS, regulator of G protein signaling, VHL, von Hippel-Lindau.

* Corresponding author. Tel.: +1 858 646 3125; fax: +1 858 646 3198.

E-mail address: ruoslahti@burnham.org (E. Ruoslahti).

identified new genes relevant to it, but because they were in vitro studies, the results may not completely reflect in vivo conditions.

Our laboratory is interested in gene expression differences among EC from different normal tissues and tumors, and has used in vivo display of peptides to identify endothelial marker molecules (Ruoslahti, 2002). Here, we undertook profiling of endothelial gene expression in two organs, lung and kidney, by cDNA microarray analysis. As with the in vivo phage display method, our primary concern was to use procedures that minimize the interpolation distance between the conditions in the analysis and those in situ. The lung and kidney vasculature are prime targets for this type of analysis because these tissues contain a high proportion of EC, and because the vasculature in these tissues carries out specialized functions. Lung vasculature is also an important site of tumor metastasis, some of which has been shown to depend on specific interactions between circulating tumor cells and the lung endothelium (Brown and Ruoslahti, 2004).

To identify genes selectively expressed in lung and kidney EC, we adapted methods for linearly amplifying RNA from small numbers of EC and parenchymal cells that had been freshly isolated from the tissue, and compared these RNAs by microarray analysis (Luo et al., 1999). We report here on genes that we found to be up-regulated in lung and kidney endothelia relative to the respective parenchymal cells. Of these, many are known in the literature as endothelial markers. We also identified for the first time many genes encoding novel endothelial markers. In many cases, the endothelial selectivity of the expression of these novel markers was as high or higher than that of known endothelial marker genes. There were also genes that only showed endothelial expression in lung but not in kidney and vice versa. These are candidates for organ-specific EC markers. The new pan-endothelial genes may be important for the development, maintenance, or normal function of endothelia, while the genes selectively expressed in EC of one tissue only may reflect the specialized endothelial functions of that tissue. These results also form a basis for comparing lung and kidney endothelia to endothelia from other tissues.

2. Materials and methods

2.1. Purification of EC

Lungs and kidneys from adult female mice were minced to around 1 mm³ pieces then subjected to 10 ml of Buffer A, containing 2 mg/ml collagenase (Sigma-Aldrich, St. Louis, Missouri, USA), 25 µg/ml DNase I (Sigma-Aldrich) in 2.4 U/ml Dispase II solution (Roche Molecular Biochemicals, Indianapolis, Indiana, USA). After 1 h incubation in a 37 °C incubator with rotation, cells were spun down in 1000×g for 5 min and the pellets were resuspended with ~1.5 ml of

Buffer A. For kidney, the resuspended cells were laid on top of 30% percoll and spun in 1600×g for 15 min as an additional step to eliminate red blood cells. The cells on the top layer were collected, washed, and resuspended in ~1.5 ml of Buffer A. The suspended cells were then filtered through a 50 µm mesh to remove big aggregates. The cells were then subjected to StemSep system for negative selection according to manufacturer's protocol, except that the lineage antibody cocktail is replaced with Mouse Lineage Panel (20 µl each; BD Pharmingen, San Diego, California, USA). Flow-through fraction was centrifuged to create pellets. The pellet was resuspended in 500 µl of Buffer B (PBS at pH 7.4, containing 2% fetal calf serum). R-Phycoerythrin (PE) conjugated rat anti-mouse CD31 (5 µl; Caltag, Burlingame California, USA) and 5 µl of 0.5 mg/ml biotin-conjugated anti-mouse CD31 (MEC13.3, BD Pharmingen) were added to the cells and incubated for 15 min in a cold room. After twice washing in Buffer B, the pellet was resuspended in 450 µl of Buffer B and passed through the MACS MS separation column (Miltenyi Biotec, Auburn, California, USA) following manufacturer's protocol. Both flow-through and elution fractions were collected and a small aliquot of cells was inspected under fluorescence microscope to evaluate the percentage of PE-positive cells with a rhodamine filter set.

2.2. Antisense RNA (aRNA) preparation

The purified EC (elution) as well as the parenchymal cells (flow-through) were subjected to RNA extraction by RNeasy Mini Kit (Qiagen, Valencia, California, USA) following manufacturer's protocol. The extracted total RNA samples (in 60 µl/sample) were dried in SpeedVac and resuspended in 10 µl of diethyl pyrocarbonate (DEPC)-treated dH₂O. The protocol described in Luo et al. (1999) for preparing a two-run amplified antisense RNA was followed, with the exception that aRNA was purified by RNeasy Mini Kit and concentrated by SpeedVac.

2.3. Microarray analysis

We used two mouse microarray chips (Arrays A and B), each containing a separate set of about 5000 cDNAs. The array design protocol is supplied as Supplemental Material. Two or more experiments were performed using cells from two different mice, along with swapping the Cy3 and Cy5 dye labels in order to reduce the probability of detecting artifactual differences. We performed two to three sets of experiments with each chip, representing 4 and 6 comparisons, respectively (Table 1S). Both technical duplicates (dye reverse) and biological duplicates (two different animals) were included in each EC/non-EC comparison. We applied the statistical model described in the Statistical analyses section and listed the genes with a lower boundary of at least 3-fold up-regulation in the EC relative to the non-EC. Direct comparison of EC from lung and kidney in

microarray assays gave results with unacceptable noise levels (data not shown). To circumvent this problem, we directly compared EC and respective parenchymal cells and used the resulting data to compare the EC populations from the lungs and kidneys. This approach is based on the assumption that the gene expression patterns of the parenchymal cell populations from these tissues are relatively similar.

For each pair of comparison, aRNA from one sample was labeled with Cy3 dye, and aRNA from the other group was labeled with Cy5 dye. To exclude the artifact that may occur with a specific dye, we also reversed the labeling dye in another comparison pair. For each labeling, 5 µg of aRNA and 3 µg of random hexamers were mixed in a total volume of 28 µl (containing DEPC-treated dH₂O), heated to 70 °C for 10 min, and chilled on ice. Then, 10 µl of 5× first-strand buffer (Invitrogen, Carlsbad, California, USA), 5 µl of 0.1 M DTT (Invitrogen), 1 µl of 40 U/µl RNasin (Promega, Madison, Wisconsin, USA), 1 µl of 10/1 dNTP mix (25 mM dGTP, 25 mM dATP, 25 mM dCTP, and 2.5 mM dTTP [Invitrogen]), 3 µl of 1 mM Cy3-dUTP (Amersham Biosciences, Piscataway, New Jersey, USA), and 2 µl of 200 U/µl Superscript RT II (Invitrogen) were added and the mixture was incubated at room temperature for 10 min and then at 37 °C for 1.5 h. To degrade the aRNA template and stop the reaction, 10 µl of 1 N NaOH and 10 µl of 0.5 M EDTA were added and incubated at 65 °C for 20 min. At this stage, Cy3 and Cy5 probes from the same pair of comparison were mixed together. Next, 50 µl of 1 M Hepes pH 7.0 and 70 µl of 3 M Sodium Acetate (pH 5.3) were added to each probe pair. The probe pairs were purified with PCR Purification Kit. Each probe pair was mixed with 20 µg human Cot-1 DNA (Invitrogen) and 20 µg poly-A RNA (Sigma-Aldrich), dried in SpeedVac, and resuspended in 25 µl of DEPC-treated dH₂O.

Printed glass slides were incubated with pre-hybridization solution (1% BSA, 5× SSC, and 0.1% SDS) at 42 °C for 1 h. After pre-hybridization, slides were rinsed with dH₂O for 10 s and then put into isopropanol. After being taken out of isopropanol, slides were spun at 1000×g for 5 min to get rid of excess isopropanol, and allowed to air dry. The probe pair was denatured at 95 °C for 2 min and mixed with 25 µl of 2× hybridization buffer (10× SSC, 50% formamide, and 0.2% SDS). For a 60×20 mm coverslip area, 46.2 µl of hybridization solution together with Cy dye-labeled probes were used to hybridize the cDNA spots in a humidified cassette (TeleChem International, Sunnyvale, California, USA) put in a 42 °C water bath for 16 h. Hybridization was carried out in the dark. After hybridization, slides were washed in a 42 °C wash I solution (1× SSC, 0.2% SDS) with agitation for 5 min, followed by 5-min room temperature wash II (0.1× SSC, 0.2% SDS) and 5-min room temperature wash III (0.1× SSC). After these three washes, slides were spun at 1000×g for 5 min to get rid of excess liquid, air-dried in the dark, and were ready to be scanned.

cDNA microarrays were scanned for Cy3 fluorescence and Cy5 fluorescence using the ScanArray 3000 (General Scanning, Watertown, Massachusetts, USA). ImaGene software (BioDiscovery, Los Angeles, California, USA) was then subsequently used for quantification. The intensity of each spot was corrected by subtracting the immediate surrounding background. The corrected intensities were normalized for each cDNA by global normalization per ImaGene software. The microarray datasets have been deposited in Gene Expression Omnibus (GEO) with accession numbers GSE 704, GSE 705, and GSE 707. The raw data are available from the authors upon request.

2.4. Statistical analyses

To calculate the expression difference of a given cDNA in the EC and non-EC pools, the average of the ratios across all the comparison sets, including the comparisons from dye reverse and from different animals, was used. We devised the formula shown below to deduce the weighted mean ratio and pseudo-standard deviation for the observations. We show here that this method gives valid ratios in our experimental setting. Since there is more variation in calculating the ratio when the raw control signal strength is low, we use raw control signal strength as weight to calculate the adjusted average. All the raw values smaller than one are set to one for calculating the ratios. The formulas we use for the weighted mean ratio (M) and pseudo standard deviation (SD^*) for each gene are:

$$M = (\sum X_n W_n) / (\sum W_n)$$

M is the weighted mean ratio for the gene. X_n is the ratio of the n th replicate for the gene. W_n is the weight of the n th comparison (raw control signal strength of the gene).

$$SD^* = \sqrt{\sum (X_n - M)^2 / \sum W_n^2}$$

SD^* is pseudo standard deviation defined here.

With M and SD^* , we calculate the lower bound $\{M - SD^*\}$ and higher bound $\{M + SD^*\}$ of the ratio. We arbitrarily chose the cDNA clones that had a $\{M - SD^*\}$ value greater or equal to 2 as the first criterion, since this cut-off will eliminate those genes that give high mean ratios due to high variability in the measurement. The second criterion was that M should be greater or equal to 3. Analysis of the data with these criteria correctly classified a large number of known EC genes, as well as allowed us to identify novel EC genes whose selective expression in EC was subsequently confirmed by quantitative RT-PCR or in situ hybridization.

2.5. Riboprobe preparation

cDNA clones corresponding to the spots of interest were retrieved from Invitrogen's mouse cDNA collection, which was used for cDNA microarray production as well. Purified

plasmids were linearized at the opposite end of the intended promoter sequence of the insert. The resulting DNA was purified with PCR Purification Kit (Qiagen) according to manufacturer's protocol. In vitro transcription reaction was set up with the following reagents: 1 µg of template (12 µl), 2 µl of 10×FITC NTP mix (Roche Molecular Biochemicals), 2 µl of 100 mM DTT, 2 µl of 10× transcription buffer (Roche Molecular Biochemicals), and 2 µl of polymerase (T3, T7, or Sp6 according to promoter) from Ampliscribe Transcription Kit (Epicenter Technologies, Madison, Wisconsin, USA). The mixture was incubated at 37 °C for 2 h, followed by 2 µl of 1 U/µl RNase-free DNase (Epicenter Technologies) treatment at 37 °C for 15 min. The riboprobe was then purified with RNeasy Mini Kit according to manufacturer's protocol and eluted in 60 µl DEPC-treated dH₂O. An aliquot of riboprobe was run on agarose gel to verify the integrity of the probe as well as for adjusting the concentration between sense and antisense probes.

2.6. In situ hybridization

In situ hybridization was done as described (Keeton et al., 1993) with modifications. Organs from 4-month-old mice were harvested and fixed with Z-fix (Anatech, Battle Creek, Michigan, USA) for 6 h. The organs were then embedded in paraffin according to standard protocol. Paraffin sections were prepared in 3 µm thickness. Before hybridization, the sections were pretreated with xylene (3×5 min); rinsed once with 50% ethanol; proceeded by the following treatments: 5 min in 50% ethanol, 5 min in 0.5× SSC, 15 min in 1 µg/ml of proteinase K (Roche Molecular Biochemicals) in Buffer C (10 mM Tris at pH 8.0 containing 0.5 M NaCl); and 0.5× in SSC (2×10 min). All incubations and washes were carried out at room temperature unless otherwise specified. Before pre-hybridization, the tissue area was dried with KimWipes and circled with Pap Pen (Research Products International, Mt. Prospect, Illinois, USA). The slides were then incubated with 200 µl pre-hybridization buffer [20 mM Tris at pH 8.0, 5 mM EDTA containing 50% formamide, 0.3 M NaCl, 1% Denhardt's solution (Sigma-Aldrich), 10% Dextran sulfate (Sigma-Aldrich), and 10 mM DTT] at 55 °C for 1–3 h. Additional 80 µl of pre-hybridization buffer, containing 1 µg tRNA and riboprobe, was added to the pre-hybridization bubble and incubated at 55 °C for 16 h.

After hybridization, the slides were washed in 2× SSC with 2.2 mM EDTA twice for 5 min each, followed by treatment with 1 µg/ml RNase A (Roche Molecular Biochemicals) in Buffer C. After RNase treatment, slides were washed twice in 2× SSC with 2.2 mM EDTA. A stringent wash (0.1× SSC, 1 mM EDTA, and 12.5 mM β-mercaptoethanol in 4 l for 2 h at 60 °C) with gentle stirring was used to get rid of non-specific binding. The slides were then subjected to 0.5× SSC washes (4×10 min). To reduce the background for horseradish peroxidase (HRP), incubation with 3% H₂O₂ in PBS for 30 min was used, followed

by one rinse with dH₂O and a 10-min incubation of dH₂O. Avidin/Biotin Blocking Kit (DAKO, Carpinteria, California, USA) was used at this stage to reduce the background associated with non-specific avidin–biotin binding according to manufacturer's protocol. GenPoint Kit (DAKO) was used for the signal amplification according to manufacturer's protocol, except that the extra step of HRP-conjugated anti-FITC antibody (1:150) with rabbit IgG (1:20) was added before Primary Streptavidin-HRP to detect FITC-labeled riboprobe. For ephrin-B1 ISH, alkaline phosphatase conjugated anti-biotin antibody (1:75, DAKO) was used in place of Secondary Streptavidin-HRP, and Sigma Fast™ Fast Red was used as substrate. Crystal mount (Biomedex, Foster City, California, USA) was used to mount the slides according to manufacturer's protocol. The detailed oligo probe in situ hybridization protocol is supplied as Supplemental Material.

2.7. Quantitative polymerase chain reaction (Q-PCR)

The Q-PCR reactions were performed according to Galang et al. (Galang et al., 2004). Briefly, a 20 µl Q-PCR reaction was used that contained 4 µl of cDNA (typically 1:30 and 1:100 dilution of the cDNA stock), 2 µl of SYBR green DNA master mix, 4 mM MgCl₂, and 0.5 mM of each primer (Table 2S). The reactions were carried out in a Roche LightCycler real-time PCR instrument with the following amplification protocol: 95 °C for 70 s, followed by 42 amplification cycles of 95 °C for 0 s, 56 °C for 7 s, and 72 °C for 20 s. Melting analysis was performed after a final melting step at 95 °C, followed by a 15 s annealing at 68 °C, then increasing the temperature to 97 °C at 0.1 °C/s with continuous fluorescence measurement.

3. Results

3.1. Microarray analysis

We used a transgenic mouse strain that expresses β-galactosidase (LacZ) under the control of the endothelial-specific Tie2 promoter (Tie2-LacZ mice) as the source of EC (Schlaeger et al., 1997). The LacZ marker was used to facilitate the establishment of the endothelial cell isolation procedure at the early stage. As we were interested in markers of mature EC, we used mice 9 months of age or older. Two selections were employed in the cell isolation procedure: first, a negative selection was used to remove known lineages that may carry the platelet-endothelial cell adhesion molecule (PECAM; CD31) as a surface marker but are not EC, followed by a positive selection to isolate PECAM-positive EC (Fig. 1). Tissues from one mouse yielded around 10,000 to 100,000 lung and kidney EC. Nearly all of the isolated cells were positive for staining with anti-PECAM antibody (Fig. 2). Purified and amplified

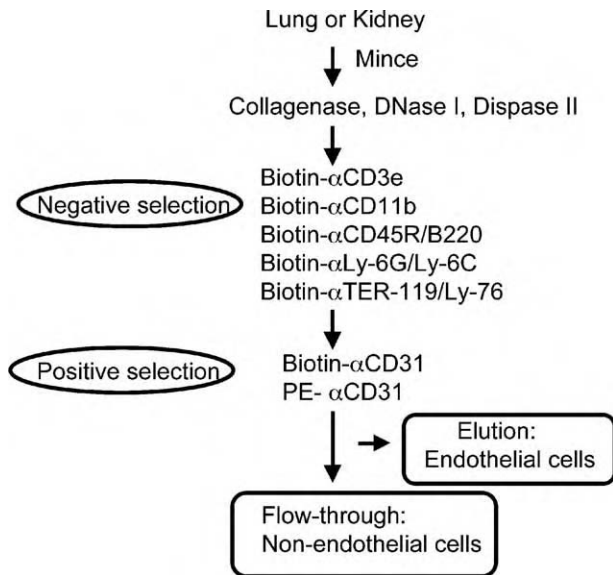


Fig. 1. Cell isolation scheme. Minced lung and kidney tissues were subjected to collagenase, dispase, and DNase treatment to generate a cell suspension. For kidney, an extra percoll gradient step was used. The cell suspensions were subjected to a negative selection to remove other cells that may carry the CD31 marker, followed by a positive selection for EC on an anti-CD31 column. The flow-through of the anti-CD31 column was designated as parenchymal cells, and the CD31-positive cells as EC.

mRNA from these cells was used to perform microarray analyses. We wanted to limit our analysis to those genes that are expressed only in EC. To this end, the initial comparison was made between EC and parenchymal cells from the same tissue, and secondary comparison was then performed between endothelial genes from the two tissues.

3.2. Genes preferentially expressed in EC

We performed microarray analysis comparing lung EC to lung parenchymal cells on two arrays containing about 5000 genes each. One of the arrays was then used in a similar comparison of EC and parenchymal cells from the kidneys.

3.2.1. Previously known endothelial genes

Our microarrays revealed a large number of genes that were highly expressed in either lung (Table 1) or kidney (Table 2) EC in comparison to the non-EC of the same tissue. The Tables list the genes with the highest EC/non-EC ratios; Tables 3S and 4S in Supplemental Material give the complete data sets. Many of the up-regulated genes shared by lung and kidney EC are well-established EC markers (Tables 3 and 5S).

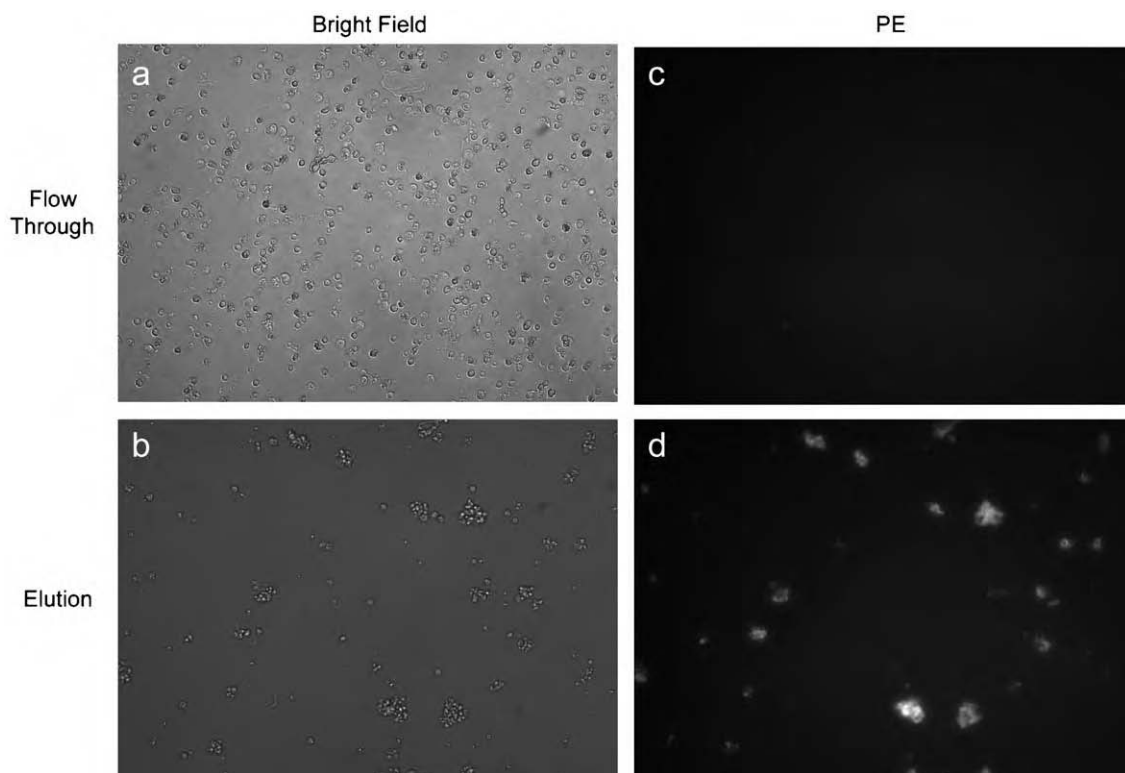


Fig. 2. Purity of cell preparations. The EC and parenchymal cells isolated as described in Fig. 1 were analyzed for CD31 expression by immunofluorescence after PE-conjugated anti-CD31 antibody staining. Only occasional CD31-positive cells were seen in the parenchymal cell preparation (c) and essentially all cells in the EC fraction were CD31-positive (d), whereas panels (a) and (b) show the corresponding bright field microscopic images (magnification=200×).

Table 1

Genes that are up-regulated in lung EC (Arrays A and B)

Accession no.	UniGene ID	Lung mean	Gene	Rank
AA274472	Mm.24615	29.57	Gja4/connexin 37	1
AA269330		24.80	Xlkd1	2
AA290107	Mm.29429	23.67	LEM3	3
AA475938		23.24	LEM4	4
AA254957		20.55	LEM5	5
AA017847	Mm.14313	20.40	Tek/Tie2	6
AA000564		19.09	Agtr11/angiotensin receptor-like 1	7
AA014250	Mm.3464	18.93	Flt1/VEGFR1	8
AA050972	Mm.394	18.64	Icam2	9
AA163827	Mm.34112	18.10	Plvap/PV1	10
AA022302	Mm.173813	17.15	Notch4	11
AA244935		16.90	LEM12	12
W16166	Mm.22152	14.83	LEM13/KEM26/PEM3	13
W59175		14.76	Cdh5/VE-cadherin	14
W84227	Mm.33798	13.73	Emilin3/multimerin 2	15
AA277779		13.63	LEM16	16
AA027569	Mm.1391	12.73	Gata2	17
AA466569	Mm.87263	11.84	LEM18	18
AA435117		11.39	Cdh5/VE-cadherin	19
W65557	Mm.1560	11.32	LEM20	20
W75674	Mm.23996	11.08	Slco2a1/solute carrier family 21	21
AA268708		10.94	LEM22	22
AA265694		10.60	Notch1	23
AA268333		10.44	LEM24	24
AA120432	Mm.23996	9.51	Slco2a1/solute carrier family 21	25
W98502	Mm.1574	9.46	Ramp2	26
W88001	Mm.29581	9.41	Hey1	27
AA537301		9.20	LEM28	28
AA036517		9.12	LEM29	29
AA016920	Mm.33762	9.04	Myct1	30
AA200135	Mm.144407	8.67	Rgs12	31
AA003899	Mm.169542	8.55	LEM32	32
AA472994		8.34	LEM33	33
W62248		8.32	Cdh5/VE-cadherin	34
AA255046	Mm.2857	8.29	Admr	35
AA038253	Mm.5376	8.24	LEM36	36
AA174397	Mm.155617	8.04	Palmd/palmdelphin	37
AA033055	Mm.21587	8.01	Slc9a3r2	38
W84056	Mm.21587	7.93	Slc9a3r2	39
AA118715	Mm.182255	7.82	Cd97	40
AA261160		7.81	Mcarn/melanoma cell adhesion molecule/MUC18	41
AA049318	Mm.4345	7.62	Tie1	42
W64238		7.62	Apln/apelin	43
AA175284	Mm.30576	7.49	LEM44	44
AA138584	Mm.22511	7.41	LEM45	45
W54099		6.99	LEM46	46
W62484	Mm.12559	6.83	Hs3st1	47
AA250558		6.78	Esam/endothelial cell-selective adhesion molecule	48
AA241237		6.78	LEM49	49
AA413050	Mm.28943	6.73	LEM50	50

The selected genes show a high EC/parenchymal cell expression ratio in lung. The top 50 genes are listed. A few genes appear twice because occasionally there is more than one cDNA clone covering the same gene. UniGene ID is listed when the *E* value is smaller than $1E-100$ for Tables 1–4.

Table 2

Genes that are up-regulated in kidney EC (Array A only)

Accession no.	UniGene ID	Kidney mean	Gene	Rank
AA017847	Mm.14313	11.51	Tek	1
AA051341	Mm.3509	9.35	Tnfrp6/tumor necrosis factor induced protein 6	2
AA023805		9.27	KEM3	3
AA109900		8.73	Hba-a1/Hemoglobin alpha, adult chain 1	4
AA034593	Mm.32135	8.69	KEM5	5
AA063802		8.38	KEM6	6
W65557		8.17	Arap3	7
AA020057	Mm.22194	8.05	Prg/proteoglycan, secretory granule	8
W97244		7.96	KEM9	9
AA139630		7.95	KEM10	10
AA003881		7.87	Zfr	11
AA059837		7.84	KEM12	12
AA000461	Mm.3453	7.77	C1qg/C1q C-chain	13
AA000712	Mm.1583	7.57	Ly6c	14
AA139452		7.46	KEM15	15
AA020470		7.40	KEM16	16
AA050212	Mm.23145	7.20	KEM17	17
W77330		7.11	KEM18	18
AA038182	Mm.29831	7.07	KEM19	19
AA111560		7.05	KEM20	20
AA002751		6.97	KEM21	21
AA002955		6.87	KEM22	22
AA047985		6.83	KEM23	23
AA139223	Mm.119713	6.78	KEM24	24
AA183727	Mm.190140	6.78	KEM25	25
W16166	Mm.22152	6.63	KEM26/LEM13/PEM3	26
AA002396	Mm.138561	6.53	KEM27	27
AA049318	Mm.4345	6.48	Tie1	28
W18362		6.47	KEM29	29
AA036499		6.39	KEM30	30
AA116465		6.38	KEM31	31
W89701		6.37	KEM32	32
W58982	Mm.117055	6.29	KEM33	33
W54421		6.29	Thy28/thymocyte protein mThy28	34
AA022302	Mm.173813	6.23	Notch4	35
AA003898		6.22	Thrap5	36
AA123007		6.22	Oasl2/2'-5' oligoadenylate synthetase-like 2	37
AA049152	Mm.29577	6.20	Brp16/brain protein 16	38
AA002904		6.20	KEM39	39
AA023914		6.17	KEM40	40
AA020272	Mm.23637	6.13	KEM41	41
AA125257		6.13	KEM42	42
AA030122	Mm.180733	6.08	KEM43	43
AA064307		5.96	Cd34	44
AA051556	Mm.2924	5.91	Pdgfra	45
AA108832		5.79	Akap8	46
AA097228	Mm.139277	5.78	KEM47	47
W84046		5.77	KEM48	48
AA000856	Mm.3317	5.77	Gus	49
AA051649		5.74	KEM50	50

Selected genes showing a high EC/parenchymal cell expression ratio in kidney. The top 50 genes are listed.

Table 3
Genes that are up-regulated in both lung and kidney EC (Array A only)

Accession no.	UniGene ID	Lung mean	Kidney mean	Gene	Rank
AA017847	Mm.14313	20.40	11.51	Tek/Tie-2	1
AA022302	Mm.173813	17.15	6.23	Notch4	2
W16166	Mm.22152	14.83	6.63	PEM3/LEM13/ KEM26	3
W65557		11.32	8.17	Arap3	4
W98502	Mm.1574	9.46	4.70	Ramp2	5
AA049318	Mm.4345	7.62	6.48	Tie1	6
AA080278	Mm.4851	6.51	5.11	Eng/endoglin	7
W10915		5.95	3.20	Rnfl44	8
AA051563		5.87	5.20	Cbfa2t3h	9
AA109900		3.78	8.73	Hba-a1/Hemoglobin alpha, adult chain 1	10
AA000712	Mm.1583	3.53	7.57	Ly6c	11
AA004178	Mm.12429	3.35	3.05	Cbfa2t3h	12
AA020057	Mm.22194	3.15	8.05	Prg/proteoglycan, secretory granule	13

The genes with EC/parenchymal cell expression ratios greater than 3 in both lung and kidney are listed. The additional criterion of $\{M-SD^*\}$ greater than 2 was used to ensure the significance of the differences in the expression ratios.

Examples of the known pan-endothelial category include Tek (Dumont et al., 1992), Tie1 (Sato et al., 1993), Notch4 (Villa et al., 2001), and endoglin (Gougous and Letarte, 1990), all of which are also known to be important for vascular development. Gja4, also known as connexin 37 (Reed et al., 1993), Icam2 (Cowan et al., 1998), VE-cadherin (Breier et al., 1996), and endothelial cell-selective adhesion molecule (Esam; Hirata et al., 2001) are endothelial-specific adhesion molecules identified from the lung cell comparison. Gja4 showed one of the highest endothelial enrichment ratios, about 30-fold, among all the genes we analyzed in this study. We also identified a known endothelial-specific membrane protein, Plvap (Stan et al., 2001).

CD31, which was used in the EC isolation, did not appear in the list because it was not included among the cDNAs on the microarray chips. Q-PCR assay showed about 170- and 20-fold enrichment in the lung and kidney EC fractions, respectively (see Table 6). Several other genes were significantly up-regulated only in lung or kidney EC, but have been previously associated with EC from various tissues. We classify these genes also as known pan-endothelial genes. Among them, GATA binding protein 2 (Gata2) and E26 avian leukemia oncogene 2 (Ets2) are transcription factors responsible for the activation of several endothelial-specific genes (Perkins and Davies, 2003). Other proteins on our list, solute carrier family 21 (St Croix et al., 2000), caveolin-1 β (Liu et al., 1999), Hs3st1 (de Agostini et al., 1990), and CD36 (Swerlick et al., 1992) have also all been previously shown to be preferentially expressed in EC. Altogether, the presence of many known endothelial genes among the ones we identified either from lung EC or kidney EC, or both, validates our analysis. In addition, unlike most of the

earlier studies, our research was carried out with cells freshly isolated from tissues without intervening cell culture. Such cells should more faithfully reflect the in vivo conditions than cultured cells. Various MHC genes were also highly expressed in EC; their expression in EC may play a role in antigen presentation and transplant rejection.

3.2.2. Novel endothelial genes

We also identified numerous genes that were selectively expressed in lung or kidney EC, or both, but that have not previously been linked to EC. These included genes that have been studied in other contexts [e.g. ARF-GTPase activating protein (ARF-GAP), Rho-GAP, ankyrin repeat and plekstrin homology domains-containing protein 3 (Arap3; Krugmann et al., 2002), Rnfl44, and multimerin 2 (Hayward et al., 1995)]. This group also included numerous genes known only as expression sequence tags [ESTs; designated as lung EC markers (LEMs), kidney EC markers (KEMs), and pan EC markers (PEMs)]. A number of these genes displayed an endothelial expression preference similar or greater than that of many well-known endothelial genes. These genes may represent novel endothelial markers.

3.3. Tissue-specific endothelial gene expression

Another group of genes identified in this study were genes that appeared to be selectively expressed in only lung or kidney EC (Tables 4 and 5). We defined such selectivity as mean ratio greater than 3-fold in one organ, and lower than 1.5-fold in the other. Again, both the genes for previously known proteins and those defined by ESTs were present in this group. Intriguingly, ephrin-B1 and a component of an ephrin-B1 regulated signaling pathway known as stromal cell-derived factor 1 (Sdf1) were preferentially expressed in lung EC (Lu et al., 2001).

Because the organ specificity was derived from separate comparisons to parenchymal cells, we performed Q-PCR assays on several of the putative tissue-specific EC genes, while a house-keeping gene, cyclophilin, served as a reference (Table 6). The results show a good general agreement between the Q-PCR and microarray results.

3.4. In situ hybridization

To confirm selective endothelial expression of some of the potentially novel endothelial markers in another independent assay, we performed in situ hybridizations with a selected panel of mRNAs. Fig. 3 shows H2-Kb, PEM3, Arap3, LEM4, and LEM45 mRNAs specifically expressed in lung EC and, where studied, also in the endocardium of the heart or EC lining the hepatic veins of the liver, suggesting that these genes are pan-EC

Table 4
Lung specific EC genes

LUNG					
Accession no.	UniGene ID	Lung mean	Kidney mean	Gene	Rank
AA027569	Mm.1391	12.73	0.11	Gata2	1
W75674	Mm.23996	11.08	1.02	Slco2a1/solute carrier family 21	2
AA120432	Mm.23996	9.51	0.53	Slco2a1/solute carrier family 21	3
W88001	Mm.29581	9.41	0.91	Hey1	4
AA003899	Mm.169542	8.55	1.26	LEM32	5
AA038253	Mm.5376	8.24	0.39	LEM36	6
W64238		7.62	1.27	Apln/apelin	7
W54099		6.99	0.29	LEM46	8
W62484	Mm.12559	6.83	1.15	Hs3st1	9
W84060	Mm.100109	6.59	0.33	Siat10	10
W98084		6.49	0.59	LEM56	11
AA027459		6.33	0.86	LEM59	12
AA030427		5.47	0.30	LEM67	13
W48139	Mm.4839	5.25	1.10	Acvrl1/ALK1	14
AA073509		5.04	1.12	LEM74	15
AA034754	Mm.29721	4.90	1.14	LEM75	16
W08694	Mm.1641	4.82	0.88	Car4/carbonic anhydrase 4	17
AA030833	Mm.2013	4.72	0.84	LEM83	18
AA032563	Mm.139674	4.62	0.29	LEM85	19
AA003297	Mm.3374	4.61	0.49	Efnb1/ephrin-B1	20
AA036623		4.42	0.68	Trim46	21
W98950		4.34	1.40	Ppm1f	22
W14540	Mm.16771	4.32	0.66	H2-Kb	23
AA123837		4.28	1.04	LEM94	24
W53959		4.27	0.44	Wars/tryptophanyl-tRNA synthetase	25
W13196	Mm.28278	4.25	0.48	Cav/caveolin-1 beta isoform	26
AA003405		4.16	0.59	LEM100	27
W97210	Mm.92659	4.09	1.25	Luzp1	28
AA027510	Mm.5376	4.08	0.54	LEM102	29
AA111732	Mm.5598	3.68	1.45	Adrb2/Adrenergic receptor, beta 2	30
AA000732		3.53	1.26	LEM120	31
AA002845	Mm.495	3.51	1.18	LEM121	32
AA014761	Mm.22365	3.47	1.16	Ets2	33
W98251	Mm.1075	3.43	0.25	St5	34
AA124535		3.43	1.19	Laf4	35
AA014511		3.38	1.00	Nrarp	36
AA030534	Mm.32985	3.25	0.70	LEM133	37
W82690		3.04	0.55	LEM139	38
AA060490		3.04	0.97	LEM140	39
AA031238		3.03	1.22	Gnaq	40
AA037991		3.00	0.93	LEM143	41
W70776	Mm.23889	3.00	1.02	Unc84a/musculus unc-84 homolog A	42

Selected genes that are highly expressed in lung and not in kidney EC. Selected lists of genes with a mean ratio greater than 3 in one organ and smaller than 1.5 in the other are shown.

markers. Hybridization with aRNA gave unacceptable levels of background in the kidney, so we used oligonucleotide hybridization to confirm the endothelial expression in the kidney of endoglin and PEM3 (Fig. 4). Endoglin signal is seen in inter-tubular and glomerular

capillaries, whereas PEM3 is expressed in intertubular capillaries and only in a subfraction of the glomerular capillaries.

Table 5
Kidney specific EC genes

Kidney					
Accession no.	UniGene ID	Lung mean	Kidney mean	Gene	Rank
AA051341	Mm.3509	0.79	9.35	Tnfrp6	1
AA023805		1.08	9.27	KEM3	2
AA034593	Mm.32135	0.87	8.69	KEM5	3
AA063802		0.79	8.38	KEM6	4
W97244		1.21	7.96	KEM9	5
AA139630		1.43	7.95	KEM10	6
AA003881		0.87	7.87	Zfr	7
AA059837		0.95	7.84	KEM12	8
AA000461	Mm.3453	0.47	7.77	C1qg/C1q C-chain	9
AA139452		1.16	7.46	KEM15	10
AA020470		0.74	7.40	KEM16	11
AA050212	Mm.23145	0.80	7.20	KEM17	12
W77330		0.75	7.11	KEM18	13
AA038182	Mm.29831	0.62	7.07	KEM19	14
AA111560		0.69	7.05	KEM20	15
AA002751		0.75	6.97	KEM21	16
AA002955		0.80	6.87	KEM22	17
AA047985		0.92	6.83	KEM23	18
AA139223	Mm.119713	0.89	6.78	KEM24	19
AA183727	Mm.190140	1.12	6.78	KEM25	20
AA002396	Mm.138561	0.81	6.53	KEM27	21
W18362		0.74	6.47	KEM29	22
AA036499		0.47	6.39	KEM30	23
AA116465		0.46	6.38	KEM31	24
W89701		0.80	6.37	KEM32	25
W54421		0.83	6.29	Thy28/thymocyte protein mThy28	26
W58982	Mm.117055	1.03	6.29	KEM33	27
AA003898		0.86	6.22	Thrap5	28
AA123007		1.19	6.22	Oasl2	29
AA002904		0.72	6.20	KEM39	30
AA049152	Mm.29577	0.75	6.20	Brp16/brain protein 16	31
AA023914		0.74	6.17	KEM40	32
AA020272	Mm.23637	0.91	6.13	KEM41	33
AA125257		1.05	6.13	KEM42	34
AA030122	Mm.180733	0.75	6.08	KEM43	35
AA064307		1.26	5.96	Cd34	36
AA051556	Mm.2924	0.81	5.91	Pdgfra	37
AA108832		0.95	5.79	Akap8	38
AA097228	Mm.139277	1.00	5.78	KEM47	39
W84046		0.75	5.77	KEM48	40
AA000856	Mm.3317	1.11	5.77	Gus	41
AA051649		0.81	5.74	KEM50	42
AA108457		0.50	5.73	Cyp20a1	43
AA035895	Mm.154671	0.76	5.73	KEM51	44
AA011778		0.79	5.69	Pip3ap	45
AA060865	Mm.23331	0.92	5.66	KEM54	46
W98666		0.98	5.64	KEM55	47
AA034788		1.14	5.63	KEM56	48
W34612	Mm.18843	1.38	5.63	Tgm2/Transglutaminase 2	49
W71365		0.78	5.61	KEM59	50

Selected genes that are highly expressed in kidney and not in lung EC. Selected lists of genes with a mean ratio greater than 3 in one organ and smaller than 1.5 in the other are shown.

Table 6
Quantitative PCR for selected up-regulated genes

Gene	Array study (EC/non-EC)		Q-PCR							
	Lung	Kidney	EC	Non-EC	Lung ratio	EC	Non-EC	Kidney ratio	Lung EC/kidney EC	Kidney EC/lung EC
<i>Both high</i>										
CD31			6998.12	41.70	167.82	1000.00	54.26	18.43		
Multimerin 2	13.73		863.55	24.60	35.10	1000.00	145.03	6.90		
Endoglin	6.51	5.11	8407.08	452.18	18.59	1000.00	695.42	1.44		
VE-cadherin	14.79	3.01	2125.24	198.31	10.72	1000.00	429.98	2.33		
Tek	20.40	11.51	1507.91	72.22	20.88	1000.00	374.13	2.67		
<i>Lung high</i>										
Gata2	12.73	0.11	10855.58	136.14	79.74	1000.00	5667.03	0.18	10.86	0.09
Ephrin-B1	4.61	0.49	20035.29	696.15	28.78	1000.00	5206.90	0.12	20.04	0.05
Siat10	6.59	0.33	4921.42	286.08	17.20	1000.00	1563.04	0.64	4.92	0.20
H2-Kb	4.32	0.66	58561.13	3430.92	17.07	1000.00	8668.33	0.12	58.56	0.02
<i>Kidney high</i>										
KEM3	1.08	9.27	421.11	345.56	0.82	1000.00	228.48	4.38	0.42	2.37
KEM20	0.69	7.05	311.63	179.61	1.74	1000.00	110.52	9.05	0.31	3.21
KEM39	0.72	6.20	463.95	358.30	1.29	1000.00	165.65	6.04	0.46	2.16

The expression of selected genes from among the pan-endothelial and organ-specific genes identified here was measured by Q-PCR with cyclophilin as a reference. The cDNAs were synthesized from aRNA and used for microarray analysis as described in the Materials and methods section. Gene expression was measured as the ratio over cyclophilin expression at two concentrations. The values are an average of two measurements. An arbitrary value of 1000 was used for kidney EC and relative numbers were calculated for lung EC, lung non-EC, and kidney non-EC. Lung EC/non-EC ratio and kidney EC/lung EC were calculated to show the relative expression of the genes in different cell types.

We also analyzed ephrin-B1 as a candidate for a lung-selective gene. In situ hybridization results showed ephrin-B1 in lung EC, but not in kidney, heart, or liver EC (Fig. 5). Thus, this mRNA may be a selective marker for lung EC.

4. Discussion

We have used a sensitive cDNA microarray method to identify genes that are selectively up-regulated in lung or kidney EC. Some of these genes are well documented in the literature as endothelial genes, but for the first time in this study, others have been localized to the endothelia and yet another group is selectively expressed in either lung or kidney EC.

To focus our study on EC gene expression as it exists in tissues, we used cells directly after isolation from the tissue. To be able to representatively analyze mRNA levels from small numbers of EC, we adapted the two-run in vitro transcription amplification method that linearly amplifies mRNA (Luo et al., 1999). The increased sensitivity of the procedure (Polacek et al., 2003) allowed us to detect low abundance transcripts in EC such as the mRNAs of the transcription factors Ets2 and Gata2. Because the EC were analyzed immediately after purification, our results are likely to reflect gene expression in vivo. The fact that we were able to successfully detect the expression of selected genes by in situ hybridization in various organs supports this notion. However, we cannot

rule out the possibility that some changes could have occurred during the cell isolation, but further changes potentially introduced in cell culture are avoided. Our search for genes that are selectively expressed in EC identified a number of genes whose protein products are known to be important for the growth, differentiation, and survival of EC. This success lends credence to the validity of the endothelial genes described here for the first time.

While this paper was being prepared, Favre et al. (2003) reported on gene expression in lung endothelia. There is a substantial overlap between their set of lung endothelial genes and ours. Among the genes found by both groups to be up-regulated in lung EC are: Rgs12, Gata2, Tie1, Tie2, Ephrin B1, CD97, Notch1, Notch4, Sdf1, Alk1, Snrk, VEGF-R1, Frizzled-4, Ece1, connexin 37(Gja4), VE-Cadherin, Esam, Palmd, Ramp2, Hey1, agrin. More than 25% of the previously named genes, which we found to be selectively expressed in lung EC, were also reported by Favre et al. Given they only listed about 50% of the named EC genes, we estimate the overlap should be close to 50%. There are also some differences. Examples of genes on our list, but not theirs are: PV1 and apelin. The reverse was true of Fmo1, Acpl1, and Plek2. The differences are mostly explained by technical factors. First, the two studies used different arrays, which comprise different sets of genes. In this regard, the two studies complement one another. Second, the methods used by the two groups differed in many details, and different criteria were used to define the significance of the expression differences observed. How-

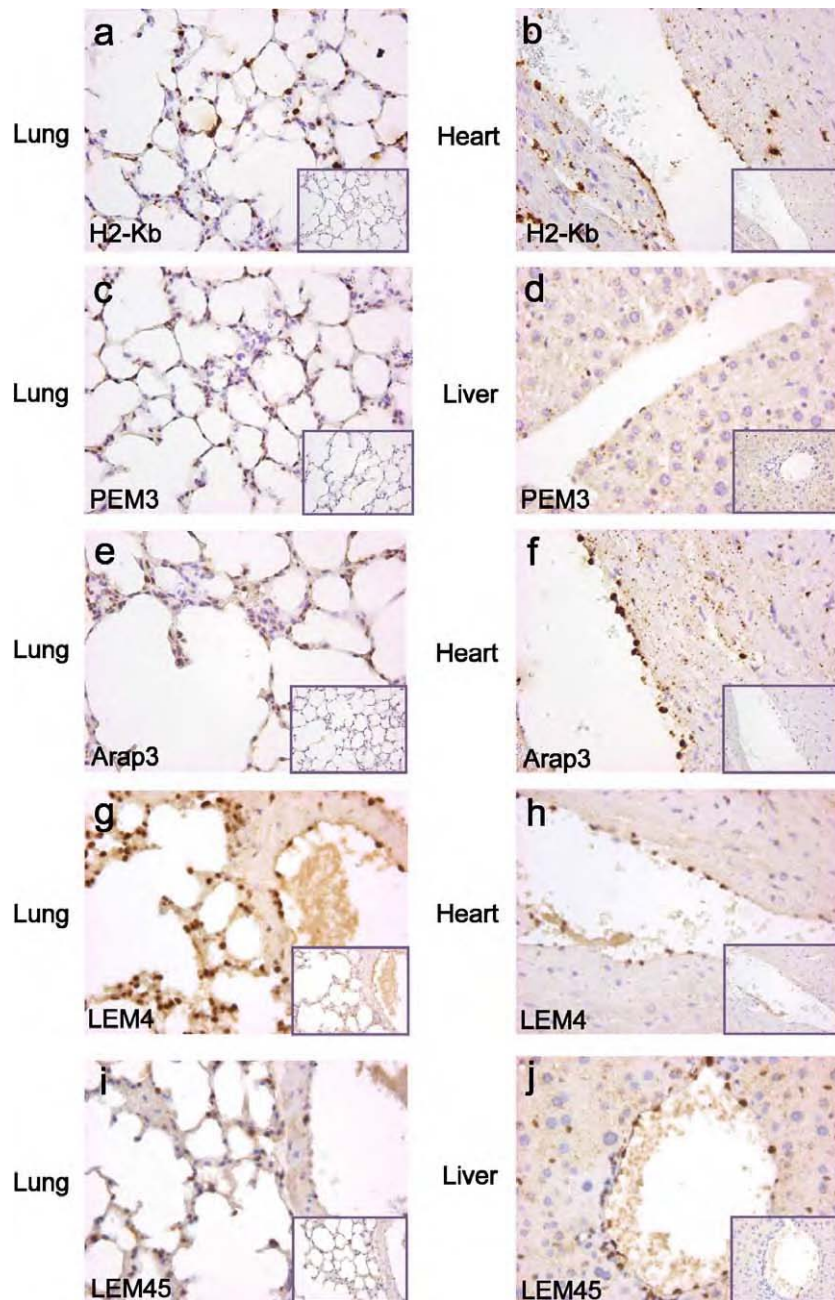


Fig. 3. Gene expression patterns revealed by in situ hybridization. The expression of H2-Kb (a), PEM3 (c), Arap3 (e), LEM4 (g), and LEM45 (i) in lung was detected by in situ hybridization. Each gene has an EC expression pattern that agrees with the microarray results. H2-Kb (b), Arap3 (f), and LEM4 (h) were also expressed in the endocardium of the heart. PEM3 (d) and LEM45 (j) were also expressed in the EC of hepatic veins in liver. The inset of each figure shows the respective in situ hybridization result of sense probe controls (magnification=400 \times).

ever, the high degree of overlap supports the value of these data sets in establishing the gene expression profile of lung EC. It also indirectly supports the validity of the kidney EC gene data we present.

Among the 350 or so genes identified here, based on selective expression by endothelia, were about 200 genes that had not been previously associated with EC. Many of these genes were up-regulated in EC relative to the parenchymal cells to a greater extent than some well-characterized endothelial genes. For example, PEM3 has an

endothelial expression ratio greater than Tie1 and endoglin. PEM3 encodes a protein around 35 kDa with an unknown function. Our data indicate strong expression of PEM3 in lung, kidney, and liver EC. Arap3 is a phosphatidylinositol 3-kinase (PI3K) effector that regulates both ARF and Rho GTPases. It was originally purified from a leucocyte lysate, but high Arap3 expression in an EC line (porcine aortic endothelial cell) has also been described (Krugmann et al., 2002). Our microarray and in situ hybridization assays show that Arap3 is expressed in EC of at least lung,

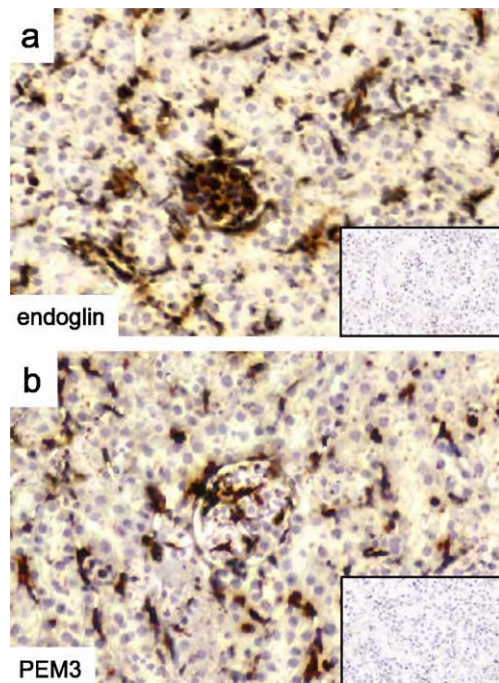


Fig. 4. Endoglin and PEM3 in the kidney. Oligonucleotide probes were used for kidney in situ hybridization. Endoglin (a) expression was detected in intertubular capillaries and the majority of glomerular cells. PEM3 (b) was detected in intertubular capillaries and in a sub-fraction of glomerular cells. The inset of each figure shows the respective in situ hybridization result of sense probe controls (magnification=400 \times).

kidney, and heart. These proteins and a number of ESTs that showed a general endothelial expression pattern await further characterization.

There were extensive differences between the gene expression patterns of the lung and kidney EC. One reason for this may be that different parenchymal cell populations were used for the comparison. However, we have been able to confirm the tissue specificity by Q-PCR for several genes we tested in this manner. We also confirmed EC expression for several additional genes by in situ hybridization. As EC from different tissues have also been shown to be molecularly distinct by other methods (Ruoslahti, 2002), it is likely that our microarray results reflect real tissue specific differences. Indeed, we were able to confirm the tissue specificity by in situ hybridization in the case of ephrin-B1. Thus, the microarray data provide candidates for the tissue-specific EC genes, but because we did not directly compare lung and kidney EC, the tissue-specificity requires confirmation.

The selective expression of ephrin-B1 in lung EC is interesting. The gene for the protein that is functionally related to ephrin-B1, Sdf1, also appeared in the lung EC microarray screening. Ephrin-B1/EphB2 ligand receptor pair inhibits Sdf1-mediated chemoattraction in the nervous system (Lu et al., 2001). The regulatory interaction is dependent on the PSD-95/Dlg/ZO-1 (PDZ) domain-binding motif of ephrin-B1 and the PDZ domain of the PDZ-regulator of G protein signaling (RGS) 3, the latter being a

GAP that functions downstream of Cxcr4, a G-protein coupled receptor for Sdf1. In this microarray study, we also showed Rgs12 to be an up-regulated gene in lung EC. Like PDZ-RGS3, Rgs12 contains both a PDZ and an RGS domain (Snow et al., 1998), and therefore could be regulated downstream of ephrin-B1 in lung EC. Ephrin/Eph signaling also plays a role in the development of the vasculature. During development, ephrin-B2 is expressed in arteries and the corresponding Eph receptor, Eph B4, is expressed in veins, suggesting that ephrin-Eph receptor interactions may guide the linking of the arterial and venous circulation (Wang et al., 1998). In addition, interactions

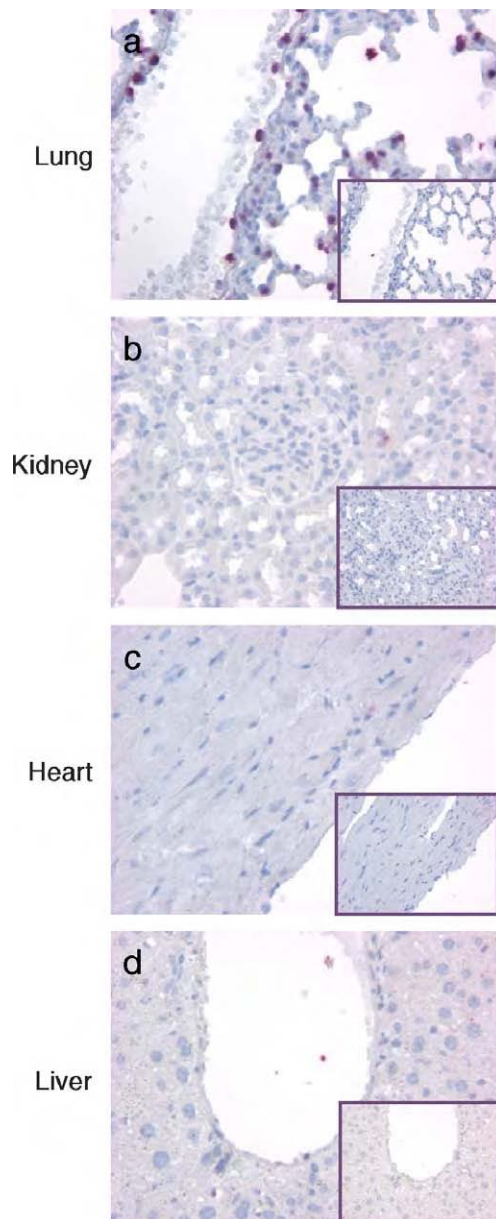


Fig. 5. Ephrin-B1 expression in EC. Ephrin-B1 was only detectable by in situ hybridization in lung EC (a). No expression was detected in kidney (b), heart (c), and liver (d). The inset of each figure shows the respective in situ hybridization result of sense probe controls (magnification=400 \times).

between ephrin and Eph receptor also occur between EC and surrounding mesenchymal cells. Ephrin-B1 is expressed in embryonic arterial and venous EC. Our data suggest that this role may be especially prominent in the adult lung vasculature and that regulating Sdf1 may be one of the ways it serves in this role.

Several of the known endothelial genes identified in our study have been linked to specific diseases. Examples of such genes include endoglin and Acvrl1/ALK1, which are involved in transforming growth factor β signaling. A loss of either one of these genes causes hereditary hemorrhagic telangiectasia syndrome (Rendu-Osler-Weber syndrome; Azuma, 2000). Frizzled homolog 4, one of the Wnt ligands was another disease-associated gene revealed by this study. Defective frizzled homolog 4 is responsible for some familial exudative vitreoretinopathies, which are characterized by a failure of peripheral retinal vascularization (Robitaille et al., 2002). Loss of the von Hippel-Lindau (VHL) gene gives rise to VHL syndrome and Chuvash polycythemia. It seems possible that the uncharacterized ESTs found in our study may also be important in vascular diseases. The lung and kidney EC genes revealed by our study, and extension of similar analyses to other tissues, may help elucidate functional specialization within the vasculature.

Acknowledgments

The authors thank Dr. David J. Loskutoff and Terri Thinnies for help with in situ hybridization, and Tristan Williams for assistance in microarray studies. We thank Dr. William Wasserman for his help at the early stages of the work. This work was supported by grants PO1 CA 82713 and Cancer Center Support Grant CA 30199 from the NCI; and DAMD17-02-1-0315 from the DOD. JTP was supported by DAMD17-99-1-9512, a fellowship from the DOD.

Appendix A. Supplemental material

Supplementary data associated with this article can be found, in the online version, at [10.1016/j.gene.2004.12.034](https://doi.org/10.1016/j.gene.2004.12.034).

References

- Azuma, H., 2000. Genetic and molecular pathogenesis of hereditary hemorrhagic telangiectasia. *J. Med. Investig.* 47, 81–90.
- Breier, G., et al., 1996. Molecular cloning and expression of murine vascular endothelial-cadherin in early stage development of cardiovascular system. *Blood* 87, 630–641.
- Brown, D., Ruoslahti, E., 2004. Metadherin, a novel cell-surface protein in breast tumors that mediates lung metastasis. *Cancer Cell* 5, 365–374.
- Cowan, P.J., et al., 1998. The human ICAM-2 promoter is endothelial cell-specific in vitro and in vivo and contains critical Sp1 and GATA binding sites. *J. Biol. Chem.* 273, 11737–11744.
- de Agostini, A.I., Watkins, S.C., Slayter, H.S., Youssoufian, H., Rosenberg, R.D., 1990. Localization of anticoagulant active heparan sulfate proteoglycans in vascular endothelium: antithrombin binding on cultured endothelial cells and perfused rat aorta. *J. Cell Biol.* 111, 1293–1304.
- Dekker, R.J., et al., 2002. Prolonged fluid shear stress induces a distinct set of endothelial cell genes, most specifically lung Kruppel-like factor (KLF2). *Blood* 100, 1689–1698.
- Dumont, D.J., Yamaguchi, T.P., Conlon, R.A., Rossant, J., Breitman, M.L., 1992. tek, a novel tyrosine kinase gene located on mouse chromosome 4, is expressed in endothelial cells and their presumptive precursors. *Oncogene* 7, 1471–1480.
- Favre, C.J., Mancuso, M., Maas, K., McLean, J.W., Baluk, P., McDonald, D.M., 2003. Expression of genes involved in vascular development and angiogenesis in endothelial cells of adult lung. *Am. J. Physiol. Heart Circ. Physiol.* 285, H1917–H1938.
- Galang, C.K., Muller, W.J., Foos, G., Oshima, R.G., Hauser, C.A., 2004. Changes in the expression of many ets family transcription factors and of potential target genes in normal mammary tissue and tumors. *J. Biol. Chem.* 279, 11281–11292.
- Gougos, A., Letarte, M., 1990. Primary structure of endoglin, an RGD-containing glycoprotein of human endothelial cells. *J. Biol. Chem.* 265, 8361–8364.
- Hayward, C.P., Hassell, J.A., Denomme, G.A., Rachubinski, R.A., Brown, C., Kelton, J.G., 1995. The cDNA sequence of human endothelial cell multimerin. A unique protein with RGDS, coiled-coil, and epidermal growth factor-like domains and a carboxyl terminus similar to the globular domain of complement C1q and collagens type VIII and X. *J. Biol. Chem.* 270, 18246–18251.
- Hirata, K., et al., 2001. Cloning of an immunoglobulin family adhesion molecule selectively expressed by endothelial cells. *J. Biol. Chem.* 276, 16223–16231.
- Ho, M., et al., 2003. Identification of endothelial cell genes by combined database mining and microarray analysis. *Physiol. Genomics* 13, 249–262.
- Keeton, M., Eguchi, Y., Sawdey, M., Ahn, C., Loskutoff, D.J., 1993. Cellular localization of type 1 plasminogen activator inhibitor messenger RNA and protein in murine renal tissue. *Am. J. Pathol.* 142, 59–70.
- Krugmann, S., et al., 2002. Identification of ARAP3, a novel PI3K effector regulating both Arf and Rho GTPases, by selective capture on phosphoinositide affinity matrices. *Mol. Cell* 9, 95–108.
- Liu, J., Razani, B., Tang, S., Terman, B.I., Ware, J.A., Lisanti, M.P., 1999. Angiogenesis activators and inhibitors differentially regulate caveolin-1 expression and caveolae formation in vascular endothelial cells. Angiogenesis inhibitors block vascular endothelial growth factor-induced down-regulation of caveolin-1. *J. Biol. Chem.* 274, 15781–15785.
- Lu, Q., Sun, E.E., Klein, R.S., Flanagan, J.G., 2001. Ephrin-B reverse signaling is mediated by a novel PDZ-RGS protein and selectively inhibits G protein-coupled chemoattraction. *Cell* 105, 69–79.
- Luo, L., et al., 1999. Gene expression profiles of laser-captured adjacent neuronal subtypes. *Nat. Med.* 5, 117–122.
- Peale Jr., F.V., Gerritsen, M.E., 2001. Gene profiling techniques and their application in angiogenesis and vascular development. *J. Pathol.* 195, 7–19.
- Perkins, K.J., Davies, K.E., 2003. Ets, Ap-1 and GATA factor families regulate the utrophin B promoter: potential regulatory mechanisms for endothelial-specific expression. *FEBS Lett.* 538, 168–172.
- Polacek, D.C., et al., 2003. Fidelity and enhanced sensitivity of differential transcription profiles following linear amplification of nanogram amounts of endothelial mRNA. *Physiol. Genomics* 13, 147–156.
- Reed, K.E., Westphale, E.M., Larson, D.M., Wang, H.Z., Veenstra, R.D., Beyer, E.C., 1993. Molecular cloning and functional expression of human connexin37, an endothelial cell gap junction protein. *J. Clin. Invest.* 91, 997–1004.

- Robitaille, J., et al., 2002. Mutant frizzled-4 disrupts retinal angiogenesis in familial exudative vitreoretinopathy. *Nat. Genet.* 32, 326–330.
- Ruoslahti, E., 2002. Specialization of tumour vasculature. *Nat. Rev., Cancer* 2, 83–90.
- Sato, T.N., Qin, Y., Kozak, C.A., Audus, K.L., 1993. Tie-1 and tie-2 define another class of putative receptor tyrosine kinase genes expressed in early embryonic vascular system. *Proc. Natl. Acad. Sci. U. S. A.* 90, 9355–9358.
- Schlaeger, T.M., et al., 1997. Uniform vascular-endothelial-cell-specific gene expression in both embryonic and adult transgenic mice. *Proc. Natl. Acad. Sci. U. S. A.* 94, 3058–3063.
- Snow, B.E., et al., 1998. GTPase activating specificity of RGS12 and binding specificity of an alternatively spliced PDZ (PSD-95/Dlg/ZO-1) domain. *J. Biol. Chem.* 273, 17749–17755.
- Stan, R.V., Arden, K.C., Palade, G.E., 2001. cDNA and protein sequence, genomic organization, and analysis of cis regulatory elements of mouse and human PLVAP genes. *Genomics* 72, 304–313.
- St Croix, B., et al., 2000. Genes expressed in human tumor endothelium. *Science* 289, 1197–1202.
- Swerlick, R.A., Lee, K.H., Wick, T.M., Lawley, T.J., 1992. Human dermal microvascular endothelial but not human umbilical vein endothelial cells express CD36 in vivo and in vitro. *J. Immunol.* 148, 78–83.
- Villa, N., Walker, L., Lindsell, C.E., Gasson, J., Iruela-Arispe, M.L., Weinmaster, G., 2001. Vascular expression of Notch pathway receptors and ligands is restricted to arterial vessels. *Mech. Dev.* 108, 161–164.
- Wang, H.U., Chen, Z.F., Anderson, D.J., 1998. Molecular distinction and angiogenic interaction between embryonic arteries and veins revealed by ephrin-B2 and its receptor Eph-B4. *Cell* 93, 741–753.
- Zhao, B., Stavchansky, S.A., Bowden, R.A., Bowman, P.D., 2003. Effect of interleukin-1beta and tumor necrosis factor-alpha on gene expression in human endothelial cells. *Am. J. Physiol., Cell Physiol.* 284, C1577–C1583.

Peptides selected for binding to clotted plasma accumulate in tumor stroma and wounds

Jan Pilch*, Darren M. Brown*†, Masanobu Komatsu*, Tero A. H. Järvinen*, Meng Yang[§], David Peters*¶, Robert M. Hoffman^{§||}, and Erkki Ruoslahti*,**

*Burnham Institute for Medical Research, 10901 North Torrey Pines Road, La Jolla, CA 92037; [§]AntiCancer, Inc., 7917 Ostrow Street, San Diego, CA 92111; and ^{||}Department of Surgery, University of California, 200 West Arbor Drive, San Diego, CA 92103-8220

Contributed by Erkki Ruoslahti, December 27, 2005

Screening of a phage library for peptides that bind to clotted plasma in the presence of liquid plasma yielded two cyclic decapeptides, CGLIIQKNEC (CLT1) and CNAGESSKNC (CLT2). When injected intravenously into mice bearing various types of tumors, fluorescein-conjugated CLT peptides accumulated in a fibrillar meshwork in the extracellular compartment of the tumors, but were not detectable in other tissues of the tumor-bearing mice. The tumor homing of both peptides was strongly reduced after coinjection with unlabeled CLT2, indicating that the two peptides recognize the same binding site. The CLT peptide fluorescence colocalized with staining for fibrin(ogen) present in the extravascular compartment of tumors, but not in other tissues. The CLT peptides did not home to tumors grown in fibrinogen-null mice or in mice that lack plasma fibronectin. The CLT peptides also accumulated at the sites of injury in arteries, skeletal muscle, and skin. We conclude that the CLT peptides recognize fibrin–fibronectin complexes formed by clotting of plasma proteins that have leaked into the extravascular space in tumors and other lesions. These peptides may be useful in targeting diagnostic and therapeutic materials into tumors and injured tissues.

fibronectin | imaging | phage display | tumor targeting | fibrin

The connective tissue (stroma) in and around malignancies is a complex and dynamic structure that integrates the tumor into the host tissue by providing a functional matrix for angiogenesis and lymphangiogenesis, for migrating bystander cells, and for invading tumor cells (1). Normal connective tissue and its extracellular matrix create an antiproliferative environment, whereas tumor extracellular matrix promotes cell migration, survival, and proliferation by providing adhesion proteins, proteases, and growth factors critical for these processes (2).

The distinctiveness of tumor extracellular matrix is reflected in its content of specific markers, such as tenascin (3) and oncofetal fibronectin (4). Moreover, high levels of collagen expression (5) and the presence of an alternatively spliced form of fibronectin (6) set the extracellular matrix of tumor blood vessels apart from that of normal vessels. The interstitial spaces of tumors also contain fibrin, presumably as a result of VEGF-induced leakage of plasma proteins into the tumor tissue (7). In a manner similar to wounds, the leaked fibrinogen becomes converted to fibrin by tissue procoagulant factors (8, 9). In the present study, we sought to determine whether the interstitial clotting could be used in tumor targeting.

Our laboratory has successfully used peptide libraries displayed on phage as a tool to identify peptides that selectively home to tumors *in vivo* (10). Homing peptides that are selected by this method have shown promise as carriers of drugs and imaging agents (11, 12). In the present study, we have used the phage methodology to identify peptides that recognize clotted plasma proteins in tumors. We screened a phage library on plasma clots *in vitro* and derived two cyclic decapeptides (CLT1 and CLT2) that specifically home to tumors and wounds *in vivo* and bind to tumor tissue in overlay of tissue sections. Tissue specificity of the peptides appears to be associated with plasma

fibronectin, which becomes bound to fibrin clots. The peptides may be useful in targeting of diagnostic and therapeutic agents into tumors and tissue lesions.

Results

Peptides Selected from Plasma Clot Bind to Tumor Stroma. The phage selection scheme was designed to amplify phage that bind to plasma clots but not to anticoagulated plasma. Three rounds of selection produced a pool with 7-fold increased binding to plasma clots. Additional selection rounds did not increase the binding. Sequencing showed that the phage encoding the peptide insert CGLIIQKNEC (CLT1 peptide) and CNAGESSKNC (CLT2 peptide) were highly enriched among the clot-binding phage. Three of 24 clones sequenced encoded CLT1, and two encoded CLT2; the rest of the clones were only represented once. The CLT phage clones bound to plasma clots with 3- to 4-fold efficiency compared to control phage. They did not significantly bind to clots made out of purified fibrin, or fibronectin immobilized on plastic (results not shown).

To determine whether the CLT peptides would recognize clotted plasma proteins *in vivo*, we synthesized the peptides as fluorescein conjugates and imaged their accumulation in tumors. Mice bearing orthotopic MDA-MB-435 xenograft tumors were intravenously injected with fluorescein-conjugated CLT1 ($n = 6$), CLT2 ($n = 4$), or a control peptide ($n = 4$) with the sequence KAREC. Examination of whole tissues from these mice under blue light 3 h after the peptide injection revealed intense fluorescence in the tumors of the mice injected with CLT1 and CLT2, whereas essentially no fluorescence was detected in tumors from the control peptide-injected mice (Fig. 1). We also detected no fluorescence in healthy organs of the CLT-injected animals.

Upon histological examination, CLT peptide fluorescence in tumors appeared in a network pattern within the tumors (Fig. 1 C and G). Tumor homing of both peptides was strongly reduced after coinjection of fluorescein-conjugated CLT1 or CLT2 in combination with unlabeled CLT2 in 5 fold excess (Fig. 1 D and H). This finding indicates that the CLT1 peptide recognizes the same binding site within the tumor as CLT2. Quantification of these results showed that the intensity of fluorescence in the MDA-MB-435 tumors of mice injected with the CLT peptides was 60–130 times stronger than in mice injected with the KAREC control peptide (Fig. 1M). Also shown in Fig. 1M is that the CLT peptides specifically accumulated in all of the various tumors we tested ($n = 2–8$). A fibrillar pattern similar to the one

Conflict of interest statement: No conflicts declared.

*Present address: Biogen-Idec, 1 Antibody Way, Oceanside, CA 92056.

†Present address: Department of Pathology, University of Alabama at Birmingham, 1670 University Boulevard, V4660, Birmingham, AL 35294-0019.

¶Present address: Burnham Institute for Medical Research at the University of California, Santa Barbara, CA 93106.

**To whom correspondence should be addressed. E-mail: ruoslahti@burnham.org.

© 2006 by The National Academy of Sciences of the USA

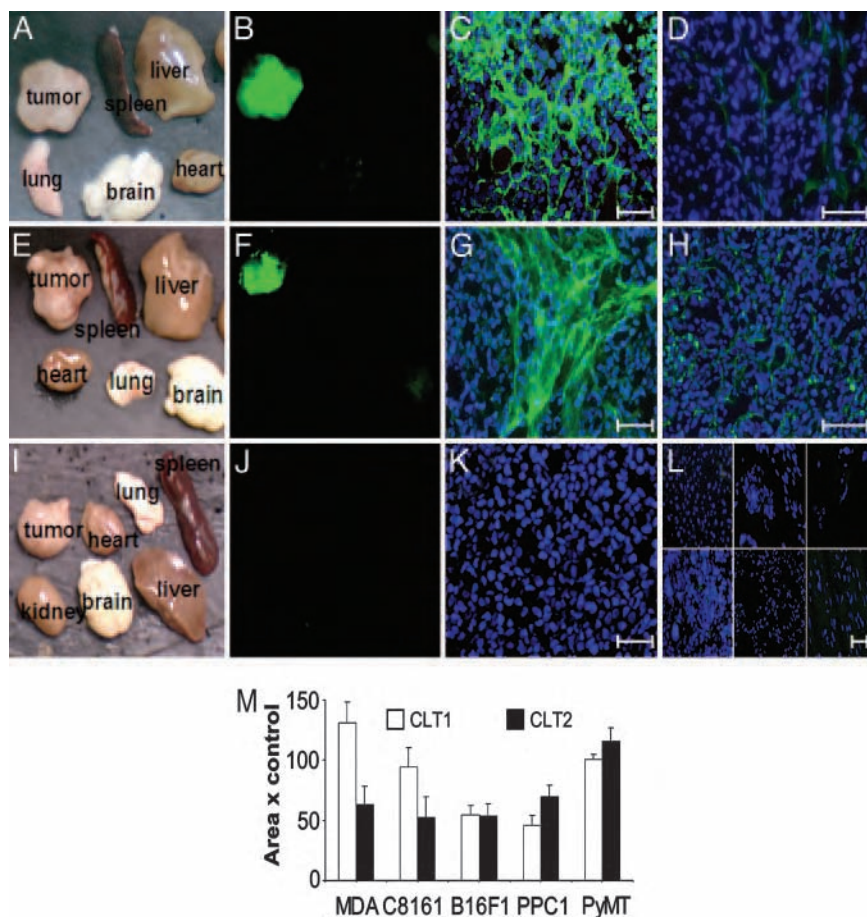


Fig. 1. CLT1 and 2 accumulate in tumor interstitial stroma. Mice bearing orthotopic MDA-MB-435 xenograft tumors were intravenously injected with 500 μ g of fluorescein-conjugated CLT1, CLT2, or control peptide (KAREC). After 3 h, the mice were perfused with PBS. The tumors and various organs were macroscopically examined for fluorescence under blue light. CLT1 (A and B) and CLT2 (E and F) produced strong fluorescence in excised tumor but not in control organs. Histological analysis ($\times 400$) showed that the fluorescein-labeled CLT1 (C) and CLT2 (G) were distributed in a network pattern within the tumor. Fluorescence was strongly reduced when fluorescein-conjugated CLT1 (D) or CLT2 (H) were coinjected with unlabeled CLT2 (5-fold excess). Fluorescein-conjugated control peptide conveyed no fluorescence to the tumors (I–K). Tumor-free tissues of the CLT peptide-injected mice were also negative (L). Representative tissue fluorescence results are shown. Quantification of fluorescence from CLT peptides as fluorescence intensity relative to a control peptide (KAREC) shows that, similar to the MDA-MB-435 tumors (MDA), various other types of tumors specifically bind to intravenously injected CLT peptides (M). Nuclei were stained with DAPI (blue). Error bars show mean \pm SEM. (Scale bars, 50 μ m.)

shown in Fig. 1 C and G was seen in each of these other tumors (data not shown). To study the ability of the CLT peptides to recognize human clinical cancers, we developed a peptide overlay assay. Overlay with the CLT1 peptide produced a fibrillar network in mouse Lewis lung carcinoma similar to that seen in the tumors after i.v. injection of the peptide (Fig. 2A). The binding of the peptide was also inhibited by unlabeled CLT1 peptide (Fig. 2B) but not by a control peptide (Fig. 2C), showing the specificity of the binding. Sections from two clinical breast cancers (Fig. 2D and E) and from PPC1 xenografts were positive in this overlay assay (Fig. 2F).

CLT Peptides Associate with Fibrin and Fibronectin in Tumor Stroma.

Staining of tumor sections with antibodies against fibrin(ogen) produces a fibrillar staining that is not seen in normal tissues (8). Fluorescence from intravenously injected CLT peptide (CLT1; Fig. 3*A*) and fibrin staining (Fig. 3*B*) colocalized (Fig. 3*C*) in tumor sections of MDA-MB-435 breast cancer xenografts. Plasma fibronectin and fibrin are deposited together into plasma clots by Factor XIII activity (13), prompting us to analyze the relationship of CLT peptide fluorescence and fibronectin staining in tumors. The results showed that CLT peptides also codistribute with fibronectin (not shown). We also studied the

distribution of the CLT peptides, fibrin, and fibronectin in MMTV-PyMT transgenic breast tumors. The results (data not shown) were identical to those obtained with the MDA-MB-435 xenografts.

CLT Peptide Tumor Homing Requires Fibrin and Plasma Fibronectin.

We next used knockout mice to study the role of fibrin(ogen) and fibronectin in the homing of the CLT peptides to tumors. Fibrinogen knockout mice are viable (14) and could be used as tumor recipients. Complete absence of fibronectin is lethal, but mice that lack plasma fibronectin can be generated by postnatally deleting the fibronectin gene in the liver (15). The CLT peptides homed to B16F1 tumors grown in wild-type C57BL/6 mice ($n = 10$) producing a fibrillar meshwork (CLT1; Fig. 3D). In contrast, only faint, evenly distributed fluorescence was present in tumors ($n = 4$) grown in the fibrinogen knockout mice (which lack the ability to produce fibrin) (Fig. 3E). B16F1 tumors grown in wild-type littermates of plasma fibronectin-deficient mice also accumulated CLT peptides in a fibrillar matrix (Fig. 3F), but mice lacking plasma fibronectin ($n = 6$) did not (Fig. 3G). Unlike in the fibrinogen knockout mice, there was no residual peptide binding to the tumors in the plasma fibronectin-deficient mice (Fig. 3H). These results show that both fibrin and fibronectin

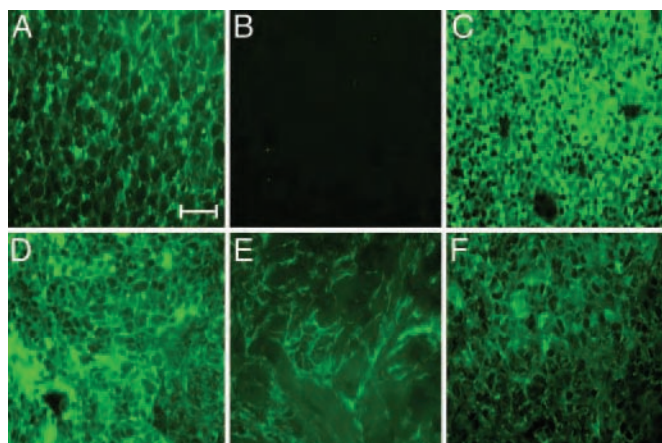


Fig. 2. Peptide overlay assay. CLT peptide binds to clinical human tumors. Frozen sections of mouse Lewis lung carcinoma were incubated with fluorescein-conjugated CLT1 peptide, washed, and analyzed for fluorescence. The fibrillar network produced by the peptide (A) was eliminated by coincubation with unlabeled CLT peptide (B) but not by a control peptide (C). Two human clinical breast cancers (D and E) and a PPC1 xenograft tumor (F) were also recognized by the CLT peptide. (Scale bar, 50 μ m for all panels.)

from plasma are needed for the CLT peptides to highlight a fibrillar matrix in tumors, but that some diffuse binding of the peptide persists in the absence of fibrin.

CLT Binds Sites of Tissue Injury *in Vivo*. Clotting is an important part of wound healing. Therefore, we tested CLT peptide homing to

tissue injuries. Fluorescein-conjugated CLT peptides homed to deendothelialized femoral arteries ($n = 5$), producing strong fluorescence in the vessel wall (Fig. 4A). CLT homing was also seen in crush injuries of the muscle ($n = 3$; Fig. 4D) and in skin wounds resulting from incisions ($n = 4$; Fig. 4E). No CLT peptide homing was observed in intact arteries, muscles, skin (Fig. 4B, F, and G), or other healthy tissues of the mice with the injuries, and a control peptide showed no homing to the injured tissues (data not shown).

Discussion

We report on two cyclic peptides that were isolated by screening phage libraries for peptides that bind to plasma clots. Fluorescein conjugates of these peptides, CLT1 and CLT2, specifically accumulate in tumor tissue after an i.v. injection in multiple cancer models. The peptides also homed to sites of tissue injury. We also show that the injected CLT peptides outline a meshwork that colocalizes with fibrin and fibronectin staining, and that peptides do not home to tumors grown in mice that lack fibrinogen or plasma fibronectin. Our results indicate that the CLT peptides bind to an epitope in a fibrin–fibronectin complex formed as a result of plasma clotting within tumors and at sites of tissue injury.

Our starting point in this work was the expectation that peptides that bind to plasma clots might specifically recognize interstitial clotting products known to be present in tumors (8). This expectation is borne out by our results. *In vitro* phage screening on plasma clots yielded two related peptide sequences, CLT1 and CLT2, that home to tumor stroma, while not being detectable in normal tissues. These peptides also homed to sites

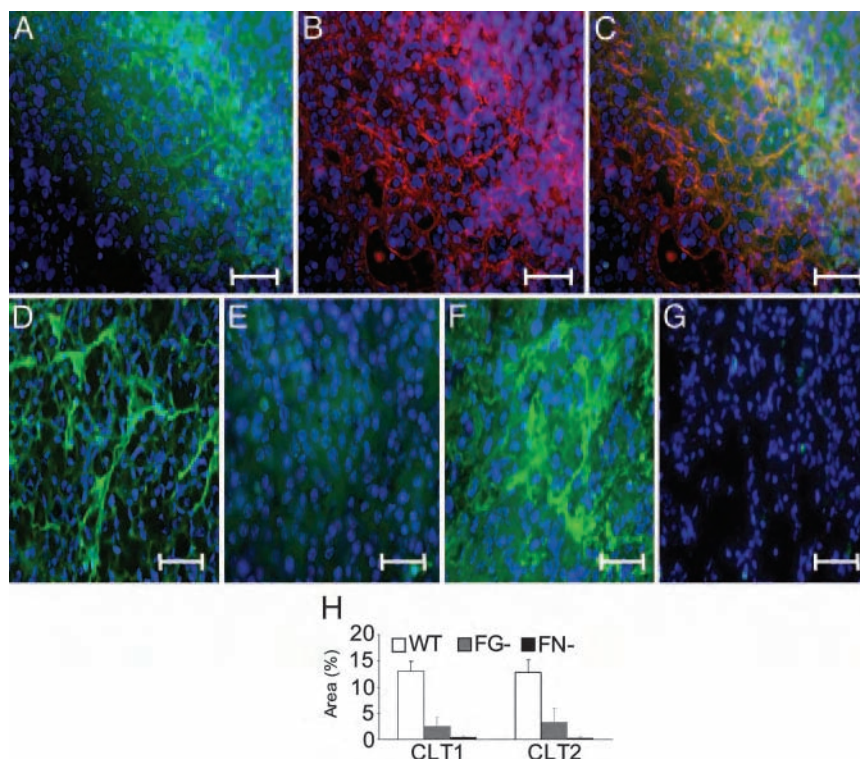


Fig. 3. CLT peptides associate with fibrin and fibronectin in tumor stroma and require a fibrin/fibronectin matrix for tumor homing. Frozen sections of MDA-MB-435 xenograft tumors from mice injected with fluorescein-conjugated CLT1 were stained for fibrin(ogen). The peptide fluorescence (A) and fibrin staining (B) show similar patterns with overlapping distribution (C). Intravenously injected CLT peptides (CLT1 is shown) produce a fluorescent meshwork in B16F1 tumors grown in C57BL/6 mice (D), but not in tumors grown in fibrinogen knockout mice (E). CLT1 also homes to B16F1 tumors in wild-type littermates of plasma fibronectin-deficient C57BL/6-Fn(fl/fl) *Mx-Cre*⁺ mice (F), but tumors of mice deficient in plasma fibronectin were negative (G). The micrographs show representative images; results are quantified and summarized in H. WT, wild-type mice; FG-, fibrinogen knockout mice; FN-, plasma fibronectin-deficient mice. Error bars show mean \pm SEM. (Scale bars, 50 μ m.)

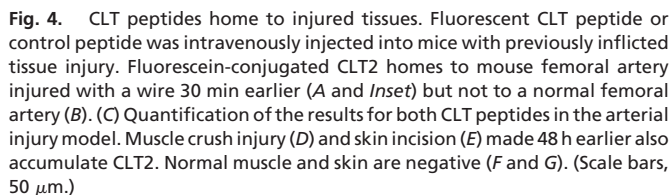


Fig. 4. CLT peptides home to injured tissues. Fluorescent CLT peptide or control peptide was intravenously injected into mice with previously inflicted tissue injury. Fluorescein-conjugated CLT2 homes to mouse femoral artery injured with a wire 30 min earlier (*A* and *Inset*) but not to a normal femoral artery (*B*). (*C*) Quantification of the results for both CLT peptides in the arterial injury model. Muscle crush injury (*D*) and skin incision (*E*) made 48 h earlier also accumulate CLT2. Normal muscle and skin are negative (*F* and *G*). (Scale bars, 50 μm .)

The CLT peptides recognized every tumor we have tested, including five tumor types in mouse and some human tumors. Thus, the CLT peptides may be useful as a general imaging or drug delivery agent for tumors, as well as for tissue injuries. Fibrin-binding peptides and antibodies have been used for imaging, but only in cardiovascular applications (19, 20). Our peptides are likely to be different from these earlier reagents in that the probable target is fibronectin rather than fibrin. Also, we have demonstrated remarkably effective tumor targeting with our CLT peptides.

Animals, Cell Lines, and Tissues. B16F1 mouse melanoma, Lewis lung carcinoma, C8161 human melanoma, MDA-MB-435 human breast cancer, and PPC-1 human prostate cancer cells (American Type Culture Collection) were maintained in RPM medium 1640 or DMEM supplemented with 10% FCS. Human tumor cells (1×10^6) were injected into the mammary fat pad or the flank of nude BALB/c *nu/nu* mice to induce tumors. Mouse mammary tumor virus (MMTV) PyMT mice were provided by Robert Oshima (Burnham Institute for Medical Research). The MMTV PyMT mice develop breast cancer under the influence of a polyoma middle T antigen driven by the mouse tumor virus promoter (21). B16F1 tumors induced by injecting 1×10^6 cells s.c. were grown in the flank of fibrinogen knockout mice (22), and of transgenic plasma fibronectin-deficient C57BL/6-Fn(fl/fl) *Mx-Cre*⁺ (15) and their wild-type littermates. Deletion of the fibronectin gene in the liver was induced by poly(I):poly(C) (15, 23). Frozen human tissues from clinical breast cancers were provided by the Western Division of the National Cancer Institute Cooperative Human Tissue Network (Vanderbilt University Medical Center, Nashville, TN).

The annealed oligonucleotide pairs were ligated to EcoRI/HindIII-digested phage vector according to the T7 Select protocol. The diversity of the peptide library was 5×10^8 primary recombinants.

Phage Screening. Human plasma clots were incubated with the CX8C peptide library at 22°C for 30 min and extensively washed with PBS. Plasma was then added to the clot to remove phage recognizing soluble plasma components. The phage pool that remained bound to the clot was quantified and amplified. The process was repeated until maximum clot binding was reached. The peptide-encoding DNA from 24 randomly picked phage clones in the selected pool was isolated and sequenced.

Imaging, Antibodies, and Immunohistology. Imaging under a blue light and examination of the distribution of fluorescein-conjugated peptides after tail vein injection have been described (24, 25).

The imaging methods are briefly described as follows. A Leica fluorescence stereomicroscope, model LZ12, equipped with a 50-W mercury lamp, was used for high-magnification imaging. Selective excitation of GFP was produced through a D425y60 band-pass filter and 470 DCXR dichroic mirror. Emitted fluorescence was collected through a long-pass filter GG475 (Chroma Technology, Brattleboro, VT) on a Hamamatsu C5810 three-chip cooled color charge-coupled device camera

(Hamamatsu Photonics, Bridgewater, NJ). Images were processed for contrast and brightness and analyzed with the use of IMAGE PRO PLUS 3.1 software (Media Cybernetics, Silver Springs, MD). Images of $1,024 \times 724$ pixels were captured directly on an IBM PC or continuously through video output on a high-resolution Sony VCR model SLV-R1000 (Sony). Imaging at lower magnification that visualized the entire animal was carried out in a light box illuminated by blue light fiber optics (Lighttools Research, Encinitas, CA) and imaged by using the thermoelectrically cooled color charge-coupled device camera as described above (26).

The mice were perfused through the heart 3 h after the peptide injection, and tissues were removed for examination. For fibrin and fibronectin immunostaining, tissues were fixed with 4% paraformaldehyde and stained with biotinylated mouse fibrin(ogen) antiserum (Nordic) or a polyclonal anti-mouse fibronectin antibody (Chemicon), followed by streptavidin Alexa Fluor 594 or anti-rabbit Alexa Fluor 594 (Molecular Probes), respectively. For peptide overlay, sections of frozen OCT-embedded tissue were incubated with 10 $\mu\text{g}/\text{ml}$ fluorescein-conjugated peptide for 30 min at room temperature. Tissue fluorescence was quantified by using IMAGE PRO PLUS software. At least two images from representative microscopic fields were analyzed

from each tissue sample, and data from individual mice that received the same treatment ($n = 2-8$) were pooled.

Wound Assays. The wire injury of the mouse femoral artery was induced as described (27). Thirty minutes after the wire injury, 250 μg of fluorescein-conjugated peptides were injected i.v. Muscle injuries were induced in mice by applying a crush injury to the quadriceps muscle, and 500 μg of fluorescein-conjugated peptides was injected i.v. 48 h later. Skin incisions were studied similarly. The mice were perfused through the heart 4 h after the peptide injection, and tissues were excised, fixed in 4% paraformaldehyde, and embedded in OCT.

We thank Drs. Reinhard Faessler (Max Planck Institute for Biochemistry, Martinsreid, Germany) and Jay Degen (Cincinnati Children's Hospital Medical Center, Cincinnati) for knockout mice, Drs. Lianglin Zhang (Burnham Institute for Medical Research) and Lionel Hebbard (Burnham Institute for Medical Research) for providing frozen tumor tissues, Dr. Fernando Ferrer for peptide synthesis, Robbin Newlin for help with histology, and Paul Kirsch for editing. This work was supported by Department of Defense Grant DAMD 17-02-1-0315 and National Cancer Institute Contract N01-CO-37007 from the National Cancer Institute. This work was supported at AntiCancer by National Institutes of Health Grants CA099258 and CA103563.

1. Bissell, M. J. & Radisky, D. (2001) *Nat. Rev. Cancer* **1**, 46–54.
2. Kalluri, R. (2003) *Nat. Rev. Cancer* **3**, 422–433.
3. Ventimiglia, J. B., Wikstrand, C. J., Ostrowski, L. E., Bourdon, M. A., Lightner, V. A. & Bigner, D. D. (1992) *J. Neuroimmunol.* **36**, 41–55.
4. Neri, D., Carnemolla, B., Nissim, A., Leprini, A., Querze, G., Balza, E., Pini, A., Tarli, L., Halin, C., Neri, P., *et al.* (1997) *Nat. Biotechnol.* **15**, 1271–1275.
5. St. Croix, B., Rago, C., Velculescu, V., Traverso, G., Romans, K. E., Montgomery, E., Lal, A., Riggins, G. J., Lengauer, C., Vogelstein, B., *et al.* (2000) *Science* **289**, 1197–1202.
6. Halin, C., Rondini, S., Nilsson, F., Berndt, A., Kosmehl, H., Zardi, L. & Neri, D. (2002) *Nat. Biotechnol.* **20**, 264–269.
7. Senger, D. R., Galli, S. J., Dvorak, A. M., Perruzzi, C. A., Harvey, V. S. & Dvorak, H. F. (1983) *Science* **219**, 983–985.
8. Dvorak, H. F., Senger, D. R., Dvorak, A. M., Harvey, V. S. & McDonagh, J. (1985) *Science* **227**, 1059–1061.
9. Abe, K., Shoji, M., Chen, J., Bierhaus, A., Danave, I., Micko, C., Casper, K., Dillehay, D. L., Nawroth, P. P. & Rickles, F. R. (1999) *Proc. Natl. Acad. Sci. USA* **96**, 8663–8668.
10. Ruoslahti, E. (2002) *Nat. Rev. Cancer* **2**, 83–90.
11. Ellerby, H. M., Wadih, A., Ellerby, L. M., Kane, R., Andrusiak, R., Del Rio, G., Krajewski, S., Lombardo, C. R., Rao, R., Ruoslahti, E., *et al.* (1999) *Nat. Med.* **5**, 1032–1038.
12. Åkerman, M. E., Warren, C. W., Chan, W. C. W., Laakkonen, P., Bhatia, S. N. & Ruoslahti, E. (2002) *Proc. Natl. Acad. Sci. USA* **99**, 12617–12621.
13. Mosher, D. F. (1975) *J. Biol. Chem.* **250**, 6614–6621.
14. Palumbo, J. S., Kombrinck, K. W., Drew, A. F., Grimes, T. S., Kiser, J. H., Degen, J. L. & Bugge, T. H. (2000) *Blood* **96**, 3302–3309.
15. Sakai, T., Johnson, K. J., Murozono, M., Sakai, K., Magnuson, M. A., Wieloch, T., Cronberg, T., Isshiki, A., Erickson, H. P. & Faessler, R. (2001) *Nat. Med.* **7**, 324–330.
16. Ten Cate, H., Bauer, K. A., Levi, M., Edgington, T. S., Sublett, R. D., Barzegar, S., Kass, B. L. & Rosenberg, R. D. (1993) *J. Clin. Invest.* **92**, 1207–1212.
17. Morla, A. & Ruoslahti, E. (1992) *J. Cell. Biol.* **118**, 421–429.
18. Baneyx, G., Baugh, L. & Vogel, V. (2001) *Proc. Natl. Acad. Sci. USA* **98**, 14464–14468.
19. Flacke, S., Fischer, S., Scott, M. J., Fuhrhop, R. J., Allen, J. S., McLean, M., Winter, P., Sicard, G. A., Gaffney, P. J., Wickline, S. A., *et al.* (2001) *Circulation* **104**, 1280–1285.
20. Jaffer, F. A., Tung, C. H., Wykrzykowska, J. J., Ho, N. H., Houg, A. K., Reed, G. L. & Weissleder, R. (2004) *Circulation* **110**, 170–176.
21. Siegel, P. M., Ryan, E. D., Cardiff, R. D., Muller, W. J. (1999) *EMBO J.* **18**, 2149–2164.
22. Suh, T. T., Holmback, K., Jensen, N. J., Daugherty, C. C., Small, K., Simon, D. I., Potter, S. & Degen, J. L. (1995) *Genes Dev.* **9**, 2020–2033.
23. Yi, M., Sakai, T., Faessler, R. & Ruoslahti, E. (2003) *Proc. Natl. Acad. Sci. USA* **100**, 11435–11438.
24. Hoffman, R. M. (2005) *Nat. Rev. Cancer* **5**, 796–806.
25. Laakkonen, P., Åkerman, M. E., Biliran, H., Yang, M., Ferrer, F., Karpanen, T., Hoffman, R. M. & Ruoslahti, E. (2004) *Proc. Natl. Acad. Sci. USA* **101**, 9381–9386.
26. Yang, M., Baranov, E., Jiang, P., Sun, F.-X., Li, X.-M., Li, L., Hasegawa, S., Bouvet, M., Al-Tuwaijri, M., Chishima, T., *et al.* (2000) *Proc. Natl. Acad. Sci. USA* **97**, 1206–1211.
27. Komatsu, M. & Ruoslahti, E. (2005) *Nat. Med.* **11**, 1346–1350.

Drug targeting to specific vascular sites

Erkki Ruoslahti

The blood vessels of individual tissues are biochemically distinct, and pathological lesions put their own signature on the vasculature. In tumors, both blood and lymphatic vessels differ from normal vessels. New methods, such as *in vivo* screening of phage libraries, have provided peptides and antibodies that recognize these vascular signatures and can be used in targeted delivery of therapeutic agents. Targeting a therapy to the diseased tissue enhances the efficacy of the treatment while reducing the side effects in mouse experiments. Results from drug delivery to tumor vessels have been particularly encouraging.

Erkki Ruoslahti

The Burnham Institute
Cancer Research Center

10901 North Torrey Pines Road

La Jolla, CA 92037, USA

tel: +1 858 646 3125

fax: +1 858 646 3198

e-mail:

ruoslahti@burnham.org

▼ The vasculature of individual tissues expresses molecules that are specific to a particular tissue or tissue type. A well-known example is the blood vessels of lymphoid tissues, in which the high endothelium expresses unique adhesion molecules for lymphocyte homing. Many, perhaps all, other tissues are now also known to put a 'signature' on their vasculature [1].

Pathological tissue processes can also put their own signature on the vasculature. Inflammation and malignancy are known to do this. Tumor vasculature continuously undergoes angiogenesis to provide the blood supply that feeds the growing tumor [2]. The activated endothelial cells and pericytes in this neovasculature express molecules that are characteristic of angiogenic vessels (not expressed or expressed at much lower levels in normal vessels). Moreover, tumor lymphatics can also express their own marker. The heterogeneity in the vasculature might provide new opportunities for targeted delivery of therapies. This review discusses these developments.

Molecular markers in blood vessels and lymphatics

Blood vessel specialization in normal tissues. Recently, an unexpected complexity of tissue-specific molecular individuality in vascular beds was uncovered. Monoclonal antibodies (MAbs) and a new technique using *in vivo*

screening of peptide and antibody libraries expressed on the surface of phage or bacteria, have been particularly informative in this regard (reviewed in Ref. [1]). Intravenous injection of mice with peptide libraries displayed on phage, followed by isolation of phage from individual tissues has yielded tissue-specific vascular homing peptides for each normal tissue and organ our laboratory has chosen for targeting so far. Preparation of MAbs against specific membrane fractions from endothelia has yielded additional tissue-specific blood vessel markers [3,4].

Special features of blood vessels in pathological tissues. Tumor blood vessels express specific markers that are not present in the blood vessels of normal tissues. Such marker molecules can be present in the endothelial cells, the pericytes or the extracellular matrix (ECM) of tumor blood vessels. Many of the marker molecules that are selectively expressed in tumor blood vessels are proteins associated with tumor-induced angiogenesis, the sprouting of new blood vessels [5]. These proteins are often functionally important in the angiogenesis process; agents that perturb their function suppress angiogenesis. Tumor blood vessels are prime targets for inhibiting tumor growth. Because these vessels are distinct from normal resting blood vessels, they can be selectively destroyed without significantly affecting normal vessels. Inflammatory lesions such as arthritic synovium are also angiogenic and can be targeted with phage-displayed peptides [6]. Atherosclerotic plaques is another lesion in which specific molecular markers are detectable with *in vivo* peptide library screening [7].

Endothelial marker molecules. The molecular nature of vascular changes that give rise to the individuality of the vessels in various tissues and pathological lesions is partially understood. Several proteases have been identified as markers of the vasculature in individual normal tissues (Table 1). Thus, two peptidases

(dipeptidyl peptidase IV [8] and membrane dipeptidase [1]) and a chloride channel are selectively expressed in lung vessels [4]. Another peptidase, aminopeptidase P, is a marker for breast gland vasculature [9].

The molecular markers of angiogenesis include additional peptidases or proteases and integrins. Aminopeptidase N is a marker of angiogenic vessels. It is a membrane-spanning 140-KDa cell surface protein that has previously been linked to cell migration and tumor invasion, but is a new marker of angiogenic endothelium. Antibodies against aminopeptidase N and enzymatic inhibitors of this enzyme block angiogenesis [10].

The cell adhesion receptors, integrins $\alpha v\beta 3$, $\alpha v\beta 5$ and $\alpha 5\beta 1$ are over-expressed in tumor vasculature [11,12]. Indeed, one of the peptides identified by *in vivo* screening of phage libraries for tumor homing recognizes $\alpha v\beta 3$ and $\alpha v\beta 5$ [Table 1; 13]. Antibodies and peptides specific for these integrins have been used as receptors for targeted delivery of anti-cancer and anti-angiogenic agents (see below).

Serial analysis of gene expression has been used to survey differences in mRNA expression between endothelial cells from human colon cancers and from adjacent normal tissue [14]. Certain ECM proteins, particularly collagens, were found to be expressed at 10- to 30-fold higher levels in tumor endothelial cells than those from the normal tissue. Some matrix metalloprotease mRNAs were also over-expressed in tumor vasculature. Yet another set of differences included 'new' tumor-specific molecules, related only to expressed sequence tags in the databases. Some of these tumor endothelial markers (TEMs) had apparent transmembrane domains, which suggests that the proteins are expressed on the cell surface. One of the TEMs is endosialin, independently shown by another group to be a marker of angiogenic blood vessels [15].

Genetic programs initiated by angiogenic growth factors produced by tumor tissue (and other tissues that require neovascularization) are likely to be responsible for the production of the angiogenesis-related markers in tumor vasculature. Upregulation of tissue factor (TF) expression in tumor endothelial cells is also likely to occur under the influence of the tumor tissue, as TF is not expressed on endothelial cells of normal vessels [16]. TF binds factor VII to initiate blood clotting, and its expression by tumor endothelia is thought to contribute to the increased incidence of thrombosis seen in cancer patients. Further analyses of tumor vessels are likely to uncover markers that are specific for individual tumor types.

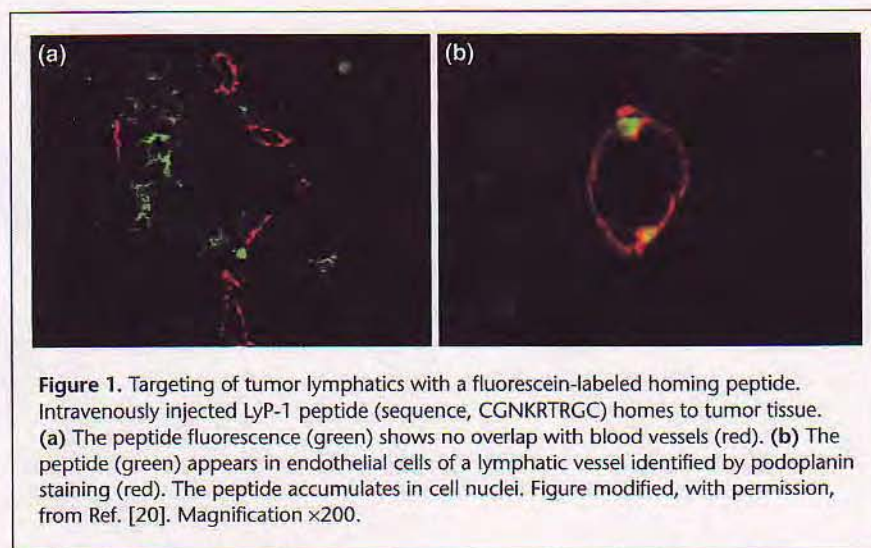
Markers in pericytes and ECM. Molecular markers of angiogenesis are not limited to the endothelium. The supporting mural cells (pericytes and smooth muscle cells)

and the ECM also carry distinct markers. NG2 proteoglycan, also known as melanoma-associated chondroitin sulfate proteoglycan, is one such marker. NG2 is a membrane-spanning cell surface protein that is expressed in the neovasculature of tumors, regenerating tissues and in fetal vessels [17]. NG2 expression is limited to pericytes; endothelial cells do not express detectable levels of NG2.

The ECM of blood vessels consists of a sub-endothelial basement membrane and the matrix surrounding the mural cells. The expression of one matrix component, an alternatively spliced form of fibronectin containing an additional type III domain, ED-B, is restricted to tumor vessels and vessels of non-malignant tissues undergoing angiogenesis [18]. Fibronectin promotes cell adhesion, migration, growth and survival; the specific function of its ED-B isoform is not known.

Lymphatics in tumors. The presence and importance of blood vessels in tumors is well-established, but it has only recently been found that lymphatic vessels can also be present within tumors. The abundance of lymphatic vessels in and around a tumor correlates with the propensity of that tumor to metastasize [19]. We have recently reported evidence indicating that lymphatic vessels in tumors can also be specialized. A nonapeptide, LyP-1, isolated by combining phage display *ex vivo* and *in vivo*, directs the homing of the phage to vessel-like structures in certain tumors [20]. These structures are not blood vessels because they stain negative for blood vessel markers. Instead, they stain for various markers of lymphatic vessels. LyP-1 recognizes these apparent lymphatic vessels in most, but not all, tumors. Fluorescein-labeled LyP-1 peptide also homes to tumors after an intravenous injection. The fluorescence appears in tumor lymphatics and accumulates in the nuclei of the lymphatic endothelial cells (Fig. 1). Fluorescent LyP-1 is not detected in normal tissues, indicating that this peptide distinguishes lymphatics in tumors from normal lymphatics of the same animal. In addition to the lymphatic endothelial cells, LyP-1 also binds to the tumor cells, accumulating in their nuclei. Thus, this peptide can selectively transport its payload (fluorescein) all the way from the systemic circulation to the nuclei of the target cells.

Tumor cells can cover a substantial fraction of the luminal surface of tumor blood vessels [21]. These tumor cells might be in the process of transmigrating through the blood vessel wall, rather than being a structural component of the vessel. Tumor cells might also form ECM-lined channels that have been proposed to function as an auxiliary vasculature in highly malignant tumors [22]. These findings suggest that peptides or antibodies that bind to tumor cells, rather than to the conventional vascular cells, might also be capable of targeting tumor vasculature.



Origin of vascular specialization. One can tentatively make two generalizations regarding tissue- and tumor-specific markers of vessels: these markers are likely to be functionally important to the tumor vessels and many of them represent special forms of otherwise common proteins. Integrins illustrate the first point. The $\alpha v\beta 3$, $\alpha v\beta 5$ and $\alpha 5\beta 1$ integrins are each upregulated in angiogenic vessels and play a role in angiogenesis [11,12]. In the fetus, $\alpha 5\beta 1$ is necessary for the development of the vasculature [23], whereas fetal or adult angiogenesis can take place without the αv integrins [24,25]. However, $\alpha v\beta 3$ and $\alpha v\beta 5$ are somehow important in adult angiogenesis because peptides and antibodies that perturb their function block angiogenesis [5,11]. Aminopeptidase N is another angiogenesis marker, which appears to be needed for angiogenesis to proceed [10].

The $\alpha v\beta 3$ and $\alpha v\beta 5$ integrins are essentially absent from the normal tissues of an adult animal and are selectively upregulated in angiogenesis. In contrast, aminopeptidase N is expressed in several epithelial tissues and in macrophages. Two factors might account for the homing specificity of the aminopeptidase N-binding peptides: (1) angiogenic vessels are the only vessels that express aminopeptidase N and (2) these vessels seem to express a specific form of this peptidase, as peptides that bind to aminopeptidase N in tumor vessels do not bind to macrophages [26]. In a similar vein, an antibody that recognizes a splice variant of fibronectin selectively recognizes the ECM of angiogenic blood vessels [18]. A peptide that homes to the vessels in normal breast tissue might similarly recognize a subset of aminopeptidase P molecules [9].

Delivery of therapeutic agents to vascular targets

Drug delivery. Peptides, peptidomimetics and antibodies that home to a specific site in the vasculature are attractive

as carriers of therapeutic and diagnostic agents. Specific drug delivery should concentrate the drug at the targeted site, increasing efficacy and also decreasing side effects in other tissues. Targeted delivery is particularly attractive in cancer therapy. The chemotherapeutic drugs currently used to treat cancer are highly toxic, which places a limit on the dose a patient can tolerate. Targeted delivery of high drug-concentrations to tumor tissue might alleviate this problem because normal tissue would be less affected. Moreover, targeting therapeutic agents to the vasculature of tumors, as opposed to the tumor cells themselves, might offer

some additional advantages. Tumors are critically dependent on a blood supply; eliminating that supply can profoundly suppress tumor growth [2]. Blood vessels are more readily accessible to intravenously administered therapy than tumor cells. Furthermore, although tumor blood vessels acquire a tumor-associated 'signature', they are composed of normal cells that do not readily acquire mutations leading to drug resistance [27]. Moreover, when a targeted anti-angiogenic agent is also active against the tumor cells, additional gains in efficiency can be expected.

Proof for the vasculature-targeted delivery principle has been obtained in studies with experimental tumors. Researchers have designed compounds that can specifically deliver anti-tumor drugs to tumor vasculature. In one approach, investigators used vascular endothelial growth factor (VEGF) to target diphtheria toxin to VEGF receptors expressed by the tumor endothelial cells [28]. We have used homing peptides to construct drugs that bind to tumor vasculature. The RGD-4C peptide specifically binds to the $\alpha v\beta 3$ and $\alpha v\beta 5$ integrins [29], and the CNGRC peptide binds to aminopeptidase N [10]. Coupling of doxorubicin to the RGD-4C and CNGRC targeting peptides yielded compounds that were more effective and less toxic than doxorubicin alone [13]. Doxorubicin, like several other cytotoxic chemotherapeutics, inhibits angiogenesis in addition to being toxic to tumor cells [30]. The vascular targeting approach is likely to enhance these anti-angiogenic effects. The targeting of doxorubicin using the RGD-4C and CNGRC peptides reduced the side effects of the treatment in the heart and liver, which are the main sites of doxorubicin toxicity.

We have developed compounds that use a homing peptide for delivery and uptake into target cells, and a proapoptotic peptide as the drug component [31]. A major advantage of

Table 1. Structure and activities of homing peptides identified by phage display^a.

	RGD-4C ^b	NGR ^c	LyP-1 ^d	F3 ^e	SMS ^f	GFE ^g
Sequence	CCDCRGDCFC	CCNGRC	cCGNKRTRGC	*	SMSIARL	cCGFECVRQCPERC
Cell surface	integrins $\alpha\beta3$ and $\alpha\beta3$	amino- peptidase N	not known	not known	not known	membrane dipeptidase
Tissue	Angiogenesis	Angiogenesis	Tumor lymphatics/ tumor cells	Angiogenesis/ vessels	Prostate	Lung
Cellular localization of the peptide	Cell surface/ cytoplasmic	Cell surface/ cytoplasmic	Cell surface/ nuclear	Cell surface/ nuclear	Cell surface/ intracellular	Cell surface

^aThe amino acid sequences of the peptides are given in the single letter code; c denotes cyclic structure formed by a disulfide bond.

^bThis is a cyclic nonapeptide containing two disulfide bonds; the form with the 1-3, 2-4 disulfide bond pattern is active in binding to the integrins [29].

^cPeptides with the NGR motif bind to aminopeptidase N, which is specifically expressed in angiogenic vessels within the vasculature [10,13].

^dA cyclic nonapeptide that recognizes tumor lymphatics and tumor cells in certain (but not all) tumors. This peptide is taken up by the cells it binds to and translocated into the nucleus [20].

^eA 31-amino acid peptide that binds to the endothelial cells in tumor blood vessels and tumor cells and is translocated into the nucleus [33].

^fA linear heptapeptide that selectively binds to the vasculature of the normal prostate [32].

^gA cyclic nonapeptide that recognizes membrane dipeptidase, which is selectively expressed by lung blood vessels within the vasculature [39].

this class of compounds is that they can be prepared by solid phase peptide synthesis. In contrast, conjugation steps are required in joining a homing peptide with conventional drugs. The proapoptotic peptide is an anti-bacterial peptide that disrupts the membranes of bacteria, but harms mammalian cells only if it is introduced into a cell. Inside a mammalian cell, the proapoptotic peptide disrupts the mitochondria, as their membranes resemble those of bacteria (mitochondria are ancestrally related to bacteria). Leakage of mitochondrial membrane, in turn, is one of the main initiators of apoptosis. The efficacy of this approach has been demonstrated in mice in two diseases associated with angiogenesis, a tumor model [31] and synovial inflammation in arthritis [6]. Moreover, combining the same proapoptotic peptide with a homing peptide that binds to the blood vessels of the normal prostate yielded a compound with a different targeting specificity. Intravenous administration of this compound to male mice resulted in partial destruction of the normal prostate tissue. In a transgenic prostate cancer model (TRAMP mice), administering the prostate-targeted compound before the appearance of the tumors delayed tumor development [32]. That the same non-selective proapoptotic peptide could be used successfully for different targets by changing the homing peptide, dramatically illustrates the potential of the targeting technology.

Specific delivery to subcellular sites. Relatively recently, we have identified peptides that selectively recognize tumor endothelial cells and tumor cells, and are capable of delivering a drug-like payload, such as fluorescein or rhodamine, into the nucleus of these cells. One of these peptides, Lyp-1, recognizes the tumor lymphatics and tumor cells [20],

whereas another peptide transports fluorescein into the nuclei of tumor blood vessel endothelial cells and tumor cells ([33]; Table 1). These peptides contain numerous basic amino acid residues, which apparently form a nuclear localization signal. They might prove to be particularly useful for delivering anti-cancer drugs that act in the nucleus. It might also be possible to develop specific targeting probes for other intracellular organelles.

Targeted gene therapy. Viral gene therapy vectors have been genetically modified with homing peptides and antibodies for targeting purposes. Inserting an RGD sequence into an adenovirus surface protein changes the tropism of the virus such that the virus infects cells expressing integrins [34,35]. A non-peptidic compound that binds to $\alpha\beta3$ integrin has been used to target a nanoparticle-based gene therapy vector to tumor vasculature [36]. The particle consisted of a lipid micelle that carries, on its surface, the $\alpha\beta3$ -binding compound and a DNA-binding cationic lipid. The particle selectively delivered a mutated *Raf-1* gene to the $\alpha\beta3$ -expressing endothelium in tumors. A single intravenous injection of the targeted nanoparticles induced apoptosis in tumor vessels, tumor regression and prolonged survival in mice.

Anti-angiogenic versus anti-vascular targeting. The experimental tumor targeting studies used fast-growing mouse tumors. The blood vessels in these tumors are 'new' and might be more likely to carry angiogenesis markers, such as the $\alpha\beta3$ integrin, than vessels in slow-growing tumors. Thus, the experimental tumors could be more responsive to anti-angiogenic therapies than human tumors, which grow over years and might have a greater proportion of mature vessels than the experimental tumors. Treating

tumors with well-established vessels is likely to require both anti-vascular and anti-angiogenic approaches. As blood vessels mature, they acquire a pericyte coating and associated ECM. Tumor-specific changes in these vascular elements, such as the NG2 proteoglycan in pericytes [17] and oncofetal fibronectin and altered collagen in the matrix [18,37], might make it possible to develop targeted delivery approaches for anti-vascular therapy. Partial damage to the vessels might suffice, as thrombosis of the affected vessels might be initiated that would further restrict blood flow to the tumor [38]. Targeting through the lymphatic vessels is another potential way of expanding the targeting strategy [20]. In the future, anti-vascular tumor therapies are likely to rely on drug combinations that provide a concerted attack at more than one of the vulnerabilities in tumor vasculature.

Concluding remarks

The homing peptides isolated by phage display have shown the great diversity of blood vessels. Vascular homing peptides for a large number of tissues have already been found, which suggests that it will be possible to identify homing peptides that are specific to blood vessels in most, if not all, tissues. It is likely that additional homing peptides specific to tumor vasculature can also be found by further screening of various tumors. Uncovering the identity of the 'receptors' for homing peptides is a priority. The already known receptors (integrins, proteases and a proteoglycan) in tumor vasculature suggests that the markers of tumor vasculature discovered by phage screening will be a heterogeneous group of proteins, predominantly associated with angiogenesis. Many of these proteins are likely to prove to be functionally significant to the process of angiogenesis. In the future, vascular markers that characterize the vasculature of one tumor type, rather than angiogenesis, might also be found.

Promising results have come from the first attempts to direct drugs to tumors by using drug-peptide conjugates that home to tumor vasculature. As the receptors for the homing peptides are identified, improved versions of these peptides and their drug conjugates can be developed. As the identity of the receptors unfolds, it will also be possible to quantitatively determine the difference between the expression of these receptors within the vasculature of tumors and normal tissues. This information can be used to improve the selectivity of drug targeting by optimizing the affinity and binding valency of the homing peptides (or their mimetics). More efficient delivery of drugs, radioactive compounds and genes into tumors will undoubtedly ensue.

So far, the only pathology extensively targeted with the phage is tumors (angiogenesis). Other pathologies might

also cause alterations in the resident vasculature. In fact, it is known that this happens in inflammation and ischemia. Thus, *in vivo* phage screening to target tissues affected by various diseases might prove rewarding. Another attractive possibility is screening for peptides (or proteins) that are able to cross certain barriers, such as the blood-brain barrier.

Translating homing peptide technology developed in the mouse into therapies for human disease should be possible. All of the peptides we have tested to date have recognized the equivalent human vascular sites, suggesting that the peptides already developed might be directly applicable in humans. However, it might be necessary to modify the peptides for optimal activity. The optimization might require converting the peptides into peptidomimetics or non-peptide chemistries, and will benefit from identification of the vascular receptors for the peptides. The available results demonstrate the potential of the homing peptide technology for affinity-based drug targeting. Clearly, what has been done so far represents only the beginning in exploiting its potential.

Acknowledgement

The author's work was supported by the National Institutes of Health grants CA 82713 and Cancer Center Support Grant CA 30199, and the DAMD 17-02-1-0315 Innovator Award from the Department of Defense.

References

- 1 Ruoslahti, E. and Rajotte, D. (2000) An address system in the vasculature of normal tissues and tumors. *Annu. Rev. Immunol.* 18, 813-827
- 2 Hanahan, D. and Folkman, J. (1996) Patterns and emerging mechanisms of the angiogenic switch during tumorigenesis. *Cell* 86, 353-364
- 3 Jacobson, B.S. *et al.* (1996) Identification of endothelial cell-surface proteins as targets for diagnosis and treatment of disease. *Nat. Med.* 2, 482-484
- 4 Elble, R.C. *et al.* (2002) Molecular and functional characterization of a murine calcium-activated chloride channel expressed in smooth muscle. *J. Biol. Chem.* 277, 18586-18591
- 5 Ruoslahti, E. (2002) Specialization of tumour vasculature. *Nat. Rev. Cancer* 2, 83-90
- 6 Gerlag, D.M. *et al.* (2001) Suppression of murine collagen-induced arthritis by targeted apoptosis of synovial neovasculature. *Arthritis Res.* 3, 357-361
- 7 Houston, P. *et al.* (2001) Homing markers for atherosclerosis: applications for drug delivery, gene delivery and vascular imaging. *FEBS Lett.* 492, 73-77
- 8 Abdel-Ghany, M. *et al.* (1998) Truncated dipeptidyl peptidase IV is a potent anti-adhesion and anti-metastasis peptide for rat breast cancer cells. *Invasion Metastasis* 18, 35-43
- 9 Essler, M. and Ruoslahti, E. (2002) Molecular specialization of breast vasculature: a breast-homing phage-displayed peptide binds to aminopeptidase P in breast vasculature. *Proc. Natl. Acad. Sci. U. S. A.* 99, 2252-2257
- 10 Pasqualini, R. *et al.* (2000) Aminopeptidase N is a receptor for tumor-homing peptides and a target for inhibiting angiogenesis. *Cancer Res.* 60, 722-727

- 11 Eliceiri, B.P. and Cheresch, D.A. (1999) The role of alphav integrins during angiogenesis: insights into potential mechanisms of action and clinical development. *J. Clin. Invest.* 103, 1227–1230
- 12 Kim, S. *et al.* (2000) A regulation of angiogenesis *in vivo* by ligation of integrin $\alpha 5\beta 1$ with the central cell-binding domain of fibronectin. *Am. J. Pathol.* 156, 1345–1362
- 13 Arap, W. *et al.* (1998) Cancer treatment by targeted drug delivery to tumor vasculature in a mouse model. *Science* 279, 377–380
- 14 St Croix, B. *et al.* (2000) Genes expressed in human tumor endothelium. *Science* 289, 1197–1202
- 15 Christian, S. *et al.* (2001) Molecular cloning and characterization of EndoGlyx-1, an EMILIN-like multisubunit glycoprotein of vascular endothelium. *J. Biol. Chem.* 276, 48588–48595
- 16 Hu, Z. and Garen, A. (2001) Targeting tissue factor on tumor vascular endothelial cells and tumor cells for immunotherapy in mouse models of prostate cancer. *Proc. Natl. Acad. Sci. U. S. A.* 98, 12180–12185
- 17 Ozerdem, U. *et al.* (2001) NG2 proteoglycan is expressed exclusively by mural cells during vascular morphogenesis. *Dev. Dyn.* 222, 218–227
- 18 Halin, C. *et al.* (2002) Enhancement of the antitumor activity of interleukin-12 by targeted delivery to neovasculature. *Nat. Biotechnol.* 20, 264–269
- 19 Alitalo, K. and Carmeliet, P. (2002) Molecular mechanisms of lymphangiogenesis in health and disease. *Cancer Cells* 1, 219–227
- 20 Laakkonen, P. *et al.* (2002) Tumor-homing peptide with a lymphatic vessel-related targeting specificity. *Nat. Med.* 8, 751–755
- 21 Chang, Y.S. *et al.* (2000) Mosaic blood vessels in tumors: frequency of cancer cells in contact with flowing blood. *Proc. Natl. Acad. Sci. U. S. A.* 97, 14608–14613
- 22 Folberg, R. *et al.* (2000) Vasculogenic mimicry and tumor angiogenesis. *Am. J. Pathol.* 156, 361–381
- 23 Yang, J.T. *et al.* (1993) Embryonic mesodermal defects in alpha 5 integrin-deficient mice. *Development* 119, 1093–1105
- 24 Bader, B.L. *et al.* (1998) Extensive vasculogenesis, angiogenesis, and organogenesis precede lethality in mice lacking all alpha v integrins. *Cell* 95, 507–519
- 25 Reynolds, L.E. *et al.* (2002) Enhanced pathological angiogenesis in mice lacking $\beta 3$ integrin or $\beta 3$ and $\beta 5$ integrins. *Nat. Med.* 8, 27–34
- 26 Curnis, F. *et al.* (2002) Differential binding of drugs containing the NGR motif to CD13 isoforms in tumor vessels, epithelia, and myeloid cells. *Cancer Res.* 62, 867–874
- 27 Kerbel, R.S. (1991) Inhibition of tumor angiogenesis as a strategy to circumvent acquired resistance to anti-cancer therapeutic agents. *BioEssays* 13, 31–36
- 28 Olson, T.A. *et al.* (1997) Targeting the tumor vasculature: inhibition of tumor growth by a vascular endothelial growth factor-toxin conjugate. *Int. J. Cancer* 73, 865–870
- 29 Assa-Munt, N. *et al.* (2001) Solution structures and integrin binding activities of an RGD peptide with two isomers. *Biochemistry* 40, 2373–2378
- 30 Browder, T. *et al.* (2000) Antiangiogenic scheduling of chemotherapy improves efficacy against experimental drug-resistant cancer. *Cancer Res.* 60, 1878–1886
- 31 Ellerby, H.M. *et al.* (1999) Anti-cancer activity of targeted pro-apoptotic peptides. *Nat. Med.* 5, 1032–1038
- 32 Arap, W. *et al.* (2002) Targeting the prostate vasculature for destruction through a vascular address. *Proc. Natl. Acad. Sci. U. S. A.* 99, 1527–1531
- 33 Porkka, K. *et al.* (2002) Targeting of peptides to the nuclei of tumor cells and tumor endothelial cells *in vivo*. *Proc. Natl. Acad. Sci. U. S. A.* 99, 7444–7449
- 34 Wickham, T.J. (2000) Targeting adenovirus. *Gene Ther.* 7, 110–114
- 35 Haviv, Y.S. *et al.* (2002) Adenoviral gene therapy for renal cancer requires retargeting to alternative cellular receptors. *Cancer Res.* 62, 4273–4281
- 36 Hood, J.D. *et al.* (2002) Tumor regression by targeted gene delivery to the neovasculature. *Science* 296, 2404–2407
- 37 Xu, J. *et al.* (2001) Proteolytic exposure of a cryptic site within collagen type IV is required for angiogenesis and tumor growth *in vivo*. *J. Cell Biol.* 154, 1069–1080
- 38 Huang, X. *et al.* (1997) Tumor infarction in mice by antibody-directed targeting of tissue factor to tumor vasculature. *Science* 275, 547–550
- 39 Rajotte, D. and Ruoslahti, E. (1999) Membrane dipeptidase is the receptor for a lung-targeting peptide identified by *in vivo* phage display. *J. Biol. Chem.* 274, 11593–11598

EDITOR'S CHOICE

bmn.com/pharmacology

As a busy scientist, searching through the wealth of information on BioMedNet can be a bit daunting – the new gateway to **pharmacology** on BioMedNet is designed to help.

The regular updates include:

News – our dedicated team of reporters from BioMedNet News provide a busy researcher with all the news to keep up-to-date on what's happening – right now.

Journal scan – learn about new reports and events in genomics every day, at a glance, without leafing through stacks of journals.

Conference reporter – daily updates on the most exciting developments revealed at key conferences in the life sciences – providing a quick but comprehensive report of what you missed by staying home.

Minireviews and Reviews – a selection of the best review and opinion articles from all *Trends* and *Current Opinion* journals and *Drug Discovery Today*.

Why not bookmark the gateway at <http://bmn.com/pharmacology> for access to all the news, reviews and informed opinion on the latest scientific advances in pharmacology.

Vascular zip codes in angiogenesis and metastasis

E. Ruoslahti¹

The Burnham Institute, Cancer Research Center, 10901 North Torrey Pines Road, La Jolla, CA 92037, U.S.A.



Jubilee Lecture

Delivered at the Chancellors Conference Centre, University of Manchester, on 1 December 2003

Erkki Ruoslahti

Abstract

In vivo screening of phage-displayed peptide libraries has revealed extensive molecular differences in the blood vessels of individual normal tissues. Pathological lesions also put their signature on the vasculature; in tumours, both blood and lymphatic vessels differ from normal vessels. The changes that characterize tumour blood vessels include selective expression of certain integrins. Peptides isolated by *in vivo* phage display for homing to tumours have been shown to be useful in directing therapeutic agents to experimental tumours. The targeting can enhance the efficacy of the therapy while reducing side effects. Phage screening has also revealed lung-specific vascular markers that promote tumour metastasis to the lungs by mediating specific adherence of tumour cells to the lung vasculature. These phage-screening studies have revealed a previously unsuspected degree of vascular specialization and provide potentially useful guidance devices for targeted therapies.

Introduction

Vascular zip codes exist in lymphoid tissues, where the specialized endothelial cells of high endothelium express adhesion molecules that direct lymphocyte homing. It is less well known that many, perhaps all, non-lymphoid tissues put a tissue-specific 'signature' on their vasculature [1]. Moreover, endothelial up-regulation of leucocyte adhesion molecules at inflammatory sites and distinct features of the vasculature in

tumours are examples of pathological tissue processes that cause changes in the vasculature [1,2].

Tumours stimulate angiogenesis to secure a blood supply for the growing tumour [3,4]. The activated endothelial cells and pericytes in this neovasculature express molecules that are not expressed or are expressed at much lower levels in normal vessels. Moreover, the endothelial cells of tumour lymphatics also express tumour-specific markers [1].

Tissue-selective tumour metastasis can be facilitated by the adhesion of tumour cells to tissue-specific zip code molecules on the surface of endothelial cells [5]. Elucidation of such adhesion mechanisms may provide molecular markers predictive of metastasis and the means of suppressing metastasis. Markers that are specific for tumour vasculature provide new opportunities for targeted delivery of therapies.

Phage display libraries expressing random peptides or protein fragments have been particularly useful in analysing vascular heterogeneity. Several years ago, we initiated *in vivo* screening of phage libraries for the purpose of identifying specific markers in the vasculature of normal tissues and tumours [6,7]. Our results reveal extensive heterogeneity in tumour blood vessels and lymphatics and we have also isolated homing peptides for a large number of individual tissues by using this method. Some of the tissue-specific endothelial markers detected with the homing peptides appear to serve as binding sites for metastasizing tumour cells. Herein, I will briefly discuss recent developments in this area.

In vivo phage display in vascular analysis

Our laboratory has used *in vivo* screening of phage libraries that express random peptides or cDNA-encoded protein fragments to identify tissue- and tumour-specific features of the vasculature. In the early studies, we injected unselected libraries into the tail vein of mice, rescued the phage from the target tissues and, by repeating the process several times, were able to isolate phage that specifically homed to the target tissue. The premise was that the phage particles would not leave the vascular space during the short (approx. 5 min) circulation time and that, as a result, only phage binding to the endothelium (and perhaps other cells in the vessel wall) would be isolated. This conjecture has been proven to be

Key words: endothelial cell, homing peptide, integrin, phage display.

¹email ruoslahti@burnham.org

Figure 1 | Vascular homing peptides and their receptors***Tumor-homing peptides*****1st generation: RGD-4C = cCDCRGDCFC**(Receptor: integrins $\alpha v\beta 3$ and $\alpha v\beta 5$)**NGR = cCNGRC**

(Receptor: aminopeptidase N)

2nd generation: F3 = 34-amino acid basic peptide from HMGN2

(Receptor: cell surface nucleolin)

cCSRPRRSEC

(Receptor: kallikrein-9?, blood vessels of pre-malignant skin lesions)

CGKRK and CDTRL

Receptors: unknown, blood vessels in skin carcinomas)

CRGRRSTReceptor: PDGFR β -associated molecule, blood vessels of islet cell carcinomas)**LyP-1 = cCGNKRTRC**

(Receptor: unknown, tumor lymphatics and tumor cells)

Peptides homing to blood vessels in normal tissues**cCGFECVRQCPERC**

Receptor: membrane dipeptidase on lung endothelial cells)

SMSIARL

Receptor: unknown, blood vessels of normal prostate

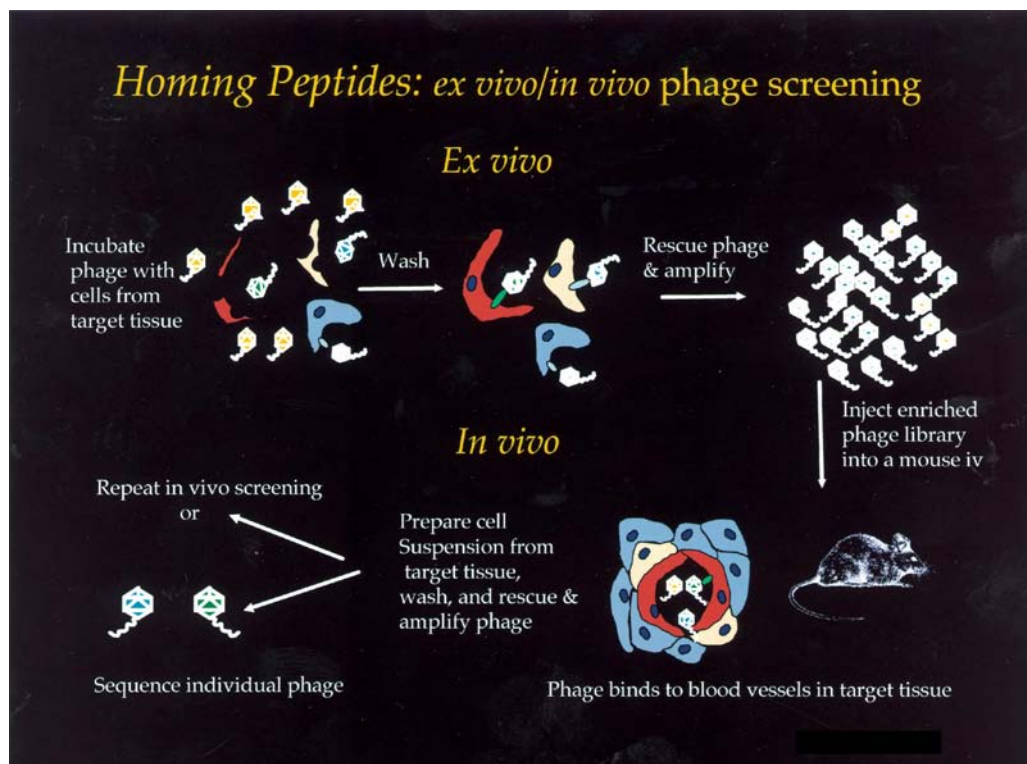
accurate. The 'first-generation' homing peptides we identified for various normal tissues or tumours bound to the blood vessels at the target [5–7] (Figure 1).

More recently, we have added an *ex vivo* step to the process to enrich the phage library on cell suspension prepared from the target tissue, and use the enriched library for *in vivo* screening [8]. A schematic representation of the *ex vivo/in vivo* phage screening procedure is shown in Figure 2. This *ex vivo/in vivo* procedure appears to favour peptides that are different from the first-generation peptides obtained by screening only *in vivo*. Two features set apart these 'second-generation' homing peptides: they effectively carry a payload to the target tissue as monovalent conjugates and many of them take the payload into the target cell [9–12]. As a result of the cell type-specific internalization, the payload (fluorescein and biotin, so far) becomes concentrated in the target cells. If the concentrating effect can be reproduced in preclinical and clinical settings, targeted therapies with enhanced efficiency may be possible. In this regard, our peptides are similar to the Tat, penetratin and VP22 peptides, which are also efficiently taken up by cells. An important difference is that these peptides are taken up by all cells, whereas our homing peptides are cell type-specific.

Blood vessel specialization in normal tissues

The phage screening studies have uncovered an unexpected extent of tissue-specific molecular heterogeneity in the vasculature of various normal tissues. We have obtained tissue-specific vascular homing peptides for each normal tissue and organ our laboratory has chosen for targeting so far. The list includes both major organs, such as the brain, lungs, heart and kidneys, and minor ones such as the prostate [5,13,14]. With our current technology [8], the selectivity of phage homing to a specific organ can be several hundredfold (L. Zhang, J. A. Hoffman and E. Ruoslahti, unpublished work). These results suggest that every tissue may express specific markers in its vasculature. Less extensive studies with monoclonal antibodies support this conclusion [15,16].

The molecular nature of vascular changes that give rise to the individuality of the vessels in various tissues and pathological lesions is only partially understood. Several proteases have been identified as markers of the vasculature in individual normal tissues. Thus two peptidases (dipeptidyl peptidase IV [17] and membrane dipeptidase [18]), and a chloride channel are selectively expressed in lung vessels

Figure 2 | Schematic representation of the *ex vivo*/*in vivo* phage screening procedure

[19]. Another peptidase, aminopeptidase P, is a marker for breast gland vasculature [13]. However, the tissue-specific endothelial markers appear to include many other types of molecules as well (L. Zhang, J. A. Hoffman and E. Ruoslahti, unpublished work).

Special features of tumour vessels

Previous studies have shown that tumour vessels express a number of markers that are characteristic of angiogenesis. For example, the expression of receptors for vascular endothelial growth factor is elevated in the endothelial cells of tumour blood vessels [3]. Certain integrins are another group of receptors elevated in angiogenic vessels. The $\alpha v\beta 3$, $\alpha v\beta 5$ and $\alpha 5\beta 1$ integrins are overexpressed in tumour vasculature [20]. Indeed, one of the peptides identified by *in vivo* screening of phage libraries for tumour homing recognizes $\alpha v\beta 3$ and $\alpha v\beta 5$ [7].

Similar to the molecular markers of normal vessels, the angiogenesis markers also include peptidases/proteases. Aminopeptidase N was established as a new marker of angiogenic vessels with our first-generation tumour-homing peptides containing the motif Asn-Gly-Arg [21]. Aminopeptidase N is a membrane protein that is expressed in some epithelial cells and immune cells; however, within the vasculature, it is specific for angiogenesis. Aminopeptidase N has been previously linked to cell migration and tumour

invasion, but not to angiogenesis. The form of aminopeptidase N expressed in tumour vasculature may be different from that in normal cells [22]. In a similar vein, an antibody that recognizes a splice variant of fibronectin selectively recognizes the ECM (extracellular matrix) of angiogenic blood vessels [23].

We have designed recently a phage-screening method aimed at yielding peptides that might recognize endothelial precursor cells. In this screen, we first selected phage for binding to bone marrow cells *ex vivo* and then for homing to tumour vasculature [10]. One of the peptides, F3, identified in this manner recognizes a small population of bone marrow cells, angiogenic endothelial cells and certain tumour cells. We have now shown that the molecule the F3 peptide binds to in the target cells is cell-surface-expressed nucleolin [24]. Antibodies prepared against nucleolin also specifically recognize blood vessels in tumours and in a non-malignant angiogenesis model. Thus cell-surface-expressed nucleolin is a new endothelial marker of angiogenic vessels, including those in tumours, where it also recognizes the tumour cells.

An unexpected degree of vascular diversity was revealed in our recent collaborative study with Dr Douglas Hanahan's laboratory [11,12]. Using transgenic mouse tumour models, we showed that pancreatic islet cell tumours and skin tumours expressed different markers in their vasculature. Another novel finding was that some homing peptides distinguished between the vessels of premalignant and malignant lesions (while not recognizing the normal vasculature). This latter

finding indicates that the molecular features of the vasculature reflect the stage of tumorigenesis.

Some of the peptides identified in the transgenic tumour study bound both to the endothelial cells and pericytes in the tumour vasculature. Previous studies have also shown that pericytes in tumour vasculature carry specific markers. The NG2 proteoglycan, also known as melanoma-associated chondroitin sulphate proteoglycan, is one such marker. NG2 is a membrane-spanning cell-surface protein that is expressed in the neovasculature of tumours, regenerating tissues and in foetal vessels [25].

We have reported recently evidence indicating that lymphatic vessels in tumours can also express tumour-specific markers. A nonapeptide, LyP-1, specifically recognizes the lymphatic vessels in some tumours, including xenografts produced with the MDA-MB-435 human breast cancer cell line [9]. LyP-1 does not recognize lymphatics in normal tissues, indicating that this peptide distinguishes lymphatics in tumours from normal lymphatics.

Significance of vascular diversity

The functional significance of the vascular diversity established by the phage studies is not well understood. However, membrane dipeptidase, which is selectively expressed in lung vessels, inactivates leukotriene D₄ [26]. It seems possible that this enzymic activity is needed to protect the lungs against systemic pro-inflammatory activity of the cytokine.

The proteins in tumour vasculature, the expression of which is linked to angiogenesis, are probably functionally important in the formation of neovasculature. The growth factor receptors and integrins that are up-regulated in angiogenic vessels are needed for angiogenesis to proceed [1], as is aminopeptidase N [21]. A tumour-homing peptide identified by targeting pancreatic islet cell tumours is homologous with a segment in the PDGF-B precursor protein, and its binding to cultured cells is dependent on the PDGF- β receptor [12]. The peptide appeared to bind both to endothelial cells and pericytes in the tumours. The molecule this peptide binds to probably plays a role in endothelial-pericyte interactions.

Delivery of therapeutic agents to vascular targets

Peptides that home to a specific site in the vasculature are attractive as carriers of therapeutic and diagnostic agents. Homing peptide-directed drug delivery should concentrate the drug at the targeted site, increasing efficacy while decreasing side effects in other tissues. Coupling of doxorubicin with the peptides that specifically bind to the $\alpha v\beta 3$ and $\alpha v\beta 5$ integrins (RGD motif peptide) or to aminopeptidase N (NGR motif peptide) yielded compounds that were more effective and less toxic than doxorubicin alone [7], and similar results were obtained when these peptides were used to target tumour necrosis factor into tumours [27]. Inserting an RGD sequence into an adenovirus surface protein changes the

tropism of the virus such that the virus infects cells expressing integrins [28,29]. A non-peptidic compound that binds to $\alpha v\beta 3$ integrin has been used to target a nanoparticle-based gene therapy vector to tumour vasculature [30].

The RGD and NGR peptides could also direct an antibacterial peptide that induces apoptosis in mammalian cells if internalized by the cells. Conjugates of the pro-apoptotic peptide with the integrin and aminopeptidase N binding peptides inhibited tumour growth in mice [31]. Systemic treatment of mice with the integrin-binding conjugate also suppressed inflammation in arthritic synovium, which exhibits strong angiogenesis [32]. Moreover, combining the same pro-apoptotic peptide with a homing peptide that binds to the blood vessels of the normal prostate yielded a compound that caused partial destruction of the normal prostate tissue [14]. Thus the *in vivo* effects of the same non-specifically toxic peptide depended on the specificity of the homing peptide, clearly illustrating the potential of the targeting technology.

Quite recently, we have identified peptides that are capable of being internalized by their target cells and delivering a drug-like payload (fluorescein, rhodamine or biotin) into the cell nucleus [9–12]. These internalizing peptides contain numerous basic amino acid residues, which apparently are important for the internalization and can form a nuclear localization signal. One of these peptides binds to cell-surface nucleolin [24]; the cellular receptors for the other peptides remain to be identified. These internalizing peptides may prove to be particularly useful for delivering anti-cancer drugs that act in the nucleus.

Tissue-specific endothelial molecules in metastasis

It is a commonly held view that much of the tissue bias in metastasis is due to non-specific trapping of circulating tumour cells in the capillaries of the tissues that the cells pass through. This mechanism would explain the frequency of metastasis in the lungs and the liver, which are the tissues that first receive the venous blood. However, there appears to be a specific adhesion component even in metastasis to the lungs. A protein with sequence homology to chloride channels, LuECAM-1, is responsible for the adhesion of B16 murine melanoma cells to lung endothelia [19]. Similarly, binding of a breast cancer cell line to dipeptidyl peptidase IV expressed on lung endothelial cells facilitates the dissemination of these cells to the lungs [33]. These examples indicate that even metastasis to the target organs that are supposed to receive circulating tumour cells is facilitated by specific cell adhesion. Tumours can also show tissue preferences that cannot depend on circulatory routing; again, binding of the tumour cells to selectively expressed endothelial surface molecules seems to be involved [19,33,34].

The identification of a presumed ion channel, protease, and a molecule with unknown function as the receptors for metastasizing tumour cells in the lungs shows that adhesive events resulting in cell homing can depend on molecules

that are distinct from what are usually considered as adhesion molecules. Classical adhesion proteins may also play a role in tissue-specific tumour metastasis. Thus forced expression of the $\alpha 4 \beta 1$ integrin on tumour cells can change the metastatic pattern of the transfected cells; having favoured the lungs as the natural site of metastasis, $\alpha 4 \beta 1$ -expressing Chinese-hamster ovary cells and K562 human erythroleukaemia cells metastasized into the lungs and bones from an intravenous injection [35]. Tumour cells that express the Lewis x carbohydrate at their surface more readily metastasize into the lungs compared with control cells lacking Lewis x [36,37]. In this case, the receptor is probably a lectin that recognizes the Lewis x epitope.

We have recently used phage display to identify a new lung-specific adhesion system that promotes lung metastasis by another breast cancer cell line, 4T1 [38]. The adhesion molecule on the tumour cells is a previously uncharacterized membrane protein, and its receptor on lung endothelial cells is not known. Thus our phage display approach probably reveals additional tissue-specific endothelial molecules that are candidate receptors for tissue-specific homing of metastatic tumour cells.

Future directions

Our homing peptide studies indicate that the endothelial cells (and possibly mural cells as well) in each vascular bed express a unique complement of cell-surface molecules. Only a few of the molecules that act as receptors for homing peptides are known, but their diversity (proteases, integrins, growth factor receptors and proteoglycans) suggests that they represent a heterogeneous group of proteins. These proteins are probably functionally significant in the vascular beds that express them. They can also function as tissue-specific receptors for metastatic tumour cells. To accelerate the discovery of homing peptide receptors, we are working on a method that allows simultaneous identification of a homing peptide and its receptor.

The tumour-homing peptides fall into two categories: (i) peptides that bind to angiogenesis-associated molecules and recognize the vasculature of all tumours (and other angiogenic lesions), and (ii) peptides that recognize the vasculature of some, but not all tumours. The latter kind would be potentially advantageous in therapeutic applications because sites of beneficial angiogenesis would not be affected. We are currently screening for peptides that would broadly recognize the vasculature of a given tumour type.

Our demonstration that tumour lymphatics are also specialized offers the possibility of attacking tumours from two directions: through the blood vessels and through the lymphatics. So far, only one homing peptide exists for tumour lymphatics, and it does not recognize all tumours. Screening is in progress to identify more lymphatic homing peptides.

Among the newest homing peptides we have described are several that are internalized by the target cells and can take a payload, such as fluorescein, into the cell nucleus. We

are conducting treatment experiments with drug conjugates to utilize these properties. We are also taking advantage of the sensor capabilities of homing peptides in designing nanodevices for tumour diagnosis and treatment.

This work was supported by the NIH grant CA 82713 and Cancer Center Support Grant CA 30199, and the DAMD 17-02-1-0315 Innovator Award from the Department of Defense. We also thank Dr Johanna Joyce for creating the initial draft of the figure.

References

- Ruoslahti, E. (2002) *Nat. Rev. Cancer* **2**, 83–90
- Hanahan, D. and Folkman, J. (1996) *Cell* (Cambridge, Mass.) **86**, 353–364
- Alitalo, K. and Carmeliet, P. (2002) *Cancer Cell* **1**, 219–227
- Hanahan, D. and Weinberg, R.A. (2000) *Cell* (Cambridge, Mass.) **100**, 57–70
- Ruoslahti, E. and Rajotte, D. (2000) *Annu. Rev. Immunol.* **18**, 813–827
- Pasqualini, R. and Ruoslahti, E. (1996) *Nature* (London) **380**, 364–366
- Arap, W., Pasqualini, R. and Ruoslahti, E. (1998) *Science* **279**, 377–380
- Hoffman, J.A., Laakkonen, P., Porkka, K., Bernasconi, M. and Ruoslahti, E. (2004) in *Phage Display: A Practical Approach* (Clarkson, T. and Lowman, H., eds.), Oxford University Press, Oxford, U.K.
- Laakkonen, P., Porkka, K., Hoffman, J.A. and Ruoslahti, E. (2002) *Nat. Med.* (N.Y.) **8**, 743–751
- Porkka, K., Laakkonen, P., Hoffman, J.A., Bernasconi, M. and Ruoslahti, E. (2002) *Proc. Natl. Acad. Sci. U.S.A.* **99**, 7444–7449
- Hoffman, J.A., Giraudo E., Singh, M., Inoue, M., Porkka, K., Hanahan, D. and Ruoslahti, E. (2003) *Cancer Cell* **4**, 383–391
- Joyce, J.A., Laakkonen, P., Bernasconi, M., Bergers, G., Ruoslahti, E. and Hanahan, D. (2003) *Cancer Cell* **4**, 393–403
- Essler, M. and Ruoslahti, E. (2002) *Proc. Natl. Acad. Sci. U.S.A.* **99**, 2252–2257
- Arap, W., Haedicke, W., Bernasconi, M., Kain, R., Rajotte, D., Krajewski, S., Ellerby, H.M., Bredesen, D.E., Pasqualini, R. and Ruoslahti, E. (2002) *Proc. Natl. Acad. Sci. U.S.A.* **99**, 1527–1531
- Jacobson, B.S., Stolz, D.B. and Schnitzer, J.E. (1996) *Nat. Med.* (N.Y.) **2**, 482–484
- Ding, B.S., Zhou, Y.J., Chen, X.Y., Zhang, J., Zhang, P.X., Sun, Z.Y., Tan, X.Y. and Liu, J.N. (2003) *Circulation* **108**, 2892–2898
- Johnson, R.C., Zhu, D., Augustin-Voss, H.G. and Pauli, B.U. (1993) *J. Cell Biol.* **121**, 1423–1432
- Rajotte, D. and Ruoslahti, E. (1999) *J. Biol. Chem.* **274**, 11593–11598
- Elble, R.C., Widom, J., Gruber, A.D., Abdel Ghany, M., Levine, R., Goodwin, A., Cheng H.C. and Pauli, B.U. (1997) *J. Biol. Chem.* **272**, 27853–27861
- Kim, S., Bell, K., Mousa, S.A. and Varner, J.A. (2000) *Am. J. Pathol.* **156**, 1345–1362
- Pasqualini, R., Koivunen, E., Kain, R., Lahdenranta, J., Sakamoto, M., Stryhn, A., Ashmun, R.A., Shapiro, L.H., Arap, W. and Ruoslahti, E. (2000) *Cancer Res.* **60**, 722–727
- Curnis, F., Arrigoni, G., Sacchi, A., Fischetti, L., Arap, W., Pasqualini, R. and Corti, A. (2002) *Cancer Res.* **62**, 867–874
- Halin, C., Rondini, S., Nilsson, F., Berndt, A., Kosmehl, H., Zardi, L. and Neri, D. (2002) *Nat. Biotechnol.* **20**, 264–269
- Christian, S., Pilch, J., Porkka, K., Laakkonen, P. and Ruoslahti, E. (2003) *J. Cell Biol.* **163**, 871–878
- Ozerdem, U., Grako, K.A., Dahlin-Huppe, K., Monosov, E. and Stallcup, W.B. (2001) *Dev. Dyn.* **222**, 218–227
- Keynan, S., Hooper, N.M. and Turner, A.J. (1996) in *Zinc Metalloproteases in Health and Disease* (Hooper, N.M., ed.), pp. 285–309, Taylor and Francis, London
- Curnis, F., Gasparri, A., Sacchi, A., Longhi, R. and Corti, A. (2004) *Cancer Res.* **64**, 565–571
- Wickham, T.J. (2000) *Gene Ther.* **7**, 110–114
- Haviv, Y.S., Blackwell, J.L., Kanerva, A., Nagi, P., Krasnykh, V., Dmitriev, I., Wang, M., Naito, S., Lei, X., Hemminki, A. et al. (2002) *Cancer Res.* **62**, 4273–4281
- Hood, J.D., Bednarski, M., Frausto, R., Guccione, S., Reisfeld, R.A., Xiang, R. and Cheresch, D.A. (2002) *Science* **296**, 2404–2407

- 31 Ellerby, H.M., Arap, W., Ellerby, L.M., Kain, R., Andrusiak, R., Rio, G.D., Krajewski, S., Lombardo, C.R., Rao, R., Ruoslahti, E. et al. (1999) *Nat. Med. (N.Y.)* **5**, 1032–1038
- 32 Gerlag, D.M., Borges, E., Tak, P.P., Ellerby, H.M., Bredesen, D.E., Pasqualini, R., Ruoslahti, E. and Firestein, G.S. (2001) *Arthritis Res.* **3**, 357–361
- 33 Cheng, H.C., Abdel-Ghany, M., Elble, R.C. and Pauli, B.U. (1998) *J. Biol. Chem.* **273**, 24207–24215
- 34 Auerbach, R., Lu, W.C., Pardon, E., Gumkowski, F., Kaminska, G. and Kaminski, M. (1987) *Cancer Res.* **47**, 1492–1496
- 35 Matsuura, N., Puzon-McLaughlin, W., Irie, A., Morikawa, Y., Kakudo, K. and Takada, Y. (1996) *Am. J. Pathol.* **148**, 55–61
- 36 Takada, A., Ohmori, K., Yoneda, T., Tsuyu-oka, K., Hasegawa, A., Kiso, M. and Kannagi, R. (1993) *Cancer Res.* **53**, 354–361
- 37 Fukuda, M.N., Ohyama, C., Lowitz, K., Matsuo, O., Pasqualini, R., Ruoslahti, E. and Fukuda, M. (2000) *Cancer Res.* **60**, 450–456
- 38 Brown, D. M. and Ruoslahti, E. (2004) *Cancer Cell*, in the press

Received 6 February 2004

Vascular Homing Peptides with Cell-Penetrating Properties

E. Ruoslahti*, T. Duza, and L. Zhang

The Burnham Institute, Cancer Research Center, 10901 North Torrey Pines Road, La Jolla, CA 92037, USA

Abstract: *In vivo* screening of phage-displayed peptide libraries has revealed extensive molecular heterogeneity in the blood vessels of individual normal tissues and shown that pathological lesions put their signature on the vasculature. In tumors, both blood and lymphatic vessels differ from normal vessels. Moreover, the molecular changes in the vasculature parallel progression in tumor development, hence making the vessels in premalignant lesions distinguishable from normal vessels and from the vessels in malignant tumors of the same tissue. Some of the tumor-homing peptides penetrate into tumor endothelial cells (and tumor cells), but not into endothelial cells in normal tissues or other normal cells. Thus, these cell-penetrating peptides are cell type-specific. Peptides that home to tumor vasculature have been shown to be useful in directing therapeutic agents to experimental tumors. The cell penetrating peptides may be particularly useful in drug delivery because they can take their payload inside the target cells and even into a specific subcellular organelle such as the nucleus.

Key Words: Phage display, endothelial cells, lymphatics, nucleolin, Tat peptide, tumor vasculature, angiogenesis.

INTRODUCTION

Many, perhaps all, normal tissues put a tissue-specific "signature" on their vasculature, and the same is true of tumors [1]. Tumors induce angiogenesis, the growth of new blood vessels, to secure a blood supply for the growing tumor [2, 3]. The activated endothelial cells in this neovasculature express molecules that are not expressed or are expressed at much lower levels in normal vessels [1]. Moreover, the endothelial cells of tumor lymphatics have in one case been shown to express a tumor-specific marker [4].

We use phage display libraries expressing random peptides or protein fragments to analyze vascular heterogeneity. Several years ago, we initiated *in vivo* screening of such libraries for the purpose of identifying specific markers in the vasculature [5, 6]. The phage library is injected into the tail vein of a mouse and phage is rescued from the tissue of interest, such as a tumor, yielding a phage pool enriched in phage that selectively binds to the target tissue. By repeating the procedure a number of times, the enrichment can be brought to a level that allows the identification of individual homing phage. More recently, we have added an *ex vivo* enrichment step to the procedure that consists of selection of phage that bind to a cell suspension isolated from the target tissue. This *ex vivo*-enriched pool is then further selected for *in vivo* homing in mice.

Our results reveal extensive heterogeneity in the vasculature of various normal tissues as well as in tumor blood vessels and lymphatics. Most recent results show that homing peptides can even distinguish the vasculature of premalignant lesions from normal vessels and from the vessels in a subsequently developing malignant tumor [7, 8]. Some of the tumor-homing peptides display cell-penetrating

properties. In this chapter, we will discuss vascular heterogeneity as detected by phage display with a focus on the cell-penetrating peptides we have encountered.

IN VIVO PHAGE LIBRARY SCREENING TARGETS THE VASCULATURE

We use *in vivo* screening of phage libraries that express random peptides or cDNA-encoded protein fragments to identify tissue-specific and tumor-specific markers in the vasculature. We have shown that injecting the library into the tail vein of a mouse that is under anesthesia, rescuing the phage from the target tissue, and repeating the process several times yields phage that selectively homes to the target tissue [1, 5, 6, 9]. The short time we allow the phage to circulate, and the large size of the phage particle are the likely reasons why we have found the procedure to exclusively target the vasculature. The phage may not leave the vascular space during the short (about 5 min) circulation time and, as a result, only phage binding to the endothelium is obtained. All the phage peptides we have isolated so far target the vasculature alone or, in some cases, the vasculature together with some other element in the tissue.

We have recently added an *ex vivo* step to the process aimed at enriching the phage library for phage that bind to the target tissue. This step consists of incubating the phage library with a cell suspension prepared from the target tissue, and using the enriched library for *in vivo* screening [4]. This *ex vivo/in vivo* procedure may favor the recovery of cell-penetrating homing peptides, as we have recently recovered a number of such peptides from our screens.

Two features set apart these "second generation" homing peptides from those we obtained by *in vivo*-only screening: the new peptides effectively carry a payload to the target tissue as monovalent conjugates, and many of them take the payload inside the target cell, i.e. these peptides are cell-penetrating [4, 7, 8, 10]. As a result of the cell type-specific internalization, the payload (fluorescein and biotin, so far)

*Address correspondence to this author at the The Burnham Institute, Cancer Research Center, 10901 North Torrey Pines Road, La Jolla, CA 92037, USA; Tel: (858) 646-3125; Fax: (858) 646-3198; E-mail: ruoslahti@burnham.org

becomes concentrated in the target cells. In this regard, our peptides are similar to the various cell-penetrating peptides described elsewhere in this issue, such as the Tat, penetratin, and VP22 peptides, which are also efficiently taken up by cells [11]. An important difference is that while these peptides indiscriminately enter any cell, our homing peptides are cell type-specific. We will discuss this aspect in more detail later in this article.

BLOOD VESSEL SPECIALIZATION IN NORMAL TISSUES

The phage screening studies have uncovered a surprising degree of tissue-specific molecular heterogeneity in the vasculature of normal tissues. We have obtained tissue-specific vascular homing peptides for a large number of major organs, such as the brain, lungs, heart and kidneys, and minor ones such as the prostate [9, 12, 13]. With our current technology [14], the selectivity of phage homing to a specific organ can be several hundred fold (L. Zhang, J.A. Hoffman, and E. Ruoslahti, unpublished results). These results suggest that every tissue may express specific markers in its vasculature. Results from studies that have used monoclonal antibodies support this conclusion [15-17]. As the peptides that home to the vessels in normal tissues have not included peptides with cell-penetrating properties, we will limit further discussion to tumor-homing peptides.

SPECIFIC MOLECULAR MARKERS IN TUMOR VESSELS

The blood vessels that nurture tumors are different from normal vessels. The best understood source of these differences is the process of angiogenesis in tumor vessels. VEGF receptors and certain integrins are expressed at greatly elevated levels in angiogenic vessels [1, 2]. The elevated integrin expression in tumor vasculature was reflected in one of our early homing peptide screens, which yielded a peptide that contains the integrin recognition sequence, RGD (arginine-glycine-aspartic acid). This peptide (referred to as RGD-4C) selectively recognizes the $\alpha v\beta 3$ and $\alpha v\beta 5$ integrins among the various RGD-binding integrins [6]. Another set of tumor-homing peptides established aminopeptidase N as a new marker of angiogenic vessels [18]. Aminopeptidase N is a membrane protein that is expressed in some epithelial cells and immune cells, but only angiogenic vessels express this enzyme within the vasculature. Moreover, the form of aminopeptidase N expressed in tumor vasculature may be different from that in normal cells [19]. The peptides that bind to aminopeptidase N contain an NGR

(asparagine-glycine-arginine) consensus motif. Despite the similarity between the NGR and RGD motifs, peptides containing the NGR sequence show very weak binding to integrins [6].

Materials bound to integrins at the cell surface tend to be internalized into the cell. Thus particles coated with integrin-binding proteins, such as fibronectin, are internalized through phagocytosis [20]. Furthermore, a number of viruses use integrins as receptors in entering cells [1]. Making use of this fact, the RGD sequence is widely used in viral gene therapy vectors to change the tropism of the virus to cells expressing RGD-directed integrins, such as endothelial cells in tumor vessels [21, 22]. The success viruses have in introducing their nucleic acid into cells *via* integrin-mediated uptake defines this system as a possible cell-penetrating pathway. Our results with a pro-apoptotic peptide are in agreement with this conclusion. Conjugates of this pro-apoptotic peptide with the RGD-4C peptide are much more potent inducers of apoptosis in cells that express the target integrin than in cells that do not [23]. As the pro-apoptotic activity is thought to depend on destabilization of mitochondrial membranes, these results are in agreement with an internalizing activity of integrin-binding peptides. However, we have found that univalent fluorescein conjugates of the RGD-4C peptide do not accumulate in tumors as effectively as our new peptides. The reason for the success with the pro-apoptotic peptide conjugates may be that the conjugates are likely to be oligomeric, and the resulting multivalency may enhance the cell binding and internalization. We have recently isolated a new set of peptides that are both tumor-specific and have stronger cell-penetrating activity. We will discuss these new peptides next.

CELL-PENETRATING PEPTIDES THAT ARE SPECIFIC FOR TUMOR VASCULATURE

We altered our homing peptide screening protocol so that it now includes an *ex vivo* step designed to enrich phage that bind to cells from the same tissue to be used *in vivo*. These procedures have yielded a number of peptides that have cell-penetrating properties (Table 1). In one screen, we isolated homing peptides that might recognize endothelial precursor cells. We selected phage for binding to bone marrow cells *ex vivo* and then further screened the *in vitro* enriched phage pool for tumor homing [10]. We discovered a peptide that recognizes a small population of bone marrow cells, angiogenic endothelial cells, certain tumor cells, and isolated cells in the gut and skin.

Table 1. Cell-Penetrating Homing Peptides

Peptide	Sequence	Specificity	Receptor	Reference
F3	34-amino acid basic peptide	Angiogenic endothelium, tumor cells	Cell surface nucleolin	Porkka <i>et al.</i> , 2002; Christian <i>et al.</i> , 2003
LyP-1	CGNKRTRGC	Tumor lymphatics, tumor cells	not known	Laakkonen <i>et al.</i> , 2002; Laakkonen <i>et al.</i> , 2004
CGKRK	CGKRK	Angiogenic endothelium, tumor cells	heparan sulfate (?)	Hoffman <i>et al.</i> , 2003
RGR	CRGRRST	Angiogenic endothelium	PDGF-R β -related	Joyce <i>et al.</i> , 2003

The cellular target molecule for the F3 peptide is cell surface-expressed nucleolin [24]. Anti-nucleolin antibodies also specifically recognize blood vessels in tumors and in a non-malignant angiogenesis model. Nucleolin is primarily a nuclear and cytoplasmic protein, but several studies show that it can also be expressed at the cell surface [24-28]. In addition to the main functions of nucleolin, which relate to rRNA maturation and ribosome assembly, nucleolin is known to shuttle between the nucleus and the cytoplasm and cell surface [27, 29-31]. Our results define cell surface nucleolin as a new endothelial marker of angiogenic vessels and F3 as a novel cell-penetrating peptide.

A striking feature of F3 is that it takes its fluorescein payload into the target cells and all the way into their nuclei. The internalization of the F3 peptide and of anti-nucleolin antibodies may reflect a physiological function of cell surface nucleolin. Midkine, a 13-kDa cytokine that, like F3, contains a high proportion of basic amino acids, enters cells in a nucleolin-dependent manner [27]. The same may be true of basic FGF, which has been shown to bind to nucleolin in nuclear extracts [32]. Thus, nucleolin appears to be responsible for the internalization of F3, midkine, and possibly also basic FGF. The molecular mechanisms underlying this nucleolin activity remain unknown.

The uptake of the F3 peptide is strongest in vigorously proliferating cells and suppressed in serum-starved cells. Nucleolin expression at the cell surface correlates with these changes [24], suggesting that the transport of nucleolin to the cell surface is related to cell proliferation. The differentiation state of the cells may contribute to nucleolin regulation, as cultured HL-60 cells induced to differentiate into non-proliferating macrophages lose their ability to bind F3 (K. Porkka and E. Ruoslahti, unpublished results). The link to proliferation and low degree of differentiation only partially explains the cell type specificity of F3, as very few cells bind F3 in the gut and skin. The identity of these cells is unknown, but their localization does not overlap with the fast-proliferating cells of these tissues [10]. These F3 positive cells could be bone marrow-derived cells.

The mechanism of F3 internalization is clearly different from that of the HIV Tat protein peptide. The internalization of Tat is independent of the cell-type, even *in vivo*. In contrast, our results show that F3 uptake is cell type-specific; F3 is selectively internalized by angiogenic endothelial and tumor cells. Other differences in the internalization of F3 and Tat include involvement of cell surface heparan sulfate in Tat peptide uptake [33], whereas heparan sulfate removal does not affect F3 uptake. Moreover, an anti-nucleolin antibody that inhibits the internalization of F3 does not affect Tat internalization [24]. As seen in Fig. (1A), the time course of the entry of these peptides into cells is also different. F3 also causes internalization of peptide-coated magnetic nanoparticles as shown in Fig. (1B). Interestingly, the particles remain in the cytoplasm and are excluded from the nucleus.

Our laboratory has recently isolated other cell-penetrating peptides with cell type-specific activity. One of these peptides is LyP-1 [4, 34]. LyP-1 is a 9-amino acid cyclic peptide (CGNKRTRGC) that, like F3, is rich in basic amino acids. F3 homes to tumor blood vessels, whereas LyP-1 recognizes tumor lymphatics. LyP-1 also binds the tumor

cells in certain tumors; it appears that when the tumor cells are positive for LyP-1 binding, the same is true of tumor lymphatics. LyP-1 does not recognize normal lymphatics. Some tumors do not bind LyP-1 even though the tumor may contain lymphatic vessels [4, 34]. LyP-1 can be extraordinarily effective as a tumor homing peptide, so much so that we have been able to image mammary fat pad tumors in intact animals by injecting fluorescein-labeled LyP-1 into the mice and visually examining the animals under blue light a day later (Fig. 2). Microscopy shows that the localization of fluorescein-conjugated LyP-1 shifts from tumor lymphatics minutes after the intravenous injection to tumor cells hours after the injection. The nuclei of the tumor cells are intensely fluorescent once that shift has occurred and excess peptide has been cleared. Another remarkable characteristic of the LyP-1 peptide is that it has an inherent anti-tumor activity; treatment of tumor-bearing mice with about 100 μ g of the free LyP-1 peptide given intravenously twice a week almost completely suppressed tumor growth [34].

The internalization of the LyP-1 peptide is distinct from that of F3 or Tat. First, the cell type specificity of these two peptides is different. Moreover, the anti-nucleolin antibody that inhibits the uptake of F3 does not affect LyP-1 internalization [10]. The pathway that internalizes LyP-1 remains to be identified, but it is clear from the data we have discussed here that there are several distinct internalization mechanisms for peptides and materials bound to them, some universal and others cell-type specific.

Cell-penetrating peptides are generally rich in basic amino acids and are transported into the nucleus after internalization. F3 and LyP-1 share these characteristics. Some of our newest tumor-homing peptides are also highly basic and accumulate in the nucleus of the target cells. CGKRRK and CRGRRST are examples of such peptides [7, 8]. It may be that the numerous basic amino acid residues, which apparently are important for the internalization, can also form a nuclear localization signal. In the case of F3, nucleolin binding could facilitate transport into the nucleus. Thus, our peptides share the cell-penetrating properties with Tat, penetratin, and other peptides in that class, but have the advantage of being cell type-specific. These peptides may be useful in tumor diagnosis and treatment.

DELIVERY OF DIAGNOSTIC AND THERAPEUTIC AGENTS TO VASCULAR TARGETS

Homing peptide-directed drug delivery can concentrate a payload, such as a drug, at a targeted site. This can be expected to increase efficacy, while decreasing side effects in other tissues. Proof of this principle was initially obtained by coupling doxorubicin to an RGD peptide that specifically binds to the $\alpha v \beta 3$ and $\alpha v \beta 5$ integrin and to a peptide that contains an NGR motif. The latter conjugate binds to aminopeptidase N in angiogenic tumor vessels. These doxorubicin conjugates were more effective in inhibiting tumor growth and less toxic than doxorubicin alone, the peptides alone, or doxorubicin conjugated to a control peptide [6]. Chimeric peptides comprised of a pro-apoptotic peptide, a linker, and either the RGD or NGR peptide, also inhibited tumor growth in mice, whereas either type of peptide alone was completely ineffective [23]. Moreover, combining the same pro-apop-

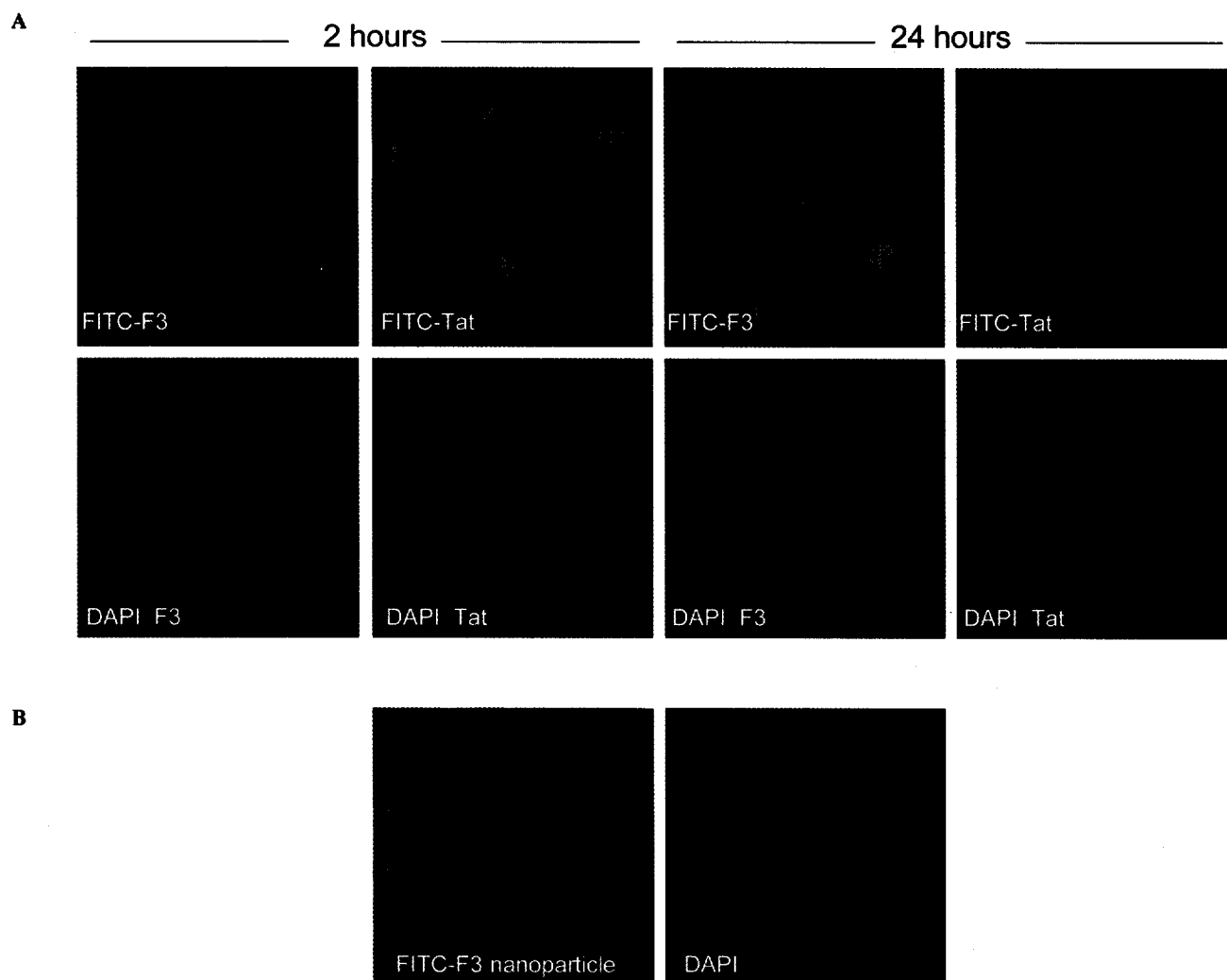


Fig. (1). Cell penetrating homing peptide. F3 is an example of recently isolated homing peptides that are internalized by their target cells. F3 binds to angiogenic endothelial cells and certain tumor cells. (A) Shown in the top panels is internalization of fluorescein-labeled F3 and Tat peptides by cultured human umbilical vein endothelial cells. Tat is found strongly internalized 2 hours after the addition of the peptide (2 μ M) to the culture, whereas F3 is slower. Bottom panels are corresponding images of cell nuclei labeled with DAPI. (B) When fluorescein-labeled F3 is coupled onto 50 nm magnetic nanoparticles, the particles are internalized by MDA-MB-435 tumor cells, but are excluded from the nucleus (left). Right panel shows the corresponding image of cell nuclei labeled with DAPI.

totic peptide with a homing peptide that binds to the blood vessels of the normal prostate yielded a compound that caused partial destruction of the normal prostate tissue [13]. Other laboratories have published similar data employing the same RGD and NGR homing peptides to target a different pro-apoptotic peptide or tumor necrosis factor. Dramatic decreases in tumor growth and suppression of toxic side effects was seen [35, 36]. Thus, the *in vivo* effects of these non-selectively toxic compounds can be altered to parallel the specificity of the homing peptide, dramatically illustrating the potential of the targeting technology.

The cell-penetrating homing peptides discussed in this review are potentially even better suited than the RGD and NGR motif peptides for the delivery of diagnostic probes or drugs into tumors. While we have only done limited testing of the new peptides in this regard, we know that they can

deliver a drug-like payload (fluorescein, rhodamine, or biotin), into the cell nucleus of tumor endothelial cells and tumor cells *in vivo* [4, 7, 8, 10]. The efficient entry of the new peptides into the target cells appears to concentrate the peptide in the tumor, making these peptides particularly efficient delivery vectors for tumor targeting. These internalizing peptides may prove to be particularly useful for delivering anti-cancer drugs that act in the nucleus or the cytoplasm.

ACKNOWLEDGEMENT

The authors' work was supported by the NIH grants CA 82713 and Cancer Center Support Grant CA 30199, and the DAMD 17-02-1-0315 Innovator Award from the Department of Defense (ER).



Fig. (2). Tumor imaging with LyP lymphatic homing peptides. Upper left panel: Fluorescein-labeled LyP-1 peptide (100 µg) was intravenously injected into mice bearing orthotopic MDA-MB-435 breast cancer xenografts. The mice were perfused through the heart about 10 min later and tumor sections were examined for fluorescence. The panel shows a lymphatic vessel (identified by podoplanin staining shown in red) in which LyP-1 fluorescence (green) has accumulated in the nuclei of the endothelial cells ([4]; reproduced with permission). Lower left panel: A tumor section from a mouse injected about 20 hrs earlier with 500 µg of LyP-1 peptide. At this time point, LyP-1 is seen in the nuclei of tumor cells in certain areas of the tumor (reproduced from [34]). Cell nuclei are stained with DAPI (blue). Upper right panel: The tumor accumulation of LyP-1b, a closely related variant of LyP-1, is so strong at 24 hrs after the injection that the tumors are visible in intact mice examined under blue light. Lower right panels: Injection of an unrelated control peptide (E3) produces no tumor fluorescence. Location of tumors is outlined in white.

REFERENCES

References 37-39 are related articles recently published in Current Pharmaceutical Design.

- [1] Ruoslahti E. Specialization of tumour vasculature. *Nature Rev Cancer* 2002; 2: 83-90.
- [2] Alitalo K, Carmeliet P. Molecular mechanisms of lymphangiogenesis in health and disease. *Cancer Cell* 2002; 1: 219-27.
- [3] Hanahan D, Weinberg RA. The hallmarks of cancer. *Cell* 2000; 100: 57-70.
- [4] Laakkonen P, Porkka K, Hoffman JA, Ruoslahti E. A tumor-homing peptide with a targeting specificity related to lymphatic vessels. *Nat Med* 2002; 8: 751-5.
- [5] Pasqualini R, Ruoslahti E. Organ targeting *in vivo* using phage display peptide libraries. *Nature* 1996; 380: 364-6.
- [6] Arap W, Pasqualini R, Ruoslahti E. Cancer treatment by targeted drug delivery to tumor vasculature in a mouse model. *Science* 1998; 279: 377-80.
- [7] Hoffman JA, Giraudo E, Singh M, Zhang L, Inoue M, Porkka K, *et al.* Progressive vascular changes in a transgenic mouse model of squamous cell carcinoma. *Cancer Cell* 2003; 4: 383-91.
- [8] Joyce JA, Laakkonen P, Bernasconi M, Bergers G, Ruoslahti E, Hanahan D. Stage-specific vascular markers revealed by phage display in a mouse model of pancreatic islet tumorigenesis. *Cancer Cell* 2003; 4: 393-403.
- [9] Ruoslahti E, Rajotte D. An address system in the vasculature of normal tissues and tumors. *Annu Rev Immunol* 2000; 18: 813-27.
- [10] Porkka K, Laakkonen P, Hoffman JA, Bernasconi M, Ruoslahti E. A fragment of the HMGN2 protein homes to the nuclei of tumor cells and tumor endothelial cells *in vivo*. *Proc Natl Acad Sci USA* 2002; 99: 7444-9.
- [11] Langel Ü. *Cell-Penetrating Peptides: Processes and Applications.*, CRC Press: Boca Raton, Florida 2002.
- [12] Essler M, Ruoslahti E. Molecular specialization of breast vasculature: A breast-homing phage-displayed peptide binds to aminopeptidase P in breast vasculature. *Proc Natl Acad Sci USA* 2002; 99: 2252-7.
- [13] Arap W, Haedicke W, Bernasconi M, Kain R, Rajotte D, Krajewski S, *et al.* Targeting the prostate for destruction through a vascular address. *Proc Natl Acad Sci USA* 2002; 99: 1527-31.
- [14] Hoffman J, Laakkonen P, Porkka K, Bernasconi M, Ruoslahti E. *In vivo* and *ex vivo* selections using phage-displayed libraries, Oxford University Press 2004.
- [15] Jacobson BS, Stolz DB, Schnitzer JE. Identification of endothelial cell-surface proteins as targets for diagnosis and treatment of disease. *Nat Med* 1996; 2: 482-4.
- [16] Ding BS, Zhou YJ, Chen XY, Zhang J, Zhang PX, Sun ZY, Tan XY, Liu JN. Lung endothelium targeting for pulmonary embolism thrombolysis. *Circulation* 2003; 108: 2892-8.
- [17] Oh P, Li Y, Yu J, Durr E, Krasinska KM, Carver LA, *et al.* Subtractive proteomic mapping of the endothelial surface in lung and solid tumours for tissue-specific therapy. *Nature* 2004; 429: 629-35.
- [18] Pasqualini R, Koivunen E, Kain R, Lahdenranta J, Sakamoto M, Stryhn A, *et al.* Aminopeptidase N is a receptor for tumor-homing peptides and a target for inhibiting angiogenesis. *Cancer Res* 2000; 60: 722-7.
- [19] Curnis F, Arrighi G, Sacchi A, Fischetti L, Arap W, Pasqualini R, *et al.* Differential binding of drugs containing the NGR motif to CD13 isoforms in tumor vessels, epithelia, and myeloid cells. *Cancer Res* 2002; 62: 867-74.
- [20] Ruoslahti E. Fibronectin and its receptors. *Annu Rev Biochem* 1988; 57: 375-413.
- [21] Wickham TJ. Targeting adenovirus. *Gene Ther* 2000; 7: 110-4.
- [22] Haviv YS, Blackwell JL, Kanerva A, Nagi P, Krasnykh V, Dmitriev I, *et al.* Adenoviral gene therapy for renal cancer requires retargeting to alternative cellular receptors. *Cancer Res* 2002; 62: 4273-81.
- [23] Ellerby HM, Arap W, Ellerby LM, Kain R, Andrusiak R, Rio GD, *et al.* Anti-cancer activity of targeted pro-apoptotic peptides. *Nat Med* 1999; 5: 1032-8.
- [24] Christian S, Pilch J, Akerman ME, Porkka K, Laakkonen P, Ruoslahti E. Nucleolin expressed at the cell surface is a marker of endothelial cells in angiogenic blood vessels. *J Cell Biol* 2003; 163: 871-8.

- [25] Deng JS, Ballou B, Hofmeister JK. Internalization of anti-nucleolin antibody into viable HEP-2 cells. *Mol Biol Rep* 1996; 23: 191-5.
- [26] Larrucea S, Gonzalez-Rubio C, Cambronero R, Ballou B, Bonay P, Lopez-Granados E, *et al.* Cellular adhesion mediated by factor J, a complement inhibitor. Evidence for nucleolin involvement. *J Biol Chem* 1998; 273: 31718-25.
- [27] Said EA, Krust B, Nisole S, Svab J, Briand JP, Hovanessian AG. The anti-HIV cytokine midkine binds the cell surface-expressed nucleolin as a low affinity receptor. *J Biol Chem* 2002; 277: 37492-502.
- [28] Sinclair JF, O'Brien AD. Cell surface-localized nucleolin is a eukaryotic receptor for the adhesin intimin-gamma of enterohemorrhagic *Escherichia coli* O157:H7. *J Biol Chem* 2002; 277: 2876-85.
- [29] Borer RA, Lehner CF, Eppenberger HM, Nigg EA. Major nucleolar proteins shuttle between nucleus and cytoplasm. *Cell* 1989; 56: 379-90.
- [30] Yu D, Schwartz MZ, Petryshyn R. Effect of laminin on the nuclear localization of nucleolin in rat intestinal epithelial IEC-6 cells. *Biochem Biophys Res Commun* 1998; 247: 186-92.
- [31] Shibata Y, Muramatsu T, Hirai M, Inui T, Kimura T, Saito H, *et al.* Nuclear targeting by the growth factor midkine. *Mol Cell Biol* 2002; 22: 6788-96.
- [32] Bonnet H, Filhol O, Truchet I, Brethenou P, Cochet C, Amalric F, *et al.* Fibroblast growth factor-2 binds to the regulatory beta subunit of CK2 and directly stimulates CK2 activity toward nucleolin. *J Biol Chem* 1996; 271: 24781-7.
- [33] Suzuki T, Futaki S, Niwa M, Tanaka S, Ueda K, Sugiura Y. Possible existence of common internalization mechanisms among arginine-rich peptides. *J Biol Chem* 2002; 277: 2437-43.
- [34] Laakkonen P, Akerman ME, Biliran H, Yang M, Ferrer F, Karpanen T, *et al.* Antitumor activity of a homing peptide that targets tumor lymphatics and tumor cells. *Proc Natl Acad Sci USA* 2004; 101: 9381-6.
- [35] Curnis F, Gasparri A, Sacchi A, Longhi R, Corti A. Coupling tumor necrosis factor-alpha with alphaV integrin ligands improves its antineoplastic activity. *Cancer Res* 2004; 64: 565-71.
- [36] Chen Y, Xu X, Hong S, Chen J, Liu N, Underhill CB, *et al.* RGD-Tachyplesin inhibits tumor growth. *Cancer Res* 2001; 61: 2434-8.
- [37] Brantley-Sieders D, Parker M, Chen J. Eph receptor tyrosine kinases in tumor and tumor microenvironment. *Curr Pharm Design* 2004; 10(27): 3431-42.
- [38] Haubner R, Wester HJ. Radiolabeled tracers for imaging of tumor angiogenesis and evaluation of anti-angiogenic therapies. *Curr Pharm Design* 2004; 10(13): 1439-55.
- [39] Stacker SA, Hughes RA, Achen MG. Molecular targeting of lymphatics for therapy. *Curr Pharm Design* 2004; 10(1): 65-74.

Cal

I. Ner

Institut
04103

Key W

INTRO

The
having
fostered
The tran
HIV Ta
Drosoph
[3]. So
number

It ha
has cell-
nasal ap
shown b
very eff
Human c
amino ac
gland (se
question
owing to
evidence
benefit t
widely us
Miacalcin
in hypoc
diseases l

Recen
(see Fig.
epitheliu
lacking [9
hCT-deriv

The m
penetratin

*Address co
Brüderstraße
97-36909; E-

Lymphatic Zip Codes in Premalignant Lesions and Tumors

Lianglin Zhang¹, Enrico Giraudo^{2,4}, Jason A. Hoffman^{3,5}, Douglas Hanahan^{2,6}
and Erkki Ruoslahti^{1,6}

1. Cancer Research Center, Burnham Institute for Medical Research, 10901 North Torrey Pines Road, La Jolla, CA 92037, USA
2. Department of Biochemistry and Biophysics, and the Diabetes and Comprehensive Cancer Centers, University of California at San Francisco, 513 Parnassus Avenue, San Francisco, CA 94143, USA
3. Program in Molecular Pathology, Burnham Institute for Medical Research and Department of Pathology, University of California San Diego, School of Medicine, 9500 Gilman Drive, La Jolla, California 92093, USA
4. Present address: Division of Molecular Angiogenesis, Institute for Cancer Research and Treatment (IRCC) and Department of Oncological Sciences, University of Turin, Str. Prov. 142 Km.3.95, 10060 Candiolo, Turin, Italy.
5. Present address: Genomics Institute of the Novartis Research Foundation, 10675 John Jay Hopkins Drive, San Diego, California 92021, USA
6. Please address correspondence to:
Erkki Ruoslahti (ruoslahti@burnham.org)
or Douglas Hanahan (dh@biochem.ucsf.edu)

ABSTRACT

Blood vessels in tumors are morphologically and functionally distinct from normal resting blood vessels. We probed lymphatic vessels in premalignant lesions and tumors by *in vivo* screening of phage-displayed peptide libraries, asking whether they too have distinctive signatures. The resulting peptides begin to define such signatures. One peptide identified the lymphatics in a human melanoma xenograft. Another recognized the lymphatics in prostate cancers, but not in premalignant prostate lesions; this peptide similarly identifies human prostate cancer lymphatics. A third was selective for the lymphatics in the premalignant prostate lesions. A fourth identified the lymphatics in dysplasias and squamous carcinomas of the cervix and skin. None recognize lymphatics in normal tissues. Thus, tumor development is associated with organ- and stage-specific changes in lymphatics. Systemic treatment of mice with fusions of a lymphatic homing peptide and a pro-apoptotic motif reduced the number of tumor lymphatics in prostate tumor and melanoma, forecasting future lymphatic targeting agents for detection and therapeutic intervention.

INTRODUCTION

The endothelial lining of blood vessels is highly diversified. Many, and perhaps all normal tissues impart a tissue-specific “signature” on their vasculature, and tumor vessels differ from normal vessels both in morphology and molecular composition (1). Tumors induce angiogenesis to support expansive growth (2) and many of the changes in tumor vessels are angiogenesis-related (3-6). Moreover, tumor blood vessels have tumor type-specific and, in some stages, stage-specific characteristics; *in vivo* screening of phage libraries has yielded distinct sets of homing peptides selectively recognizing angiogenic signatures in two transgenic mouse models of organ specific tumorigenesis. Homing peptides can also distinguish the angiogenic blood vessels of premalignant lesions from those of fully malignant lesions in the same tumor model (7, 8), indicating that vascular changes mirror the stage of tumor development.

The lymphatic system constitutes a second vascular system, one that has only an efferent arm. Tumors frequently induce lymphangiogenesis, as well as co-opt existing lymphatics (9-11). Tumors may contain intratumoral lymphatics, but, more commonly, an extensive network of lymphatic vessels is present around tumor tissue (12-14). The lymphatics within tumors, when present, are generally non-functional in fluid transport (14), possibly reflecting compression by interstitial pressure and blockage by intraluminal tumor cells. The lymphatic vessels in and around tumors are an important conduit of metastasis. Indeed, growth factor-stimulated enhancement of lymphatic vessel expression in tumors increases metastasis (15, 16). Conversely, inhibiting lymphangiogenesis suppresses lymphatic metastasis, but generally does not affect tumor growth (17).

A peptide that selectively binds to the endothelial cells of lymphatics associated with a xenotransplanted human breast tumor has been described (13). This was the first demonstration that tumor lymphatics can differ from normal lymphatics, but the larger question of whether tumor lymphatics are generally distinguishable from normal lymphatics has been unanswered.

Here, we identify homing peptides that specifically recognize tumor lymphatics or lymphatics in premalignant lesions in a set of distinctive organ-specific tumor models in mice. Our results show that tumor lymphatics, like tumor blood vessels, express specific markers, and that these lymphatic markers are tumor type-specific and distinct from blood vessel markers in the same tumors. The tumor-specific lymphatic vessel markers may be useful in early detection and tumor targeting.

EXPERIMENTAL PROCEDURES

Cell lines, mice, and tumors

The following cell lines were maintained in DMEM supplemented with 10% FCS: C8161 human melanoma, MDA-MB-435 human breast cancer, KRIB human osteosarcoma,

and human prostate cancer cells PPC1 and DU145. LNCaP human prostate cancer cell line was grown in RPMI 1640 medium with 10 mM HEPES, 1 mM sodium pyruvate and 1.5 g/L sodium bicarbonate supplemented with 10% FCS. M12 human prostate cancer cell line was cultured in RPMI 1640 with 5 µg/ml insulin-transferrin-sodium selenite (ITS), 2.5 µg/ml fungizone, 50 µg/ml gentamycin, 0.2 µM dexamethasone, 10 ng/ml epidermal growth factor (EGF), and 5% FCS (18). To produce tumors, nude BALB/c and C56BL/6 mice were subcutaneously (C8161, KRIB, and PPC1) or orthotopically (MDA-MB-453, PPC1, DU145, M12, and LNCaP) injected with 1×10^6 tumor cells. Transgenic mouse tumor models included TRAMP prostate cancer, MMTV-PyMT breast cancer, and K14-HPV16 cervical cancer. To initiate cervical carcinogenesis, female K14-HPV16 mice (19) were treated with 17β -estradiol [E_2 ; (20, 21)]. Briefly, one-month-old virgin female transgenic (heterozygous K14-HPV16, 1203#1) and nontransgenic (FVB/n) mice were anesthetized with isoflurane, and continuous release pellets that deliver E_2 at doses of 0.05 mg over 60 days (Innovative Research of America, Sarasota, Florida, USA) were implanted subcutaneously in the dorsal back skin. Subsequent pellets were implanted at 3 and 5 months of age for a total of 6 months of hormone treatment. K14-HPV16 mice were maintained in the FVB/n background (FVB/n; The Jackson Laboratory, Bar Harbor, ME). The mice were maintained in accordance with the University of California, San Francisco (UCSF) institutional guidelines governing the care of laboratory mice. The animal experimentation was approved by Animal Research Committees at UCSF or Burnham Institute for Medical Research.

Phage library and screening

An NNK-encoded CX7C library display on T7Select415-1 phage (Novagen, Madison, WI) was prepared as previously described (13). Phage selection and validation have been described (22). A two-step procedure was designed for the selection of peptides targeting the tumor lymphatic vessels of premalignant prostate lesions and prostate tumor. First, the phage library was incubated with cells derived from normal prostate to subtract the phage that bind to normal prostate. Second, the anti-podoplanin magnetic

beads were used to isolate lymphatic endothelial cells. We performed 2-3 rounds of *ex vivo* selection and 2-3 rounds of *in vivo* selections.

For the *ex vivo* selections, cell suspensions were prepared from normal prostates of tumor-free littermates of TRAMP mice, premalignant prostates of 14- to 16-week-old TRAMP mice, and tumor tissues of 25- to 28-week-old TRAMP mice. The C57BL6 TRAMP mice display mild to severe hyperplasia by the time they are 12 weeks of age, and severe hyperplasia has developed by 18 weeks (23, 24). Thus, the premalignant lesions of prostate we used represent a mixture of mild or severe hyperplasia.

Collagenase IA (1 mg/ml; Sigma, St. Louis, MO) was used to disperse the tissues. About 1×10^7 normal prostate cells were incubated at 4°C for 3 hrs with 5×10^{10} plaque forming units (pfu) of T7 phage displaying a CX7C peptide library. The samples were centrifuged at 1200 rpm for 10 min, the supernatant (the normal prostate-subtracted phage library) was recovered and then incubated overnight at 4 °C with 5×10^7 cells derived from premalignant prostate tissue or prostate tumor. The cells were washed to remove unbound phage, incubated with rat anti-mouse podoplanin for 45 min at 4°C, and washed three times with cold PBS containing 0.5% BSA. Podoplanin-positive cells were then isolated using M450 sheep anti-rat IgG Dynabeads (M450; Dynal, Oslo, Norway). Phage that bound to the podoplanin-positive cell population were rescued and amplified in *E.coli*. *In vivo* phage library screening was performed as described (13).

Homing specificity of phage

In vivo homing specificity of phage was tested as described (22). Briefly, mice bearing tumors were anesthetized and intravenously injected with 5×10^9 pfu of phage. After 7 min, the mice were perfused through the heart with PBS containing 0.5% BSA. The tumor and control organs were dissected from each mouse and the phage were rescued and tittered. For histology analysis, the mice were perfused with 4% PFA 30 min after the injection of phage. Tissues were embedded in Tissue-Tek O.C.T. and 5 µm sections were prepared for phage immunostaining.

Antibodies and immunohistology

Custom immunization to produce a rabbit antiserum against mouse Prox-1 was performed by Proteintech Inc. New Zealand White rabbits were immunized with a fusion protein of GST-C-terminal fragment of Prox-1 protein. The antibody was affinity purified on the fusion protein and absorbed with GST. The resulting antibody preparation (1.8 mg/ml) gave a titer of 1:10,000 against the fusion protein in ELISA. Immunofluorescence staining of tissue sections with the anti-Prox-1 antibody gave a pattern of nuclear staining. Antibodies against the lymphatic markers anti-LYVE-1 (13) and anti-podoplanin (kindly provided by T. Petrova and K. Alitalo), rat monoclonal anti-mouse CD31 (BD Pharmingen, San Diego, CA), rat anti-mouse MECA-32 (Pharmingen), rabbit polyclonal anti-T7 phage, rabbit anti-mouse cleaved caspase-3 (ASP175) (Cell Signaling Technology, Danvers, MA) and rat anti-mouse VEGFR3 (provided by H. Kubo and K. Alitalo) were used for immunohistochemical staining of frozen tissue sections as described (8, 13).

The corresponding secondary antibodies were added and incubated for 1 hr at room temperature: AlexaFluor-488 goat anti-rat or rabbit IgG (1:1000; Molecular Probes, Eugene, OR), AlexaFluor-594 goat anti-rat or rabbit IgG (1:1000, Molecular Probes), AlexaFluor-594 donkey anti-mouse or goat IgG (1:1000, Molecular Probes), and AlexaFluor-488 donkey anti-mouse or goat IgG (1:1000; Molecular Probes). The slides were washed three times with PBS and mounted in Vectashield Mounting Medium with DAPI (Vector Laboratories, Burlingame, CA). Blood vessels were also visualized by intravenously injecting *Lycopersicon esculentum* (tomato) lectin conjugated to fluorescein (100 µg of lectin in 200 µl of PBS; Vector Laboratories).

Tissue distribution of fluorescein-labeled peptides (25) was studied by intravenously injecting the peptide (100-150 µg in 200 µl PBS) into the mice. The injected peptides were allowed to circulate 30 min to 2 hrs, and the mice were perfused with 4% paraformaldehyde through the left ventricle of heart. Tissues were dissected and frozen in OCT embedding medium (Tissue-Tek, Elkhart, IN). The frozen sections were prepared for immunohistological analysis.

Peptide synthesis

Peptides were synthesized in our peptide facility, using Fmoc chemistry in a solid-phase synthesizer. The peptides were purified by HPLC and confirmed by mass spectrometry. Fluorescein-conjugated peptides were synthesized as described (25). The LSD and REA peptides were synthesized as the chimera with the pro-apoptotic motif $D(KLAKLAK)_2$ (26).

Targeted proapoptotic peptide treatment of tumor-bearing mice

Prostate cancer model. Orthotopic xenografted prostate tumors were established by injecting 1×10^6 PPC1 human prostate cancer cells into the mouse prostate. Fifteen days post inoculation, the mice were intravenously injected with $D(KLAKLAK)_2$ -CREAGRKAC, an equimolar mixture of $D(KLAKLAK)_2$ and CREAGRKAC, or PBS. Mice were given 200 μ g of the conjugate per week divided into two injections (26, 27) .

Melanoma model. Nude BALB/c mice were subcutaneously injected with 1×10^6 C8161 human melanoma cells. Treatment started when mean tumor volumes reached about 100 mm³. Mice with size-matched tumors were randomized into three groups. The therapeutic group received a chimera of tumor homing peptide with the proapoptotic motif [$D(KLAKLAK)_2$ -CLSDCGKRKC]. The control groups received an equimolar mixture of CLSDGKRKC and $D(KLAKLAK)_2$, or PBS alone. The tumor-bearing mice were intravenously injected with 200 μ g/dose/mouse once a week for three weeks (26, 27).

The mice were monitored for weight loss, and tumors were dissected and weighed at the termination of the experiment. Histological analysis was performed to evaluate the density of tumor lymphatics and blood vessels. Apoptotic lymphatic endothelial cells were visualized by double staining with anti-cleaved caspase-3 and anti-podoplanin antibodies. The animal experiments reported here were approved by the Animal Research Committee of Burnham Institute for Medical Research.

Phage overlay of tissue sections from human cancer

The frozen sections of human prostate tumor specimens were obtained from Dr. Daniel Mercola (Sidney Kimmel Cancer Center, La Jolla, CA). The sections (5 μm) were pre-incubated with blocking buffer (5% normal goat serum and 0.5% BSA in 1xPBS) for 1 hr at room temperature, washed three times with diluted blocking buffer (1:10), and phage (3×10^9 pfu) were incubated on the section for 4 hrs. After 3 washes, rabbit anti-phage antibody (10 $\mu\text{g}/\text{ml}$) was added and the phage incubated for 2 hrs. The slides were washed and incubated with AlexaFluor-488 goat anti-rabbit IgG for 1 hr. After further washes, the slides were mounted with Vectashield (Vector Laboratories).

Statistical analysis

Student's t test was used in statistical analysis of the results. The bar diagrams show mean and standard deviation.

RESULTS

Phage targeting of lymphatics in C8161 melanoma

We chose the C8161 human melanoma as the first topic because xenografts of tumors generated with this cell line in nude mice contain lymphatic vessels that are not recognized by the homing peptide LyP-1, which binds to lymphatic endothelial cells in breast carcinomas (13). Our experimental design was aimed to determine whether lymphatic homing peptides having analogous specificity for the melanoma-associated lymphatics could be identified. We modified our earlier protocols to increase the probability of obtaining peptides that recognize tumor lymphatics. We incubated a phage display library with a cell suspension of whole C8161 tumor tissue, allowing phage to bind, and then used immuno-magnetic beads to isolate lymphatic endothelial cells that carried along any phage bound to these cells. This enrichment step yielded a phage pool that bound 250-fold more efficiently to the isolated cells than nonrecombinant phage (Fig. S1A). The enriched phage pool was used in subsequent *in vivo* rounds to select phage that homed to C8161 xenograft tumors. Two rounds of selection *in vivo* produced a 40-fold enrichment of phage (Fig. S1B). There was no enrichment in the several control organs tested.

The 48 phage clones from the second *in vivo* round of phage pool selection included five clones that appeared most frequently, and these were analyzed further. Two clones displaying peptides with related amino acid sequences (CLSDGKRKC and CLDGGRPKC) bound to cell suspensions prepared from C8161 tumors; the stronger binder, CLSDGKRKC, bound 100-fold more than control phage. Intravenous injection of phage into nude mice bearing C8161 tumors showed that both phage homed selectively to the tumors; CLSDGKRKC was about twice as efficient as CLDGGRPKC (the results for CLSDGKRKC are shown in Fig. 1A). The CLSDGKRKC peptide (referred to below as LSD) was chosen for further study.

To establish that the homing ability of LSD phage is due to the displayed peptide sequence, we chemically synthesized the peptide as a fluorescein-conjugate peptide and intravenously injected the conjugate into C8161 tumor mice. After 2 hrs of circulation, the peptide was detected within the tumors (Fig. 1B), but not in control organs (Fig. S1C). Staining of tissue sections with the lymphatic vessel markers podoplanin, Prox-1, LYVE-1, and VEGFR3, showed colocalization of the LSD fluorescence with them (Fig. 1C), whereas there was no colocalization with the blood vessel markers MECA-32 and CD31 (Fig. 1D). Quantification showed that 85% of the lymphatic vessels that were positive for the peptide were also positive for podoplanin.

We further tested the homing of LSD phage to other types of cancer, including the MDA-MB-435 human breast cancer xenografts recognized by the previously described lymphatic homing peptide, LyP-1 (13). Intravenously injected LSD phage did not appreciably home to MDA-MB-435 tumors (see below). These data show that LSD-peptide selectively homes to the lymphatic vessels in C8161 melanoma.

Phage targeting of lymphatics in premalignant lesions and tumors of prostate

Seeking to further generalize the proposition that tumor-associated lymphatics might have organ specific signatures, we selected lymphatic homing peptides in the TRAMP transgenic mouse model of *de novo* prostate carcinogenesis (28). Immunohistochemical

analysis had revealed abundant lymphatics associated both with premalignant lesions and tumors in this model (Fig. S2A). As it is possible to access premalignant lesions in this system, we also explored the possibility of distinguishing the lymphatics of such lesions from those of fully developed tumors. We studied TRAMP mice inbred into C57BL6, a genetic background wherein prostate tumorigenesis occurs over a 30 week time course to terminal disease, with a discernable premalignant phase (~10-20 weeks).

To isolate peptides that selectively home to fully developed tumors in the TRAMP model, we first pre-treated the phage library with cell suspensions derived from normal prostate to decrease the abundance of phage that bind to normal prostate. The normal prostate-subtracted library was then enriched by two rounds of *ex vivo* selection on lymphatic endothelial cells immuno-purified from tumors of 25- to 28-week-old TRAMP mice. Three subsequent *in vivo* selection rounds yielded a phage pool that showed nearly 50-fold enrichment for tumor homing. Five peptide sequences were represented more than once in this pool. Three of these phage clones with amino acid sequences CREAGRKAC, CSMSAKKKC, and CKTRVSCGV showed robust binding to tumor-derived cell suspensions and were further tested *in vivo*. Intravenously injected CREAGRKAC phage became 50-fold enriched in TRAMP tumors relative to nonrecombinant phage, while the other two phage showed about 30-fold enrichment. We chose the CREAGRKAC (REA) for further study.

To screen for peptides recognizing the premalignant lymphatics, we first treated the phage library with cell suspensions derived from normal prostate, and the subtracted library was then enriched on immuno-purified lymphatic endothelial cell suspensions derived from prostates containing premalignant lesions, so called prostatic intraepithelial neoplasia, or PIN (in 14- to 16-week-old mice). The sequential *ex vivo* selections yielded a phage pool that was 60-fold enriched for binding to the target cells, and a 30-fold enrichment for homing to prostate with PIN lesions was obtained in a subsequent *in vivo* selection. Five phage clones were chosen for evaluation of *in vivo* homing based on their frequent appearance among 64 clones sequenced (32 clones each from the second *ex vivo* round and the third *in vivo* round). Of these, three clones with amino

acid sequences CAGRRSAYC, CASLSCR, and CSGGKVLDC, bound to cell suspension derived from PIN lesions (data not shown). These candidates were further tested *in vivo* individually. Phage displayed peptides CAGRRSAYC, CSGGKVLDC, and CASLSCR showed 24-, 14-, and 12-fold enrichment to PIN lesions relative to nonrecombinant phage, respectively. The CAGRRSAYC (AGR) was chosen for further study.

To evaluate the specificity of the REA and AGR peptides, we intravenously injected the phage into TRAMP mice with either premalignant PIN lesions or prostate tumors, or into their tumor-free (transgene negative) male littermates with normal prostates. The results showed that the REA phage homes to tumors, but not to PIN lesions or normal prostate, whereas the AGR phage homes only to PIN (Fig. 2A). Neither phage was found in other tissues, including lymph nodes, kidneys, lungs, skin, or intestine, at levels higher than the nonrecombinant control phage.

In vivo distribution of fluorescein-conjugated REA and AGR peptides after intravenous injection confirmed the phage results. The REA peptide accumulated in prostate tumors, showing 90% overlap with podoplanin-positive lymphatic vessels, whereas PIN lesions, normal prostate (Fig. 2B), and control organs (Fig. S2B) were negative. The AGR peptide selectively homed to PIN lesions, but little or no peptide was seen in prostate tumors, normal prostate tissue (Fig. 2B), or in control tissues (Fig. S2C).

To study the association of REA and AGR peptides with the vasculature, the phage or fluorescein-labeled peptides were intravenously injected into TRAMP mice, and phage and peptide localization was compared to lymphatic and blood vessel markers localized with antibodies. The phage and their cognate peptides each showed substantial colocalization with the lymphatic markers podoplanin, VEGFR3, LYVE-1, and Prox-1 in their respective lesions, whereas their localization was entirely distinct from that of the blood vessel markers CD31 and MECA-32. The overlap of the peptides with Prox-1 was less obvious than with the other markers, presumably because Prox-1 is nuclear,

whereas the peptides associate with the cell membrane. The results for the REA and AGR peptides are shown in Figures 2C and D, and for the REA phage in Figure S2D.

Homing peptide for lymphatic vessels in cervical cancer

In a previous study from our laboratories, we identified a homing peptide for dysplastic skin lesions in K14-HPV16 transgenic mice, which develop skin cancers (7). This peptide, CNRRTKAGC, is similar to LyP-1 (CGNKRTRGC), which selectively recognizes lymphatic vessels and tumor cells in breast cancers (13). Because of this similarity, we asked whether the CNRRTKAGC peptide (LyP-2) also recognizes tumor lymphatics. We tested the LyP-1 and LyP-2 peptides in skin and cervical cancers of the K14-HPV16 transgenic mice. In addition to spontaneously developing angiogenic dysplasias and then squamous cell carcinomas of the skin (Coussens et al 1996), female K14-HPV16 mice develop cervical cancers when their normally cyclic estrogen levels are sustained with time release pellets (20). The estrogen-treated females undergo neoplastic progression in the cervix mimicking, that inferred for human cervical carcinogenesis (20, 21, 29). The premalignant cervical lesions (also called cervical intraepithelial neoplasia, CIN) and cervical tumors of these mice contain abundant lymphatic vessels as detected by immunostaining for lymphatic markers (Fig. S3A).

Intravenously injected LyP-2 phage showed robust homing both to the premalignant and malignant lesions in the cervix, but not to normal cervix (Fig. 3A). Fluorescein-labeled LyP-2 peptide also accumulated in the cervical lesions, colocalizing with LYVE-1 (Fig. 3B, upper panels) and podoplanin (82% overlap; data not shown), but not with MECA-32 (Fig. 3B, lower panel). Additionally, occasional foci of scattered cells in the stroma were labeled, with some apparent intracellular localization; the identity of these cells is currently unresolved. No peptide accumulation was observed in normal cervix (Fig. 3B) or in other control tissues, either in lymphatics or in non-vascular cells (Fig. S3B). LyP-2 also homed to the lymphatics associated with dysplasias and squamous cell carcinomas of the skin in male and female K14-HPV16 mice, but not to normal skin lymphatics (data not shown).

Specificity of lymphatic homing-peptides for different types of tumors

Having isolated phage-displayed peptides that homed to the lymphatics of melanoma, prostate, or cervix (the origin and specificity of these peptides is summarized in Table 1), we asked whether they recognized common determinants of the tumor-associated lymphatic vasculature or organ/tumor selective signatures. The lymphatic homing peptides derived from the different tumor models were tested for their ability to recognize the lymphatics of other tumors. Intravenously injected LSD phage did not home to xenotransplant tumors derived from the MDA-MB-435 breast tumor cell line (Fig. 4A, left panel). This phage also did not appreciably home to transgenic mouse tumors of the breast or prostate, or to PPC1 human prostate cancer xenografts; possible low-level homing was seen to squamous carcinomas of the skin in K14-HPV16 mice, and to KRIB human osteosarcoma xenografts. *In vivo* injection of fluorescein-labeled LSD peptide followed by histological analysis of peptide distribution, agreed well with the phage results. As shown in Figure 4A (right panel), strong LSD peptide fluorescence was seen in the C8161 derived tumors, the model in which the peptide was selected. The C8161 tumors were positive in nude mice representing two different genetic backgrounds (BALB/c and C57BL/6; shown for the BALB/c strain in Figure 4A, right panel). In agreement with the phage data, KRIB tumors were weakly positive with the fluorescent peptide, and the other tumors, including the skin cancers, were negative. These results show that the LSD peptide selectively recognizes the lymphatics in the C8161 melanoma-derived tumors.

To profile the homing peptide specificity of the AGR peptide in different types of premalignant lesions, we used three transgenic mouse models: TRAMP, K14-HPV16/E₂, and MMTV-PyMT, which respectively develop prostate, cervical, or breast neoplasias that subsequently progress to overt cancer. Both AGR phage (Figs. 2A and 4B) and fluorescent peptide (Figs. 2B and D) showed marked preference for the PIN lesions in TRAMP mice; there was little homing of the phage and no detectable homing of the peptide to similar premalignant lesions or malignant tumors in the other two models (Figs. 4B and S2G).

The REA phage, which was identified in the TRAMP model, also homed to xenografts obtained by orthotopically inoculating into nude mice cells from the human prostate cancer cell lines PPC1, M12, DU145, and LNCaP (Fig. 4C). These xenografted tumors were also positive with the fluorescein-conjugated REA peptide (the results for PPC1 are shown in Fig. 4D). In contrast, the MDA-MB-435, C8161, and KRIB xenografts, as well as the *de novo* breast and skin cancers arising in MMTV-PyMT or K14-HPV16 mice, respectively, were negative for REA binding (Fig. 4C and D). The cervical tumors of K14-HPV16/E₂ mice were slightly positive for REA peptide binding, but markedly less so than the prostate tumors. Immunohistochemical analysis showed that FITC-REA peptide colocalized with lymphatic vessels both within tumor tissues (Fig. 4D, first row, middle panel) and tumor periphery (Fig. 4D, first row, right panel). This was the case with orthotopic prostate tumor xenografts arising from multiple human prostate tumor-derived cell lines (results for PPC1 tumors are shown in Fig. 4D). This peptide homed to a lesser extent to K14-HPV16/E₂ cervical tumors (Fig. 4D). Interestingly, REA-phage homed less efficiently to subcutaneous xenografts of PPC1 than to orthotopic xenografts of the same tumor cell line (Fig. S2E). The REA-phage strongly bound to PPC1 tumor-derived cell suspensions, but did not bind to cultured PPC1 cells (Fig. S2F). Thus, REA appears to primarily recognize prostate cancer lymphatics.

We also asked whether the REA peptide recognizes human prostate cancers, by using phage overlay of tissue sections. Immunohistochemical staining with antibodies against lymphatic markers Prox-1 and podoplanin revealed abundant lymphatic vessels in human prostate tumors (Fig 4D, bottom row, red). Overlay of tissue sections from two primary human prostate cancers with REA phage indicated that this phage recognizes the lymphatics of human prostate tumors (Fig 4D, bottom row, green). The AGR phage did not bind to the human tumor sections (not shown).

LyP-1 and LyP-2 have different specificities

Given the similar amino acid sequences of the LyP-1 and LyP-2 peptides, and the fact that they both bind to tumor lymphatics, we were interested in comparing their specificities. Surprisingly, these peptides recognize different tumors. While both

peptides homed to the K14-HPV16 skin cancer lymphatics (data not shown), LyP-1 phage homed to MDA-MB-435 breast tumors growing s.c. but not to the *de novo* cervical tumors, whereas the opposite was true of LyP-2 (Fig. 5A). Neither phage homed to the normal cervix or normal breast tissue. To confirm these differences in specificity, we co-injected one peptide as a fluorescein conjugate and the other conjugated to rhodamine, and vice versa. Both LyP-2 conjugates homed to cervical tumors, whereas neither LyP-1 conjugate did so. The opposite result was obtained when the same conjugates were tested in MDA-MB-435 tumor-bearing mice (Fig. 5B). These data indicate that different binding sites exist for the two LyP peptides in different types of tumors.

Lymphatic homing peptide conjugates destroy tumor lymphatics

One potential application of peptides that home and bind to the distinctive lymphatic vasculature of tumors is to target delivery of toxic payloads aiming to disrupt the tumor lymphatics, thereby assessing their functional importance and prospects as a therapeutic target. We began this assessment by linking two of our signature-finding peptides to a toxic agent, assessing its effects on the tumor lymphatics. As a toxic agent, we used conjugates with an apoptosis-inducing peptide, $_D(KLAKLAK)_2$. In a previous study, this peptide was linked to blood vascular tumor-homing peptides and shown to be selectively cytotoxic to angiogenic endothelial cells and to have demonstrable anti-tumor activity (26). To determine whether peptides recognizing tumor lymphatics could be used to target those lymphatics, we synthesized the REA and LSD peptides as conjugates with $_D(KLAKLAK)_2$ and systemically treated mice bearing PPC1 or C8161 xenografts.

Treatment with the REA conjugate had no effect on tumor blood vessel density in the PPC1 tumors, but significantly reduced the number of tumor lymphatics; the uncoupled mixture had no effect on the lymphatics compared to the PBS control (Fig. 6A). The conjugate had no effect on tumor growth (Fig. 6B), indicating (perhaps not surprisingly) that the tumor-associated lymphatics were not essential for primary tumor growth. Examination of lymphatics in normal skin revealed no discernible effect by the REA or

LSD conjugates, and no significant differences were observed in the weight of the mice belonging to the various treatment groups, indicating lack of general lymphatic effects or overt toxicity (data not shown). Reduced density of tumor lymphatics was also seen in C8161 melanoma xenografts of mice treated with the LSD conjugate (data not shown).

To study the mechanism of the lymphatic disruption by the REA conjugate, we examined the frequency of apoptosis in lymphatic endothelial cells in PPC1 tumors using caspase-3, as a marker. The tumors of the mice treated with the REA conjugate had a significant increase in lymphatic endothelial cells expressing active caspase-3 compared to tumors of mice treated with PBS, REA, or a mixture of REA and $D(KLAKLAK)_2$ (Fig. 6C). These data indicate that the REA conjugate reduced the lymphatic vessel counts by inducing apoptosis in lymphatic endothelial cells.

DISCUSSION

In this paper, we demonstrate an extensive heterogeneity of tumor lymphatics. We have identified peptides that recognize the lymphatics of individual tumor types, including transgenic mouse tumors arising *de novo* in different organs, as well as human tumor xenografts. We also describe a peptide that distinguishes the lymphatics of premalignant prostatic lesions, both from normal lymphatics and from those of fully developed tumors in the same transgenic mouse model of prostate carcinogenesis. The lymphatic markers detected by the homing peptides are specific for lymphatic vessels, i.e. the peptides do not bind to the blood vessels of the same tumors or premalignant lesions. Several prostate cancers shared the same lymphatic marker. These results show that the lymphatics express a zip code system that is akin to the one in blood vessels, but distinct from it. In beginning to assess the applications of this knowledge, we showed that systemic treatment of tumor-bearing mice with a lymphatic homing peptide linked to a pro-apoptotic compound could selectively destroy tumor lymphatics.

We employed a new screening method based on the immuno-isolation of lymphatic endothelial cells from whole tumor cell suspensions that had been preincubated with

phage display libraries, thereby enriching for phage bound to this rare cell type. This method allowed us to focus on the selection of phage displayed peptides that identify specific features in the lymphatics of the target tissue. We show in each of the tumor models that peptides strongly represented in the selected phage pools specifically homed to tumors, and extensively colocalized with markers of lymphatic endothelial cells in the tumor tissue after an intravenous injection. In contrast, there was no colocalization with blood vessel endothelial markers. Co-staining with the lymphatic markers LYVE-1, podoplanin, Prox-1, and VEGFR3, were consistent in supporting this result. The use of multiple markers is an important standard, as none of the lymphatic endothelial markers is completely specific for lymphatics (30, 31). In aggregate, however, they provide strong evidence for a lymphatic vessel identity of the structures our peptide recognizes in tumors.

We have now demonstrated lymphatic vessel specialization in every one of the 5 tumor types studied. These tumors consisted of xenograft models of melanoma, breast, and prostate carcinomas, as well as transgenic mouse models developing prostate, skin, and cervical cancers. In addition, the LSD, REA, and LyP peptides each recognized tumor lymphatics in more than one inbred mouse strain. For example, the REA peptide homed to prostate cancers in TRAMP mice (C57BL/6 background) and prostate cancer xenograft tumors grown in nude mice (BALB/c), demonstrating that their specificity is not limited to any given mouse strain. Previous studies have defined a peptide that distinguishes the lymphatics of MDA-MB-435 breast cancer xenografts tumors from normal lymphatics (13, 25). The present results show that such molecular specialization of tumor lymphatics is not limited to this tumor, but is likely to be a generalized phenomenon. The peptides we identified in this study as being specific for lymphatic vessels in the various tumor models were essentially specific for the tumor type used in the screening. Interestingly, the only other tumors with lymphatics recognized by the TRAMP tumor-homing peptide REA were xenograft tumors generated with 4 different human prostate cancer cell lines. This result suggests that the changes detected by our peptides in tumor lymphatics may be tumor type-specific. Similar experiments with tumor blood vessels have revealed two classes of peptides

identifying signatures of the angiogenic neovasculature. One pan-specific class recognizes markers that are generally associated with angiogenesis in most tumor types and organs (1, 4, 32, 33), while a second class of peptides detected tumor-type-specific vascular signatures (7, 8). While we did not isolate any peptides that identified pan-specific markers of tumor (but not normal) lymphatics, we anticipate additional screens could reveal such entities.

Stage-specific lymphatic signatures during tumorigenesis

We obtained two stage-specific lymphatic-homing peptides using different neoplastic lesions in the TRAMP model. The REA peptide selectively recognizes the lymphatics in fully developed TRAMP tumors, whereas the AGR peptide was only reactive with the lymphatics in PIN lesions. Our laboratories have previously obtained homing peptides that distinguish the blood vessels of premalignant lesions from normal blood vessels and those of malignant tumors arising subsequently in the same transgenic mouse models (7, 8). The present results suggest that lymphatic vessels display a similar evolution of molecular specificities as tumorigenesis progresses.

A prospective family of lymphatic signatures?

The mutually exclusive tumor specificity of the LyP-1 and LyP-2 peptides is interesting given the close sequence similarity of these peptides (CGNKRTRGC versus CNRRTKAGC). LyP-1 recognizes lymphatics and tumor cells in MDA-MB-435 and MMTV-PyMT breast cancers (8). Careful comparison of the ability of the two peptides to accumulate in MDA-MB-435 tumors and cervical carcinomas after intravenous injection showed that MDA-MB-435 tumors were positive for LyP-1, whereas cervical carcinomas were not, while LyP-2 had the opposite specificity. Interesting, both peptides bound to other cell types in the neoplastic lesions: LyP-1 binds to and is internalized by breast tumor cells, whereas LyP-2 binds to scattered cells in the neoplastic cervix. The bases for and implications of these distinctive lymphatic and non-lymphatic binding specificities are presently unclear, and deserve future investigation. We have encountered a third peptide in the LyP series, CNKRTRGGC. We did not include that peptide in this study, but its specificity appears to parallel that of

LyP-1 (25). Comparison of the 3 sequences indicates that shifting the glycine residue from the N-terminal to the C-terminal end is not important to the specificity of the peptide, but that the arrangement of the basic residues in the K/RRTR/K motif can alter specificity. Our attempts to identify the binding molecules (receptors) for the LyP peptides (and indeed for other of the lymphatic signature-finding peptides identified in this study) have not been successful thus far, and this remains an agenda for future studies. The closely related sequences of the LyP peptides predict the existence of a family of related receptors with tumor type-specific expression in lymphatics. The distinctive specificity of peptides containing the RGD motif in different sequence contexts for individual integrins (34) exemplifies the archetype.

Prospects for therapeutic and diagnostic targeting of the lymphatics

The peptides we describe here have potentially important uses. Early targeting of the tumor lymphatics for destruction may serve to reduce metastatic spread, as lymphatic vessels provide one of the main routes for the spreading of many types of cancer (15-17, 35, 36).. In the present study, we were able to reduce the abundance of lymphatics in melanoma xenograft tumors by using lymphatic homing peptides to direct a toxic peptide to the lymphatics in these tumors. In agreement with earlier studies (36), the destruction of the lymphatics had little effect on the growth of the melanoma tumors. These data support the proposition that primary tumor growth is not in general dependent on the lymphatic neovasculature. However, targeted destruction of tumor lymphatics with homing peptide conjugates has prospect to limit metastatic dissemination, as has been exemplified in other studies that genetically manipulated lymphatic growth factors to eliminate tumor lymphatics (15-17, 35, 36).

While studying the effect of the lymphatic homing peptide-drug conjugates on metastasis is one of our long-term aims, we foresee considerable potential in more general applications aimed at producing anti-tumor effects with homing peptides for tumor lymphatics. Lymphatic homing peptides can be harnessed to deliver a payload into the tumor, as illustrated herein for fluorescein and for the $D(KLAKLAK)_2$ pro-apoptotic peptide. Targeted drug conjugates can potentially have broader effects than what can

be obtained by destroying peri-tumoral lymphatics. Homing peptides for tumor blood vessels have been used in targeted delivery of therapeutic agents into tumors. As a result of such targeting, the efficacy of the drug increased, while its side effects were reduced (26, 32, 37, 38). Our lymphatic homing peptides present another potential route for targeted delivery of drugs into tumors.

Tumor-specific changes in the lymphatics may also have applications in diagnostic molecular imaging of tumor growth, progression, and response to therapy, as well as for early detection of incipient organ-specific cancers (or premalignant progenitor lesions) that evidently have both blood and lymphatic vascular signatures.

ACKNOWLEDGMENTS

We thank Dr. Rania Kairouz for her participation in the early stages of this work; Dr. Fernando Ferrer for peptide syntheses; Dr. Daniel Mercola for human prostate cancer samples; Robbin Newlin, Cherry Concengco, and Katie Gilliland for technical assistance with histology; and Roslind Varghese for editing. This work was supported by National Institutes of Health grants PO1 CA 82713 (ER and DH), PO1 CA 104898, RO1 CA115410 (ER), Cancer Center Support Grant P30 CA 30199 (The Burnham Institute), and other grants from the NCI/NIH (DH), and by Department of Defense grant DAMD 17-02-1-0315 (ER). LZ was supported by fellowship DAMD17-02-0309 from the Department of Defense, and JAH by National Cancer Institute training grant T32 CA77109-05. DH is an American Cancer Society Research Professor.

REFERENCES

1. Ruoslahti E. Specialization of tumour vasculature. *Nat Rev Cancer* 2002 Feb;2(2):83-90.
2. Hanahan D, Weinberg RA. The hallmarks of cancer. *Cell* 2000 Jan 7;100(1):57-70.
3. Brooks PG, Clouse J, Morris LS. Hysterectomy vs. resectoscopic endometrial ablation for the control of abnormal uterine bleeding. A cost-comparative study. *J Reprod Med* 1994 Oct;39(10):755-60.
4. Christian S, Pilch J, Akerman ME, Porkka K, Laakkonen P, Ruoslahti E. Nucleolin expressed at the cell surface is a marker of endothelial cells in angiogenic blood vessels. *J Cell Biol* 2003 Nov 24;163(4):871-8.
5. Ferrara N, Alitalo K. Clinical applications of angiogenic growth factors and their inhibitors. *Nat Med* 1999 Dec;5(12):1359-64.
6. Pasqualini R, Koivunen E, Kain R, *et al.* Aminopeptidase N is a receptor for tumor-homing peptides and a target for inhibiting angiogenesis. *Cancer Res* 2000 Feb 1;60(3):722-7.
7. Hoffman JA, Giraudo E, Singh M, *et al.* Progressive vascular changes in a transgenic mouse model of squamous cell carcinoma. *Cancer Cell* 2003 Nov;4(5):383-91.
8. Joyce JA, Laakkonen P, Bernasconi M, Bergers G, Ruoslahti E, Hanahan D. Stage-specific vascular markers revealed by phage display in a mouse model of pancreatic islet tumorigenesis. *Cancer Cell* 2003 Nov;4(5):393-403.
9. Cao R, Bjorndahl MA, Religa P, *et al.* PDGF-BB induces intratumoral lymphangiogenesis and promotes lymphatic metastasis. *Cancer Cell* 2004 Oct;6(4):333-45.
10. Cassella M, Skobe M. Lymphatic vessel activation in cancer. *Ann N Y Acad Sci* 2002 Dec;979:120-30.
11. Stacker SA, Achen MG, Jussila L, Baldwin ME, Alitalo K. Lymphangiogenesis and cancer metastasis. *Nat Rev Cancer* 2002 Aug;2(8):573-83.
12. Jackson DG, Prevo R, Clasper S, Banerji S. LYVE-1, the lymphatic system and tumor lymphangiogenesis. *Trends Immunol* 2001 Jun;22(6):317-21.
13. Laakkonen P, Porkka K, Hoffman JA, Ruoslahti E. A tumor-homing peptide with a targeting specificity related to lymphatic vessels. *Nat Med* 2002 Jul;8(7):751-5.
14. Padera TP, Kadambi A, di Tomaso E, *et al.* Lymphatic metastasis in the absence of functional intratumor lymphatics. *Science* 2002 Jun 7;296(5574):1883-6.
15. Mandriota SJ, Jussila L, Jeltsch M, *et al.* Vascular endothelial growth factor-C-mediated lymphangiogenesis promotes tumour metastasis. *Embo J* 2001 Feb 15;20(4):672-82.
16. Skobe M, Hawighorst T, Jackson DG, *et al.* Induction of tumor lymphangiogenesis by VEGF-C promotes breast cancer metastasis. *Nat Med* 2001 Feb;7(2):192-8.
17. Saharinen P, Tammela T, Karkkainen MJ, Alitalo K. Lymphatic vasculature: development, molecular regulation and role in tumor metastasis and inflammation. *Trends Immunol* 2004 Jul;25(7):387-95.

18. Bae VL, Jackson-Cook CK, Maygarden SJ, Plymate SR, Chen J, Ware JL. Metastatic sublines of an SV40 large T antigen immortalized human prostate epithelial cell line. *Prostate* 1998 Mar 1;34(4):275-82.
19. Arbeit JM, Munger K, Howley PM, Hanahan D. Progressive squamous epithelial neoplasia in K14-human papillomavirus type 16 transgenic mice. *J Virol* 1994 Jul;68(7):4358-68.
20. Arbeit JM, Howley PM, Hanahan D. Chronic estrogen-induced cervical and vaginal squamous carcinogenesis in human papillomavirus type 16 transgenic mice. *Proc Natl Acad Sci U S A* 1996 Apr 2;93(7):2930-5.
21. Giraudo E, Inoue M, Hanahan D. An amino-bisphosphonate targets MMP-9-expressing macrophages and angiogenesis to impair cervical carcinogenesis. *J Clin Invest* 2004 Sep;114(5):623-33.
22. Hoffman J, Laakkonen, P., Porkka, K., Bernasconi, M., and Ruoslahti, E. In vivo and ex vivo selections using phage-displayed libraries. In: Clackson T, Lowman HB editors *Phage Display* New York: Oxford University Press; 2004:p.171-92.
23. Greenberg NM, DeMayo F, Finegold MJ, *et al.* Prostate cancer in a transgenic mouse. *Proc Natl Acad Sci U S A* 1995 Apr 11;92(8):3439-43.
24. Gingrich JR, Greenberg NM. A transgenic mouse prostate cancer model. *Toxicol Pathol* 1996 Jul-Aug;24(4):502-4.
25. Laakkonen P, Akerman ME, Biliran H, *et al.* Antitumor activity of a homing peptide that targets tumor lymphatics and tumor cells. *Proc Natl Acad Sci U S A* 2004 Jun 22;101(25):9381-6.
26. Ellerby HM, Arap W, Ellerby LM, *et al.* Anti-cancer activity of targeted pro-apoptotic peptides. *Nat Med* 1999 Sep;5(9):1032-8.
27. Arap W, Haedicke W, Bernasconi M, *et al.* Targeting the prostate for destruction through a vascular address. *Proc Natl Acad Sci U S A* 2002 Feb 5;99(3):1527-31.
28. Hsu CX, Ross BD, Chrisp CE, *et al.* Longitudinal cohort analysis of lethal prostate cancer progression in transgenic mice. *J Urol* 1998 Oct;160(4):1500-5.
29. Coussens LM, Hanahan D, Arbeit JM. Genetic predisposition and parameters of malignant progression in K14-HPV16 transgenic mice. *Am J Pathol* 1996 Dec;149(6):1899-917.
30. Mouta Carreira C, Nasser SM, di Tomaso E, *et al.* LYVE-1 is not restricted to the lymph vessels: expression in normal liver blood sinusoids and down-regulation in human liver cancer and cirrhosis. *Cancer Res* 2001 Nov 15;61(22):8079-84.
31. Valtola R, Salven P, Heikkila P, *et al.* VEGFR-3 and its ligand VEGF-C are associated with angiogenesis in breast cancer. *Am J Pathol* 1999 May;154(5):1381-90.
32. Arap W, Pasqualini R, Ruoslahti E. Chemotherapy targeted to tumor vasculature. *Curr Opin Oncol* 1998 Nov;10(6):560-5.
33. Yao VJ, Ozawa MG, Trepel M, Arap W, McDonald DM, Pasqualini R. Targeting pancreatic islets with phage display assisted by laser pressure catapult microdissection. *Am J Pathol* 2005 Feb;166(2):625-36.
34. Ruoslahti E. The RGD story: a personal account. *Matrix Biol* 2003 Nov;22(6):459-65.
35. Stacker SA, Caesar C, Baldwin ME, *et al.* VEGF-D promotes the metastatic spread of tumor cells via the lymphatics. *Nat Med* 2001 Feb;7(2):186-91.

36. Lin J, Lalani AS, Harding TC, *et al.* Inhibition of lymphogenous metastasis using adeno-associated virus-mediated gene transfer of a soluble VEGFR-3 decoy receptor. *Cancer Res* 2005 Aug 1;65(15):6901-9.
37. Curnis F, Gasparri A, Sacchi A, Longhi R, Corti A. Coupling tumor necrosis factor-alpha with alphaV integrin ligands improves its antineoplastic activity. *Cancer Res* 2004 Jan 15;64(2):565-71.
38. Curnis F, Sacchi A, Borgna L, Magni F, Gasparri A, Corti A. Enhancement of tumor necrosis factor alpha antitumor immunotherapeutic properties by targeted delivery to aminopeptidase N (CD13). *Nat Biotechnol* 2000 Nov;18(11):1185-90.

FIGURE LEGENDS

Fig. 1. A homing peptide recognizes C8161 melanoma lymphatics. A. Homing of LSD-phage to C8161 xenografts. The LSD phage clone (2×10^9 pfu) was injected intravenously into mice bearing C8161 xenograft tumors and allowed to circulate for 7 min. Phage titers recovered from tumors and control tissues are shown. Phage accumulation in C8161 tumor tissue was significantly higher than in normal tissues [$P < 0.03$ relative to the normal tissue with the highest phage uptake, the skin; ($n=3$)]. B. *In vivo* localization of fluorescein-labeled LSD peptide. The peptide (150 μ g) was intravenously injected into C8161 tumor mice, and the tumors and various control tissues were collected for histological analysis 2 hrs after the injection. Green fluorescence indicates the presence of the peptide; nuclei are blue (DAPI staining). Original magnification: 200x. C. Colocalization of the LSD peptide with lymphatic markers. The green FITC fluorescence colocalizes with red staining for the lymphatic vessel markers podoplanin, VEGFR3, Prox-1, and LYVE-1 in vessel-like structures within the tumor tissue and at tumor periphery (lower left). D. LSD-peptide does not colocalize with blood vessel markers. Tumor blood vessels were stained with anti-MECA-32 or anti-CD31 (red). Original magnification in C and D: 400x.

Fig. 2. Stage-specific peptides distinguish premalignant lesions and tumors in the prostate of TRAMP mice and colocalize with lymphatic vessels. Phage isolated by screening for homing to TRAMP tumors (REA) or to TRAMP premalignant lesions (AGR) were individually tested in TRAMP mice bearing tumors, or premalignant lesions, and in tumor-free littermates of TRAMP mice with normal prostate. TRAMP mice were intravenously injected with phage or fluorescein-conjugated peptides, and the localization of the phage was studied by phage titration or immunohistochemistry in frozen tissue sections. The peptides were detected in tissue sections by examining fluorescence. The REA-phage (A, black bars) and peptide (B, top panels) accumulate in TRAMP tumors, whereas the AGR phage (A, gray bars) and peptide (B, bottom panels) selectively home to premalignant lesions. The difference between tumor tissue and premalignant tissue was significant for both peptides ($P < 0.01$; $n=3$ to 6) Original magnification: 400x. C. Intravenously injected fluorescein-labeled REA peptide (green)

colocalizes TRAMP tumor sections with the lymphatic vessel markers podoplanin, Prox-1, and LYVE-1 (upper row), but not with blood vessel markers (lower row); a premalignant TRAMP lesion does not bind the REA peptide (lower row, right panel). Original magnification: 400x D, Fluorescein-labeled AGR peptide (green) colocalizes with podoplanin and LYVE-1 (red) in dysplastic prostate lesions, but there is no colocalization with blood vessels detected with MECA-32 staining; a TRAMP tumor does not bind the AGR peptide. Original magnification: 400x.

Fig. 3. LyP-2 peptide homes to lymphatics in premalignant lesions and tumors of cervix in K14-HPV16/E₂ transgenic mice. A. LyP-2 phage (1.5×10^9 pfu) was intravenously injected into mice bearing CIN-3 lesions or tumors of the cervix and phage titers from the indicated tissues were determined. Significantly more of the LyP-2 phage accumulated in the tumors and dysplastic lesions than in normal cervix ($P < 0.005$; $n = 3$). B. FITC-LyP-2 peptide (100 μ g) was injected into the tail vein of mice bearing dysplastic lesions or tumors of the cervix and allowed to circulate for 2 hrs. FITC-LyP-2 selectively localized within premalignant lesions and tumors, colocalizing with lymphatic vessel markers (shown for LYVE-1; upper row), but not with the blood vessel markers (shown for MECA-32; lower row). Original magnification: 400x (upper panels) and 200x (lower panels).

Fig. 4. Homing specificity of the LSD, REA and AGR peptides in different types of tumors and premalignant lesions. *In vivo* homing of the LSD phage (A, left) and fluorescein-labeled LSD peptide (A, right) to six types of tumors was tested as in Figure 1 ($n = 3$ to 6). Robust phage homing and peptide fluorescence was only observed in C8161 tumors. KRIB xenograft tumors were slightly positive for phage and peptide homing, but phage homing to C8161 tumors was significantly higher than to this or any of the other tumors ($P < 0.005$). Original magnification: 400x. B. *In vivo* homing of intravenously injected AGR phage in TRAMP mice, K14-HPV16/E₂ mice bearing CIN-3 lesions or tumors ($n = 3$), and in MMTV-PyMT mice with dysplastic lesions or breast tumors. The AGR phage homed significantly more to TRAMP premalignant lesions than to comparable lesions in the other tumor models ($P < 0.03$). *In vivo* homing of the

REA-phage (C) and fluorescein-labeled REA peptide (D) to eleven types of tumors was tested (n=3 to 6). Significant phage homing and peptide fluorescence was observed in prostate tumors of TRAMP mice, and in PPC1, M12, DU145, and LNCaP human prostate cancer xenograft tumors (peptide fluorescence is shown for PPC1 in 4D). Four out of 5 prostate cancers (DU145 was the exception) accumulated significantly more REA phage than the other types of tumors ($P<0.03$). Cervical tumors in K14-HPV16/E₂ mice were slightly positive. REA-phage overlay of primary human prostate cancer is shown in 4D, bottom row. Human tumor tissue sections were stained with Prox-1 or anti-podoplanin. A serial section from the podoplanin staining was used for REA-phage overlay showing correspondence of the podoplanin and the REA phage localization.

Fig. 5. Differential tumor-homing specificity of LyP-1 and LyP-2 peptides. A. LyP-1 and LyP-2 phage were intravenously injected into mice bearing MDA-MB-435 breast cancer xenografts or K14-HPV16/E₂ tumors (n=3). B. Fluorescein-labeled LyP-1 and rhodamine-labeled LyP-2 (upper row) were intravenously injected (100 µg of each peptide) into the mice bearing tumors or premalignant lesions. Alternatively, the injection consisted of rhodamine-labeled LyP-1 and fluorescein-labeled LyP-2 (lower row). Tissues were collected and processed for histological analysis 2 hrs later. LyP-1 homes to the MDA-MB-435 tumors, whereas LyP-2 homes to the cervical cancers and premalignant lesions. Phage homing to the premalignant lesions was significantly higher than to the corresponding tumors in both models ($P<0.01$). Original magnification: 400x.

Fig. 6. Targeting the tumor-associated lymphatics with homing peptides linked to a pro-apoptotic peptide. The PPC1 orthotopic xenografted mice (10 mice/group) were systemically treated with 100 µg/dose/mouse/biweekly of $_D(KLAKLAK)_2$ -CREAGRKAC, equimolar amounts of the uncoupled peptides, or with the vehicle (PBS). At termination, tumor weights were recorded and frozen tissue sections were prepared for immunohistochemical analysis. A. The $_D(KLAKLAK)_2$ -CREAGRKAC chimeric peptide greatly reduces the number of tumor lymphatics ($P<0.01$) as determined from podoplanin staining, whereas the blood vessel count (MECA-32 staining) and tumor

volume (B) were unaffected. C. $D(KLAKLAK)_2$ -CREAGRKAC induced apoptosis of lymphatic endothelial cells in PPC1 tumors. The apoptotic lymphatic endothelial cells were detected by double staining with anti-active caspase-3 and anti-podoplanin antibodies. A significant increase in apoptosis of lymphatic endothelial cells in PPC1 tumors was observed in tumors of mice treated with the $D(KLAKLAK)_2$ -CREAGRKAC conjugate compared with controls ($P < 0.001$).

SUPPLEMENTARY FIGURES

Fig. S1. Phage library screening for peptides homing to lymphatic vessels in C8161 xenograft tumors. A. *Ex vivo* selection. The CX7C phage library (5×10^{10} pfu) was incubated with 5×10^7 cells derived from C8161 xenograft tumors at 4°C overnight. Lymphatic endothelial cells were isolated with anti-mouse podoplanin captured onto magnetic beads. The phage that bound to lymphatic endothelial cells were rescued and amplified for subsequent screening. Three rounds of *ex vivo* selection yielded 250-fold enrichment of phage as compared to the background obtained with nonrecombinant phage. B. *In vivo* selection. The enriched phage pool from the third *ex vivo* selection round was injected into the tail vein of a C8161 tumor mouse. Phage were recovered from tumor tissue, amplified, and the selection was repeated. A 40-fold enrichment relative to nonrecombinant phage was obtained in two *in vivo* rounds. C. Distribution of fluorescein-labeled LSD peptide in tumor-free tissues of mice bearing C8161 xenograft tumors. FITC-LSD (150 μg) was intravenously injected into tumor mice and allowed to circulate for 2 hrs. The tumor and various tissues were collected and processed for histological analysis. A few spots of LSD fluorescence were seen in the kidneys; all other tissues, with the exception of the tumors (Fig. 1B-D), were negative. Original magnification: 200x.

Fig. S2. Peptides selectively home to lymphatics in premalignant lesions and tumors of TRAMP mice. A. Presence of lymphatic vessels in premalignant prostate lesions and tumors of TRAMP mice. Premalignant prostate tissue and tumor tissue were obtained from TRAMP mice at the ages of 14-16 and 25-28 weeks, respectively. Lymphatics were visualized by staining frozen sections with rabbit anti-mouse LYVE-1

(red) and blood vessels were stained with rat anti-mouse MECA-32 (green). Original magnification: 200x. B. Distribution of fluorescein-labeled REA peptide in tumor-free tissues of TRAMP mice. The peptide (150 µg) was intravenously injected into TRAMP tumor mice, and the tumors and various control tissues were collected for histological analysis 2 hrs later. No FITC-REA was detected in the skin, lungs, gut, or brain. The liver and kidneys contained fluorescence at levels far lower than the TRAMP tumors (see Fig. 2C). Original magnification: 400x. C. Distribution of fluorescein-labeled AGR peptide in control tissues of TRAMP mice with premalignant prostate lesion. The peptide (150 µg) was intravenously injected into 14- to 16-week-old TRAMP mice and the tumors and various control tissues were collected for histological analysis 2 hrs later. No FITC-AGR was detected in the skin, lungs, gut, brain, or heart. The kidneys contained fluorescence at levels far lower than the premalignant lesions (Fig. 2C). D. Intravenously injected REA-phage was localized with anti-T7 antibodies and lymphatic vessels were visualized by using podoplanin, VEGFR3, and LYVE-1 staining. The phage (red) colocalizes with the lymphatic markers (upper row; green), but not with the blood vessel markers CD31, MECA-32, or tomato lectin (lower row; green). E. Comparison of the homing of REA phage to orthotopic vs. subcutaneously xenografted PPC1 tumors in nude mice. The REA phage (5×10^9 pfu) were injected into tumor mice by tail vein. After circulation for 7 min, the bound phage were recovered from the tumors and various control organs and titrated ($P < 0.03$ for orthotopic versus subcutaneous tumors; $n=3$). F. REA-phage binds to cell suspensions derived from PPC1 tumors, but not to cultured PPC1 cells. The *in vitro* phage binding assay was performed as described in Experimental Procedures. G. Fluorescein-labeled AGR peptide, which homes strongly to TRAMP premalignant lesions (Fig. 2D), does not detectably recognize cervical or breast premalignant lesions (K14 CIN-3; PyMT dysplastic) or tumors (K14 tumor; PyMT tumor). Original magnification: 400x.

Fig. S3. Evaluation of LyP-2 peptide specificity in K14-HPV 16/E₂ mice. A. Lymphatic vessels in tumors and dysplasias of the cervix in K14-HPV16/E₂ mice. Hematoxylin/eosin and anti-LYVE-1 staining of a cervical carcinoma and CIN-3 lesions. LYVE-1 positive structures are seen in both the carcinoma and CIN-3 lesion. Similar

results were obtained with another lymphatic marker, Prox-1 (not shown). Original magnification: 100x; inset, 400x. B. Fluorescein labeled-LyP-2 peptide homes to cervical carcinoma in K14-HPV16/E₂ mice. FITC-LyP-2 peptide (100 µg) was injected intravenously into tumor-bearing mice, and tissues were processed for histological analysis 2 hrs later. Little or no fluorescence was seen in normal cervix, skin, liver, or brain. Original magnification: 200x.

Table1. Main characteristics of lymphatic homing peptides

Peptide	Tumor used to isolate homing peptide	Tumors tested for phage homing <i>in vivo</i> ⁽¹⁾	Specific Homing ⁽²⁾	Fold over control phage
LSD	C8161 subcutaneous xenografts	C8161 xenografts KRIB xenografts K14-HPV16 skin cancer MDA-MB-435 orthotopic xenografts MMTV-PyMT breast tumors PPC1 orthotopic xenografts TRAMP prostate tumors	Yes Yes No No No No No	39 7 ³ 5 3 3 3 1
REA	TRAMP prostate tumors	TRAMP prostate tumors PPC1 orthotopic xenografts M12 orthotopic xenografts LNCaP orthotopic xenografts DU145 orthotopic xenografts MMTV-PyMT breast tumors K14-HPV16/E2 cervical cancer KRIB xenografts PPC1 subcutaneous xenografts C8161 subcutaneous xenografts K14-HPV16 skin cancer MDA-MB-435 orthotopic xenografts	Yes Yes Yes Yes Yes Yes Yes Yes No No No No	46 25 24 20 14 8 ³ 7 ³ 7 ³ 6 5 4 4
AGR	TRAMP prostatic intraepithelial neoplastic (PIN) lesions	TRAMP PIN lesions Tramp prostate tumors K14-HPV16/E2 cervical dysplasia K14-HPV16/E2 cervical tumors MMTV-PyMT pre-malignant lesions MMTV-PyMT breast tumors	Yes No No No No No	18 4 5 4 2 4
LyP-2	K14-HPV16 skin cancer	K14-HPV16/E2 cervical dysplasia K14-HPV16/E2 cervical tumors MDA-MB-435 orthotopic xenografts	Yes Yes No	17 22 3

(1) TRAMP, MMTV-PyMT and K14-HPV16 are genetically engineered mouse models of organ specific carcinogenesis, each of which presents first with angiogenic dysplasia and subsequently carcinoma.

(2) The specific homing of phage is considered to be strong (above 10 fold compared to control), weak (between 5-10 fold) or non-specific (below 5 fold).

(3) Phage homing corroborated by fluorescent peptide homing.

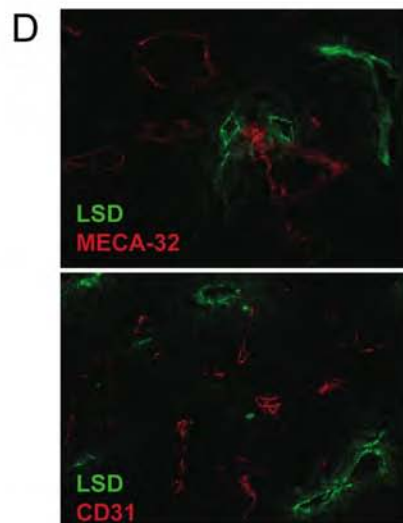
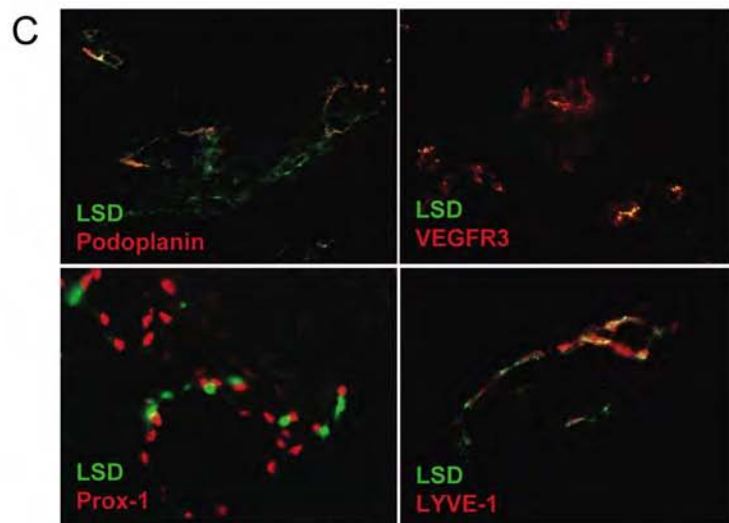
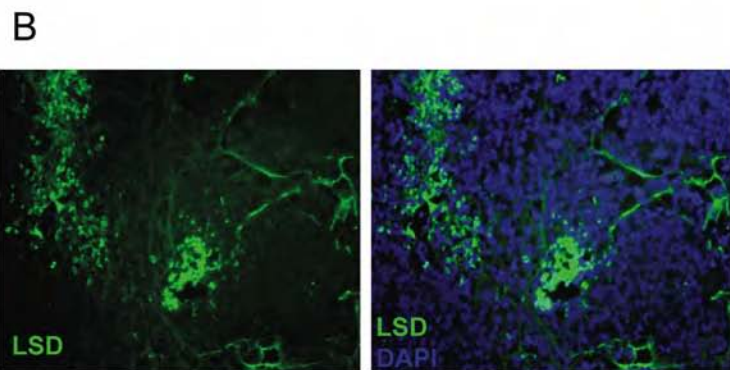
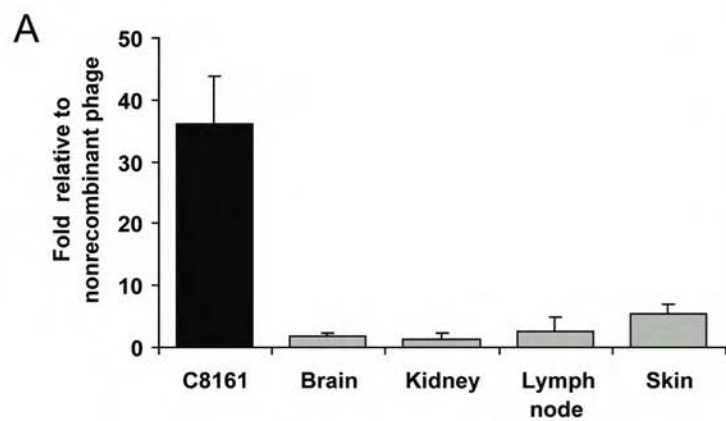


Figure 1 Zhang et al.

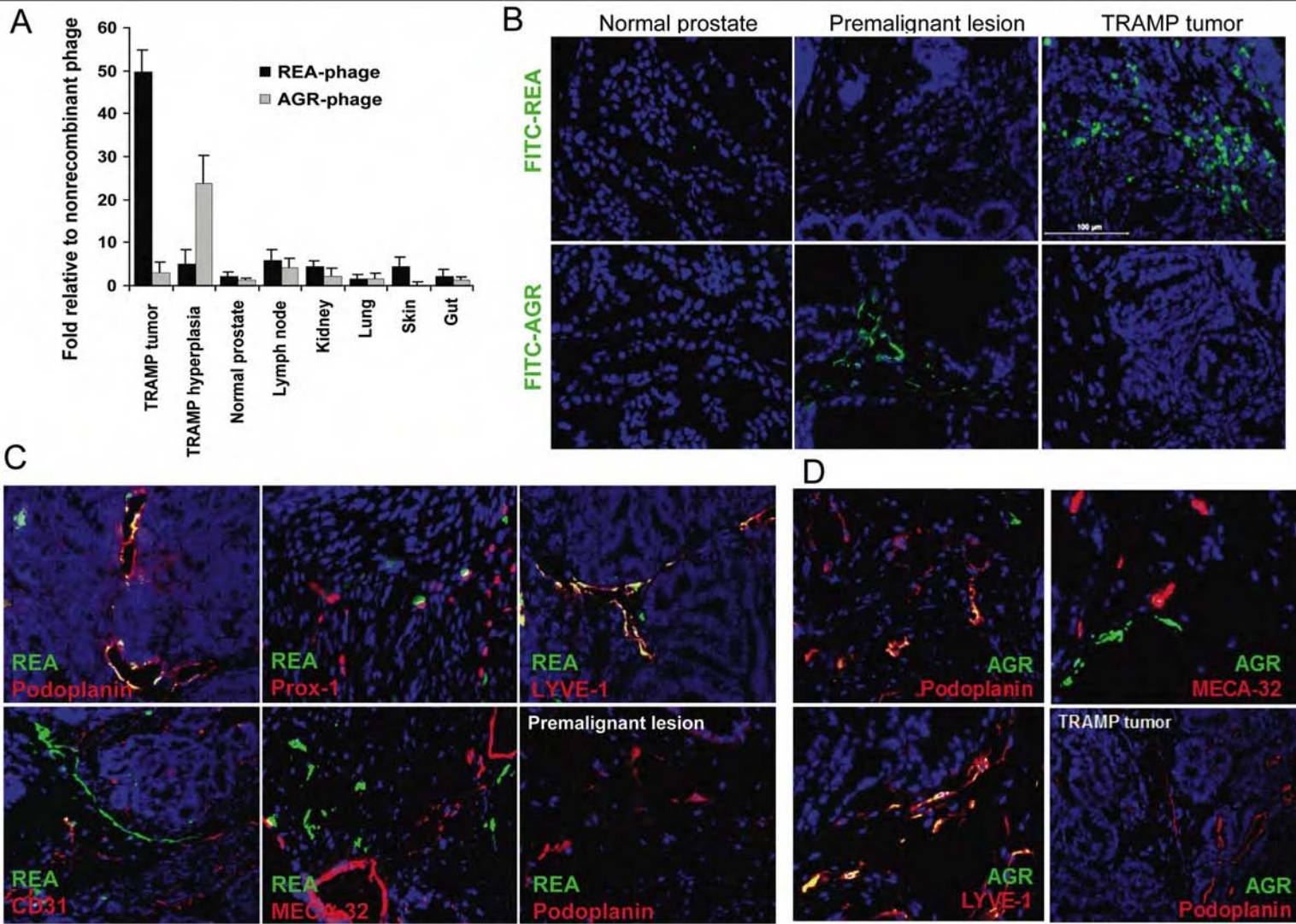
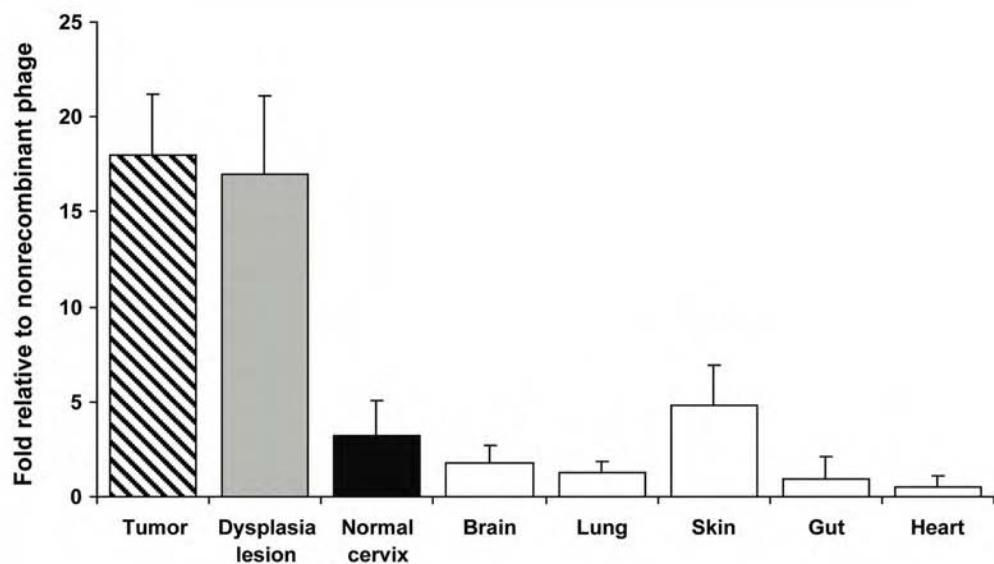


Figure 2 Zhang et al.

A



B

Normal cervix

CIN-3 lesion

Cervical tumor

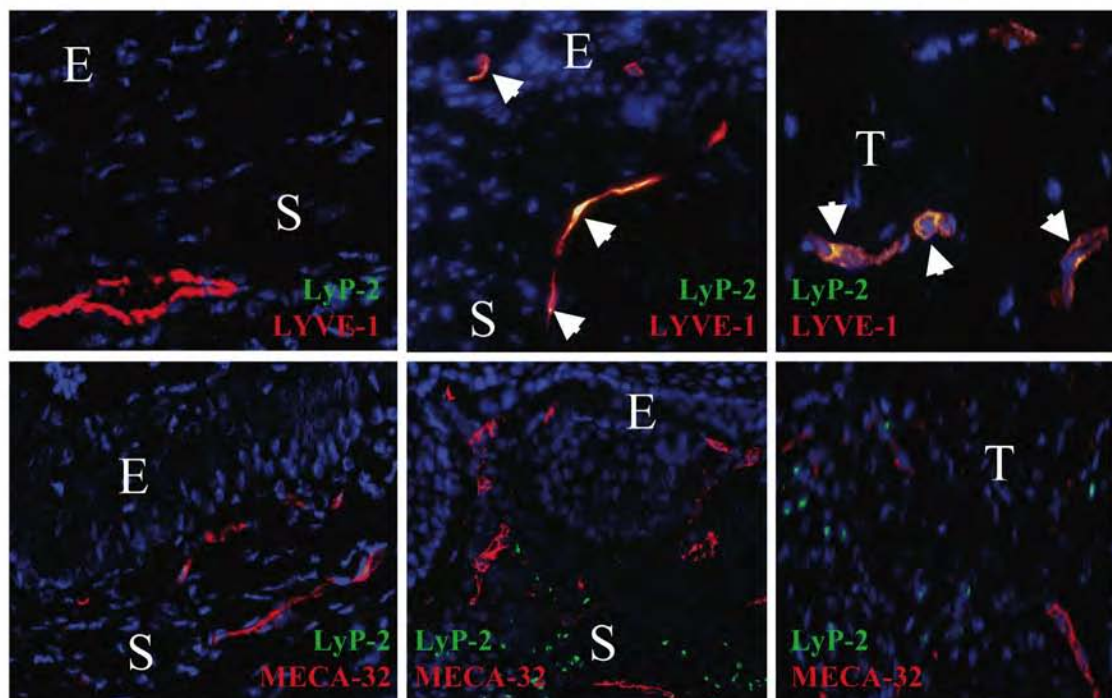
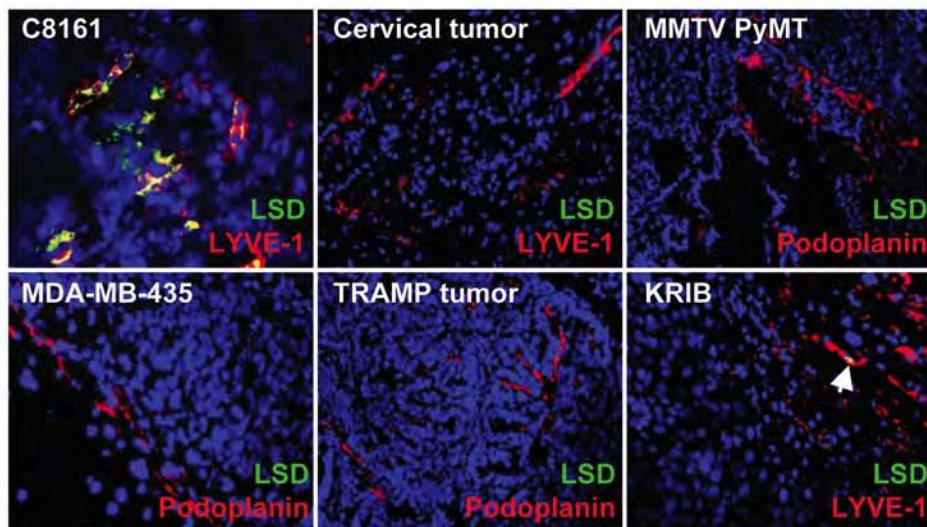
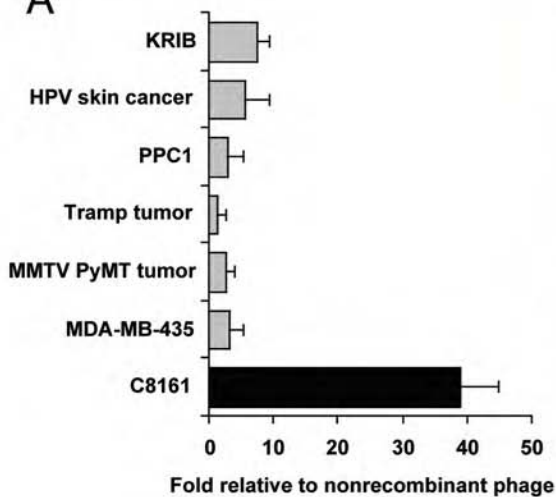


Figure 3 Zhang et al.

A



B

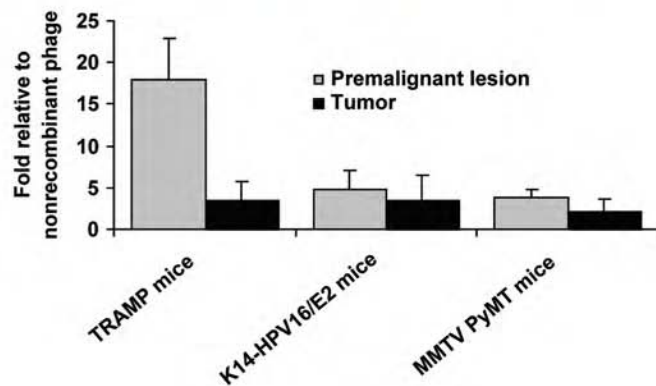
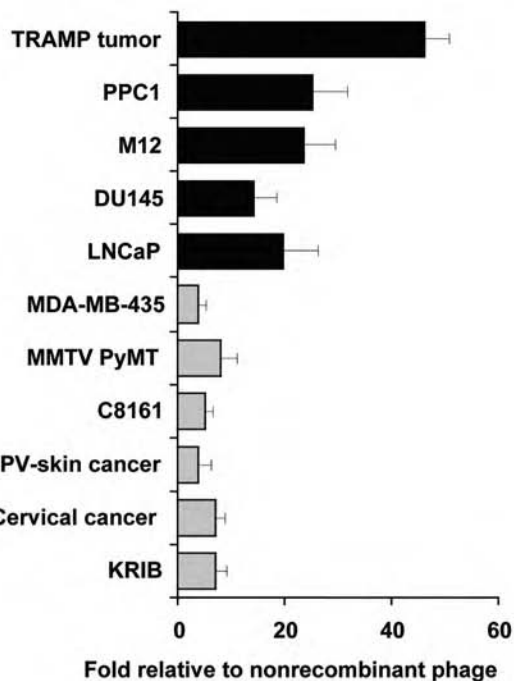


Figure 4 Zhang et al

C



D

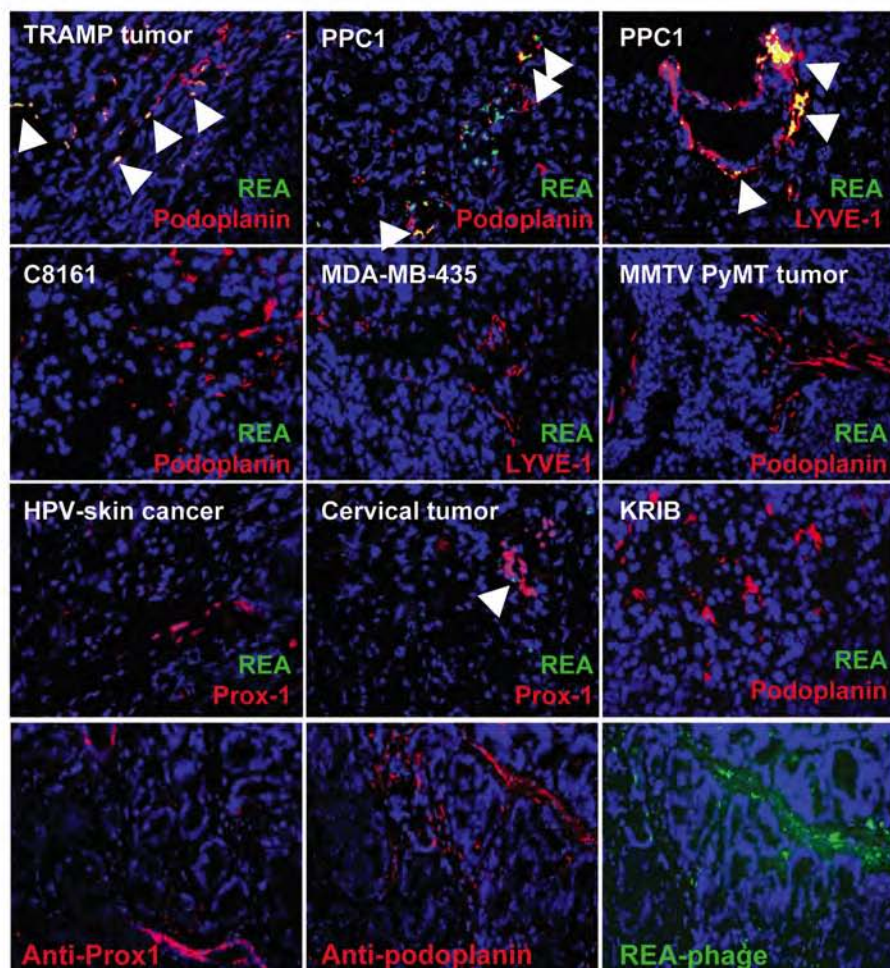
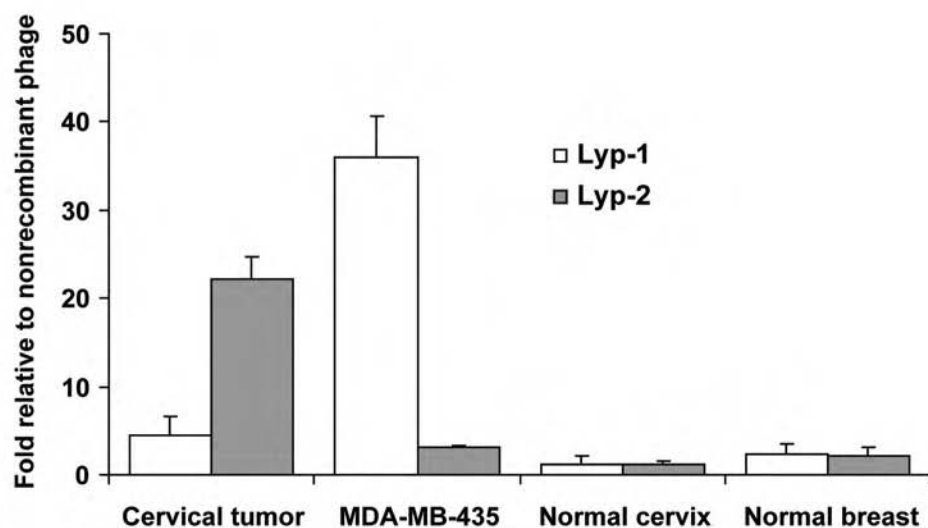


Figure 4 CONTD Zhang et al

A



B

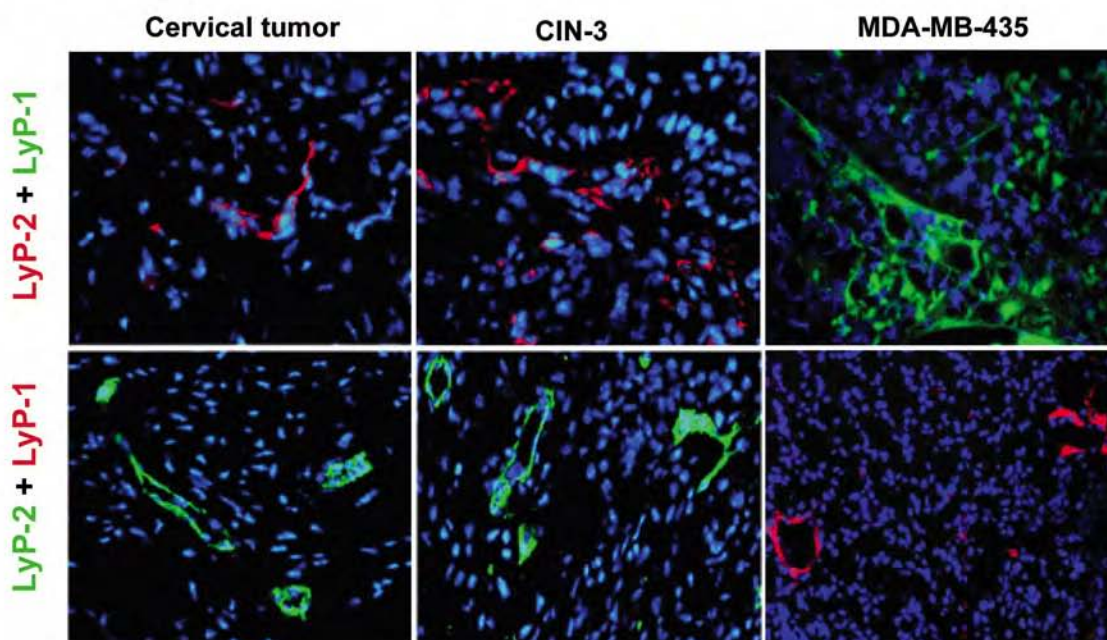
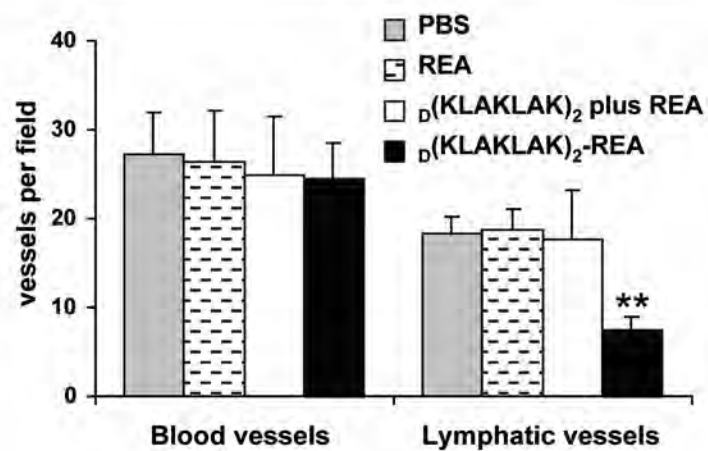
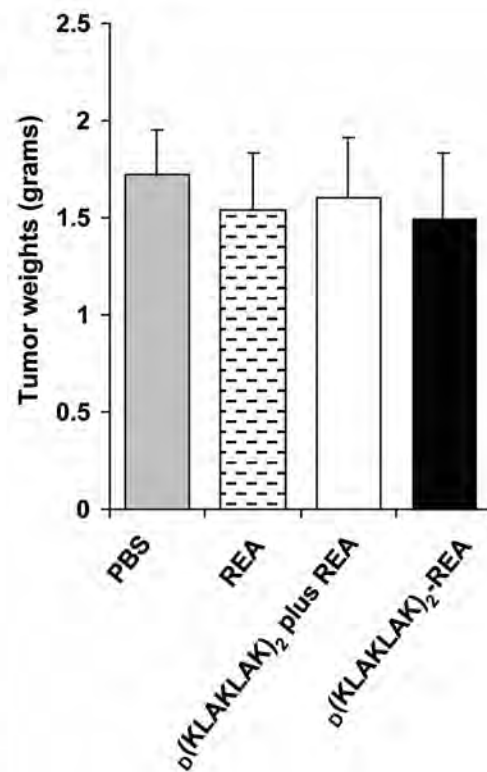


Figure 5. Zhang et al

A



B



C

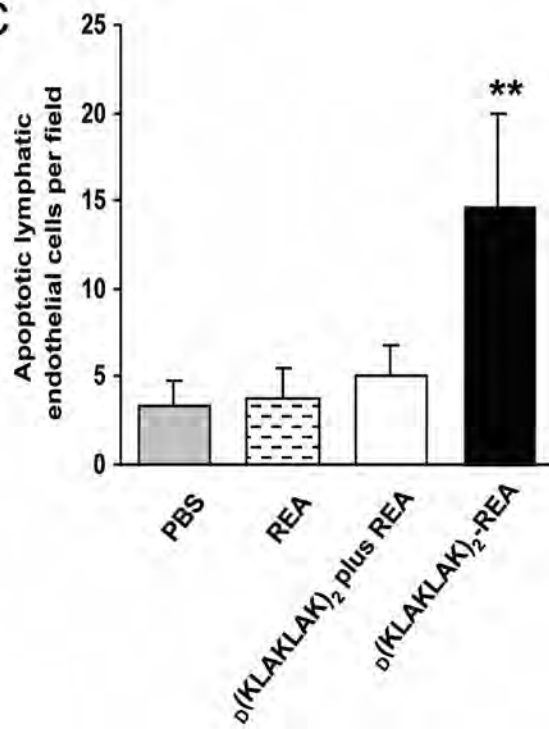


Figure 6. Zhang et al